Tailoring the Properties of Organic Semiconductors through Heteroatoms

Julia A. Schneider

McGill University

Department of Chemistry

Montreal, CANADA

A thesis submitted to McGill University in partial fulfillment of the requirements of the degree of Doctor of Philosophy.

Julia A. Schneider

Tailoring the Properties of Organic Semiconductors through Heteroatoms

February 2016

Supervisor: Dmitrii F. Perepichka

McGill University

Department of Chemistry

801 Sherbrooke St. West

Montreal, H3A 0B8

Abstract

Incorporating heteroatoms is a powerful technique to tune the properties of organic semiconductors. Understanding the structure-property relationships associated with heteroatoms is imperative for the design of new materials for organic electronics. In this dissertation we study the effect of sulfur and nitrogen heteroatoms on the electronic, optical, and supramolecular assembly properties of organic semiconductors. This work focuses on the synthesis of new polymers and small molecules that contain heteroatoms in the π–conjugated core and/or in substituents, as well as the full characterization of these materials. The structures presented include thienothiophene vinylene polymers with alkylsulfanyl and alkylsulfonyl substituents, a thienothiophene—thiazolothiazole trimer, diazabenzopyrene, and diazaperylene. Device studies in photovoltaics and field-effect transistors were performed to gain insight on structure-property relationships and the effect of heteroatoms.

Résumé

L'incorporation d'hétéroatomes est une technique puissante permettant de mettre au point les propriétés de semi-conducteurs organiques. Comprendre les relations entre les structures et les propriétés associées au hétéroatomes est impératif pour la conception de nouveaux matériaux pour l'électronique organique. Dans cette thèse nous étudions l'effet des hétéroatomes de soufre et d'azote sur les propriétés électroniques, optiques et d'assemblage supramoléculaire de semi-conducteurs organiques. Ce travail se concentre sur la synthèse de nouveaux polymères et des molécules qui contiennent des hétéroatomes dans le centre π–conjugué et/ou dans des substituants, ainsi que sur la caractérisation complète de ces matériaux. Les structures présentées comprennent des polymères thiénothiophène vinylène avec des substituants d' alkylsulfanyle et alkylsulfonyle, un trimère de thiénothiophène - thiazolothiazole, diazabenzopyrene et diazaperylene. Afin de mieux comprendre les relations entre les structures et les propriétés et l'effet des hétéroatomes, des études de ces matériaux dans des photovoltaïques et des transistors à effet de champ ont été effectuées.

Acknowledgements

My profound thanks and appreciation to my supervisor, Prof. Dmitrii Perepichka, without whose counsel this work would not have been possible.

I am indebted to all the members of the Perepichka group. Special thanks to Chaoying Fu, my dissertation companion, Mykola Kondratenko, who showed great bravery in the face of flaming t-Buli, to Afshin Dadvand, who always believed in me, and to Hayden Black and Rajesh Malakalapalli, the world's best post-docs. Thank you to Alan Blayney and Jorge Rubio for the chicken nuggets and late night Civ games. My apologies to Yaroslav Zem, and all the other group members I may have yelled at when startled.

I would like to acknowledge the assistance of Francine Belanger-Gariepy with X-ray crystallographic analysis, Fred Morin with solid-state NMR experiments, Nadim Saadé and Alexander Wahba with mass spectroscopy, Michelle Bezanson and Dmitrii Xanthopoulos with HPLC, and Violetta Toader with synthesis.

I wish to extend my gratitude to Robert Godin, not only for his assistance with single-crystal fluorescence and lifetime measurements, but for his invaluable friendship.

My time at UCSB would not have been as productive or enjoyable without the help of Dr. Wen Wen, the members of Prof. Bazan's research group, and most of the geology department. Thank you to the Continental for being my home away from home.

I would like to thank my family for their patience, Agnes and Ed Bolton for their love and support, Matthew Beale for the fish bowl, I would not have had the wherewithal to finish this thing if it weren't for you.

Finally, to my fellow chemists and friends, Michelle Bezanson, Laure Kayzer, Monika Rak and Mary Bateman. It was a long road and I am so glad we walked it together.

Contribution of Authors

Chapter 2 reprinted with permission from:

Schneider, J. A.; Dadvand, A.; Wen, W.; Perepichka, D. F. *Macromolecules* **2013**, *46*, 9231–9239. Copyright (2013) American Chemical Society

Afshin Dadvand was responsible for making and measuring thin-film transistors of **S-PTTVc**. Solar cell devices of **S/SO2-PTTV** with additives were made and measured by Dr. Wen Wen from Prof. Bazan's group at UCSB. Solar cell devices of **S-PTTV** were made by the first author. AFM images were taken by Dr. Wen. All the modeling, synthesis, and optical and electrochemical characterization of the polymers and dimers was performed by the first author.

Chapter 3 reprinted with permission from:

Schneider, J. A.; Black, H.; Lin, H.-P.; Perepichka, D. F. *ChemPhysChem* **2015**, *16*, 1173-1178. Copyright (2013) John Wiley & Sons, Inc.

Dr. Hua-ping Lin made and measured the thin-film transistors of **3.2**. Dr. Hayden Black made and measured the single-crystal transistors of **3.1-Yellow**. The first author is responsible for the single-crystal transistors of **3.1-Red**, as well as the synthesis, optical and electrochemical characterization of the trimers.

Introduction

Organic electronics are a class of devices in which molecules or polymers serve as the electrically active material. Notably, the properties of these organic materials can be endlessly tuned through structural modifications. The ability to tailor a semiconductor for a specific application is one of the most attractive aspects of organic electronics. Additionally, solution-processable materials offer the possibility of inexpensive, large area devices, via roll-to-roll or inkjet printing for example. Solar cells produced in this way could potentially satisfy the world's increasing energy demands in a sustainable manner. Organic electronics made entirely from biodegradable materials would help stem the accumulation of e-waste in landfills. For organic electronics to become widely adopted and compete with existing inorganic materials, however, they need to demonstrate sufficiently long lifetimes and enhanced electrical properties. This has fueled the discovery of many new high-performance, stable materials, as well as extensive research into what factors dictate charge transport and how to control them. The motivation of this thesis is to contribute new design strategies for the synthesis of organic semiconductors and to better our understanding of structure-property relationships.

While some design strategies yield predictable results, many structure-property relationships are still not well understood, especially as they relate to supramolecular ordering. In the last three decades, multitudes of organic semiconductors have been synthesized, primarily by trial and error. A material's solid-state packing and associated device performance is only discussed after the fact. The work in this thesis focuses on a series of carefully designed structures meant to probe a specific structure-property relationship: the role of the heteroatom.

The incorporation of heteroatoms in a molecule or polymer is an efficient way to tune the properties of a material, but how a heteroatom is incorporated, either as a substituent or as part of the π–conjugated core, will alter its effect on energy levels and supramolecular ordering. DFT calculations can be used to accurately predict how an electron rich or electron deficient heteroatom will modify a molecule's frontier orbitals, but how heteroatoms influence self-assembly is much harder to ascertain. The structures studied in this thesis feature sulfur and nitrogen, the two most prevalent heteroatoms in organic semiconductors. Sulfur is of particular interest in organic electronics because sulfur-sulfur interactions between neighboring molecules have been linked to high electrical conductivity. Nitrogen can be used to lower the energy levels of a material and facilitate electron charge transport, while protonating nitrogen atoms can further alter a material's electronic and optical properties (eg, acid-doping of polyaniline). The following chapters explore the affects of these heteroatoms in side-chain substituents and within aromatic rings.

Chapter One offers a brief overview of the field of organic electronics. It discusses the theories of charge transport, devices that employ organic semiconductors, and existing design strategies utilized to achieve desired properties. Among these strategies, the use of heteroatoms is discussed in more details. The chapter concludes with a selection of reported organic semiconductors of relevance to the presented research.

Chapter Two presents novel thienothiophene vinylene polymers with alkylsulfanyl side chains. Our original goal was to incorporate more sulfur atoms along the periphery of the polymer backbone to see if sulfur-sulfur contacts could lead to better intrachain organization. The electronic effect of the sulfur atom as a side-chain substituent was further explored by oxidation to electron withdrawing sulfonyl groups (as well as sulfoxyl, Appendix A.2). By varying the ratio of alkylsulfanyl and alkylsulfonyl-substituted monomer units in random copolymers, the energy levels of the polymers could be tuned. The result is one of the few examples of a donor-acceptor polymer with a structurally homogeneous backbone. The semiconducting properties of the polymers were measured in transistor and photovoltaic devices.

Chapter Three explores the effect of combining sulfur and nitrogen heteroatoms, while highlighting the role polymorphism plays in charge transport. We synthesized a trimer made of structurally similar thienothiophene and thiazolothiazole building blocks, placing the focus on the role of sulfur and nitrogen heteroatoms. Two polymorphs of this molecule were grown using temperature gradients and through crystal structure analysis, DFT calculations, and single-crystal field-effect transistor devices, we studied the role of heteroatom close contacts in different packing motifs.

Chapter Four is a primarily synthetic investigation repurposing the long-known Hemetsberger reaction to incorporate nitrogen heteroatoms in arenes. This work presents the previously unreported azide insertion on peri-substituted arenes to form fused pyridines using only visible light. Two polycyclic N-heteroaromatic compounds are reported, namely diazabenzopyrene and diazaperylene, and the effect of the nitrogen heteroatoms on their optical properties is investigated.

Chapter Five presents a summary of the work in this thesis, as well as general conclusions and perspectives.

The Appendix contains brief descriptions of other related projects that though interesting, were unsuccessful or deemed inappropriate for publication.

Abbreviations

Å	Ångström
λ	Reorganization energy
μ_h, μ_e	Hole, electron mobility
APCI	Atmospheric pressure chemical ionization
BHJ	Bulk heterojunction
BLA	Bond length alternation
°C	Degrees celcius
$CHCl_3$	Chloroform
CH_2Cl_2	Dichloromethane
CV	Cyclic voltammetry
DFT	Density functional theory
DMF	Dimethylformamide
DMSO	Dimethylsulfoxide
E_g	HOMO-LUMO gap or band gap
eq.	Equivalent
Et_2O	Diethyl ether
EtOH	Ethanol
ESI	Electrospray ionisation
FF	Fill factor
FWHM	Full width at half maximum
HCL	Hydrochloric acid
HMDS	Hexamethyldisilazane
HOMO	Highest occupied molecular orbital
HPLC	High Performance Liquid Chromatography
HRMS	High resolution mass spectrometry
IR	Infrared (spectroscopy)
I_{SC}	Short-circuit current
ITO	Indium tin oxide
K	Kelvin
LUMO	Lowest unoccupied molecular orbital
m-CPBA	Meta-chloroperoxybenzoic acid
MeCN	Acetonitrile

MeOH	Methanol
MW	Molecular weight
NaOEt	Sodium ethoxide
NaOH	Sodium hydroxide
Na_2SO_4	Sodium sulfate
NMR	Nuclear magnetic resonance
N-PAH	Polycyclic N-heteroaromatic
OFET	Organic field-effect transistor
OLED	Orgainic light emitting diode
OPV	Organic photovoltaic
OSC	Orgainic semiconductor
P3HT	Poly(3-hexylthiophene)
PAH	Polycyclic Aromatic Hydrocarbon
PCBM	Phenyl-C61-butyric acid methyl ester
PCE	Power conversion efficiency
PDI	Polydispersity index
PEDOT:PSS	Poly(3,4-ethylenedioxythiophene) polystyrene sulfonate
PLQY	Photoluminescent quantum yield
PMMA	Poly(methyl methacrylate)
PP	Poly(phenylene)
PPV	Poly(phenylene vinylene)
PPy	Poly(pyrrole)
PT	Poly(thiophene)
PTTV	Poly(thienothiophene vinylene)
PTV	Poly(thiophene vinylene)
PVT	Physical vapor transport
Py	Pyrrole
UV-vis	Ultraviolet – Visible (spectroscopy)
t	Electronic coupling
$TBAPF_6$	Tetrabutylammonium hexafluorophosphate
TFA	Trifluoroacetic Acid
TFT	Thin-film transistor
THF	Tetrahydrofuran
TLC	Thin-layer chromatography
TMEDA	Tetramethylethylenediamine
TT	Thienothiophene
TzTz	Thiazolothiazole
SCFET	Single-crystal field-effect transistors
-SR	Alkylsulfanyl
$–SO_2R$	Alkylsulfonyl
V_{OC}	Open-circuit voltage
XRD	X-Ray Diffraction

Contents

1 An Introduction to Organic Electronics and the Molecular Design of Organic Semiconductors

1.1 History of Organic Semiconductors

Semiconductors are ubiquitous in modern technology: they can be found in the transistors and diodes that all our electronic devices use. The first transistor device was invented in 1947 while Bardeen, Brattain, and Shockley were studying surface states in a germanium crystal. Ever since, inorganic materials like silicon or gallium arsenide have been predominantly used in our electronic components. Conductive organic materials, however, had already been discovered, though perhaps unbeknownst to the discoverer. In 1862, Letheby observed conductive and electrochromic behavior in a unidentified "dirty blueish-black powder" now thought to be polyaniline.[1] Many small organic molecules were also known to be conductive, such as tetrathiafulvalene (TTF) chloride salts, as shown by Wudl in 1972.[2][3] An enormous body of work then evolved around TTF complexes when they were suspected of superconductivity.[4] Controlled doping via impurities to modulate the conductivity of an organic material was perhaps first described in iodine-doped polypyrroles by Bolto et al. in 1963.[5] Their results led them to conclude that the "orbital overlap between adjacent pyrrole rings in polypyrrole suffices to impart a relatively high level of conductivity." The work that popularized conjugated polymers for organic electronics, however, was the famous discovery in 1977 by MacDiarmid and Heeger that thin-films of polyacetylene (synthesized by Shirakawa) are also conductive when doped with halogens.[6] This discovery earned the trio the 2000 Nobel Prize in Chemistry.[7] Suddenly conductive materials could be synthesized according to chemists' designs. Synthetic strategies from organic chemistry

were married to charge transport theories from physics and the field of organic electronics was born.

Initially the impetus for organic electronics was to recreate the conducting properties of inorganic materials, which led to extensive studies on the conductivity of molecular crystals and conjugated polymers. The current prominence of the field, however, came about due to breakthroughs in device fabrication. While working for Eastman Kodak in the early 1980s, Tang filed patents for the first heterogeneous organic solar cell and the first electroluminescent device, earning him the title "father of organic electronics." His organic light emitting diode (OLED) demonstrated not only that organic material could produce light in response to an electrical current, but that organic materials could be used in commercially viable electronic devices.[8] A few years later the Friend group, working at the Cavendish Laboratory, reported the first OLED based on a conjugated polymer, poly(phenylene vinylene) (PPV), paving the way for solution-processable devices.[9]

In the late 1980s, Friend and co-authors were also making breakthroughs in organic field-effect transistors (OFET). An important contribution was the demonstration that charge carriers could be introduced into conjugated polymers, such as polyacetylene, through the use of a surface electric field.[10] Also paramount in the advancement of the field was Garnier's work with oligothiophene-based OFETs.[11] Early measurements of evaporated films of sexithiophene only displayed mobilities on the order of 10^{-4} cm^2/Vs, but the possibility of using organic semiconductors in conventional electronics was established.

Since these early discoveries many organic semiconductors (OSCs) – polymers and small molecules – have been synthesized and tested in devices. Organic electronics exhibit four key beneficial properties: flexibility, transparency, expendability and the potential to be processed at low-cost over large surfaces through solution printing techniques.[12] Due to these properties, organic electronics can be advantageous for certain applications where inorganic materials would not be appropriate, though they do often suffer from low conductivities and poor operational stability. The incorporation of thin-film printed OSCs in Radio Frequency IDentification (RFID) tags, for example, would lower the tag's cost and improve their mechanical properties, making them viable for tracking large inventories,

such as in supermarkets.[13] OSCs have also been heavily studied as biosensors, where cost, flexibility and disposability can be important factors, but fast switching speeds are not necessary because the sensing process is limited by biochemical reactions and adsorption rates.[14] The first commercial use of OSCs was in OLED displays, which are thinner and use less energy than their inorganic analogues. The emission color of an OLED can also be tuned by modifying the organic chromophore. Organic photovoltaics (OPVs) are an example of devices which greatly benefit from the large-scale printing processes available to OSCs. Solution-processable OPVs can be light, flexible, and transparent, something that would be impossible in silicon-based solar cells.[15] Complimentary circuits, which rely on a combination of p- and n-type transistors, have also been made from OSCs, though their development has been slow due in part to the relative scarcity of n-type semiconductors.[16] All the applications have made organic electronics a hotly researched field over the last several decades. Ongoing research focuses on selectively tuning a material's electronic properties, on increasing solubility and stability, and on understanding and controlling supramolecular assemblies.

1.2 Band gap

Organic semiconductors are π–conjugated molecules or polymers, meaning they contain alternating single and double bonds such that their π–orbitals overlap and form a network of delocalized electrons (Figure 1.1). These overlapping molecular orbitals and the energy levels of the electrons within, is referred to as a band. The bonding molecular orbitals below the Fermi level form the valence band and the higher energy anti-bonding orbitals above the Fermi level form the conductance band. The energy difference between these bands is called the band gap and it is bound by the highest energy occupied molecular orbital (HOMO) and the lowest energy unoccupied molecular orbital (LUMO).

In a material with no band gap, termed "metallic," electrons can easily move into the empty states of the conductance band, creating "free" charge carriers which provide high conductivities. Conversely, insulators exhibit poor conductivities because their large band gap inhibits the movement of electrons into the conductance band.

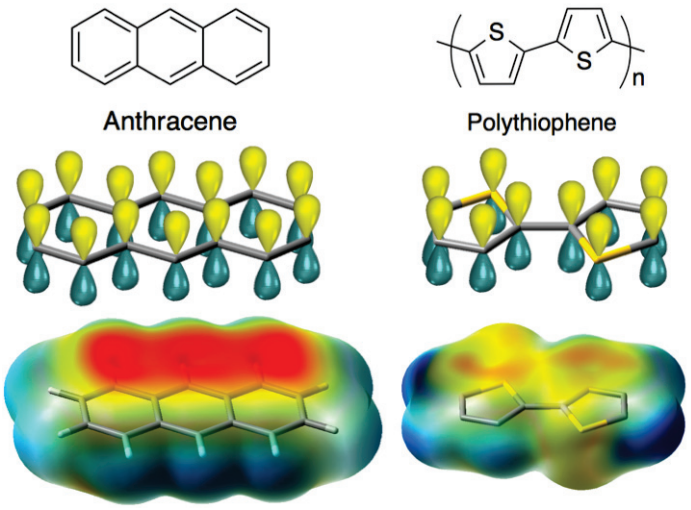

Fig. 1.1.: Conjugated molecules have alternating double and single bonds. Overlap between π–orbitals causes electrons to be delocalized throughout the structure giving rise to electron density above and below the aromatic cores, as seen in the calculated electrostatic potential surfaces.

Charge carriers need an open path in order to move through a material, i.e. the bands must be only partially filled. This is achieved when an electron moves from the full valence band into the empty conductance band, leaving a "hole" behind. A neighboring electron can then move over to the new hole, leaving its own hole behind. In effect, the hole is acting as a positive charge carrier moving through the valence band, while electrons move through the conductance band. OSCs are ambipolar and can be used in p-type or n-type transistors, in which holes or electrons, respectively, are the charge carriers. All OSCs are "extrinsic semiconductors," meaning that they must be doped to be conductive. Dopants supply holes or electrons to the material and contract the band gap by creating intermediate states (Figure 1.2). A material can chemically or photochemically doped through oxidation or reduction, or it can be doped via the injection of charge carriers by an electric field.

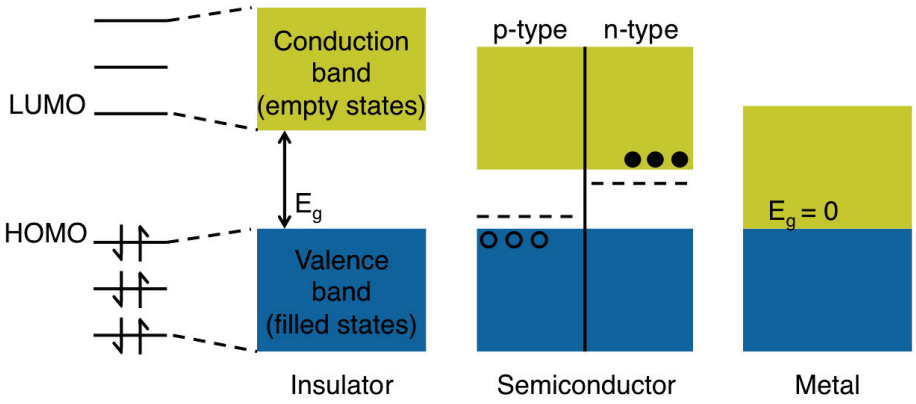

Fig. 1.2.: Molecular orbitals make up the energy bands and the size of the band gap determines the conductivity. P-type and n-type doping of the band gap with respective charge accumulation is shown in the semiconductor. (Electrons are filled and holes are unfilled circles.)

1.3 Theoretical Models for Charge Transport

Before looking at the design strategies for synthesizing OSCs, it is useful to understand, at least qualitatively, the theoretical models describing charge transport in small molecules and polymers. Charge transport in OSCs is characterized by measuring the charge mobility, or the time it takes an electron or hole to move through the material under an electric field. OSCs encompass materials with a large range of mobilities, making it hard for a single theoretical model to accurately describe charge transport in all OSCs. Charge transport in an ultra-pure crystal is different than in an amorphous film, which will also be different from transport in semi-crystalline polymer films. Several theories were developed and expanded upon to explain the observed characteristics of OSC devices, namely temperature-dependent, field-dependent, and film-thickness dependent charge-carrier mobility. Unfortunately it is still hard to predict the effects of microstructures in inhomogeneous OSC films, such as crystalline domains in polymer films.[17][18] The existing theories are generally characterized as band theory, hopping theory, and hybrid theories of the two.

Band theory is based on a model where charges are fully delocalized over several molecular units and exist in bands (equivalent to the conductance and valence bands introduced in

Section 1.2). For band transport to occur the interaction energy between nearest neighbors, called the electronic coupling (t), must be greater than disorder induced energy barriers. Band transport is characterized by a decrease in charge carrier mobility with increasing temperatures, a property common to crystalline inorganic semiconductors, but rarely seen in organic semiconductors. Karl and coworkers measured the hole and electron transport in assiduously purified naphthalene crystals at temperatures from 4–300 K, and proved that band transport can take place in ultra-pure OSC crystals below 300 K.[19] When measuring electron transport along the three crystallographic directions of naphthalene crystals a strong anistropy was observed that coincided with the electronic couplings acquired from DFT calculations–a fact that emphasizes the dependence of band transport on crystallinity.[20]

In amorphous OSCs, however, disorder effects become large and transport through a single delocalized band is no longer feasible. Disorder effects can be dynamic, such as vibrational changes when a molecule (or "site") becomes charged (seen in crystalline OSCs as well) or static, such as pre-existing variations in site energies and inter-site distances.[21] In such an environment a charge is localized on a single site and must "hop" to another localized site in order for conductivity to be observed. This process had been previously described by Marcus in the electron transfer between identical molecules in solutions – a theory for which he was awarded the 1992 Nobel Prize in Chemistry.[22][23] Hopping theory in OSCs was spearheaded by, among others, Mott and Holstein, who developed small polaron hopping theory.[24] A polaron is the combination of a charge carrier and the lattice deformations associated with that carrier's movement. The distortions to the molecules and their environment lead to an energetic cost to charge transfer called the reorganization energy (λ). As a result, charge transfer is thermally activated and we observe an increase in mobility as temperature increases. Holstein's model for the rate of electron transfer is a function of the electronic coupling (t), the polaron binding energy (E_{pol}), and thermal energy ($k_B T$) shown in equation 1.1.

$$k_{ET} = \frac{t^2}{\hbar}\sqrt{\frac{\pi}{2E_{pol}k_B T}}\exp\left[-\frac{E_{pol}}{2k_B T}\right] \tag{1.1}$$

The polaron binding energy is defined as the relaxation energy of an ionized molecule, while reorganization energy is the sum of the relaxation energies of the initial neutral molecule and the resulting ionized molecule. Recognizing that the polaron binding energy is equal to half to reorganization energy ($E_{pol} = \lambda/2$), equation 1.1 is identical to the semiclassical Marcus equation. The simplicity of this model, that relates transfer rates directly to electronic coupling (t) and reorganization energy (λ), has made it popular among chemists as a reasonable approximation for charge transport in OSCs.

Neither band theory nor two-state hopping theories, however, address the defects present in the majority of OSC thin-films, which are poly/semicrystalline. In these cases, static disorder effects give rise to anisotropic charge transport, due to different t values. Variations in site energies and inter-site distances leads to asymmetric rates and therefore time-dependent mobilities. The Gaussian Disorder Model (GDM) assumes a Gaussian energy distribution of these variations and takes into account the life-time of the charge carrier.[25]

As device preparation techniques improved, OSCs started to show higher measured mobilities even in amorphous films. Current theories therefore reconciled band-like and hopping transport into trap-limited transport.[26] The multiple-trap-and-release model (MTR) was first proposed by Shur and Hack to describe hydrogenated amorphous silicon.[27] The model assumes band-like charge transport occurs through delocalized states, but that trap-states capture injected charge carriers, where they may be further excited into the conduction band (Figure 1.3). This model describes materials with a large range of mobilities, since the mobility is affected by the ratio of free to trapped charges. Horowitz successfully applied the MTR model to OSCs when explaining the changing temperature and field-dependence of mobilities observed in polycrystalline films of sexithiophene.[28]

In the context of molecular design for OSCs, maximizing nearest neighbor interactions and minimizing reorganization energy is crucial to increased charge mobilities. In the end, though, charge transport is often limited by the number of trap states. The efficacy of a trap depends on its energy level relative to the HOMO or LUMO, for hole or electron trapping, respectively.[29] Trapping sites can either be structural faults or chemical impurities. A

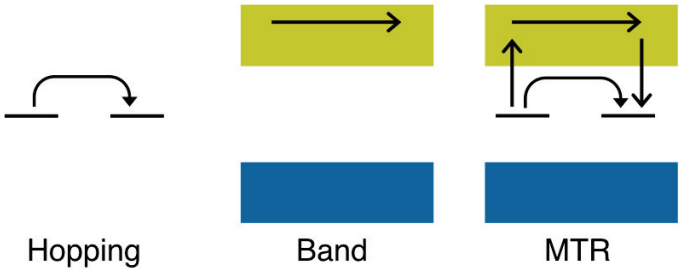

Fig. 1.3.: Theoretical charge transport models. On the left is the hopping method where only localized states exist. In the middle is band theory where all charges travel through the conductance band. On the right is the multiple-trap-and-release model in which trapped charges can still move into the conductance band. (Note that these examples are depicting n-type transport.)

commonly seen trap is oxygen or oxidation products, but not all such impurities need act as traps. If the energy level of the potential trap lies above or below the material's band gap, the trap remains ineffective. The nature of the traps present, especially oxidation products, depend on the OSC and can sometimes be predicted and avoided.

1.4 OSC Devices

Organic semiconductors have been used in a wide range of electronics. While OSC's exhibit lower mobilities than their inorganic counterparts, their tunability and processing versatility give them a strong advantage for light-weight or one-time-use applications. OSCs can be printed from solution onto practically any surface, including flexible plastics[30] and paper.[31] This is advantageous for medical applications, such as electronic skin or bio-compatible sensors.[32] This section will give a brief overview of three types of OSC devices.

1.4.1 Organic Light-Emitting Diodes

In terms of the commercialization of OSCs, organic light-emitting diodes (OLEDs) are undoubtedly leading the way. OLED-based displays can be found in a myriad of smartphone

screens, including Samsung's Galaxy series, Google's Nexus 6, the Nokia Lumina, and LG's G Flex, as well as in some tablets, television displays, and solid-state lighting panels.[33]

An OLED device consists of an emissive layer and transport layer, made of organic molecules or polymers. These layers are sandwiched between two electrodes and when a voltage is applied across the electrodes, electrons are injected into the emissive layer. The electrons drift to the interface with the transporting layer where the recombination with holes found there causes radiative emission. Since OLED devices directly generate light, there is no need for a backlight as in LCD displays, and creating true black is easily achieved by switching off the emitting pixel. OLED displays are therefore thinner and more energy efficient than LCD displays. OLEDs can be patterned into pixel-sized devices (much smaller than LED devices) or printed into large sheets for solid-state lighting (Figure 1.4).[34] Historically, blue OLEDs have trailed behind red and green emitting devices in terms of efficiency and life-times, but recent research is closing this gap.[35]

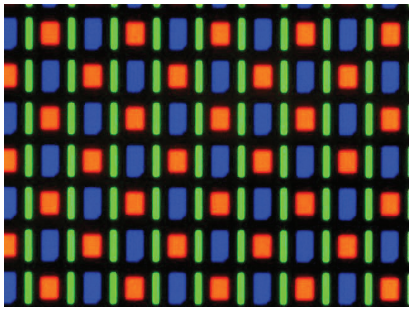

Fig. 1.4.: A 200x magnification of Google's Nexus One AMOLED screen shows the RGB arrangement of OLED pixels. Photograph by Matthew Rollings, distributed under a CC-BY 3.0 license.

1.4.2 Solar Cells

Organic photovoltaics (OPVs), though still tailing silicon-based solar panels in terms of efficiency, can be printed into lightweight, flexible, and transparent solar cells. These qualities are important mechanistic and aesthetic features when incorporating solar windows into urban architecture.[36] The solution-processability of materials for roll-to-roll printing is especially important for OPVs due to the large-scale nature of this application.

OPVs produce electricity through the photoelectric effect illustrated in Figure 1.5 for a simple p-n junction. A p-n junction describes the interface between a p-type (donor) and n-type (acceptor) semiconductor. Incident light excites an electron into the conductance band of the donor or acceptor material, leaving a hole behind, thus creating an "electron-hole pair" or "exciton." This exciton must diffuse to the p-n junction where the charges can be separated: the hole into the p-type donor material and the electron into the n-type acceptor material. The charges are then channeled to their respective electrodes and produce an electric current.

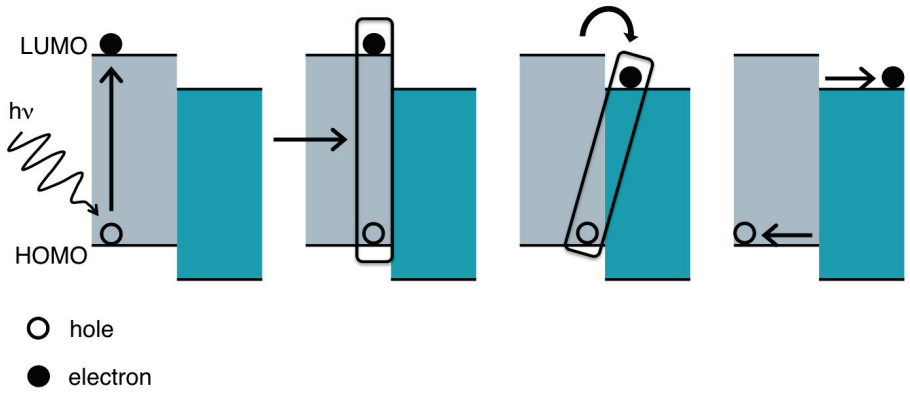

Fig. 1.5.: Once an exciton is generated (left) it must diffuse to the p-n junction before undergoing charge separation (right).

Efficient solar cells are constructed with a few key factors in mind.

- First, the active layer should have a broad absorbance spectrum that captures a majority of the sun's energy. This means a semiconductor with a small band gap (≈ 1.5 eV). The band gap cannot be too small, however, to account for energy loss from exciton thermalization and the HOMO-LUMO offset of the cell.[37]
- The lifetime of an exciton is on the order of nanoseconds and its diffusion length only approximately 10 nm, necessitating small, regularly spaced domains of donor and acceptor phases to minimize exciton recombination.
- Once at the p-n junction the driving force for charge separation (the electro potential drop from the LUMO of the donor to the LUMO of the acceptor) needs to be greater than the exciton binding energy to drive exciton dissociation.

- The charge mobilities of the donor and acceptor materials should be reasonably high ($> 10^{-4}$ cm^2/Vs). They should also be balanced to avoid a build-up of electrons or holes, which leads to accelerated charge recombination.

Controlling the morphology of the donor and acceptor domains is an integral part of fabricating efficient devices. The most common practice is to dissolve the two materials in a common solvent and to create a blended active layer called a bulk-heterojunction (Figure 1.6). Annealing and adding solvent additives can alter how each material crystallizes and thus affect the resulting domain sizes.

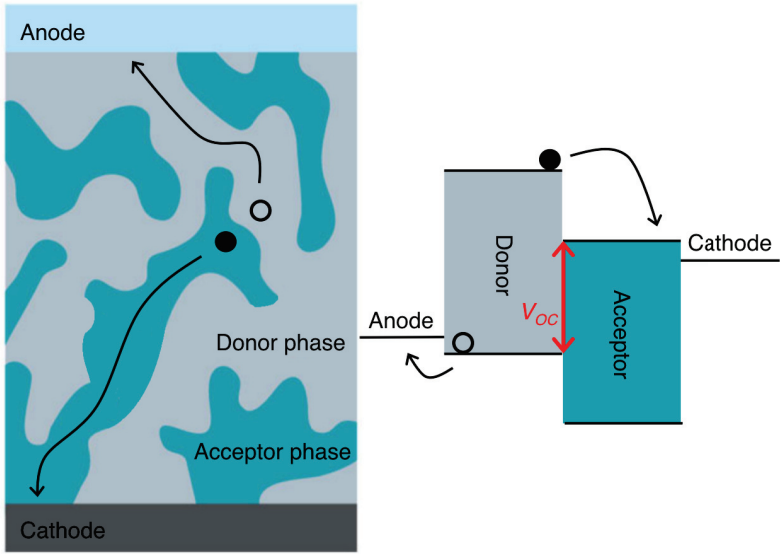

Fig. 1.6.: On the left is a simplified depiction of a bulk heterojunction showing the blended donor and acceptor domains. On the right is shown the V_{OC} as it relates to the HOMO of the donor and the LUMO of the acceptor, i.e. the band gap of the cell.

The power efficiency of a solar cell is defined by three parameters: the short-circuit current (I_{SC}), the open-circuit voltage (V_{OC}), and the fill-factor (FF). These parameters are calculated from the current-voltage relationship of the device plotted in an I-V curve (Figure 1.7). The short-circuit current is the largest current which may be drawn from the solar cell and occurs when the bias across the cell is zero. While in the open-circuit state, charge carriers generated under illumination accumulate at the anode and cathode. When this growing potential difference cancels out the built-in potential the current is zero and the measured open-circuit voltage is the maximum voltage the solar cell can provide to an external circuit.[38] In OPVs the upper limit of the V_{OC} is equal to the band gap of the cell, or

$|LUMO_{Acceptor} - HOMO_{Donor}|$ (Figure 1.6), but empirically loss is always observed due to the recombination of charges.[39]

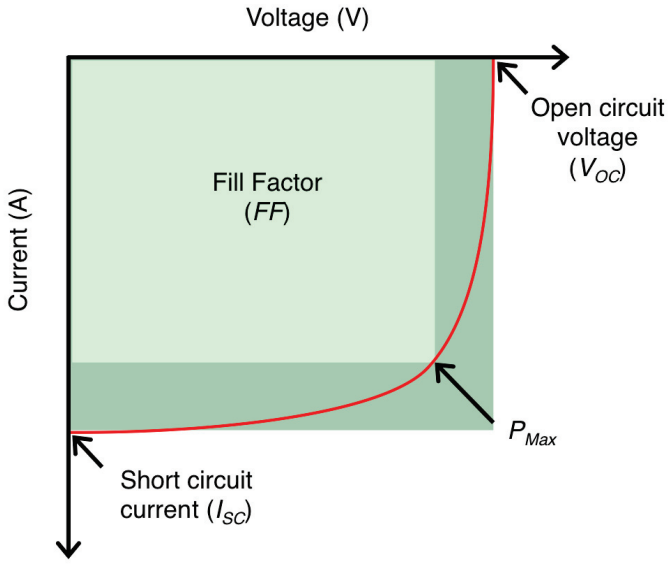

Fig. 1.7.: A characteristic IV curve for an irradiated solar cell showing the V_{OC}, the I_{SC}, and P_{Max}. The FF is the ratio between the two shaded areas.

Power is the product of the current and voltage ($P = I \times V$), with the maximum power of the cell (P_{Max}) representing the point of peak efficiency. The fill factor, FF, is the ratio of the area bound by the I_{SC} and V_{OC} to the area bound by the current and voltage at P_{Max} as seen in equation 1.2 and Figure 1.7. Fill factor is often described as the "squareness" of the IV curve with an ideal value of 1.

$$FF = \frac{I_{Max} V_{Max}}{I_{SC} V_{OC}} \tag{1.2}$$

The overall power efficiency of the cell is then defined as:

$$PCE = \frac{P_{Max}}{P_{In}} = \frac{FF(I_{SC} V_{OC})}{P_{In}} \tag{1.3}$$

How do these parameters relate to the design of organic semiconductors? Lowering the band gap of the donor material means more light is harvested, which has a direct beneficial impact on the I_{SC}. Unfortunately, if shrinking the band gap increases the HOMO level of the donor material, this will limit the V_{OC}, therefore simultaneously lowering the band gap and

the HOMO level of the material is extremely desirable. Chen et al. observed that for each 0.1 eV drop in the HOMO level of differently substituted poly(benzodithiophene-thieno[3,4-*b*]thiophene), they increased the V_{OC} by 0.07 volts.[40]

The I_{SC} and the V_{OC} are both limited by charge recombination as well. Exciton dissociation and charge recombination both occur at the donor-acceptor interface. It is therefore important to augment charge mobility with smooth, ordered films while maintaining adequate domain sizes for exciton dissociation. Efficient charge extraction at the electrodes will also help reduce recombination loss.

Polymers have been extensively tested as donor materials for BHJ solar cells, and a key property that influences the morphology of the films is molecular weight.[41] Larger molecular weight polymers show a propensity to form nanofibrillar morphologies and exhibit higher charge mobilities. For example, batches of poly(dioctylfluorene-dithienylbenzothiadiazole) displayed higher I_{SC}s with increasing MWs, though the V_{OC}s stayed constant.[42] Too large a MW, however, may decrease the mobility due to entanglement, which hinders intrachain transport.[43]

To ensure the solution-processability of high MW conjugated polymers, solubilizing side chains are required, which will affect film morphology as well. The position, length, and bulkiness of alkyl side chains affects the π–π interactions between polymer chains. Increased π–π interactions lead to higher mobilities and I_{SC}s, but may have a detrimental effect on the film blends.[44] More examples of side chain engineering is discussed in Section 1.5.4.

1.4.3 Field-effect transistors

A field-effect transistor is an electronic switch that uses an electric field to control the conductivity of a semiconductor. In this thesis, OFETs were used to test the electrical properties of novel polymers and small molecules. OFETs consist of an active semiconductor layer, an insulating layer, and three contacts: the source, the drain, and the gate (Figure 1.8). The substrate for the device typically doubles as the gate electrode, as is the case with silicon wafers. Above the gate is an insulating layer, called the gate dielectric layer, typically SiO_2. When an electric field is applied to the gate charges accumulate in the dielectric

layer. This causes an accumulation of complementary charges in the semiconductor at the semiconductor-dielectric interface. Once turned "on" by the electric field, the semiconductor becomes conductive and charges can migrate along the narrow transistor channel. Since charge migration occurs only at the semiconductor-dielectric interface, any defects can easily limit charge mobilities. "Smoothing" the dielectric layer, with polystyrene for example, has been shown to greatly improve mobilities.[45]

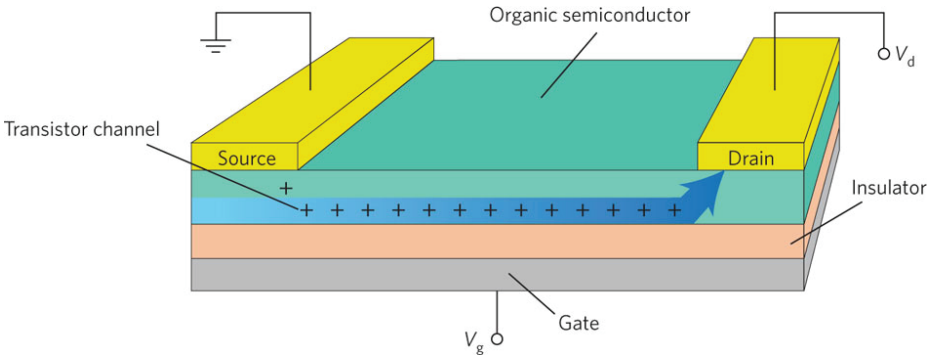

Fig. 1.8.: Schematic diagram of a bottom-gate, top-contact OFET showing the gate-induced charge transport channel. Reprinted by permission from Macmillan Publishers Ltd: Nature Materials [46], copyright 2010.

In the case of poorly soluble small molecules, films are deposited using vacuum vapor deposition, but for polymers or soluble small molecules, solution-processing techniques, such as spin-coating, are used. A single crystal can also be used as the active layer, enabling the measurement of mobilities specific to that packing architecture. The physical morphology of the OSC plays an important part in device performance, so the method used to deposit the material can vastly affect charge mobility. This is starkly evident in the case of pentacene thin films, which are practically insulating ($\mu_h \approx 10^{-9}$ cm^2/Vs) as amorphous films deposited at low temperatures, but display high mobilities in ordered films deposited at room temperature ($\mu_h \approx 1$ cm^2/Vs).[47]

The charge mobility of an OFET is determined by recording the drain-source current (I_{DS}) as a function of drain-source bias (V_{DS}) at different gate voltages (V_G). When a small drain-source voltage V_{DS} is applied (smaller than the gate voltage minus the threshold voltage, $<(V_G\text{-}V_T)$) the device operates in the linear regime. As drain-source voltage increases and surpasses ($V_G\text{-}V_T$) the device operates in a saturation regime (Figure 1.9). Charge mobilities

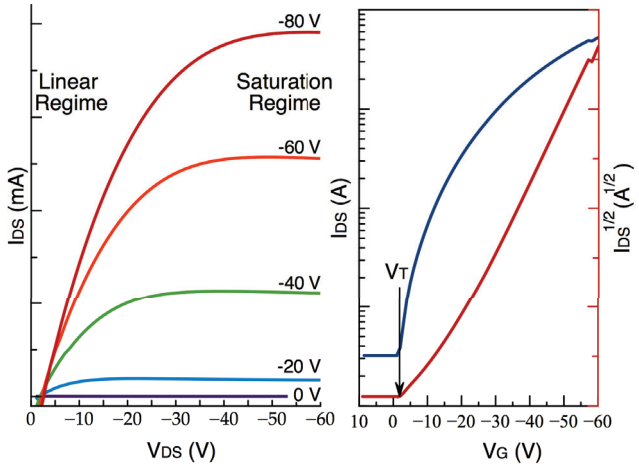

Fig. 1.9.: Typical electrical characteristics of a p-channel OFET device: (left) output curve and (right) transfer curve.

can be calculated from either regime. In the saturation regime, drain current is independent of drain-source voltage, but rather varies as the square of the gate voltage as seen in equation 1.4.

$$I_{DS} = -\frac{W}{2L} C_i \mu (V_G - V_T)^2 \tag{1.4}$$

Where W and L are the channel width and length and C_i is the capacitance of the dielectric. The threshold voltage, V_T, is the minimum gate voltage that is needed to generate the transistor channel. Rewriting this equation, it is clear that the field-effect carrier mobility, μ, can be determined from the slope of the curve plotting the square root of the saturation current as a function of gate voltage according to equation 1.5.

$$\mu = \frac{2L}{W} \frac{1}{C_i} \left(\frac{\delta \sqrt{I_{DS}}}{\delta V_G} \right)^2 \tag{1.5}$$

It must be pointed out, however, that these equations are approximations. Equation 1.5 assumes that the mobility is independent of the gate voltage, which is not the case for several reasons. For example, at low gate voltages charges will be trapped by localized traps, limiting mobility.[48][49] The charge mobility in equation 1.5 is also not corrected for contact resistance at the metal/organic interface, which is a common issues in OFETs.

Contact resistance can occur due to an energy level mismatch between the electrode metal and the OSC or disorder in the OSC film at the interface.

1.5 Molecular Design Strategies

The most attractive aspect of OSCs from a chemist's point of view is the opportunity to rationally design and synthesize a desired material. By altering the molecular structure of a material and testing its electronic properties, structure-property relationships can be defined and the factors affecting charge transport in OSCs illuminated. Charge transport in OSCs is highly dependent on the solid-phase morphology of the material and not solely on the molecule's electronic properties and since structure-property relationships encompass both the individual molecules' characteristics and the characteristics of the bulk material, it can be very difficult to ascertain if a modification is responsible for an observed property. In this thesis we try to divorce molecular structure from morphological aspects and study both separately, so as to better delineate structure-property relationships in OSCs.

Depending on its final application, an OSC can be designed to have vastly different properties. Will it be used for p-type or n-type transport? Does it need to be highly soluble? Should it form amorphous films or be highly crystalline? Is broad absorption important or is strong emission at a specific wavelength required? The molecular design of an OSC will naturally reflect these sought-after properties, though the toolbox of design strategies available to realize them remains the same.

The first requirement for an OSC is a finite band gap. Since the 1980s, many strategies for controlling the band gap have been established. In an OSC the energy bands are made of overlapping π–orbitals, so that manipulating these energy levels is all about maintaining conjugation and expanding electron delocalization. There are four main factors (depicted in Figure 1.10) that influence band gap: 1) planarity, 2) bond-length alternation, 3) aromaticity, and 4) the electronic effect of substituents. A single design choice can easily affect all of these factors, so it is easier to consider specific strategies and discuss the affects on these factors as they apply.

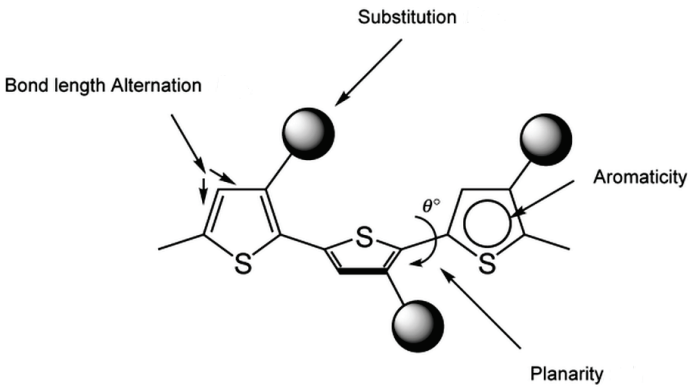

Fig. 1.10.: Factors that influence band gap labeled on polythiophene. Reprinted with permission from [50]. Copyright 2007 John Wiley & Sons, Inc.

1.5.1 Extending Conjugation with Spacer Groups

The most basic and prevalent unit in conjugated molecules is the benzene ring. The benzene ring contains 6 electrons in delocalized π–orbitals, but its ring structure gives it more resonance stabilization than linear hexatriene. Benzene is a very small conjugated system, so its HOMO-LUMO gap is large (ca. 5.5 eV).

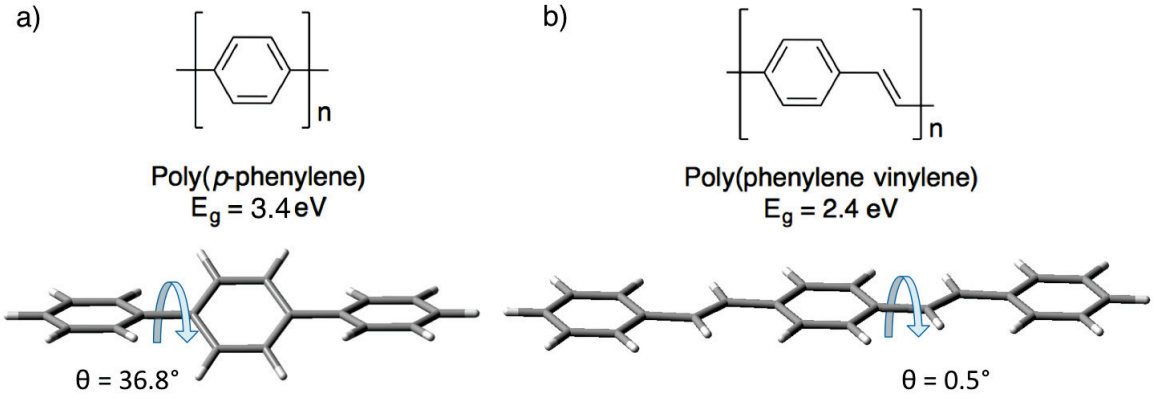

Fig. 1.11.: Simple polyphenylene has a twisted backbone (left) leading to a large band gap, which can be lowered by introducing a vinylene spacer, such as in poly(phenylene vinylene) (right). DFT calculations of the dihedral angles performed using B3LYP, 6-31G(d).

To shrink the band gap, there are two ways of expanding the conjugation. The first is to connect multiple benzene rings together with C–C single bonds, forming an oligomer or polymer. This method preserves the aromatic stability of each ring, but planarity is lost due

to steric hindrance between the benzene rings. The short distance between benzene rings will not accommodate the C–H bonds on each ring, requiring the backbone of the polymer to twist (Figure 1.11a). When larger substituents need to be added, steric hindrances can cause serious torsional twists, interrupting the orbital overlaps between rings. A simple solution to planarize the polymer is to introduce a spacer group between each ring. The spacer group must also be conjugated and, in effect, it will "dilute" the aromaticity of the benzene rings. This promotes delocalization of electrons along the entire polymer, not just within nodes of the aromatic rings. Examples of such conjugated spacers are vinylene, seen in Figure 1.11b, and ethynylene. The ethynylene spacer has no hydrogen atoms to contribute to sterics and therefore produces rod-like, planar polymers.[51] The disadvantage comes in the form of increased bond length alternation, caused by the large difference in lengths between the C–C single bond and the much shorter C≡C triple bond.

Bond length alternation (BLA) is defined as the average of the differences in length of adjacent carbon-carbon bonds. Conjugated molecules can be thought to contain two competing resonance structures: the aromatic and the quinoidal (Figure 1.12), both containing alternating single and double (or triple) bonds. In a structure with a non-degenerate ground state, like polyphenylene or polythiophene, where the aromatic form is preferred, the BLA is proportional to the band gap and decreases with increasing quinoidal character.[52] Even polyacetylene, a polymer with a degenerate ground state, has a BLA of 0.08 Å as a consequence of Peierls' distortion. In a 1-D crystal lattice a net energy gain is brought about by distorting the periodicity of the lattice into "dimers," or if the 1-D lattice is a carbon chain, into double and single bonds.[53][54]

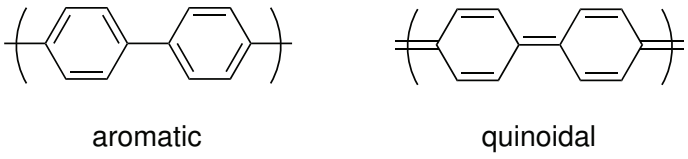

Fig. 1.12.: Shown are the aromatic resonance structure (left) and quinoidal resonance structure (right) of polyphenylene.

An early approach to minimize BLA is to design a monomer unit which contains an aromatic cycle when the polymer backbone is in its quinoidal form. This counter–balances the aromaticity of the polymer core and favors delocalization, lowering the band gap and

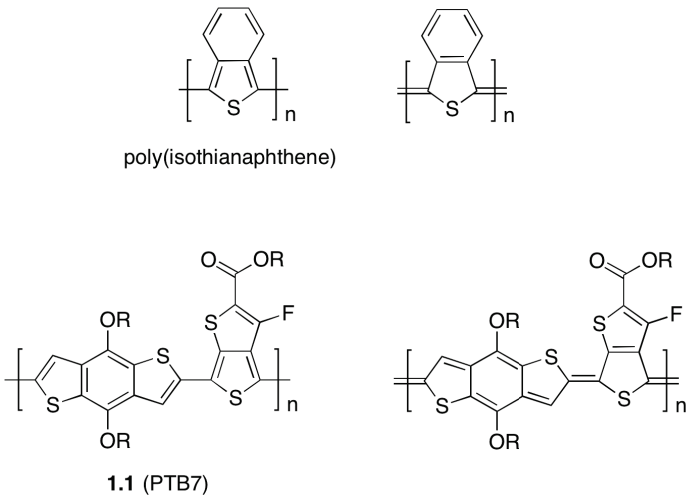

Fig. 1.13.: Isothianaphthene and thieno[3,4-*b*]thiophene both contain a fused aromatic ring when the polymer is in quinoidal form.

BLA. This approach was pioneered by Wudl in the synthesis of poly(isothianaphthene) which exhibits a very low band gap of 1.0 eV (Figure 1.13).[55] A more recent example can be seen in polymer **1.1** (also known as PTB7), well known for achieving 9% efficiencies in OPVs.[56] In the thieno[3,4-*b*]thiophene unit the fused thiophene ring is in its aromatic form when the backbone thiophene ring is is its quinoidal form and vice versa (Figure 1.13).[57]

Besides acting as a measure for electron delocalization through the balance of aromatic and quinoidal character, BLA is extremely important as it relates to the polarizability of the molecule. Polarizability is the measure of electron cloud displacement (or induced dipole moment) in the presence of an electric field and it is inversely proportional to the polaron binding energy. As was described in Section 1.3, the polaron binding energy is one to the key parameters affecting the rate of charge transfer in organic semiconductors. The relationship between BLA and polarizability was experimentally proven by testing a series of donor–acceptor polyenes with end groups of increasing acceptor strength, yielding a range of BLAs from 0.11 Å for decatetraene to $\approx$ 0 Å for cyanine. The results indicated that molecular polarizability (α) is maximized as BLA approaches zero.[58][59][60]

One method to planarize aromatic rings and reduce BLA is to use a spacer group that impedes torsional twisting. The most successful example of this is fluorene, which is

essentially two benzene rings fused by a C–C single bond and an sp^2 carbon. Fusing the rings ensures better π–orbital interactions, but also shortens the C–C linking bond and elongates the C–C bonds within the five-membered rings, thus reducing the BLA (Figure 1.14). Polyfluorenes, therefore, are extremely popular organic semiconductors, exhibiting good stability, interesting liquid-crystalline properties, as well as being excellent blue-light emitters.[61] In many other π conjugated systems, such as polythiophenes, the rigidification of molecules has proved to be a useful approach towards low-band gap materials.[62][63]

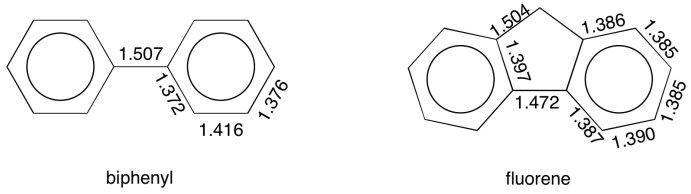

Fig. 1.14.: The fused spacer group in fluorene lowers BLA as compared to biphenyl. Averaged bond lengths (Å) from [64] for biphenyl and from [65] for fluorene.

1.5.2 Fusing rings: Polycyclic Arenes

A different approach towards molecular rigidification, which does not require a spacer group, is fusing aromatic rings together. Multiple fused rings will share π–orbitals so that electrons are delocalized throughout the molecule, lowering the band gap of the molecule and raising the HOMO levels. In acenes, however, extending the conjugation linearly leads to increased biradical or "open-shell" character, making it vulnerable to oxidation (Figure 1.15). Hexacene is the longest acene which is stable under ambient conditions.[66] Higher order acenes form biradicaloids that are prone to intermolecular dimerization and oxidation.[67]

Nonlinear polycyclic aromatic hydrocarbons (PAHs) exhibit higher band gaps and lower HOMO levels than their linear counterparts. Phenanthrene, for example, with a HOMO of -5.7 eV and a band gap of 4.7 eV, has energy levels closer to naphthalene than its linear analogue anthracene. This increased stability is explained by Clar's rule: the more aromatic sextets present in a molecule, the more stable that molecule will be. This is also

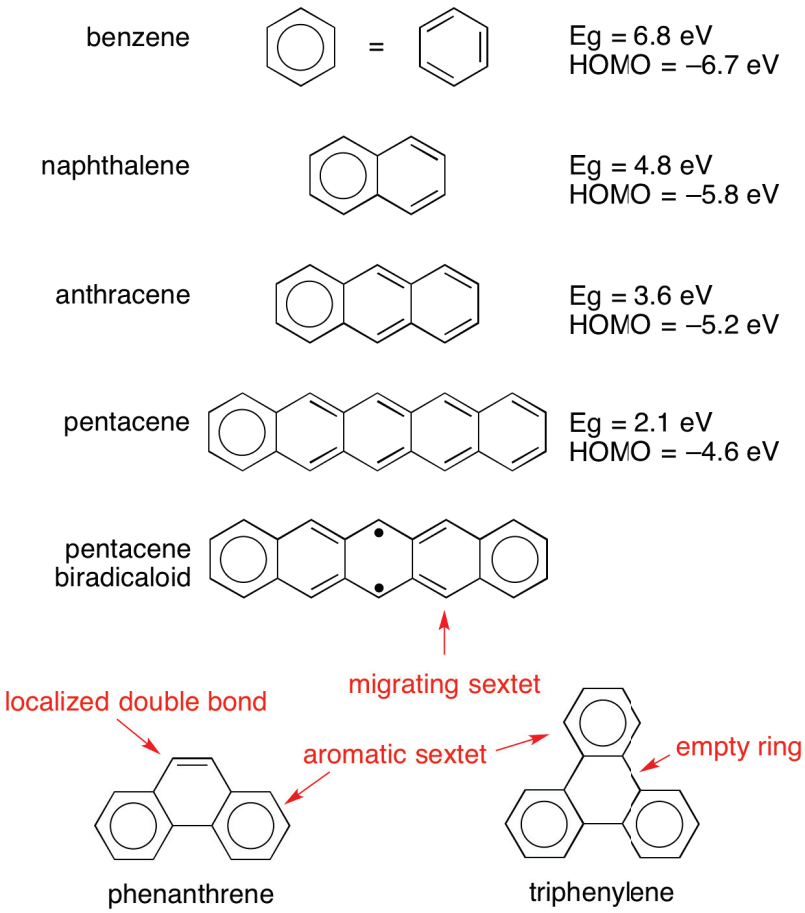

Fig. 1.15.: A drop in band gap and a raising of HOMO levels can be observed with the expansion of linear acenes. Below are non-linear PAHs illustrating Clar's classification of 6-membered rings.

the rationalization behind the formation of open-shell species. Clar's Rule classifies 6-membered rings into four types: aromatic sextets, migrating sextets, empty rings, and rings with localized double bonds (Figure 1.15). Fusing linear acenes can yield molecules with two aromatic sextets, such as bistetracene. Bistetracene (two tetracenes fused at the 1,2,12 positions and substituted with triisopropylsilyl acetylene groups) contains 8 fused rings, but its HOMO level is only -5.1 eV, allowing for air-stable FET devices and high mobilities ($\mu_h = 6.1\ cm^2/Vs$).[68] Picene, the "zigzag" analogue of pentacene, contains three aromatic sextets and shows better environmental stability in p-channel FETs than pentacene.[69] Thermally deposited thin films of alkylated-picene have, like pentacene, shown extremely high mobilities (up to $\mu_h = 20\ cm^2/Vs$), but are stable under atmospheric conditions.[70]

Extending the conjugation does more than affect energy levels: it also lowers the BLA (as discussed previously) and lowers the reorganization energy. As was discussed in Section 1.3 when a neutral molecule becomes charged it undergoes geometry modifications at an energy cost called the reorganization energy, an important factor in charge transport. Figure 1.16 shows how reorganization energy decreases as the number of rings increase in a series of molecules with different fused geometries. Reorganization energy is also affected by heteroatoms, which are discussed next.

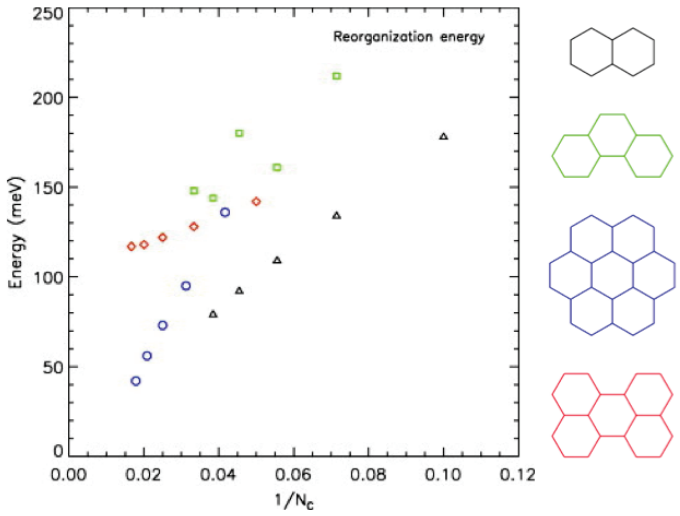

Fig. 1.16.: Molecular reorganization energies computed for (oligo)acenes (black triangles), phenacenes (green squares), circum(oligo)acenes (blue circles), and (oligo)perylenes (red diamonds), as a function of the inverse of the total number of carbon atoms N_C. Reprinted from [71] Copyright 2014 with permission from Elsevier.

1.5.3 Heteroatoms

Another design strategy in organic electronics is the use of heteroaromatics. Inserting heteroatoms into a polycyclic system will have a large impact on the structure and the electronic properties of the molecule or polymer. The work presented in this thesis focuses on two heteroatoms: sulfur and nitrogen. Sulfur and nitrogen both have lone electron pairs which can contribute to the aromaticity of a cycle, thus making aromatic five-membered rings possible (Figure 1.17). These five-membered rings, thiophene and pyrrole, are smaller and exhibit less torsional twisting in polymers than polyphenylenes. Thiophene and pyrrole are less aromatic than benzene (according to thermodynamic stabilization), and thus polythiophenes (PT) and polypyrroles (PPy) have stabler quinoidal forms, leading to more delocalized electrons and smaller band gaps than poly(*p*-phenylene) (PPP) (theoretical E_g PT = 2.0 eV, PPy = 2.9 eV, PPP = 3.8 eV).[72]

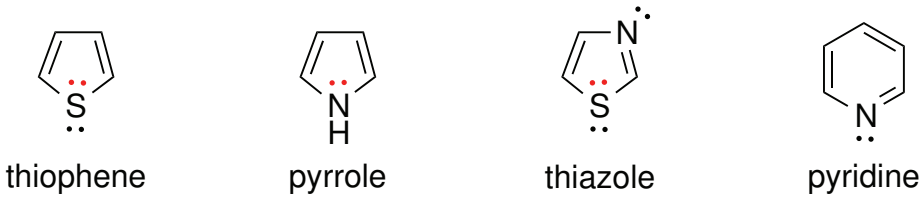

Fig. 1.17.: Pictured are several heteroaromatic structures. Electrons participating in the aromaticity are labeled in red.

Though polypyrroles were among the first conductive organic materials studied[73][74], it is polythiophene and thiophene-containing molecules that predominate in the field of organic electronics. Thiophenes present many advantages,[1] not the least of which is their well established and versatile chemistry. Derivatives of thiophene can be synthesized by selective substitution via lithiation chemistry. Thiophene monomers are easily oxidized, either electrochemically or chemically, to form radical cations which polymerize. If thiophene is substituted unsymmetrically, this method produces to a regiorandom polymer. Brominated thiophenes can be polymerized through transition metal-catalyzed cross-coupling reactions to give regioregular homopolymers or to make copolymers. Thiophenes are electron rich and oxidatively stable, making them good for p-type transport, and they self-assemble with close π–π stacks. Furthermore the increased polarizability of the sulfur atom compared to

carbon helps lower reorganization energies and can lead to intermolecular sulfur-sulfur interactions. These interactions are described in more detail in Section 1.6.

Nitrogen heteroatoms can be incorporated into OSCs in 5- or 6-membered rings. In 5-membered pyrroles, the lone pair on nitrogen contributes to the aromaticity of the ring making the heterocycle electron rich. Conversely, in 6-membered pyridine, the lone pair is perpendicular to the π–orbitals of the ring and therefore does not contribute to the aromaticity, but rather enhances basicity. In this case the electronegativity of the nitrogen atom makes the ring electron-poor and lowers the HOMO/LUMO levels of the molecule. As a result OSCs containing nitrogen have been shown to be p-type, ambipolar, or n-type. (See examples in Figure 1.31 in Section 1.7)

Thiazoles are five-membered rings containing both sulfur and nitrogen heteroatoms (Figure 1.17). They belong to the azole family of molecules, along with oxazoles and imidazoles. Thiazole is slightly less aromatic than thiophene[75][76], with sulfur's lone pair contributing to the aromaticity of the ring, while the nitrogen atom is electron-withdrawing. This makes thiazole an electron-accepting heterocycle in OSCs. (See examples in Figure 1.30 in Section 1.7)

1.5.4 Substituents

Introducing substituents is a convenient way to tune the properties of a molecule or polymer since they provide an enormous potential for structural and electronic variation (Figure 1.18). They are also necessary for solution-processable materials. Substituents can affect the energy levels of a material, as well as impact planarity, and reorganization energy.

Long alkyl chains are commonly used to impart solubility to a polymer or large polycyclic molecule. The nature of that chain, linear or branched, and its location, will have an impact on the solid-state packing of the material.[44] In polymers, a large part of the reorganization energy comes from the rotation of the inter-ring dihedral angles between the neutral and charged species. This rotational energy is greatly impacted by the size and type of substituent present on the polymer backbone. Using substituents that form non-covalent interactions that "lock" the conformation of the polymer backbone is advantageous for this

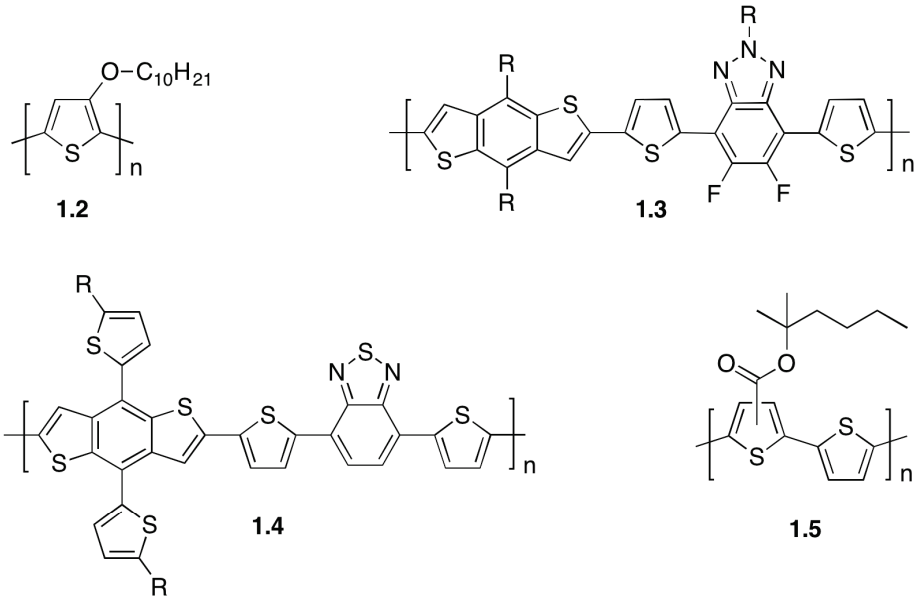

Fig. 1.18.: A selection polymers illustrating different substituents.

reason. One recent example is the use of alkoxy or fluorine substituents on benzotriazole in a benzotriazole-thiophene copolymer (Figure 1.19). The authors attribute tight interchain ordering and improved carrier mobilities on the non-covalent interactions between thiophene's sulfur and the substituents.[77] A computational study on through-space interactions performed by Jackson et al., however, warns that while S-S, O-S, N-S, and F-S interactions all have some stabilizing influence, their non-covalent binding energies are too low to provide conformational control in polymers. Only hydrogen-bonding interactions, such as CH-N and CH-O, have high enough binding energies (≈2 kcal/mol) to act as "locking" mechanisms.[78]

Electron-donating or electron-withdrawing substituents are often used to fine-tune the HOMO and LUMO energy levels of a material. Replacing the hexyl chain in P3HT with an alkoxy chain (see polymer **1.2**) results in a 0.3 eV increase in the HOMO level, shrinking the band gap of the polymer (1.6 eV compared to 1.9 eV for P3HT).[79] Fluorine is a popular electron-withdrawing substituent because its van der Waals radius is not much larger than hydrogen's (135 pm vs. 120 pm) and therefore won't significantly increase torsional twisting when placed on a monomer unit, such as on benzotriazole in polymer **1.3**.[80]

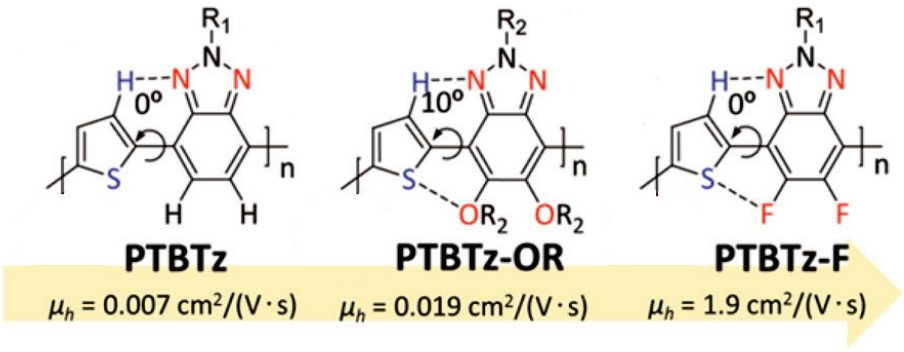

Fig. 1.19.: Varying the benzotriazole substituents in these copolymers did not affect the band gap, but led to tighter interchain ordering and higher mobilities. Reprinted with permission from [77]. Copyright 2014 American Chemical Society.

Aromatic substituents can also be used to extend the conjugation pathway orthogonal to the core of the molecule or polymer. Polymer **1.4** is an example of this strategy. Huo et al. found that when alkylthienyl substituents were used in place of alkoxy groups on benzodithiophene, the resulting material had a smaller band gap, higher hole mobilities, and performed better in BHJ-solar cells.[81] Though sometimes improperly called "2D" polymers, polymers with aromatic substituents exhibit high molecular ordering with strong π–π stacking.[82]

Finally, a substituent can be designed to be removable[83], as in polymer **1.5**. A thermally cleavable ester substituent was used by Fréchet and then Krebs as a sacrificial solubilizing group.[84][85] Once the material has been solution-processed, the ester functionality can be removed to give insoluble, but planar, poly(thiophene).

1.5.5 Donor-Acceptor Strategy

One more design strategy for manipulating the band gap of a material is the donor-acceptor strategy, which calls for combining electron-deficient units with electron-rich units. When these units are in conjugation their orbital splitting results in a narrower band gap with lower HOMO/LUMO levels (Figure 1.20a). This strategy is widely used in polymers for OPVs where broad absorption is desired, but raising the HOMO would be detrimental to the V_{OC}. Using D-A units, the band gap of a material can be fine-tuned, either by altering a

unit or by altering its ratio relative to other units. The "push-pull system" in D-A polymers has other benefits as well. As was introduced in Section 1.5.1, BLA can be decreased and polarizability increased by increasing the strength of the donor and acceptor moieties. This has been extensively studied in polyenes [86], as well as other conjugated systems.[87][88] As a result of their high polarizability, materials with D-A structures can exhibit nonlinear optical properties, such as two photon absorption.[89][90]

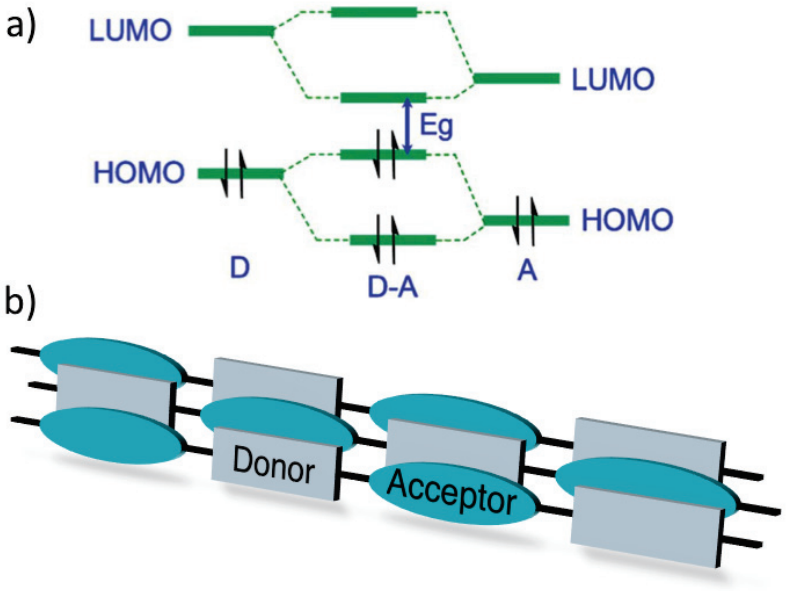

Fig. 1.20.: a) The orbital splitting of donor and acceptor units results in a smaller band gap without raising HOMO levels. Reproduced from [91] with permission of The Royal Society of Chemistry. b) Tight interchain packing in D-A polymers is favored by alternating donor-acceptor π–stacks.

Electron-rich and electron-deficient aromatics are well known to assemble in a face-to-face manner.[92][93] The "push-pull" behavior of D-A units promotes intramolecular charge transfer between units, leading to intramolecular dipoles. Thus dipole-dipole interactions between polymer chains are expected to lead to smaller interchain distances and therefore better charge transport between chains (Figure 1.20b). Indeed, short π–π distances are frequently observed in X-ray diffraction experiments of D-A polymer films.[94][95] D-A polymer PTB7, shown in Figure 1.18, has been used in OPVs with PCEs exceeding 9%. Yet when Yu's group attempted to make a similar polymer with a D-A-A structure, their highest PCE was only 2%. By using two acceptor units, they lowered the local dipole

moment causing charges to remain trapped in the A-A unit, and as a result observed faster recombination rates and lower I_{SC}s.[96]

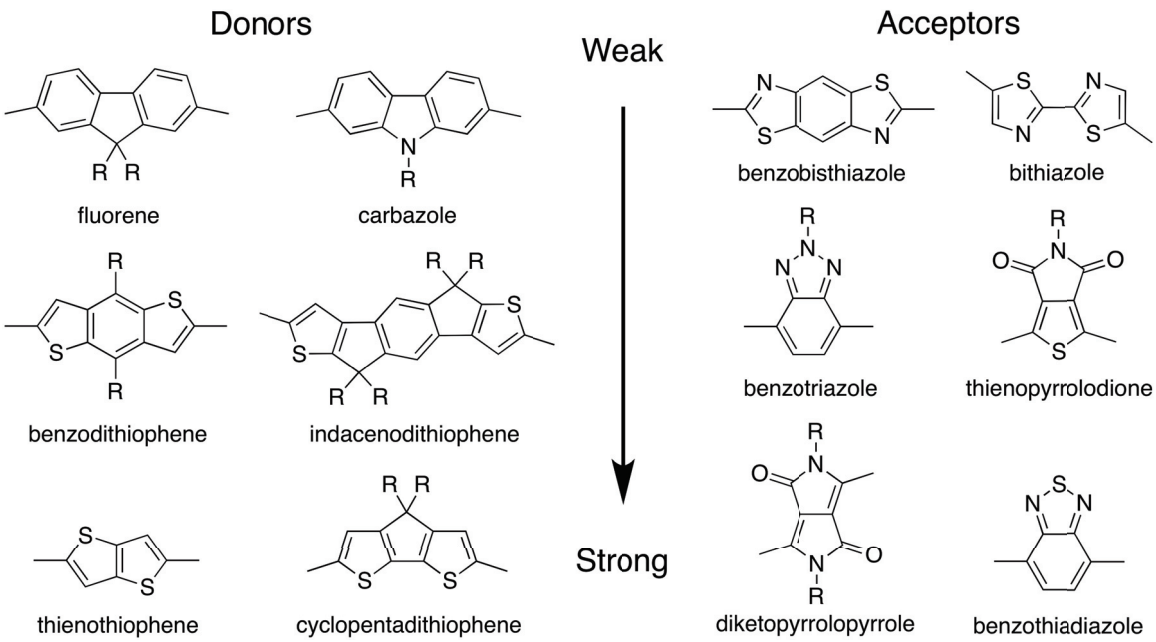

Fig. 1.21.: A selection of electron-donating and electron-accepting monomers that have been used in D–A copolymers.

Examples of oft-used donor and acceptor units are shown in Figure 1.21. Though these are usually found in polymers, the D-A strategy is applicable to oligomeric molecules, unimolecular rectifiers, or simply to the choice of substituents. Examples of D-A copolymers using different building blocks are shown in Figure 1.22. All have shown excellent properties in OPVs or OFETs. Bronstein et al. combined thieno[3,2-*b*]thiophene and diketopyrrolopyrrole, two particularly well studied units known for forming crystalline films with good mobilities, in polymer **1.6**. Though as-spun films of **1.6** showed no signs of crystallinity in X-ray diffraction or differential scanning calorimetry studies, their charge mobilities were among the highest for polymer FETs ($\mu_h = 1.95\ cm^2/Vs$). Polymer/$PC_{71}BM$ OPV devices gave a max PCE of 5.4%.[97] With polymer **1.7**, Chen et al. present a heptacyclic unit where the benzodithiophene core is covalently rigidified by two flanking thiophene units. This monomer was copolymerized with thienopyrrolodione. FET devices of **1.7** exhibited modest mobilities ($\mu_h = 6.8 \times 10^{-2}\ cm^2/Vs$), but OPV devices with $PC_{71}BM$ gave PCEs of 6.6%, a vast improvement compared to the un-rigidified analogue with a PCE

of 0.2%.[98] Osaka et al. also utilized a fused ring approach with their D-A polymer **1.8** which features naphthodithiophene and naphthobisthiadiazole. The first iteration of **1.8** had no solubilizing chains on the naphthodithiophene units (R′ = 2-decyltetradecyl, R" = H) and displayed an edge-on orientation with a π–stack distance of 3.43 Å. This polymer yielded high performing FET and polymer/PCBM OPV devices ($\mu_h = 0.5\ cm^2/Vs$, PCE = 5.2%). Adding linear dodecyl chains to naphthodithiophene changed the orientation of the polymer films to have face-on π–stacks with a distance of 3.51 Å. The improved solubility led to even higher PCEs of 8.0% while only lowering mobilities to $\mu_h = 0.1\ cm^2/Vs$.[15]

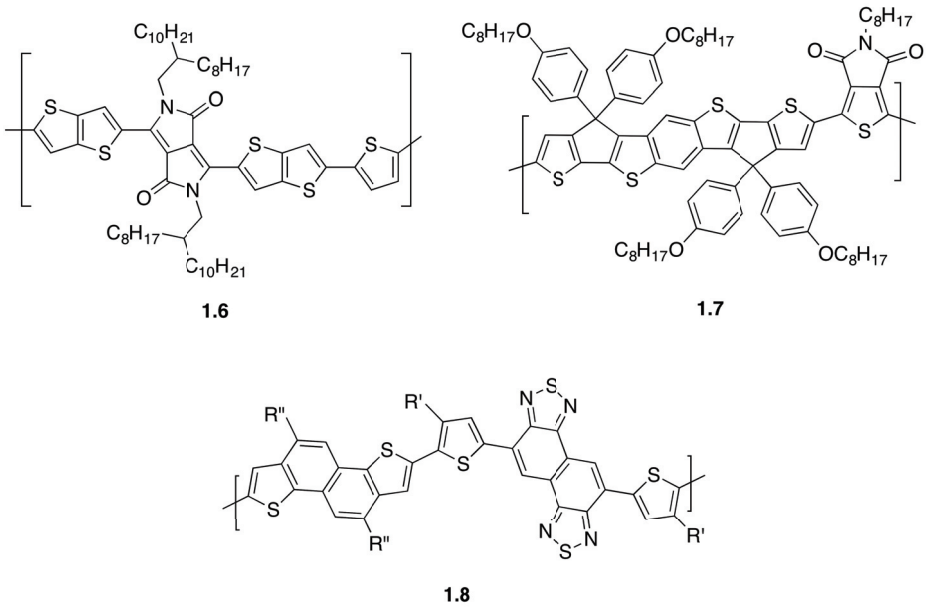

Fig. 1.22.: Shown are three examples of D–A copolymers with impressive properties in OFET or OPV devices.

1.6 Supramolecular Solid-State Assembly

Though design strategies can be used to tune the energy levels and reorganization energy of a material, the electronic coupling will be dictated by the solid-state assembly of that material. It is the sum of intermolecular π–orbital interactions in three-dimensions that will determine the efficacy of charge transport. Four main types of packing-motifs, shown in Figure 1.23 have been observed for most organic semiconductors. Close packing that favors strong π–π overlap is beneficial for charge transport, but strong anisotropy may yield poor

mobilities in the bulk material, where π–stacks many not align with the direction of current measurement.

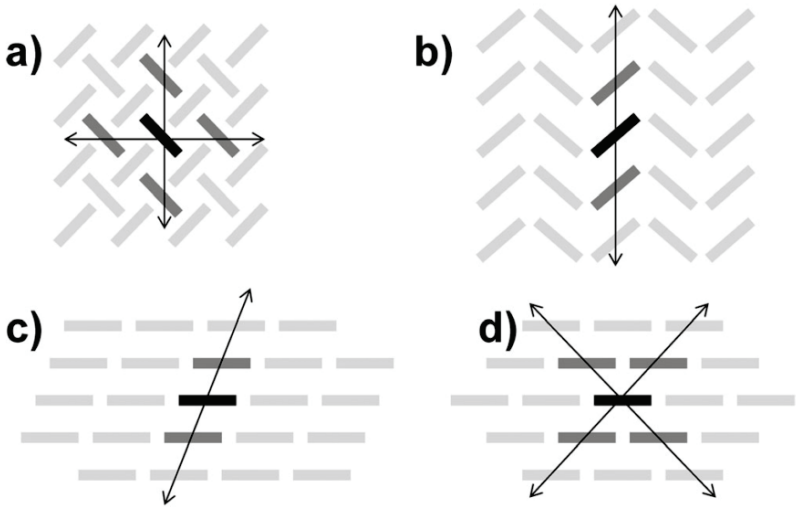

Fig. 1.23.: The four common packing motifs are a) herringbone, b) cofacial herringbone, c) 1-D lamellar "slipped stacks", and c) 2-D lamellar "brickwork" packing. Directions of preferred charge transfer are shown by arrows. Reprinted with permission from [21]. Copyright 2014 John Wiley & Sons, Inc.

It is important to remember that the conductance and valence bands are formed by molecular orbital interactions, so not only must the molecules be closely packed, but their frontier molecular orbitals should be aligned as well. Figure 1.24 maps the electron coupling (t) of two cofacial pentacene molecules with respect to long axis displacement. The molecular overlap is at its maximum when the molecules are perfectly aligned and decreases in an oscillatory pattern that correlates with the nodes of the HOMO orbitals. The electronic coupling (t) in a material can be calculated from the crystal structures. In symmetric systems, t can be approximated by the energy splitting of the frontier orbitals in a dimer (for example, $\Delta E = (HOMO - HOMO^{-1})/2$ for hole transport).[99] This approximation, called the energy-splitting-in-dimer approach (ESID), assumes both molecules in the dimer have the same site energies, which will not be the case if the molecules inhabit different environments in the crystal lattice. The ESID method is therefore not reliable for extended systems where polarization effects of the crystal environment on the site energies should

be taken into account.[100] A better calculation of t is the direct-coupling method, which calculates t from the wave function of each molecule according to equation 1.6

$$t = \frac{J - \frac{1}{2}(\epsilon_1 + \epsilon_2)S}{1 - S^2} \tag{1.6}$$

where J is the charge transfer integral, S is the orbital overlap, and ϵ_1 and ϵ_2 are the site energies of the molecules.

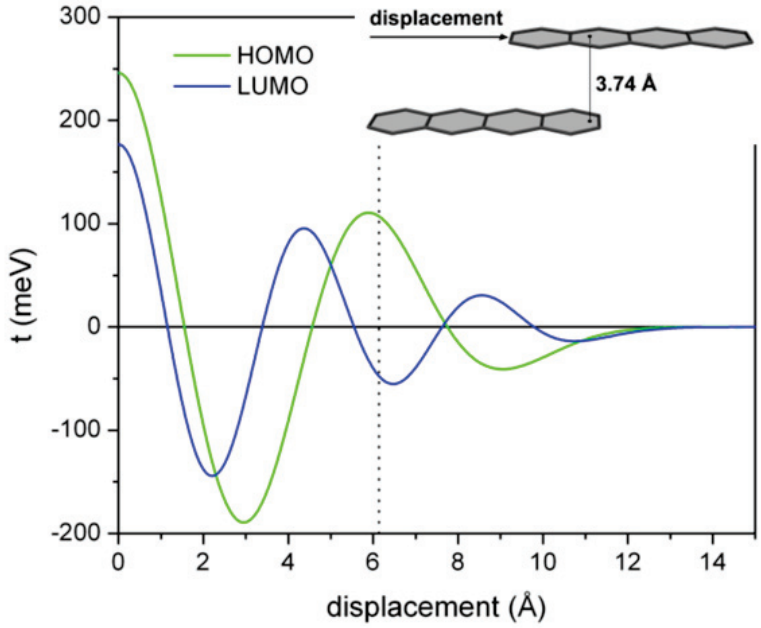

Fig. 1.24.: Evolution of the HOMO and LUMO intermolecular electronic coupling (t) as a function of displacement for two tetracene molecules with a π–stacking distance of 3.74 Å. The dotted line indicates the magnitude of long-axis displacement found in rubrene crystals. Reprinted with permission from [101]. Copyright 2005 John Wiley & Sons, Inc.

While predicting exact packing motifs is not yet possible, and the chance of polymorphism is likely, morphological changes can be induced through molecular design. A few recent reviews have addressed this subject as it applies to polymers and small molecules.[102][103] What follows are a few examples of design strategies based on non-covalent intermolecular interactions.

The solid-state packing of molecules is controlled by non-covalent effects, namely van der Waals and coulombic interactions. For example, in pentacene, electron density lies in

the π–orbitals above and below the plane of the molecule and slightly positively charged hydrogen atoms lie along the periphery of the pentacene backbone. The equal, but opposing dipoles normal to the plane of the molecule generate a quadrupole moment, represented as a partial positive charge density sandwiched between two partial negative charge densities (Figure 1.25a). Pentacene has many polymorphs[104], but all of them adopt a herringbone arrangement in order to maximize electrostatic interactions between its partially negative "face" and partially positive "edge." (Figure 1.25a). This face-to-edge packing still allows for high electronic coupling between the different molecular dimers, leading to high mobilities in pentacene films ($\mu_h \approx 1\ cm^2/Vs$)[105] and single crystals ($\mu_h \approx 40\ cm^2/Vs$).[106]

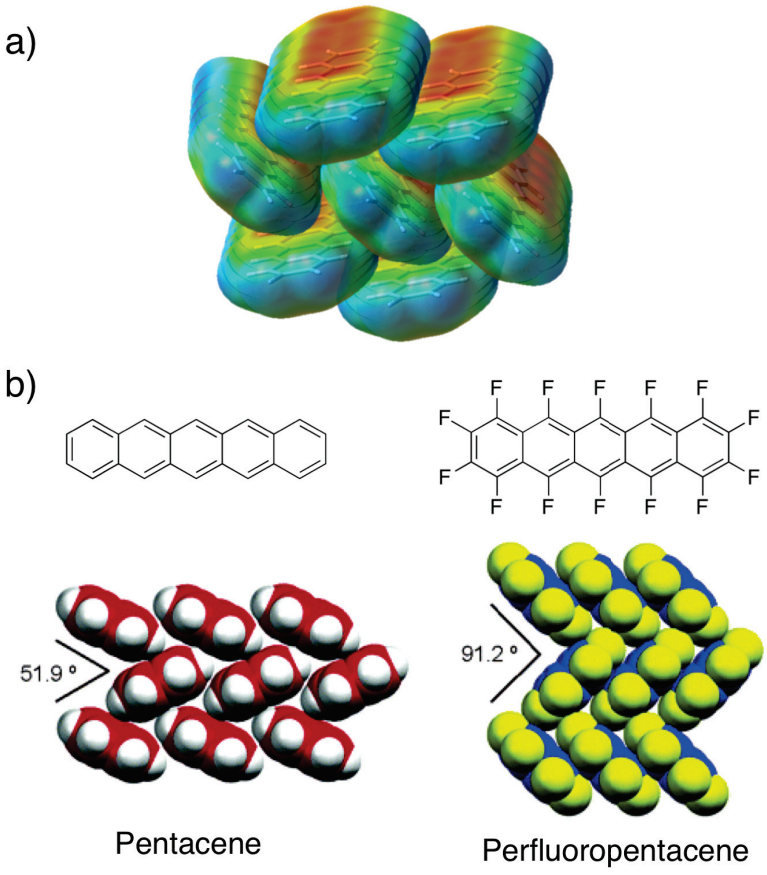

Fig. 1.25.: a) Pentacene's herringbone face-to-edge packing is due to its quadrupole moment. b) In perfluoropentacene the herringbone packing is orthogonal with tighter π–π stacks. Section b) reprinted with permission from [11]. Copyright 2004 American Chemical Society

There are several ways to disrupt these electrostatic CH–π interactions and get tighter π–π stacks. One way is to replace the hydrogens with heteroatoms. Perfluoropentacene, for

example, has an inverse electron density distribution to pentacene and is a well known OSC for n-type transport due to the electron-withdrawing nature of fluorine. The fluorine atoms affect the packing of the molecules, in which CH–π interactions are replaced by F-F interactions between nearly perpendicular molecules (Figure 1.25b). The CF–π interactions between molecules of the same π–stack also greatly reduce their short-axis displacement (3.15 Å vs. 5.34 Å in pentacene), thereby increasing the electronic coupling between cofacial molecules.[11][107]

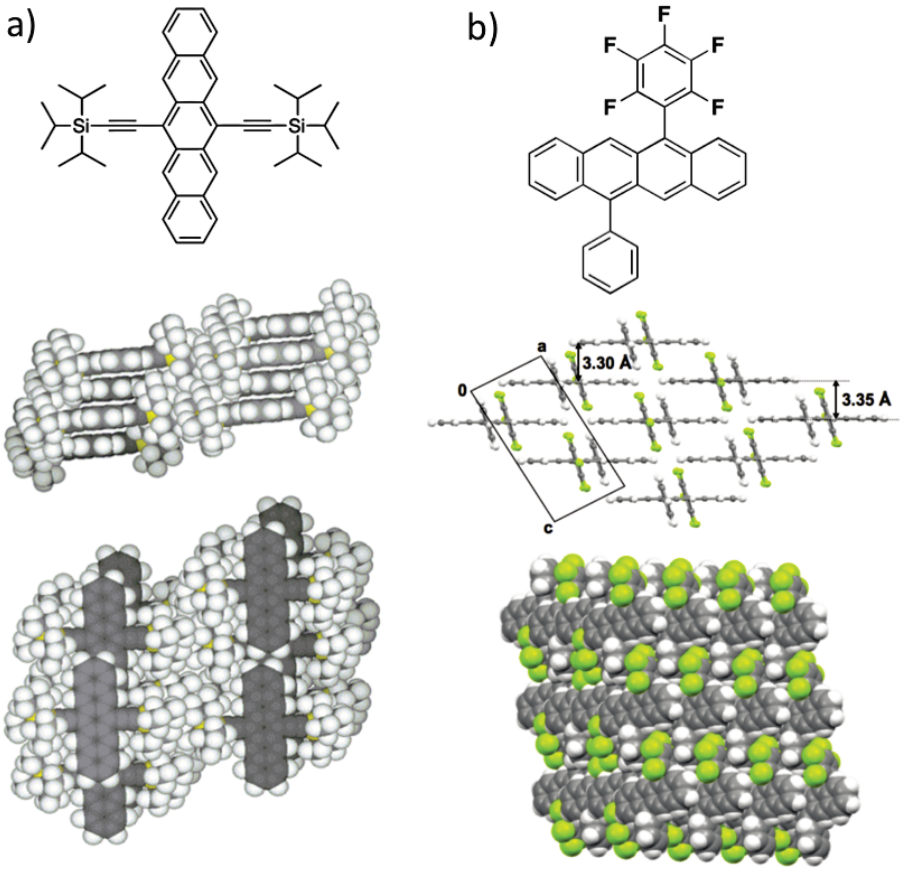

Fig. 1.26.: a) Brickwork packing of TIPS-pentacene induced through bulky substituents. Reprinted with permission from [108]. Copyright 2001 American Chemical Society. b) Aromatic donor-acceptor interactions between substituents gives a lamellar brickwork assembly in 5-perfluorophenyl-11-phenyltetracene. Reprinted with permission from [109]. Copyright 2011 American Chemical Society.

The use of bulky substituents is another oft-used strategy for controlling crystal packing. Trialkylsilylethynyl groups have been extensively studied as substituents on oligoacenes because their size can be easily controlled. Anthony et al. found that with smaller alkylsilyl

groups ($SiMe_3$, for example), pentacene derivatives assemble into slipped stacked, but if the size of the substituent is approximately half the length of the acene backbone, then a lamellar "brickwork" arrangement is observed.[110] This type of packing is observed in crystals of bis(triisopropylsilylethynyl)pentacene (TIPS-pentacene) with good electronic coupling between overlapping pentacene cores (54 and 65 meV) leading to high mobilities ($\mu_h = 1.8\ cm^2/Vs$) (Figure 1.26a).[111][112]

Okamoto et al. designed aryl and perfluoroaryl substituted tetracene as another way to induce face-to-face packing of the acene core. Here, aromatic donor-acceptor interactions between the substituents of coplanar tetracenes causes lamellar packing and close π–π distances between tetracene layers (Figure 1.26b).[109] Without the donor-acceptor interactions, bis(phenyl)tetracene adopts a herringbone conformation with no π–π stacks.

Alkyl chains placed along the long axis of the molecule, on the other hand, do not disrupt the packing of the molecules, but rather bring them closer together through van der Waals interactions. Inoue et al. studied the crystal packing of phenyl–benzothieno[3,2-*b*]benzothiophene (Ph-BTBT) with increasing lengths of alkyl chain substituents.[113] They found that by increasing chain length (n = 10) they saw stronger attractive dispersion forces between the chains, leading to much higher electronic couplings.

CH–π interactions can also be weakened by replacing carbon with heteroatoms along the periphery of the molecule. Some heteroatoms, like O or N, can partake in hydrogen-bonding which could compete for morphological control.[114] OSCs containing sulfur, a larger and more polarizable atom than carbon, may benefit from intermolecular interactions through S$\cdots$S contacts. For such contacts to be useful to hole transport, however, there must be large HOMO orbital coefficients on the sulfur atoms.[115] Even without short S$\cdots$S distances, having high orbital coefficients over the sulfur atoms can lead to better electronic coupling. Figure 1.27 shows several thiophene containing OSCs, their HOMO orbital contours, and hole transport mobilities in FETs.[116][117] The intensity of orbital coefficients on sulfur varies with structure. Notably, [5]thienoacene has virtually no orbital coefficients on its sulfurs, so that its HOMO orbital does not extend along its periphery. This explains its relatively low mobility ($\mu_h = 0.045\ cm^2/Vs$).[118] In DNT-V ($\mu_h = 1.1\ cm^2/Vs$),

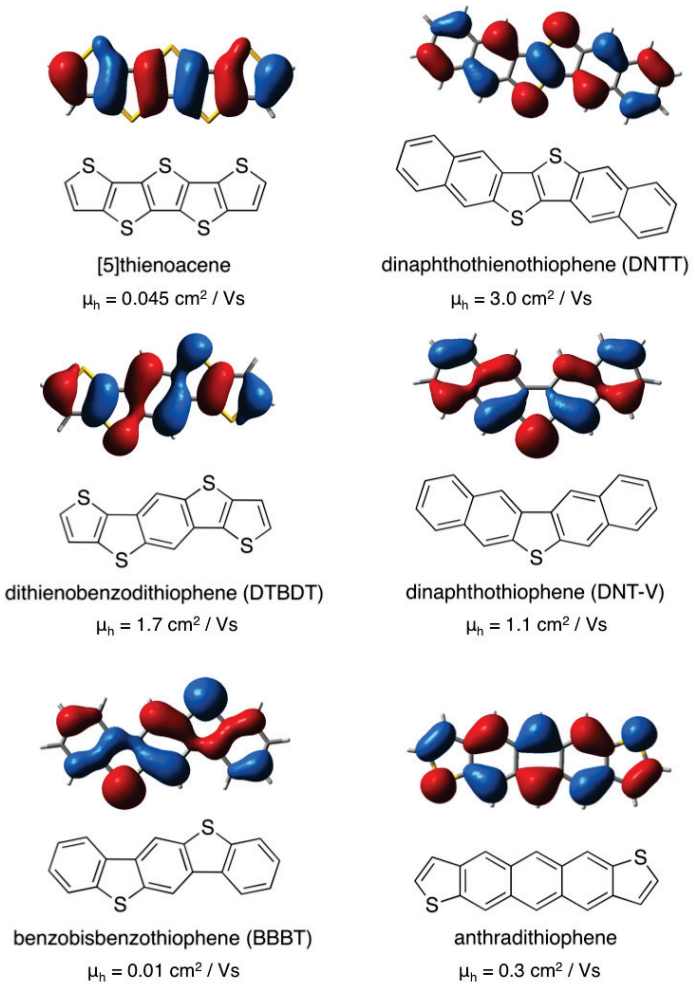

Fig. 1.27.: Calculated HOMO orbital contours (B3LYP/6-31G(d)) and hole transport mobilities for several thiophene-containing OSCs.

on the other hand, the HOMO coefficients reside heavily on the central sulfur atom.[119] Unfortunately, other factors may affect charge mobilities. For example, the low lying HOMO of BBBT (-5.6 eV) is thought to cause a large hole injection barrier and limit its mobilities ($\mu_h = 0.01\ cm^2/Vs$).[120][121]

In Figure 1.28 we see how changes in the linearity of a molecule affect preferences for face-to-edge CH–π interactions versus face-to-face π–stacking. Dinaphtho[2,3-*b*:2′,3′-*f*]thieno[3,2-*b*]thiophene (DNTT) is an excellent p-type semiconductor, due in part to its acene-like structure and electronic coupling in several directions.[122][123] "Bent" structural isomers of DNTT, however, exhibit much lower charge mobilities due to one-dimensional electronic

coupling or electronic coupling between isolated dimers. In addition, of the three isomers, only DNTT shows HOMO orbital coefficients on the sulfur atoms.

Finally, processing techniques can have a huge impact on the morphology of the material.[124] The same molecule will display vastly different electronic properties depending on whether it was drop cast, spin coated, evaporated, annealed, or grown as a single crystal. New solution processing techniques like solution-shearing, in which a top wafer is dragged across the evaporating OSC solution, have succeeded in forming oriented crystalline thin films by physically straining the molecules as the solvent evaporates. Bao et al. showed closer intermolecular distances and a five-time increase in mobility for thin films of TIPS-pentacene using this solution-shearing technique.[125]

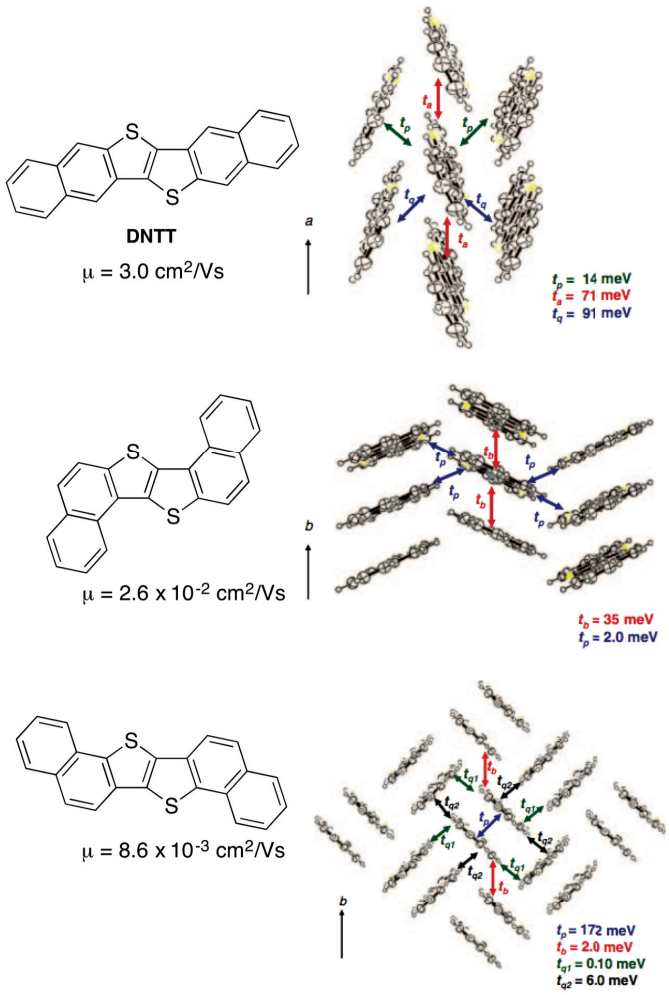

Fig. 1.28.: Crystal packing of DNTT and two isomers, showing hole mobilities and electronic coupling t. Adapted with permission from [123]. Copyright 2010 Chemical Society of Japan.

1.7 Relevant Small Molecule OSCs

1.7.1 Sulfur-containing OSCs

Sulfur-containing molecules were the first high-mobility materials studied in organic electronics (Figure 1.29). It was the metal-like transport properties of tetrathiafulvalene (TTF) complexes, in which TTF forms stable radical cations, that launched the quest for superconductivity in organic materials. In the process countless derivatives of TTF were synthesized and their conductive properties explored.[104] Crystals of TTF exist as two

types of polymorphs: monoclinic or triclinic, each featuring S···S interactions. The monoclinic phase consists of infinite π–stacks, allowing for better charge transport than in the triclinic phase where no π–stacks are formed ($\mu_h = 1.2\ cm^2/Vs$ vs. $\mu_h = 0.2\ cm^2/Vs$).[126] Oligothiophenes were among the first structures to be used in FETs. Of the unsubstitued oligothiohenes, which are planar and adopt herringbone packing motifs, **α-8T** has the highest reported mobility of $0.33\ cm^2/Vs$.[127] Many derivatives of oligothiophenes have since been studied, including liquid crystalline **1.9** with long alkoxy side chains.[128] As spun films of **1.9** exhibited good hole mobilities of $0.1\ cm^2/Vs$, but single crystal devices gave mobilities up to $6.2\ cm^2/Vs$, one of the highest values amongst non-fused oligothiophene semiconductors.

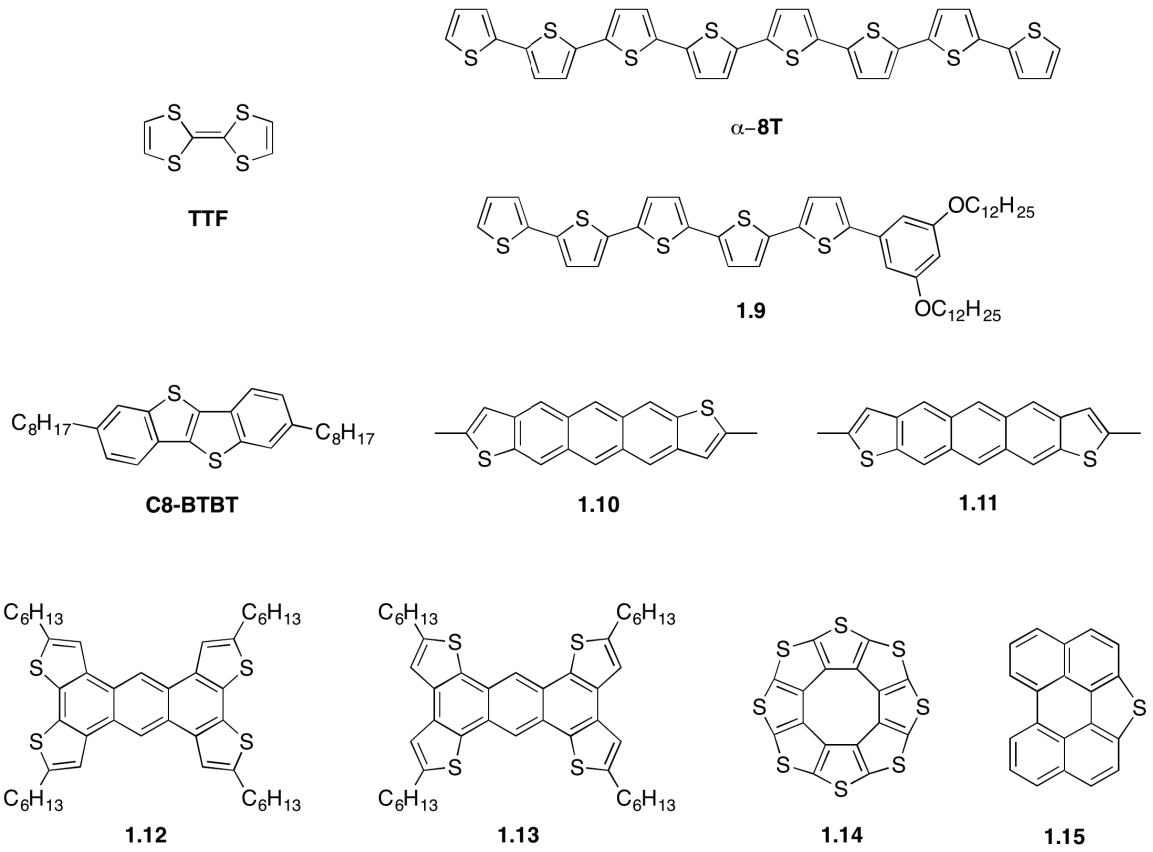

Fig. 1.29.: A selection of small molecule OSCs featuring thiophene.

Fused thienoacenes were introduced in the previous section and are a class of excellent hole transporting materials. A record high mobility for thienoacenes of $9.1\ cm^2/Vs$ was recorded for single crystals of **C8-BTBT**.[129] Average values were lower, however, indicating a

preferred pathway for charge carriers in the crystal growth orientation. Anthradithiophene was synthesized as a stable analogue to pentacene and is an example of the effect isomers can have on charge transport. Isomerically pure anti (**1.10**) and syn (**1.11**) isomers of 2,8-dimethyl-anthradithiophene were synthesized and tested in thin film FET devices.[130] **1.10** displayed a hole mobility five times higher than **1.11** (anti $\mu_h = 0.41\ cm^2/Vs$ vs. syn $\mu_h = 0.084\ cm^2/Vs$), a fact attributed to its centrosymmetric space group in the crystal structure. Takimiya et. al. saw a similar 6-fold difference in the mobilities of unsubstituted anthradithiophenes and reported stronger isomer effects in naphthodithiophenes (NDT), where anti-NDT displayed hole mobilities over an order of magnitude higher than in syn-NDT.[15] Contrarily, isomer effects were not observed with silylethynylated thienoacenes, where the large substituents dictate solid-state packing and the heteroatoms are scrambled in the crystal structure.[131] These examples demonstrate the subtler influences molecular structure can have on supramolecular assembly and charge transport.

Many 2D-extended semiconductors have also been studied. Isomers of tetrathienoanthracene, **1.12** and **1.13**, for example, have two different conjugation pathways, which only extends into the thiophene moieties in **1.13**. Both molecules adopt a cofacial herringbone arrangement, but the peripheral sulfur atoms in **1.12** allow for more close S$\cdots$S contacts and leads to an order of magnitude higher hole mobilities in **1.12**, highlighting the importance of these contacts to charge transport.[132] Octathio[8]circulene (**1.14**), nicknamed "sulflower," which was synthesized by Chernichenko et. al., is entirely composed of peripheral sulfur atoms. Without the possibility of CH–π interactions, the molecule adopts a cofacial herringbone packing motif with very close S$\cdots$S distances (3.25 Å).[133] A low hole mobility of $9 \times 10^{-3}\ cm^2/Vs$ was reported for **1.14** due to pronounced one-dimensional growth in its films, as evidenced by atomic force microscopy.[134] Perylothiophene **1.15** exhibits a similar packing motif as **1.14** with short S$\cdots$S contacts (3.51 Å) between neighboring columns. Sun et. al. found that by modifying their SiO_2 substrate they could promote the growth of single-crystal micrometer sized wires. These wires showed better hole transport properties ($\mu_h = 0.8\ cm^2/Vs$) than thin films of deposited **1.15** ($\mu_h = 0.05\ cm^2/Vs$).[135]

1.7.2 Thiazolo-containing OSCs

Thiazoles are electron-accepting heterocycles and are often used as acceptors in donor-acceptor polymers.[136] Small molecules with thiazole cores can be tuned to exhibit p-type or n-ype charge transport through the use of electron donating or withdrawing substituents (Figure 1.30). For example, benzobisthiazole **1.16**, flanked by alkylated thiophenes displays p-type transport ($\mu_h = 10^{-2}$ cm^2/Vs).[137] Single crystals of **1.16** showed an interesting packing motif consisting of orthogonal π–π stacks with close S$\cdots$N contacts linking the orthogonal stacks (3.02 Å vs. 3.35 Å for the sum of the van der Waals radii). With electron withdrawing substituents, such as perfluoroalkyl groups, thiazole-containing molecules exhibit n-type charge transport. **1.17** and **1.18**, synthesized by Ando et. al., have very similar chemical structures, but vastly different conformations in the solid state.[138] While **1.17** displays excellent electron transport properties ($\mu_e = 1.83$ cm^2/Vs), devices of **1.18** showed no transport properties at all. This sharp difference in performance is attributed to small torsional twists in **1.18**, caused by sterics between the hydrogen atoms on the thiazole unit and the phenyl end group. So while **1.17** is planar and forms an ordered brickwork network, the unit cell of **1.18** contains molecules with different torsional angles creating a disordered columnar structure. Fused thiazolothiazole moeties have no hydrogen bonds and are therefore attractive building blocks for planar OSCs. **1.19**, for example is nearly planar with thiophene units adopting an all-trans conformation.[139] Short S$\cdots$S contacts (3.25 Å) were observed between the thiazolo sulfur atoms on neighboring slipped stacks. High electron charge transport with mobilites up to 1.2 cm^2/Vs was measured for thin films of **1.19** on SiO_2 modified with octadecyl-trichlorosilane.[140]

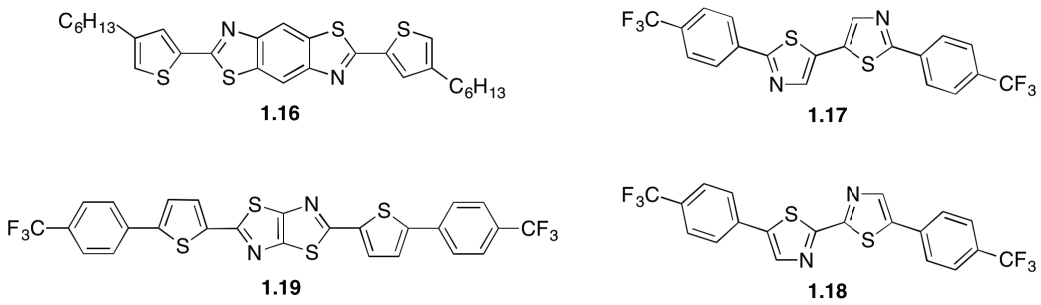

Fig. 1.30.: A selection of small molecule OSCs featuring thiazole.

1.7.3 Nitrogen-containing OSCs

Hydrogenated N-heteroacenes, such as **1.20**, were reported several decades before the synthesis of their hydrocarbon analogue, pentacene in 1935 (Figure 1.31).[141] Unlike pentacene, which oxidizes quickly in solutions, hydrogenated N-heteroacenes are stabilized by multiple, isolated Clar's sextets, though they can be oxidized to their fully conjugated forms. In 2003 Miao et. al. demonstrated that **1.20** could serve as an environmentally stable hole transport layer in FETs, exhibiting a mobility of 6×10^{-3} cm^2/Vs.[142] In their oxidized forms N-heteropentacenes have similar band gaps as pentacene, but their frontier molecular orbitals can be lowered according to the number and location of the nitrogen heteroatoms. Two isomers of silylethynylated N-heteropentacene were synthesized by Liang et. al. with either internal (**1.21**) or terminal (**1.22**) pyrazine units.[13] They found that N-heteroatoms placed internally were twice as effective at lowering the frontier orbitals of the molecule as terminally N-heteroatoms. To date, **1.21** is still the most effective azaacene for n-type transport with an electron mobility of 3.3 cm^2/Vs. The silylethynyl groups on **1.21** lead to a brickwork packing motif in the solid state, as is seen for TIPS-pentacene in Figure 1.26. Efficient charge transport is observed, however, even in **1.21**'s precursor **1.23**. **1.23** self-assembles into infinite π–stacks with quadruple C–H$\cdots$N/O hydrogen bonds between stacks in a DDAA–AADD pattern. Thin films of deposited **1.23** behave as n-type semiconductors with mobilities of 0.04 to 0.12 cm^2/Vs.[143]

A few non-linear azaarene OSCs are known, such as **1.24**, in which each azaacene is separated by a pyrene core.[144] Asymmetrically pure chiral azahelicenes (**1.25**) have also been studied in OFETs.[145] Although mobilities were low ($\mu_h = 1 \times 10^{-4}$ cm^2/Vs), a highly specific photo-response to circularly polarized light was found.[146]

OSCs containing pyrrole nitrogens have been extensively studied as well. The carbazole unit has a rich history in the xerographic industry, which used poly(vinyl carbazole) in charge transfer complexes as photoconductors.[147] Carbazoles are attractive units for OSCs because of their chemical and environmental stability, as well as the possibility to tune the energy levels and solid-state packing of the material by altering the substituents on the nitrogen atom. Indolo[3,2-*b*]carbazole **1.26** crystals, for example, adopt a herringbone

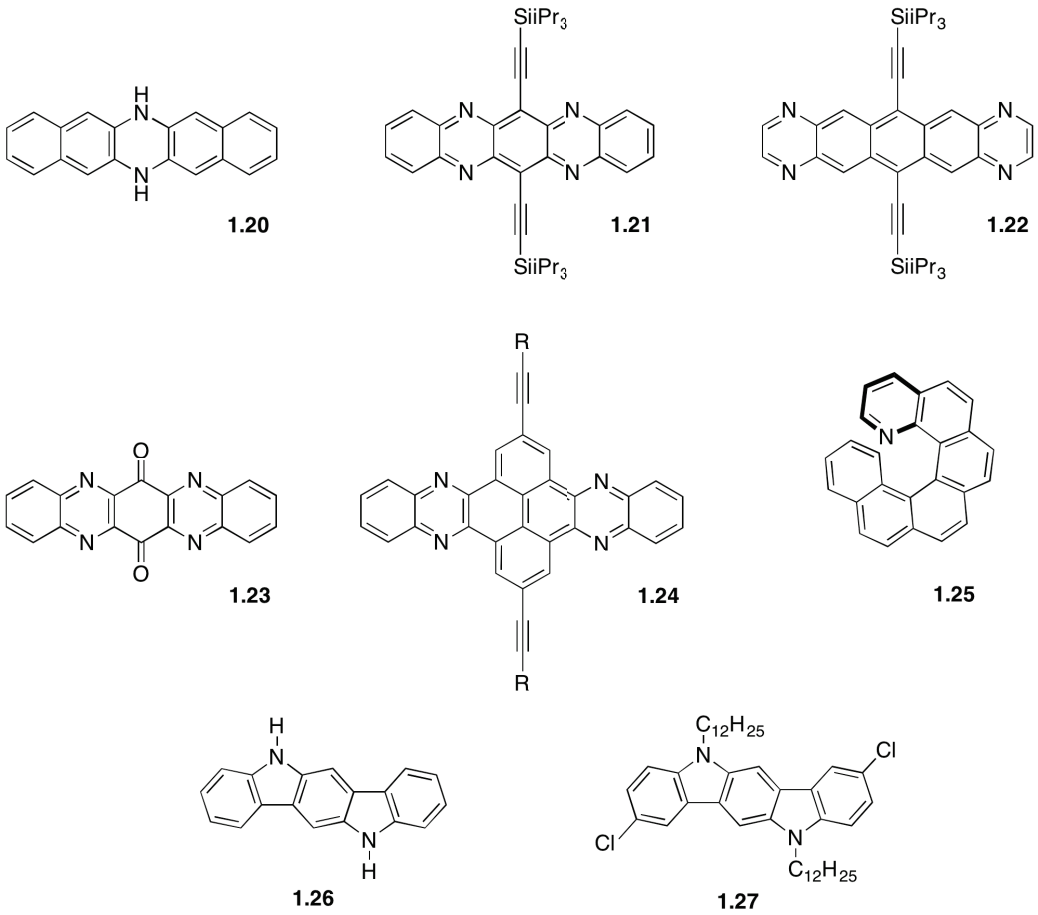

Fig. 1.31.: A selection of small molecule OSCs featuring nitrogen heteroatoms.

arrangement that includes N–H$\cdots\pi$ interactions, as well as C–H$\cdots\pi$ interactions. Thin film devices displayed good hole transport properties with a mobility of 0.1 cm^2/Vs, an order of magnitude more than was measured for N-substituted analogues in which there were no N–H$\cdots\pi$ interactions.[148] Of the many derivatives of indolo[3,2-*b*]carbazole, the highest hole mobility was measured in thin films of **1.27** ($\mu_h = 0.14\ cm^2/Vs$).[149]

Even a brief survey of the literature such as this illustrates a key issue in the study of organic semiconductors: the charge mobilities acquired from devices, especially thin-film devices, are far from the intrinsic charge mobility of the material. It is often the case that substrate modifications or different annealing temperatures will lead to orders of magnitude increases in mobility. Charge mobility measurements are therefore more a measure of morphology and supramolecular ordering than of molecular structure properties. That

being said, by studying many similar molecules, several structure-property relationships can be defined. Substituents, for example, tend to dominate solid-state assembly. Long linear alkyl chains can form ordered films through van der Waals interactions allowing for solution-processed devices with mobilities matching those made from vacuum deposition. Planar molecules generally outperform those that contain torsional twists, as those lead to disorder in the solid-state. Finally, heteroatom placement has been shown to influence not only HOMO/LUMO levels, but supramolecular assembly, with a preference for symmetrical placement.

References

(1) Letheby, H. XXIX. On the production of a blue substance by the electrolysis of sulphate of aniline. *J. Chem. Soc.* **1862**, *15*, 161.

(2) Wudl, F.; Wobschall, D.; Hufnagel, E. J. Electrical conductivity by the bis (1,3-dithiole)-bis (1,3-dithiolium) system. *J. Am. Chem. Soc.* **1972**, *94*, 670.

(3) Ferraris, J.; Cowan, D. O.; Walatka, V.; Perlstein, J. H. Electron transfer in a new highly conducting donor-acceptor complex. *J. Am. Chem. Soc.* **1973**, *95*, 948.

(4) Coleman, L.; Cohen, M.; Sandman, D.; Yamagishi, F.; Garito, A.; Heeger, A. Superconducting fluctuations and the peierls instability in an organic solid. *Solid State Commun.* **1973**, *12*, 1125.

(5) Bolto, B.; McNeill, R.; Weiss, D. Electronic Conduction in Polymers. III. Electronic Properties of Polypyrrole. *Aust. J. Chem.* **1963**, *16*, 1090.

(6) Shirakawa, H.; Louis, E. J.; MacDiarmid, A. G.; Chiang, C. K.; Heeger, A. J. Synthesis of electrically conducting organic polymers: halogen derivatives of polyacetylene, (CH)x. *J. Chem. Soc. Chem. Commun.* **1977**, 578.

(7) Heeger, A.; MacDiarmid, A. G.; Shirakawa, H. The Nobel Prize in chemistry, 2000: conductive polymers. *Stock. Sweden R. Swedish Acad. Sci.* **2000**, 1.

(8) Tang, C. W.; VanSlyke, S. A. Organic electroluminescent diodes. *Appl. Phys. Lett.* **1987**, *51*, 913.

(9) Burroughes, J. H.; Bradley, D. D. C.; Brown, A. R.; Marks, R. N.; Mackay, K.; Friend, R. H.; Burns, P. L.; Holmes, A. B. Light-emitting diodes based on conjugated polymers. *Nature* **1990**, *347*, 539.

(10) Burroughes, J. H.; Jones, C. A.; Friend, R. H. New semiconductor device physics in polymer diodes and transistors. *Nature* **1988**, *335*, 137.

(11) Horowitz, G.; Peng, X.; Fichou, D.; Garnier, F. The oligothiophene-based field-effect transistor: How it works and how to improve it. *J. Appl. Phys.* **1990**, *67*, 528.

(12) Berggren, M.; Nilsson, D.; Robinson, N. D. Organic materials for printed electronics. *Nat. Mater.* **2007**, *6*, 3.

(13) Myny, K.; Steudel, S.; Vicca, P.; Smout, S.; Beenhakkers, J.; Aerle, N. A. J. M. V.; Furthner, F.; Van, B.; Putten, D.; Tripathi, A. K.; Gelinck, G. H.; Genoe, J. In *Appl. Org. Print. Electron.* Cantatore, E., Ed.; Springer US: Boston, MA, 2013; Chapter Organic RF.

(14) Huang, W.; Diallo, A. K.; Dailey, J. L.; Besar, K.; Katz, H. E. Electrochemical processes and mechanistic aspects of field-effect sensors for biomolecules. *J. Mater. Chem. C* **2015**, *3*, 6445.

(15) Sekine, C.; Tsubata, Y.; Yamada, T.; Kitano, M.; Doi, S. Recent progress of high performance polymer OLED and OPV materials for organic printed electronics. *Sci. Technol. Adv. Mater.* **2014**, *15*, 034203.

(16) Usta, H.; Facchetti, A.; Marks, T. J. N-channel semiconductor materials design for organic complementary circuits. *Acc. Chem. Res.* **2011**, *44*, 501.

(17) Street, R. A.; Northrup, J. E.; Salleo, A. Transport in polycrystalline polymer thin-film transistors. *Phys. Rev. B* **2005**, *71*, 165202.

(18) Salleo, A.; Kline, R. J.; DeLongchamp, D. M.; Chabinyc, M. L. Microstructural characterization and charge transport in thin films of conjugated polymers. *Adv. Mater.* **2010**, *22*, 3812.

(19) Warta, W.; Karl, N. Hot holes in naphthalene: High, electric-field-dependent mobilities. *Phys. Rev. B* **1985**, *32*, 1172.

(20) Kenkre, V. M.; Andersen, J. D.; Dunlap, D. H.; Duke, C. B. Unified theory of the mobilities of photoinjected electrons in naphthalene. *Phys. Rev. Lett.* **1989**, *62*, 1165.

(21) Schweicher, G.; Olivier, Y.; Lemaur, V.; Geerts, Y. H. What Currently Limits Charge Carrier Mobility in Crystals of Molecular Semiconductors? *Isr. J. Chem.* **2014**, *54*, 595.

(22) Marcus, R. A. On the Theory of Oxidation-Reduction Reactions Involving Electron Transfer. I. *J. Chem. Phys.* **1956**, *24*, 966.

(23) Marcus, R. A. Electron transfer reactions in chemistry. Theory and experiment. *Rev. Mod. Phys.* **1993**, *65*, 599.

(24) Holstein, T. Studies of Polaron Motion: Part I. The Molecular-Crystal Model. *Ann. Phys. (N. Y).* **1959**, *8*, 343.

(25) Bässler, H. Charge Transport in Disordered Organic Photoconductors a Monte Carlo Simulation Study. *Phys. Status Solidi B* **1993**, *175*, 15.

(26) Stallinga, P. Electronic transport in organic materials: Comparison of band theory with percolation/(variable range) hopping theory. *Adv. Mater.* **2011**, *23*, 3356.

(27) Shur, M.; Hack, M. Physics of Amorphous Silicon Based Alloy Field-Effect Transistors. *J. Appl. Phys.* **1984**, *55*, 3831.

(28) Horowitz, G.; Hajlaoui, M. E.; Hajlaoui, R. Temperature and gate voltage dependence of hole mobility in polycrystalline oligothiophene thin film transistors. *J. Appl. Phys.* **2000**, *87*, 4456.

(29) Köhler, A.; Bässler, H. In *Electron. Process. Org. Semicond.* April; Wiley-VCH Verlag GmbH & Co. KGaA: Weinheim, Germany, 2015, pp 193–305.

(30) Sekitani, T.; Zschieschang, U.; Klauk, H.; Someya, T. Flexible organic transistors and circuits with extreme bending stability. *Nat. Mater.* **2010**, *9*, 1015.

(31) Barr, M. C.; Rowehl, J. A.; Lunt, R. R.; Xu, J.; Wang, A.; Boyce, C. M.; Im, S. G.; Bulović, V.; Gleason, K. K. Direct Monolithic Integration of Organic Photovoltaic Circuits on Unmodified Paper. *Adv. Mater.* **2011**, *23*, 3500.

(32) Tee, B. C.-. K.; Chortos, A.; Berndt, A.; Nguyen, A. K.; Tom, A.; McGuire, A.; Lin, Z. C.; Tien, K.; Bae, W.-G.; Wang, H.; Mei, P.; Chou, H.-H.; Cui, B.; Deisseroth, K.; Ng, T. N.; Bao, Z. A skin-inspired organic digital mechanoreceptor. *Science* **2015**, *350*, 313.

(33) Mertens, R.; Peleg, R. OLED mobile phones: an introduction and market status. http://www.oled-info.com/oled-mobile-phones (accessed Nov 19, 2015).

(34) Loo, Y.-L.; McCulloch, I. Progress and Challenges in Commercialization of Organic Electronics. *MRS Bull.* **2012**, *33*, 653.

(35) Lee, J.; Chen, H.-F.; Batagoda, T.; Coburn, C.; Djurovich, P. I.; Thompson, M. E.; Forrest, S. R. Deep blue phosphorescent organic light-emitting diodes with very high brightness and efficiency. *Nat. Mater.* **2015**, *15*, DOI: 10.1038/nmat4446.

(36) BELECTRIC OPV GmbH, Solarte. http://www.solarte.de/index.php/en/ (accessed Nov 19, 2015).

(37) Coakley, K. M.; McGehee, M. D. Conjugated Polymer Photovoltaic Cells. *Chem. Mater.* **2004**, *16*, 4533.

(38) Qi, B.; Wang, J. Open-circuit voltage in organic solar cells. *J. Mater. Chem.* **2012**, *22*, 24315.

(39) Scharber, M. C.; Mühlbacher, D.; Koppe, M.; Denk, P.; Waldauf, C.; Heeger, A. J.; Brabec, C. J. Design Rules for Donors in Bulk-Heterojunction Solar Cells—Towards 10 % Energy-Conversion Efficiency. *Adv. Mater.* **2006**, *18*, 789.

(40) Chen, H. Y.; Hou, J. H.; Zhang, S. Q.; Liang, Y. Y.; Yang, G. W.; Yang, Y.; Yu, L. P.; Wu, Y.; Li, G. Polymer solar cells with enhanced open-circuit voltage and efficiency. *Nat. Photonics* **2009**, *3*, 649.

(41) Beaujuge, P. M.; Fréchet, J. M. J. Molecular design and ordering effects in π-functional materials for transistor and solar cell applications. *J. Am. Chem. Soc.* **2011**, *133*, 20009.

(42) Müller, C.; Wang, E.; Andersson, L. M.; Tvingstedt, K.; Zhou, Y.; Andersson, M. R.; Inganäs, O. Influence of Molecular Weight on the Performance of Organic Solar Cells Based on a Fluorene Derivative. *Adv. Funct. Mater.* **2010**, *20*, 2124.

(43) Ballantyne, A. M.; Chen, L.; Dane, J.; Hammant, T.; Braun, F. M.; Heeney, M.; Duffy, W.; McCulloch, I.; Bradley, D. D. C.; Nelson, J. The Effect of Poly(3-hexylthiophene) Molecular Weight on Charge Transport and the Performance of Polymer:Fullerene Solar Cells. *Adv. Funct. Mater.* **2008**, *18*, 2373.

(44) Mei, J.; Bao, Z. Side chain engineering in solution-processable conjugated polymers. *Chem. Mater.* **2014**, *26*, 604.

(45) Fritz, S. E.; Kelley, T. W.; Frisbie, C. D. Effect of dielectric roughness on performance of pentacene TFTs and restoration of performance with a polymeric smoothing layer. *J. Phys. Chem. B* **2005**, *109*, 10574.

(46) Melzer, C.; von Seggern, H. Organic electronics: Enlightened organic transistors. *Nat. Mater.* **2010**, *9*, 470.

(47) Dimitrakopoulos, C.; Malenfant, P. Organic Thin Film Transistors for Large Area Electronics. *Adv. Mater.* **2002**, *14*, 99.

(48) Noh, Y.-Y.; Chang, J.-F.; Cheng, X.; Baeg, K.-J. In, Meng, H.-f., Ed.; CRC Press: Boca Raton, Fl, 2013; Chapter Polymer Fi.

(49) Merlo, J. A.; Frisbie, C. D. Field effect transport and trapping in regioregular polythiophene nanofibers. *J. Phys. Chem. B* **2004**, *108*, 19169.

(50) Roncali, J. Molecular engineering of the band gap of pi-conjugated systems: Facing technological applications. *Macromol. Rapid Commun.* **2007**, *28*, 1761.

(51) Pizzoferrato, R.; Berliocchi, M.; Di Carlo, A.; Lugli, P.; Venanzi, M.; Micozzi, A.; Ricci, A.; Lo Sterzo, C. Improvement of the extended one-pot (EOP) procedure to form poly(aryleneethynylene)s and investigation of their electrical and optical properties. *Macromolecules* **2003**, *36*, 2215.

(52) Brédas, J. L. Relationship between band gap and bond length alternation in organic conjugated polymers. *J. Chem. Phys.* **1985**, *82*, 3808.

(53) Longuet-Higgins, H. C.; Salem, L. The Alternation of Bond Lengths in Long Conjugated Chain Molecules. *Proc. R. Soc. A Math. Phys. Eng. Sci.* **1959**, *251*, 172.

(54) Heeger, A.; Blanchet, G.; Chung, T.-C.; Fincher, C. Solitons or not in polyacetylene (and does it matter?) *Synth. Met.* **1984**, *9*, 173.

(55) Wudl, F.; Kobayashi, M.; Heeger, A. J. Poly(isothianaphthene). *J. Org. Chem.* **1984**, *49*, 3382.

(56) He, Z.; Zhong, C.; Su, S.; Xu, M.; Wu, H.; Cao, Y. Enhanced power-conversion efficiency in polymer solar cells using an inverted device structure. *Nat. Photonics* **2012**, *6*, 593.

(57) Lu, L.; Yu, L. Understanding Low Bandgap Polymer PTB7 and Optimizing Polymer Solar Cells Based on It. *Adv. Mater.* **2014**, *26*, 4413.

(58) Marder, S. R.; Beratan, D. N.; Cheng, L. T. Approaches for optimizing the first electronic hyperpolarizability of conjugated organic molecules. *Science* **1991**, *252*, 103.

(59) Marder, S. R.; Perry, J. W.; Bourhill, G.; Gorman, C. B.; Tiemann, B. G.; Mansour, K. Conjugated Organic Molecules. *Science* **1993**, *261*, 186.

(60) Gorman, C. B.; Marder, S. R. Effect of Molecular-Polarization on Bond-Length Alternation, Linear Polarizability, First and Second Hyperpolarizability in Donor-Acceptor Polyenes As a Function of Chain-Length. *Chem. Mater.* **1995**, *7*, 215.

(61) Kanibolotsky, A. L.; Berridge, R.; Skabara, P. J.; Perepichka, I. F.; Bradley, D. D. C.; Koeberg, M. Synthesis and properties of monodisperse oligofluorene-funcfionalized truxenes: Highly fluorescent star-shaped architectures. *J. Am. Chem. Soc.* **2004**, *126*, 13695.

(62) Brisset, H.; Blanchard, P.; Illien, B.; Riou, A.; Roncali, J. Bandgap control through reduction of bond length alternation in bridged poly(diethienylethylene)s. *Chem. Commun.* **1997**, 569.

(63) Roncali, J.; Thobie-Gautier, C. An efficient strategy towards small bandgap polymers: The rigidification of the p-conjugated system. *Adv. Mater.* **1994**, *6*, 846.

(64) Trotter, J. The crystal and molecular structure of biphenyl. *Acta Crystallogr.* **1961**, *14*, 1135.

(65) Gerkin, R. E.; Lundstedt, A. P.; Reppart, W. J. Structure of fluorene, C13H10, at 159 K. *Acta Crystallogr. Sect. C Cryst. Struct. Commun.* **1984**, *40*, 1892.

(66) Watanabe, M.; Chang, Y. J.; Liu, S.-W.; Chao, T.-H.; Goto, K.; Islam, M. M.; Yuan, C.-H.; Tao, Y.-T.; Shinmyozu, T.; Chow, T. J. The synthesis, crystal structure and charge-transport properties of hexacene. *Nat. Chem.* **2012**, *4*, 574.

(67) Sun, Z.; Wu, J. Open-shell polycyclic aromatic hydrocarbons. *J. Mater. Chem.* **2012**, *22*, 4151.

(68) Zhang, L.; Fonari, A.; Liu, Y.; Hoyt, A. L.; Lee, H.; Granger, D.; Parkin, S.; Russell, T. P.; Anthony, J. E.; Bredas, J. L.; Coropceanu, V.; Briseno, A. L. Bis-tetracene: an air-stable, high-mobility organic semiconductor with extended conjugation. *J. Am. Chem. Soc.* **2014**, *136*, 9248.

(69) Okamoto, H.; Kawasaki, N.; Kaji, Y.; Kubozono, Y.; Fujiwara, A.; Yamaji, M. Air-assisted High-performance Field-effect Transistor with Thin Films of Picene. *J. Am. Chem. Soc.* **2008**, *130*, 10470.

(70) Okamoto, H.; Hamao, S.; Goto, H.; Sakai, Y.; Izumi, M.; Gohda, S.; Kubozono, Y.; Eguchi, R. Transistor application of alkyl-substituted picene. *Sci. Rep.* **2014**, *4*, 5048.

(71) Malloci, G.; Cappellini, G.; Mulas, G.; Mattoni, A. Electronic and optical properties of families of polycyclic aromatic hydrocarbons: A systematic (time-dependent) density functional theory study. *Chem. Phys.* **2011**, *384*, 19.

(72) Patra, A.; Bendikov, M. Polyselenophenes. *J. Mater. Chem.* **2010**, *20*, 422.

(73) Dall'Olio, A.; Dascola, G.; Varacca, V.; Bocchio, V. Résonance paramagnétique électronique et conductivité d'un noir d'oxypyrrol électrolytique. *C. R. Acad. Sci. Paris Série C* **1968**, *267*, 433.

(74) Diaz, A. F.; Kanazawa, K. K.; Gardini, G. P. Electrochemical polymerization of pyrrole. *J. Chem. Soc. Chem. Commun.* **1979**, *160*, 635.

(75) Ramsden, C. A. The influence of aza-substitution on azole aromaticity. *Tetrahedron* **2010**, *66*, 2695.

(76) Horner, K. E.; Karadakov, P. B. Shielding in and around Oxazole, Imidazole, and Thiazole: How Does the Second Heteroatom Affect Aromaticity and Bonding? *J. Org. Chem.* **2015**, *80*, 7150.

(77) Yum, S.; An, T. K.; Wang, X.; Lee, W.; Uddin, M. A.; Kim, Y. J.; Nguyen, T. L.; Xu, S.; Hwang, S.; Park, C. E.; Woo, H. Y. Benzotriazole-Containing Planar Conjugated Polymers with Noncovalent Conformational Locks for Thermally Stable and Efficient Polymer Field-Effect Transistors. *Chem. Mater.* **2014**, *26*, 2147.

(78) Jackson, N. E.; Savoie, B. M.; Kohlstedt, K. L.; Olvera De La Cruz, M.; Schatz, G. C.; Chen, L. X.; Ratner, M. a. Controlling conformations of conjugated polymers and small molecules: The role of nonbonding interactions. *J. Am. Chem. Soc.* **2013**, *135*, 10475.

(79) Shi, C.; Yao, Y.; Yang, Y.; Pei, Q. Regioregular copolymers of 3-alkoxythiophene and their photovoltaic application. *J. Am. Chem. Soc.* **2006**, *128*, 8980.

(80) Price, S.; Stuart, A.; Yang, L.; Zhou, H.; You, W. Fluorine Substituted Conjugated Polymer of Medium Band Gap Yields 7% Efficiency in Polymer-Fullerene Solar Cells. *J. Am. Chem. Soc.* **2011**, *133*, 4625.

(81) Huo, L.; Zhang, S.; Guo, X.; Xu, F.; Li, Y.; Hou, J. Replacing alkoxy groups with alkylthienyl groups: a feasible approach to improve the properties of photovoltaic polymers. *Angew. Chem. Int. Ed. Engl.* **2011**, *50*, 9697.

(82) Kim, J. H.; Song, C. E.; Kim, B.; Kang, I. N.; Shin, W. S.; Hwang, D. H. Thieno[3,2-b]thiophene-substituted benzo[1,2-b:4,5-b′]dithiophene as a promising building block for low bandgap semiconducting polymers for high-performance single and tandem organic photovoltaic cells. *Chem. Mater.* **2014**, *26*, 1234.

(83) Yu, J.; Holdcroft, S. Chemically amplified soft lithography of a low band gap polymer. *Chem. Commun.* **2001**, 1274.

(84) Liu, J.; Kadnikova, E. N.; Liu, Y.; McGehee, M. D.; Fréchet, J. M. J. Polythiophene containing thermally removable solubilizing groups enhances the interface and the performance of polymer-titania hybrid solar cells. *J. Am. Chem. Soc.* **2004**, *126*, 9486.

(85) Gevorgyan, S. a.; Krebs, F. C. Bulk heterojunctions based on native polythiophene. *Chem. Mater.* **2008**, *20*, 4386.

(86) Sheng, Y.; Jiang, Y.; Wang, X.-C. AM1 study of the relationship between the donor-acceptor strength and the polarizabilities of push-pull polyenes. *J. Chem. Soc. Faraday Trans.* **1998**, *94*, 47.

(87) Dehu, C.; Meyers, F.; Bredas, J. L. Donor-acceptor diphenylacetylenes: geometric structure, electronic structure, and second-order nonlinear optical properties. *J. Am. Chem. Soc.* **1993**, *115*, 6198.

(88) Würthner, F.; Effenberger, F.; Wortmann, R.; Krämer, P. Second-order polarizability of donor—acceptor substituted oligothiophenes: substituent variation and conjugation length dependence. *Chem. Phys.* **1993**, *173*, 305.

(89) An, Z.; Odom, S. a.; Kelley, R. F.; Huang, C.; Zhang, X.; Barlow, S.; Padilha, L. a.; Fu, J.; Webster, S.; Hagan, D. J.; Van Stryland, E. W.; Wasielewski, M. R.; Marder, S. R. Synthesis and photophysical properties of donor- and acceptor-substituted 1,7-bis(arylalkynyl)perylene-3,4:9,10-bis(dicarboximide)s. *J. Phys. Chem. A* **2009**, *113*, 5585.

(90) Ellinger, S.; Graham, K. R.; Shi, P.; Farley, R. T.; Steckler, T. T.; Brookins, R. N.; Taranekar, P.; Mei, J.; Padilha, L. a.; Ensley, T. R.; Hu, H.; Webster, S.; Hagan, D. J.; Van Stryland, E. W.; Schanze, K. S.; Reynolds, J. R. Donor-acceptor-donor-based π-conjugated oligomers for nonlinear optics and near-IR emission. *Chem. Mater.* **2011**, *23*, 3805.

(91) Zhang, Z.; Wang, J. Structures and properties of conjugated Donor–Acceptor copolymers for solar cell applications. *J. Mater. Chem.* **2012**, *22*, 4178.

(92) Martinez, C. R.; Iverson, B. L. Rethinking the term "pi-stacking". *Chem. Sci.* **2012**, *3*, 2191.

(93) Reczek, J. J.; Villazor, K. R.; Lynch, V.; Swager, T. M.; Iverson, B. L. Tunable columnar mesophases utilizing C2 symmetric aromatic donor-acceptor complexes. *J. Am. Chem. Soc.* **2006**, *128*, 7995.

(94) Tsao, H. N.; Cho, D. M.; Park, I.; Hansen, M. R.; Mavrinskiy, A.; Yoon, D. Y.; Graf, R.; Pisula, W.; Spiess, H. W.; Müllen, K. Ultrahigh mobility in polymer field-effect transistors by design. *J. Am. Chem. Soc.* **2011**, *133*, 2605.

(95) Li, Y. N.; Sonar, P.; Murphy, L.; Hong, W. High mobility diketopyrrolopyrrole (DPP)-based organic semiconductor materials for organic thin film transistors and photovoltaics. *Energy Environ. Sci.* **2013**, *6*, 1684.

(96) Carsten, B.; Szarko, J. M.; Son, H. J.; Wang, W.; Lu, L.; He, F.; Rolczynski, B. S.; Lou, S. J.; Chen, L. X.; Yu, L. Examining the effect of the dipole moment on charge separation in donor-acceptor polymers for organic photovoltaic applications. *J. Am. Chem. Soc.* **2011**, *133*, 20468.

(97) Bronstein, H.; Chen, Z.; Ashraf, R. S.; Zhang, W.; Du, J.; Durrant, J. R.; Tuladhar, P. S.; Song, K.; Watkins, S. E.; Geerts, Y.; Wienk, M. M.; Janssen, R. a. J.; Anthopoulos, T.; Sirringhaus, H.; Heeney, M.; McCulloch, I. Thieno[3,2-b]thiophene-diketopyrrolopyrrole-containing polymers for high-performance organic field-effect transistors and organic photovoltaic devices. *J. Am. Chem. Soc.* **2011**, *133*, 3272.

(98) Chen, Y. L.; Chang, C. Y.; Cheng, Y. J.; Hsu, C. S. Synthesis of a new ladder-type benzodi(cyclopentadithiophene) arene with forced planarization leading to an enhanced efficiency of organic photovoltaics. *Chem. Mater.* **2012**, *24*, 3964.

(99) Newton, M. D. Quantum chemical probes of electron-transfer kinetics: the nature of donor-acceptor interactions. *Chem. Rev.* **1991**, *91*, 767.

(100) Valeev, E. F.; Coropceanu, V.; Da Silva Filho, D. a.; Salman, S.; Brédas, J. L. Effect of electronic polarization on charge-transport parameters in molecular organic semiconductors. *J. Am. Chem. Soc.* **2006**, *128*, 9882.

(101) Da Silva Filho, D. A.; Kim, E. G.; Br??das, J. L. Transport properties in the rubrene crystal: Electronic coupling and vibrational reorganization energy. *Adv. Mater.* **2005**, *17*, 1072.

(102) Noriega, R.; Rivnay, J.; Vandewal, K.; Koch, F. P. V.; Stingelin, N.; Smith, P.; Toney, M. F.; Salleo, A. A general relationship between disorder, aggregation and charge transport in conjugated polymers. *Nat. Mater.* **2013**, *12*, 1038.

(103) Sutton, C.; Risko, C.; Brédas, J.-L. Noncovalent Intermolecular Interactions in Organic Electronic Materials: Implications for the Molecular Packing vs Electronic Properties of Acenes. *Chem. Mater.* **2016**, *28*, 3.

(104) Bendikov, M.; Wudl, F.; Perepichka, D. F. Tetrathiafulvalenes, oligoacenenes, and their buckminsterfullerene derivatives: the brick and mortar of organic electronics. *Chem. Rev.* **2004**, *104*, 4891.

(105) Gundlach, D.; Lin, Y.; Jackson, T.; Nelson, S.; Schlom, D. Pentacene organic thin-film transistors-molecular ordering and\nmobility. *IEEE Electron Device Lett.* **1997**, *18*, 87.

(106) Jurchescu, O. D.; Baas, J.; Palstra, T. T. M. Effect of impurities on the mobility of single crystal pentacene. *Appl. Phys. Lett.* **2004**, *84*, 3061.

(107) Delgado, M. C. R.; Pigg, K. R.; da Silva Filho, D. A.; Gruhn, N. E.; Sakamoto, Y.; Suzuki, T.; Osuna, R. M.; Casado, J.; Hernández, V.; Navarrete, J. T. L.; Martinelli, N. G.; Cornil, J.; Sánchez-Carrera, R. S.; Coropceanu, V.; Brédas, J.-L. Impact of Perfluorination on the Charge-Transport Parameters of Oligoacene Crystals. *J. Am. Chem. Soc.* **2009**, *131*, 1502.

(108) Anthony, J. E.; Brooks, J. S.; Eaton, D. L.; Parkin, S. R. Functionalized pentacene: improved electronic properties from control of solid-state order. *J. Am. Chem. Soc.* **2001**, *123*, 9482.

(109) Okamoto, T.; Nakahara, K.; Saeki, A.; Seki, S.; Oh, J. H.; Akkerman, H. B.; Bao, Z.; Matsuo, Y. Aryl-Perfluoroaryl Substituted Tetracene: Induction of Face-to-Face π-π Stacking and Enhancement of Charge Carrier Properties. *Chem. Mater.* **2011**, *23*, 1646.

(110) Anthony, J. E.; Eaton, D. L.; Parkin, S. R. A road map to stable, soluble, easily crystallized pentacene derivatives. *Org. Lett.* **2002**, *4*, 15.

(111) Park, S. K.; Jackson, T. N.; Anthony, J. E.; Mourey, D. a. High mobility solution processed 6,13-bis(triisopropyl-silylethynyl) pentacene organic thin film transistors. *Appl. Phys. Lett.* **2007**, *91*, 10.

(112) Wade, J.; Steiner, F.; Niedzialek, D.; James, D. T.; Jung, Y.; Yun, D.-J.; Bradley, D. D. C.; Nelson, J.; Kim, J.-S. Charge mobility anisotropy of functionalized pentacenes in organic field effect transistors fabricated by solution processing. *J. Mater. Chem. C* **2014**, *2*, 10110.

(113) Inoue, S.; Minemawari, H.; Tsutsumi, J.; Chikamatsu, M.; Yamada, T.; Horiuchi, S.; Tanaka, M.; Kumai, R.; Yoneya, M.; Hasegawa, T. Effects of Substituted Alkyl Chain Length on Solution-Processable Layered Organic Semiconductor Crystals. *Chem. Mater.* **2015**, *27*, 3809.

(114) Black, H. T.; Perepichka, D. F. Crystal engineering of dual channel p/n organic semiconductors by complementary hydrogenbonding. *Angew. Chem. Int. Ed.* **2014**, *53*, 2138.

(115) Osaka, I.; Shinamura, S.; Abe, T.; Takimiya, K. Naphthodithiophenes as building units for small molecules to polymers; a case study for in-depth understanding of structure–property relationships in organic semiconductors. *J. Mater. Chem. C* **2013**, *1*, 1297.

(116) Gao, P.; Beckmann, D.; Tsao, H. N.; Feng, X.; Enkelmann, V.; Baumgarten, M.; Pisula, W.; Müllen, K. Dithieno[2,3-d;2′,3′-d′]benzo[1,2-b;4,5-b′]dithiophene (DTBDT) as Semiconductor for High-Performance, Solution-Processed Organic Field-Effect Transistors. *Adv. Mater.* **2009**, *21*, 213.

(117) Nakano, M.; Niimi, K.; Miyazaki, E.; Osaka, I.; Takimiya, K. Isomerically Pure Anthra[2,3-b:6,7- b′]-difuran (anti-ADF),-dithiophene (anti-ADT), and -diselenophene (anti -ADS): Selective Synthesis, Electronic Structures, and Application to Organic Field-Effect Transistors. *J. Org. Chem.* **2012**, *77*, 8099.

(118) Xiao, K.; Liu, Y.; Qi, T.; Zhang, W.; Wang, F.; Gao, J.; Qiu, W.; Ma, Y.; Cui, G.; Chen, S.; Zhan, X.; Yu, G.; Qin, J.; Hu, W.; Zhu, D. A Highly p-Stacked Organic Semiconductor for Field-Effect Transistors Based on Linearly Condensed Pentathienoacene. *J. Am. Chem. Soc.* **2005**, *127*, 13281.

(119) Okamoto, T.; Mitsui, C.; Yamagishi, M.; Nakahara, K.; Soeda, J.; Hirose, Y.; Miwa, K.; Sato, H.; Yamano, A.; Matsushita, T.; Uemura, T.; Takeya, J. V-shaped organic semiconductors with solution processability, high mobility, and high thermal durability. *Adv. Mater.* **2013**, *25*, 6392.

(120) Gao, P.; Beckmann, D.; Tsao, H. N.; Feng, X.; Enkelmann, V.; Pisula, W.; Müllen, K. Benzo[1,2-b:4,5-b′]bis[b]benzothiophene as solution processible organic semiconductor for field-effect transistors. *Chem. Commun.* **2008**, 1548.

(121) Ebata, H.; Miyazaki, E.; Yamamoto, T.; Takimiya, K. Synthesis, Properties, and Structures of Benzo[1,2-b:4,5-b′]bis[b]benzothiophene and Benzo[1,2-b:4,5-b′]bis[b]benzoselenophene. *Org. Lett.* **2007**, *9*, 4499.

(122) Yamamoto, T.; Takimiya, K. Facile Synthesis of Highly π-Extended Heteroarenes, Dinaphtho[2,3-b:2′,3′-f]chalcogenopheno[3,2-b]chalcogenophenes, and Their Application to Field-Effect Transistors. *J. Am. Chem. Soc.* **2007**, *129*, 2224.

(123) Yamamoto, T.; Shinamura, S.; Miyazaki, E.; Takimiya, K. Three structural isomers of dinaphthothieno[3,2-b]thiophenes: Elucidation of physicochemical properties, crystal structures, and field-effect transistor characteristics. *Bull. Chem. Soc. Jpn.* **2010**, *83*, 120.

(124) Virkar, A. a.; Mannsfeld, S.; Bao, Z.; Stingelin, N. Organic semiconductor growth and morphology considerations for organic thin-film transistors. *Adv. Mater.* **2010**, *22*, 3857.

(125) Giri, G.; Verploegen, E.; Mannsfeld, S. C. B.; Atahan-Evrenk, S.; Kim, D. H.; Lee, S. Y.; Becerril, H. a.; Aspuru-Guzik, A.; Toney, M. F.; Bao, Z. Tuning charge transport in solution-sheared organic semiconductors using lattice strain. *Nature* **2011**, *480*, 504.

(126) Jiang, H.; Yang, X.; Cui, Z.; Liu, Y.; Li, H.; Hu, W.; Liu, Y.; Zhu, D. Phase dependence of single crystalline transistors of tetrathiafulvalene. *Appl. Phys. Lett.* **2007**, *91*, 123505.

(127) Murphy, A. R.; Fréchet, J. M. J. Organic semiconducting oligomers for use in thin film transistors. *Chem. Rev.* **2007**, *107*, 1066.

(128) Dong, S.; Zhang, H.; Yang, L.; Bai, M.; Yao, Y.; Chen, H.; Gan, L.; Yang, T.; Jiang, H.; Hou, S.; Wan, L.; Guo, X. Solution-crystallized organic semiconductors with high carrier mobility and air stability. *Adv. Mater.* **2012**, *24*, 5576.

(129) Liu, C.; Minari, T.; Lu, X.; Kumatani, A.; Takimiya, K.; Tsukagoshi, K. Solution-Processable Organic Single Crystals with Bandlike Transport in Field-Effect Transistors. *Adv. Mater.* **2011**, *23*, 523.

(130) Mamada, M.; Minamiki, T.; Katagiri, H.; Tokito, S. Synthesis, physical properties, and field-effect mobility of isomerically pure syn -/ anti -anthradithiophene derivatives. *Org. Lett.* **2012**, *14*, 4062.

(131) Lehnherr, D.; Waterloo, A. R.; Goetz, K. P.; Payne, M. M.; Hampel, F.; Anthony, J. E.; Jurchescu, O. D.; Tykwinski, R. R. Isomerically Pure syn -Anthradithiophenes: Synthesis, Properties, and FET Performance. *Org. Lett.* **2012**, *14*, 3660.

(132) Brusso, J. L.; Hirst, O. D.; Dadvand, A.; Ganesan, S.; Cicoira, F.; Robertson, C. M.; Oakley, R. T.; Rosei, F.; Perepichka, D. F. Two-Dimensional Structural Motif in Thienoacene Semiconductors: Synthesis, Structure, and Properties of Tetrathienoanthracene Isomers. *Chem. Mater.* **2008**, *20*, 2484.

(133) Chernichenko, K. Y.; Sumerin, V. V.; Shpanchenko, R. V.; Balenkova, E. S.; Nenajdenko, V. G. "Sulflower": A new form of carbon sulfide. *Angew. Chemie - Int. Ed.* **2006**, *45*, 7367.

(134) Dadvand, A.; Cicoira, F.; Chernichenko, K. Y.; Balenkova, E. S.; Osuna, R. M.; Rosei, F.; Nenajdenko, V. G.; Perepichka, D. F. Heterocirculenes as a new class of organic semiconductors. *Chem. Commun. (Camb).* **2008**, 5354.

(135) Sun, Y.; Tan, L.; Jiang, S.; Qian, H.; Wang, Z.; Yan, D.; Di, C.; Wang, Y.; Wu, W.; Yu, G.; Yan, S.; Wang, C.; Hu, W.; Liu, Y.; Zhu, D. High-Performance Transistor Based on Individual Single-Crystalline Micrometer Wire of Perylo[1,12-b,c,d]thiophene. *J. Am. Chem. Soc.* **2007**, *129*, 1882.

(136) Lin, Y.; Fan, H.; Li, Y.; Zhan, X. Thiazole-based organic semiconductors for organic electronics. *Adv. Mater.* **2012**, *24*, 3087, 3081.

(137) Pang, H.; Vilela, F.; Skabara, P. J.; McDouall, J. J. W.; Crouch, D. J.; Anthopoulos, T. D.; Bradley, D. D. C.; de Leeuw, D. M.; Horton, P. N.; Hursthouse, M. B. Advantageous 3D Ordering of π-Conjugated Systems: A New Approach Towards Efficient Charge Transport in any Direction. *Adv. Mater.* **2007**, *19*, 4438.

(138) Ando, S.; Murakami, R.; Nishida, J.-i.; Tada, H.; Inoue, Y.; Tokito, S.; Yamashita, Y. n-type organic field-effect transistors with very high electron mobility based on thiazole oligomers with trifluoromethylphenyl groups. *J. Am. Chem. Soc.* **2005**, *127*, 14996.

(139) Ando, S.; Nishida, J.-i.; Tada, H.; Inoue, Y.; Tokito, S.; Yamashita, Y. High performance n-type organic field-effect transistors based on pi-electronic systems with trifluoromethylphenyl groups. *J. Am. Chem. Soc.* **2005**, *127*, 5336.

(140) Kumaki, D.; Ando, S.; Shimono, S.; Yamashita, Y.; Umeda, T.; Tokito, S. Significant improvement of electron mobility in organic thin-film transistors based on thiazolothiazole derivative by employing self-assembled monolayer. *Appl. Phys. Lett.* **2007**, *90*, 053506.

(141) Hinsberg, O. Ueber mehrgliedrige stickstoffhaltige Ringsysteme. *Justus Liebig's Ann. der Chemie* **1901**, *319*, 257.

(142) Miao, Q.; Nguyen, T. Q.; Someya, T.; Blanchet, G. B.; Nuckolls, C. Synthesis, assembly, and thin film transistors of dihydrodiazapentacene: An isostructural motif for pentacene. *J. Am. Chem. Soc.* **2003**, *125*, 10284.

(143) Tang, Q.; Liang, Z.; Liu, J.; Xu, J.; Miao, Q. N-heteroquinones: quadruple weak hydrogen bonds and n-channel transistors. *Chem. Commun. (Camb).* **2010**, *46*, 2977.

(144) More, S.; Bhosale, R.; Choudhary, S.; Mateo-Alonso, A. Versatile 2,7-substituted pyrene synthons for the synthesis of pyrene-fused azaacenes. *Org. Lett.* **2012**, *14*, 4170.

(145) Takenaka, N.; Sarangthem, R. S.; Captain, B. Helical-Chiral Pyridine N-Oxides, a New Family of Asymmetric Catalysts. *Angew. Chem. Int. Ed.* **2008**, *47*, 9708.

(146) Yang, Y.; da Costa, R. C.; Fuchter, M. J.; Campbell, a. J. Circularly polarized light detection by a chiral organic semiconductor transistor. *Nat. Photonics* **2013**, *7*, 634.

(147) Law, K. Y. Organic photoconductive materials: recent trends and developments. *Chem. Rev.* **1993**, *93*, 449.

(148) Zhao, H.; Jiang, L.; Dong, H.; Li, H.; Hu, W.; Ong, B. S. Influence of intermolecular N-H...pi interactions on molecular packing and field-effect performance of organic semiconductors. *Chemphyschem* **2009**, *10*, 2345.

(149) Li, Y.; Wu, Y.; Gardner, S.; Ong, B. S. Novel Peripherally Substituted Indolo[3,2-b]carbazoles for High-Mobility Organic Thin-Film Transistors. *Adv. Mater.* **2005**, *17*, 849.

2

Tuning the Electronic Properties of Poly(thienothiophene vinylene)s via Alkylsulfanyl and Alkysulfonyl Substituents

In this chapter, all five of the design strategies discussed in Chapter 1 are utilized to design low band gap polymers for solar cells. A vinylene spacer group is adopted to ensure a planar conjugated backbone. The thienothiophene monomer unit is chosen for its fused aromatic structure, which lowers BLA and promotes π–π stacking in the solid-state. Sulfur heteroatoms are incorporated as heterocycles in the thienothiophene core and as substituents in alkylsulfanyl and alkylsulfonyl side chains. The electronic effects of the substituents are tuned via the oxidation of alkylsulfanyl to alkylsulfonyl. The role of the substituents in the supramolecular ordering of the materials is also explored in the crystal analysis of model dimers. Crystal analysis allows us to determine whether the substituents' sulfur atoms form beneficial S···S contacts. Finally donor–acceptor polymers are synthesized through the copolymerization of thienothiophene monomer units bearing alkylsulfanyl or sulfonyl substituents.

Reprinted with permission from: Schneider, J. A.; Dadvand, A.; Wen, W.; Perepichka, D. F. *Macromolecules* **2013**, *46*, 9231–9239. Copyright (2013) American Chemical Society

2.1 Abstract

The use of alkylsulfanyl and alkylsulfonyl side chains are demonstrated to be a useful synthetic strategy for tuning the electronic properties of organic semiconductors, as shown in thienothiophene vinylene polymers. By changing the oxidation state of sulfanyl to sulfonyl, we lower the HOMO and LUMO energy levels of our substituted polymers, as well as enhance their fluorescence. Fine-tuning of the energy levels was achieved by combining sulfanyl and sulfonyl substituted thienothiophene monomers through random polymerization, yielding polymers with low-band gaps (1.5 eV) yet benefiting from a structurally uniform conjugated backbone. The effects of these functional side chains are presented through DFT calculations, UV-vis, fluorescence, and electrochemical measurements, as well as crystallographic analysis of sulfanyl substituted oligomers. The semiconducting properties of the new polymers are studied in OFET and OPV devices.

2.2 Introduction

Thiophene-based conjugated polymers are important semiconducting materials with widespread applications in organic light-emitting diodes (OLEDs), field-effect transistors (OFETs), and photovoltaic solar cells (OPVs).[1] Polythiophenes are now ubiquitous in the field of organic semiconductors since they are easily functionalized and show great charge transport properties. Poly(3-hexylthiophene) (P3HT) for example, has become the benchmark donor material for bulk heterojunction solar cells, though its efficiency is limited by a relatively large band gap (Eg = 1.9 eV) and high HOMO level (–5.1 eV).[2]

Since P3HT, thiophene-based polymers have been tirelessly modified to create new high performance materials. The dominant approach is incorporating electron-deficient monomer units with electron-rich thiophene to create donor-acceptor systems that promote intrachain charge transfer, lowering the band gap of the polymer.[3] This, however, requires the synthesis of two different monomer units, complicates the structure-properties relationships and creates a polarization along the conjugation backbone. Instead of altering the backbone,

a polymer's energy levels can be directly tuned through substituents, a method that is underutilized in conjugated polymer chemistry.

For example, poly(3-alkoxythiophene) showed a smaller band-gap (1.60 eV) than P3HT due to increased rigidity ascribed to S$\cdots$O interactions, but the electron donating effect of the alkoxy group raised the HOMO level (–4.47 eV).[4] Poly(3-cyano-4-hexylthiophene), conversely, was found to have a lower HOMO level (–6.1 eV), but a larger band gap (2.3 eV).[5] Substituents such as fluorine,[6] fluoroalkyl,[7] thienyl,[8] dicyanoethene,[9] alkoxy groups,[10] nitro groups[11] and esters[12] have also been explored in polythiophenes. Alkylsulfanyl substituents are of particular interest for several reasons: the van der Waals radius of sulfur (0.18 nm) is less than that of –CH_2 (0.20 nm) which slightly reduces steric strain compared to alkyl substituents;[13] they impart solubility to the polymer; and, in polythiophenes, they can act as mild electron acceptors, lowering the HOMO levels.[14][15] Furthermore, their electron withdrawing effect can be tuned by changing the oxidation state of sulfur from sulfanyl (–SR) to sulfoxyl (–SOR) or sulfonyl (–SO_2R). Sulfonyl groups have been shown to increase fluorescence in polymers[16] and oligomers.[17] They were also employed as electron withdrawing substituents in donor-acceptor conjugated polymers for OPV,[18] but there exists no detailed or comparative studies of their electronic effects in semiconducting materials.

We were interested in a comparative analysis of the effect of alkylsulfanyl and alkylsulfonyl substituents on the electronic properties and behavior of conjugated polymers in semiconducting device applications. We have chosen poly(thieno[3,2-*b*]thiophene vinylene) as the conjugated backbone, taking into consideration relative structural simplicity, planarity, and a low expected band gap. Thieno[3,2-*b*]thiophene's (TT) fused unit fosters electron delocalization by reducing the bond length alternation (compared to simple thiophene).[19] Owing to the 180° coupling geometry of TT (cf. $\approx$150° for thiophene), its polymers strongly prefer a linear rod-like structure and show increased crystallinity and charge mobilities.[20][21] A vinylene spacer reduces the twist caused by repulsions between substituents and "dilutes" the aromatic nature of the TT moieties. Both of these effects promote electron delocalization and shrink the band-gap of the polymer. In this paper we report the synthesis and spectroscopic, structural and device characterization

of poly(3,6-dialkylsulfanylthieno[3,2-*b*]thiophene vinylene), **S-PTTV**, its oxidized derivative poly(3,6-dialkylsulfonylthieno[3,2-*b*]thiophene vinylene), **SO_2-PTTV**, and the random copolymer incorporating both sulfanyl and sulfonyl units, **S/SO_2-PTTV**. Comparing their properties to the model unsubstituted **H-PTTV** and similarly substituted polymer without vinylene linker (**S-PTT**) we explore the complex effect that substituents play in these conjugated systems. Two dimers **S-2TTV** and **SO_2-2TTV** were also synthesized to understand the substituent effects in a simplified system.

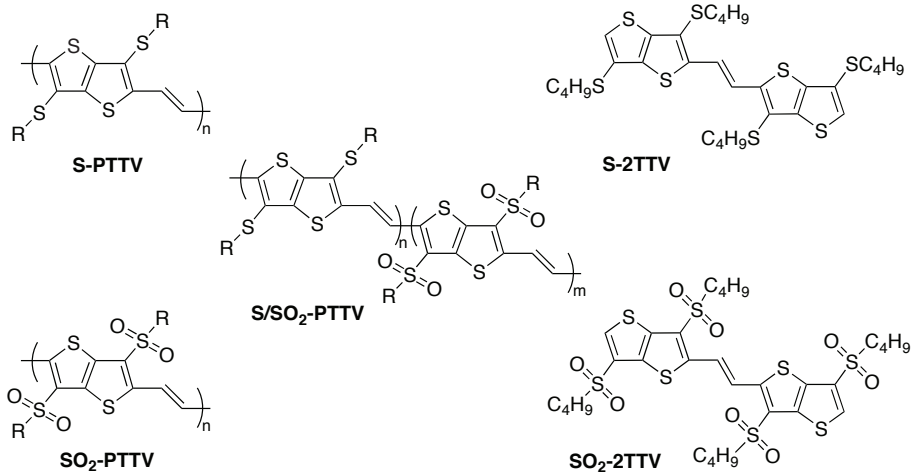

Fig. 2.1.: Polymer structures reported or discussed in this chapter.

2.3 Results and Discussion

2.3.1 Theoretical Calculations

Density functional theory (DFT) calculations at the B3LYP/6-31G(d) level were performed on a series of substituted TT oligomers (n=1, 2...7) as well as for the infinite polymers, under periodic boundary conditions (PBC). The side chains were modeled with methyl groups. The HOMO, LUMO, and band gap values of the corresponding polymers, along with optimized dihedral angles are listed in Table 2.1. The model polymers **S-PTT**, **H-PTTV** and **P3MT** (a model of regioregular poly(3-alkylthiophene)[19]) were not experimentally studied in this paper, but are given for comparison.

Tab. 2.1.: Calculated Energy Levels and Geometry of the Polymers.

	HOMO (eV)	LUMO (eV)	E_g (eV)	dihedral (deg)[a]
P3MT	–4.31	–2.32	1.99	0
H-PTTV	–4.53	–2.74	1.79	0
S-PTT	–5.45	–2.23	3.22	55
	–4.72	–2.79	1.93	0[b]
S-PTTV	–4.67	–2.93	1.74	1
SO_2-PTTV	–5.60	–3.76	1.84	10
S/SO_2-PTTV[c]	–5.15	–3.34	1.81	4

[a] The dihedral angle between the thiophene ring and the next conjugated unit.
[b] The dihedral angle is restrained to 0°, which destabilizes the structure by 1.35 kcal/mol.
[c] PBC calculations of an alternating polymer structure (AD)n. The block-copolymer (AADD)n showed a 0.06 eV lower band gap: HOMO = –5.12 eV; LUMO = –3.37 eV.

As expected based on the behavior of sulfanyl-substituted oligothiophenes,[22] the alkyl-sulfanyl groups cause a large twist (55°) in poly(thienothiophene) **S-PTT**, disrupting the conjugation. Consequently, a very large band gap of 3.22 eV is predicted for this polymer by DFT. This is higher than the ≈2.2 eV optical band gap reported[13] for alkylated **S-PTT** in solution (in the solid state the band gap was further lowered to 1.74 eV). These observations suggest planarization of the polymer chain (see below); indeed, calculations of a fully planarized **S-PTT** polymer predict a band gap of 1.93 eV. The steric repulsions of the substituents is removed by separating the TT units with a vinylene spacer. Therefore, **S-PTTV** is planar and is predicted to have a much smaller band gap of 1.74 eV. According to calculations, the sulfonyl substituents in **SO_2-PTTV** only cause a small twist (10°) in the polymer's backbone, increasing the band gap by 0.10 eV. Both substituents induce an electron-withdrawing effect, lowering both frontier orbitals by ≈0.15 eV for **S-PTTV** and ≈1.0 eV for **SO_2-PTTV**, compared to unsubstituted H-PTTV (Figure 1). Lower HOMO levels are beneficial for increased stability in air and are expected to produce larger open circuit voltages (V_{OC}) in OPVs.[23] At the same time, the substituents do not significantly affect the π-conjugation along the chains. The trends of MO energy vs. reciprocal length of oligomers (Figure 2.2) are shifted along the energy axis, but are otherwise nearly superimposable. Also, the topology of the HOMO and LUMO of the **S-PTTV**, **SO_2-PTTV** homopolymers

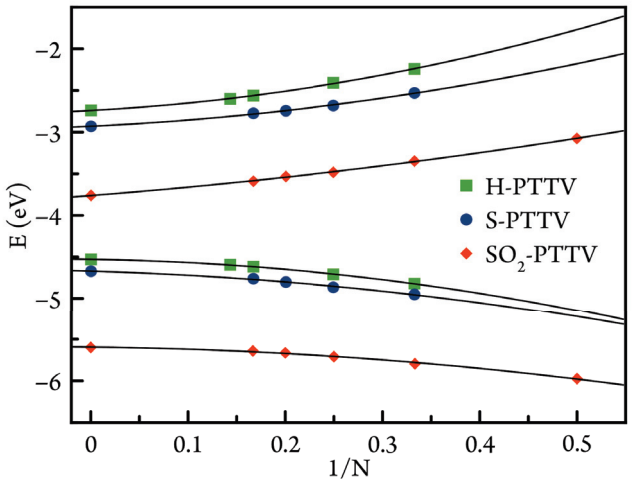

Fig. 2.2.: Calculated HOMO and LUMO energy levels of oligomers and infinite chains modeled with PBC. (N = number of repeat units.)

and the (alternating) copolymer **S/SO_2-PTTV** are nearly superimposable (Figure 2.3). Thus, the donor-acceptor motif should not alter the electron delocalization along the backbone or the intermolecular orbital coupling. The rigidity of the conjugated backbone is an important factor defining the material properties of polythiophenes and related structures.[24] DFT predicts a very shallow rotation barrier (≈1.5 kcal/mol) for both TT-TT and SO_2TT-V connections (Figure 2.4). This means that non-planar **S-PTT** could planarize due to solid state packing forces (as was in fact observed[13]). Similarly, **SO_2-PTTV**, predicted to be nearly planar in the gas phase, could adopt a twisted conformation under external factors (solvation, inter-chain interactions). In fact, the energy penalty for twisting the TT/vinylene dihedral angle by 50° is smaller than RT (0.6 kcal/mol at room temperature). In contrast, a much larger rotation barrier (7.9 kcal/mol per TT/vinylene connection), which can be considered a stabilization of the planar conformation, is predicted for **S-PTTV**. This can be attributed to the smaller size of the alkylsulfanyl group and perhaps to weak attractive S···H interactions with the vinylene protons (the calculated S···H distance is 2.80 Å).

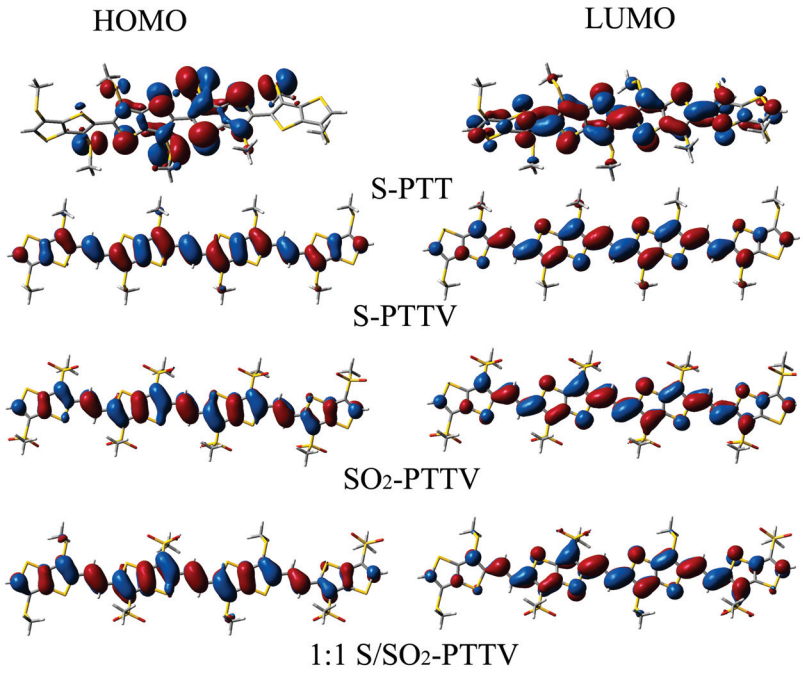

Fig. 2.3.: DFT-optimized structures of tetramers showing the topology of HOMOs and LUMOs.

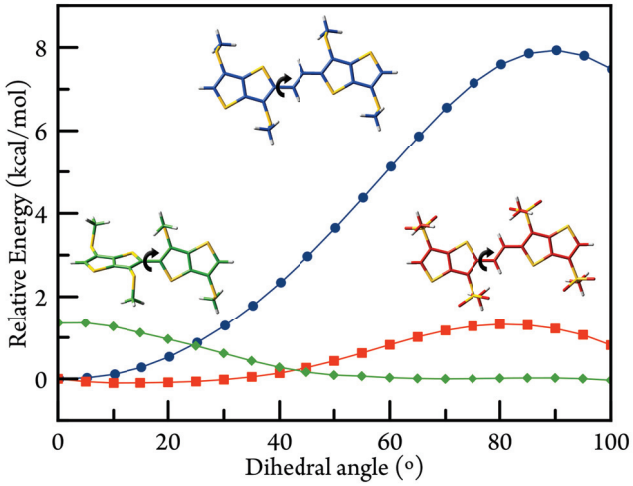

Fig. 2.4.: Energy barrier of rotation of thiophene/vinylene dihedral angles for **S-2TT** (green), **S-2TTV** (blue), **SO_2-2TTV** (red).

2.3.2 Synthesis

Bisalkylsulfanyl-TT **2.1** was obtained from 3,6-dibromothieno[3,2-*b*]thiophene[25] by stepwise lithiation, followed by quenching of the carbanion intermediate with dialkyldisulfide (Scheme 2.1).[26] Brominating **2.1** with NBS yielded monomer **2.2**. We note that partial oxidation of the sulfanyl chains was occasionally observed, unless the excess of NBS is quenched before an aqueous workup. Full oxidation of the alkylsulfanyl substituents into alkylsulfonyl was achieved with meta-chloroperoxybenzoic acid (m-CPBA) to give monomer **2.3**. Polymers were synthesized through the Stille polycondensation of monomers

Scheme 2.1: Synthesis of Monomers **2.2** and **2.3**

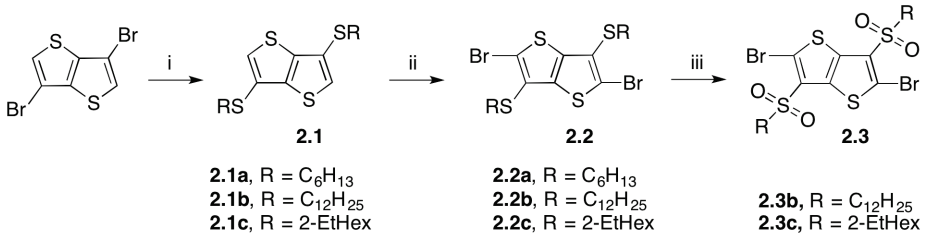

2.1

2.1a, R = C_6H_{13}
2.1b, R = $C_{12}H_{25}$
2.1c, R = 2-EtHex

2.2

2.2a, R = C_6H_{13}
2.2b, R = $C_{12}H_{25}$
2.2c, R = 2-EtHex

2.3

2.3b, R = $C_{12}H_{25}$
2.3c, R = 2-EtHex

(i) [1 eq nBuLi, 1 eq RS-SR]x2, Et_2O, –78°C to 20°C; (ii) NBS, $CHCl_3$, –5°C to 20°C, $Na_2S_2O_3$ work-up; (iii) m-CPBA, $CHCl_3$, 0°C to 20°C.

2.2 and **2.3** with (E)-1,2-bis(tributylstannyl)ethene followed by end-capping with an excess of the stannylated mono-mer, followed by iodobenzene (Scheme 2.2). The polymers were isolated by precipitation into MeOH and washed in a Soxhlet apparatus with EtOH, acetone, hexane, and finally extracted with chloroform and chlorobenzene. **S-PTTV** was obtained as a dark, shiny material. Hexylsulfanyl **S-PTTVa** precipitated during the reaction and displayed poor solubility, signaling the need for longer side chains. Both dodecyl-substituted **S-PTTVb** and branched 2-ethyhexyl substituted **S-PTTVc** showed high MWs, but only **S-PTTVc** was soluble enough for film spin-coating. **SO_2-PTTV** gave a lower percent yield of soluble material and only low MWs could be achieved for both **SO_2-PTTVb** and **SO_2-PTTVc**. Solid state ^{13}C NMR confirmed the structure of the insoluble fractions (see Supporting Information). This low solubility is likely attributable to dipole-dipole interactions of the sulfonyl substituents.

Scheme 2.2: Polymerization Reaction

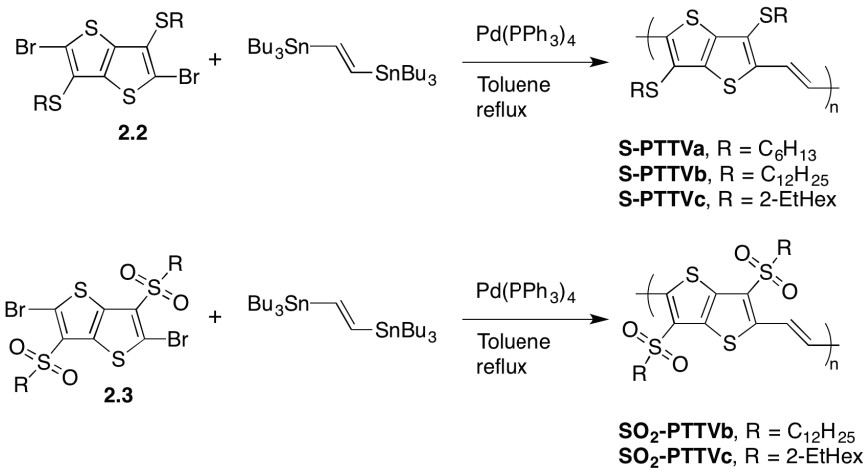

Random copolymers have only recently been applied in OPVs, but they are easy to synthesize and can show increased solubility and efficiencies.[27] It is also possible to quickly realize a series of random copolymers by simply varying the feed ratios and thereby quantify the effect of a certain unit.

S/SO$_2$-PTTV was synthesized by the random copolymerization of a mixture of monomers **2.2** and **2.3** with (E)-1,2-bis(tributylstannyl)ethene. The copolymer was soluble, with a MW that averaged those of **S-PTTV** and **SO$_2$-PTTV** (Table 2.2). The relative fraction of the sulfanyl/sulfonyl substituted TT units can be tuned by varying the ratio of the starting monomers and easily quantified by ^{1}H NMR. A 1:1 and 1:2 feed ratio of monomers **2.2**:**2.3** gave measured ratios of 1:0.88 and 1:1.6, respectively. Along with the lower MW of **SO$_2$-PTTV**, this indicates a reactivity preference for monomer **2.2** over **2.3**, likely due to the steric effect of the bulkier sulfonyl group and/or coordination to palladium in the catalytic complex.[28]

To gain insight into the solid-state packing of the substituted TTV systems, we synthesized two model dimers by the Stille coupling of monobrominated TTs **2.4** and **2.5** with (E)-1,2-bis(tributylstannyl)ethene to afford dimers **S-2TTV** and **SO$_2$-2TTV**, respectively. Monobromination of **2.1d** was accomplished by lithiation (nBuLi) followed by treatment with carbon tetrabromide. **2.4** was then oxidized to **2.5** as described above (Scheme 2.3). Single crystals of dimer **S-2TTV** were prepared as orange needles from a mixture of ethanol,

Tab. 2.2.: Molecular Weights, Polydispersities, and UV-Vis Absorption of Synthesized Polymers.

	MW (kg/mol)	PDI	yield (%)	$\lambda_{max/onset}$ soln (nm)	$\lambda_{max/onset}$ film (nm)	E_g^{opt} film[c] (eV)	fwhm (cm^{-1}) soln/film
S-PTTVa	13.0	1.9	73[a]	544/697	580/760	1.63	
S-PTTVb	43.4	1.3	62[b]	607/730	585/770	1.61	4450/5980
S-PTTVc	42.7	2.2	62[b]	610/740	608/765	1.62	4540/6250
SO_2-PTTVb	6.3	1.1	70[b]	486/640	471/680	1.82	4680/5130
SO_2-PTTVc	7.6	1.3	41[b]	517/625	529/720	1.72	4810/5810
S/SO_2-PTTV-1:1	27.0	2.1	75[b]	597/760	594/810	1.53	4770/6540
S/SO_2-PTTV-1:2	12.9	2.5	54[b]	561/748	547/755	1.64	5340/6190

[a] Total yield of the MeOH precipitated product.
[b] Yield of polymer fraction(s) soluble in $CHCl_3$ and PhCl.
[c] $E_g^{opt} = 1240/\lambda_{edge}$ of film.

hexane, and toluene, and were subjected to X-ray analysis (Figure 2.5). In accordance with

Scheme 2.3: Synthesis of Model Dimers

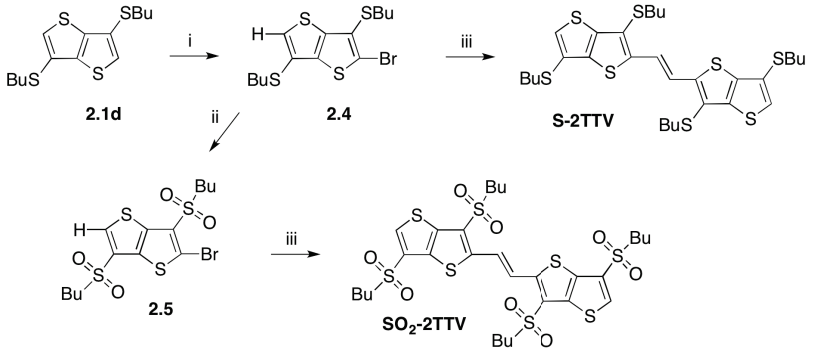

(i) 1 eq nBuLi, 1 eq CBr_4, Et_2O, –78°C to 20°C; (ii) mCPBA, $CHCl_3$, 0°C to 20°C; (iii) 0.5 eq of $Bu_3SnCH{=}CHSnBu_3$, $Pd(PPh_3)_4$, 100°C.

the DFT calculations, the conjugated backbone of **S-2TTV** is nearly planar (TT-vinylene dihedral angle = 5.2°). The crystals formed a slipped-stacked structure with an interplane distance of 3.50 Å(Figure 2.5a). Importantly, the "inner" alkylsulfanyl substituents bend out of the plane at ≈ 80°, thus protruding above and below the aromatic plane. This confirms the DFT prediction that placing this substituent in plane destabilizes the structure by ≈4 kcal/mol, compared to the optimal 83° twisted geometry (Figure S2.2). Similar out-of-plane

geometry and even larger planarization penalty was calculated for **SO_2-2TTV** (Figure S2.2). To accommodate the out-of-plane protruding substituents, the molecules have to slip vs one another along the short molecular axis, which significantly limits $\pi \cdots \pi$ overlap between the TT units (Figure 2.5b).

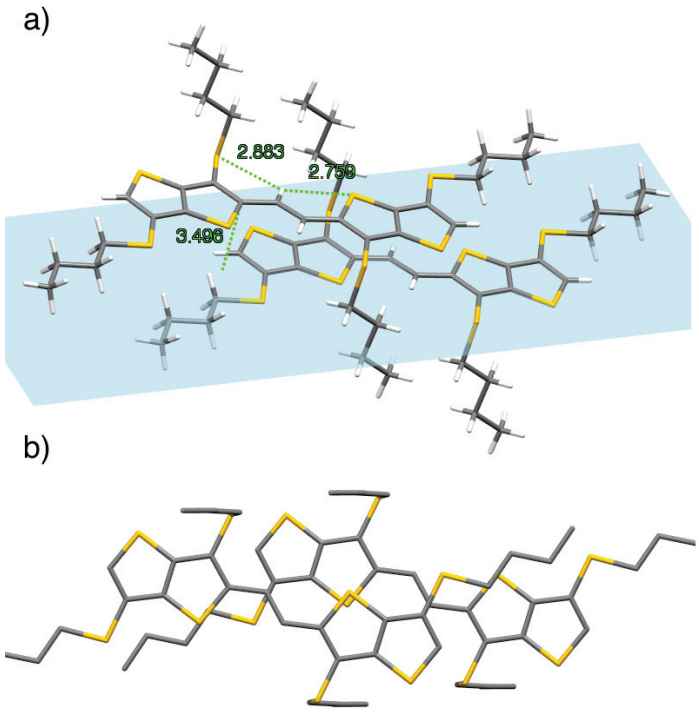

Fig. 2.5.: Crystal structure of **S-TTV** showing (a) S$\cdots$H distances with vinylene hydrogen and the interplane distance and (b) the lack of π-overlap between TT units.

2.3.3 Optical Properties

The UV-vis absorption spectra of the prepared polymers were studied in chloroform solution and in thin films (Figure 2.6, Table 2.2). All the polymers displayed broader absorption spectra and red-shifts of the band edge in the solid state compared to solution. The spin-coated films are highly reflective, with characteristic metallic luster (Figure 2.6b). The variation of the solution absorption band with different alkyl side-chains (**S-PTTVa/b/c**) are in line with the changes in molecular weights of these polymers. Interestingly, very little difference was observed in the solid state. The absorption of solid **S-PTTVc**, λedge = 765 nm (Eg = 1.62 eV) is red-shifted from analogous alkyl-substituted poly(3,6-dihexyl)thieno[3,2-

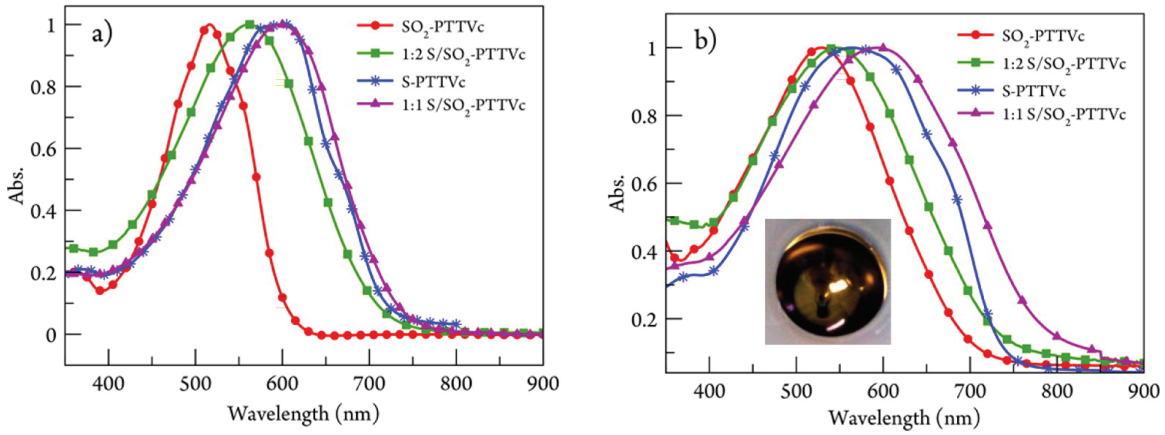

Fig. 2.6.: Absorption spectra of polymers in (a) chloroform solutions and (b) thin films. The Inset shows a flask coated in a film of **S-PTTVc**.

b]thiophene vinylene **C_6-PTTV** which showed a band edge at 700 nm (1.77 eV)[29] and from poly(3,6-dioctylsulfanylthieno[3,2-*b*]thiophene), **SC_8-PTT**, whose band edge appears at 713 nm (1.74 eV).[13] Evidently, both the sulfanyl substituents and the vinylene spacer play a part in shrinking the band gap.

Replacing sulfanyl sides chains with sulfonyl (**SO_2-PTTV**) results in a ≈0.1 eV increase of the optical band gap (720 nm, 1.72 eV), as predicted by DFT (Table 2.1). This increase should in part be attributed to the low MW[30] of **SO_2-PTTV** (Table 2.2) although its lower rigidity (Figure 2.4) should also play a role and must be responsible for the unexpectedly large band gap in solution (1.98 eV). **SO_2-PTTV** displays the smallest increase in the FWHM between solution and solid state, which suggests a weakened intermolecular exciton coupling caused by the sulfonyl substituents.

Copolymer **S/SO_2-PTTV-1:1** retains the broad absorption (FWHM=6540cm^{-}1) of **S-PTTV** and shows a further lowered band gap of 1.53 eV, that can be attributed to the donor-acceptor interactions between sulfanyl and sulfonyl-substituted units. The balance between the latter appears important as the increased amount of –SO_2 substituted TT units in **S/SO_2-PTTV-1:2** increases the band gap (1.64 eV), possibly due to disrupted solid-state packing (cf. small $\Delta FWHM_{film\text{-}sol}$ = 850 cm^{-1}, Table 2.2), but also due to a lower MW.

Comparing the absorption of the dimers **S-2TTV** and **SO_2-2TTV**, unperturbed by the uncertainty of polymer lengths, supports the above observations. Their 0-0 transitions (450

and 444 nm, determined as a crossing of the absorption and emission curves) are 2.76 eV and 2.79 eV for **S-2TTV** and **SO_2-2TTV**, respectively (Figure 2.7). DFT calculations predicted somewhat higher HOMO-LUMO gaps of 3.14 eV and 3.08 eV, respectively. The sulfanyl-substituted **S-2TTV** showed a more pronounced vibronic splitting of the absorption band, as expected based on its predicted rigidity (Figure 2.4). Generally, oligo- and polythiophenes

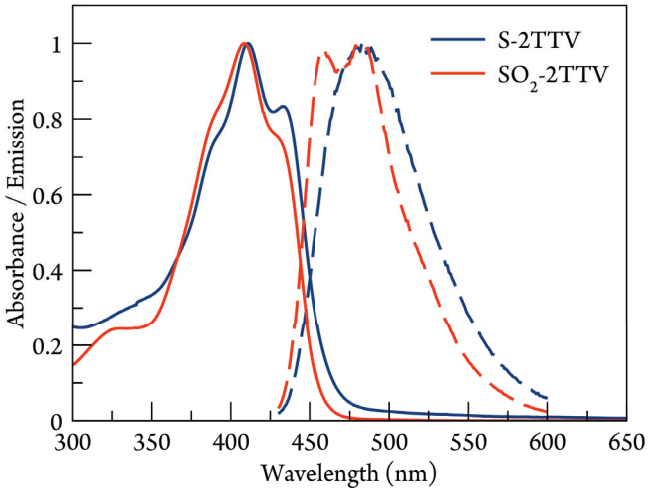

Fig. 2.7.: Absorption (—) and emission (- -) spectra of **S-2TTV** and **SO_2-2TTV**.

are weak-to-moderate emitters, a fact attributed to the heavy atom effect of sulfur enhancing the intersystem crossing.[31] A majority of thienylenevinylene oligomers and polymers and their derivatives are almost completely nonemissive. We have earlier reported a dramatic enhancement of fluorescence in thienylene-vinylene oligomers and polymers upon the introduction of sulfanyl side chains, which was unexpected due to the additional sulfur atoms.[32] As a further surprise, we now observed that **S-PTTV** containing fused thienothiophene rings, is again nonemissive, although the model dimer **S-2TTV** exhibits a moderate emissivity (λ_{max} = 485 nm, PLQY = 15%, Figure 2.5). We could not find a good explanation for these variations, but we note that both alkyl-substituted PTTV (**C_6-PTTV**)[29] and alkylsulfanyl-substituted PTT (**SC_8-PTT**, PLQY = 26%)[13] are reported to show strong photoluminescence.

In line with previous reports,[16] oxidizing the sulfanyl group into sulfonyl enhances the photoluminescence. The dimer **SO_2-2TTV** shows a quantum yield three times larger (λ_{max} = 483nm, PLQY = 45%) than its sulfanyl analogue **S-2TTV** (Figure 6). Moderately strong

luminescence was also observed for **SO_2-PTTV** at λ_{max} = 585 nm (PLQY = 17%), but introducing sulfanyl-substituted units in the copolymer again quenches the luminescence, and only very weak emission at 690 nm was observed for **S/SO_2-PTTV-1:1** (see Supporting Information).

2.3.4 Electrochemical Properties

The redox behavior of the synthesized polymers was studied by cyclic voltammetry (CV) for thin films drop-casted on Pt electrodes (Figure 2.8, Table 2.3). All three polymers

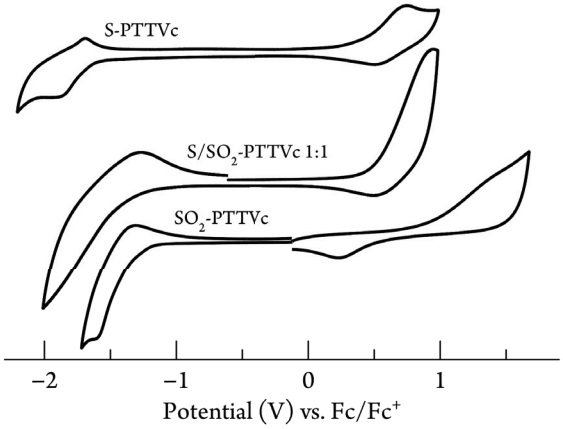

Fig. 2.8.: Cyclic voltammograms of synthesized polymers (0.1 M Bu_4NPF_6 / propylene carbonate as electrolyte; scan rate 0.1 V/s).

show reversible reduction (n-doping) and oxidation (p-doping) waves, except for the most electron-deficient **SO_2-PTTV**, which revealed a quasi-reversible oxidation (ie. corresponding cathodic peaks at much more negative potentials), indicating trapping of the positive charges.

Compared to the alkyl-substituted **C_6-PTTV**[29] the sulfanyl substituents show a moderate electron withdrawing effect, shifting the oxidation and reduction of **S-PTTV** by 0.08 eV and 0.20 eV, respectively (Table 2.3). A much larger shift is observed for sulfonyl-substituted polymer, **SO_2-PTTV** (0.67 V and 0.63 V shifts for oxidation and reduction, respectively). The random copolymers **S/SO_2-PTTV-1:1** and **S/SO_2-PTTV-1:2** show the electronic effects

Tab. 2.3.: Redox Potentials[a], HOMO-LUMO Levels[b], and Band Gaps[c] of Polymers Determined by CV of Thin Films.

	E_{red} (V)	E_{ox} (V)	LUMO (eV)	HOMO (eV)	E_g^{CV} (eV)
C_6-PTTV[29]	–1.83	0.24	–2.97	–5.04	2.07
S-PTTV	–1.63	0.32	–3.17	–5.12	1.95
SO_2-PTTV	–1.20	0.91	–3.60	–5.71	2.11
S/SO_2-PTTV-1:1	–1.37	0.50	–3.43	–5.30	1.87
S/SO_2-PTTV-1:2	–1.14	0.74	–3.66	–5.54	1.88

[a] All potentials reported versus Fc/Fc^+ in 0.1 M Bu_4NPF_6/propylene carbonate.
[b] Calculated from the onset of the oxidation and reduction potentials, assuming HOMO of Fc at –4.8 eV.[33]
[c] E_g^{CV} = HOMO – LUMO.

of both monomer units with reduction and oxidation onsets between those of **S-PTTV** and **SO_2-PTTV**, giving them the smallest electrochemical gaps at 1.87 eV and 1.88 eV, respectively.

2.3.5 Device Studies

S-PTTV and copolymer **S/SO_2-PTTV-1:1** were tested in OFETs and OPVs, but unfortunately **SO_2-PTTV** was not soluble enough to be spin cast into working devices.

Thin-film transistors were prepared from toluene solutions of the polymers spin-cast on Si/SiO_2 followed by the deposition of patterned Au electrodes. The output and transfer characteristics of the **S-PTTVc** transistor are shown in Figure 2.9. A rather low hole mobility of $\approx 1x10^{-5} cm^2/Vs$ was measured for **S-PTTVc**, and no further improvement was achieved upon annealing. The copolymer-based devices showed no transistor activity ($\mu_h < 10^{-7} cm^2/Vs$) and no n-channel activity (electron conductance) was observed for either polymers. This compares unfavorably with the reported OFETs based on **C_6-PTTV** with hole mobilities up to $1.9x10^{-2} cm^2/Vs$ (for annealed films, a 40× increase from unannealed). The out-of-plane protrusion of the side chains and the resulting poor overlap between TT units, as observed in the **S-2TTV** crystals, is likely the reason for poor transistor characteristics of these materials.

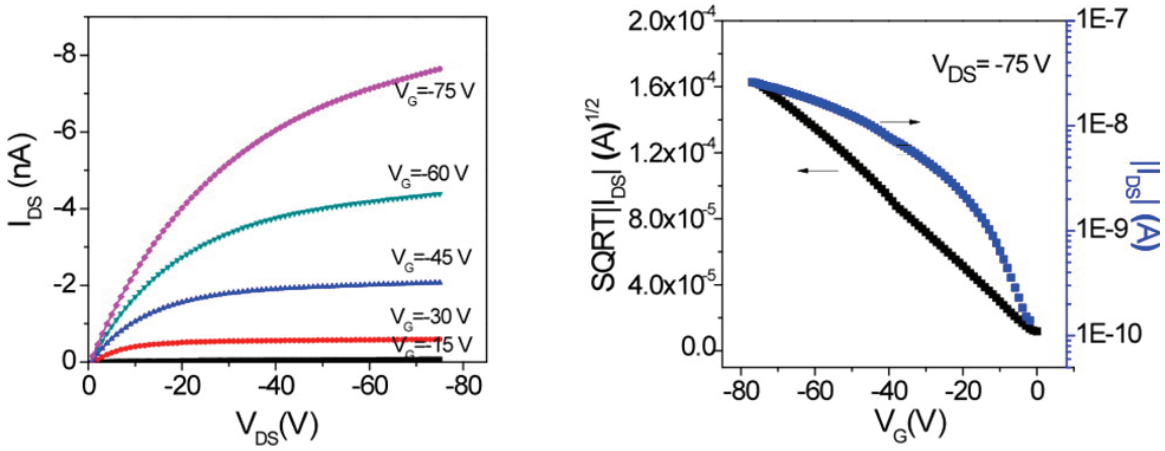

Fig. 2.9.: Output (left) and transfer (right) characteristics of transistors made from **S-PTTVc** ($\mu_h \approx 1x10^{-5}cm^2/Vs$).

Tab. 2.4.: Photovoltaic Properties of ITO/PEDOT:PSS/Polymer:PC_70BM (1:1)/Ca/Al Devices.

	$HOMO^{CV}$ (eV)	I_{SC} (mA/cm^2)	V_{OC} (V)	FF	PCE (%)
C_6-PTTV[29]	–5.0	1.27	0.60	0.37	0.28
S-PTTV	–5.12	3.16	0.68	0.37	0.79
S/SO_2-PTTV-1:1	–5.30	1.64	0.82	0.29	0.39
S/SO_2-PTTV-1:1 and 3% CN		4.46	0.70	0.27	0.84
S/SO_2-PTTV-1:2 and 0.5% DIO		4.07	0.66	0.29	0.78

Bulk-heterojunction solar cell devices from polymer:$PC_{70}BM$ blends were tested. Figure 2.10 shows the I-V curves of two of the polymers and the photovoltaic characteristics obtained are listed in Table 2.4.

S-PTTV displayed slightly higher open-circuit voltages (V_{OC}) than reported for **C_6-PTTV**, as is expected due to its lower HOMO level. The trend continues for **S/SO_2-PTTV-1:1**, which has a high V_{OC} of 0.8 V.

The performances of both the **S-PTTV** and **S/SO_2-PTTV-1:1** devices are limited by low short-circuit currents (I_{SC}) and fill factors (FF). This can be related to the low charge mobility seen in the transistor devices, although **C_6-PTTV**, that showed higher hole mobility in OFETs, produced even lower I_{SC} in analogous OPV devices. Poor mobilities mean more

chances for recombination at the interface before the hole and electron can diffuse away and increase the serial resistance which leads to the low FFs observed.[34] Similar results were obtained with Ca vs Al electrodes, so poor charge extraction at the electrode interface is unlikely to be the issue.

Preliminary optimizations attempts for **S/SO$_2$-PTTV-1:1** using chloronaphthalene (CN) and 1,8-diiodooctane (DIO) additives led to improvements in the current densities, but not to FFs. The best I_{SC} (4.5 mA/cm^2) was achieved for devices with 3% CN additive, which is still half the I_{SC} seen in analogous P3HT devices without additives. The fact that the FFs did not increase suggests that while the additives may reduce the phase segregation, thereby improving the exciton dissociation, the larger interface area also increases charge recombination, leaving the low mobility of the polymers as the limiting factor.

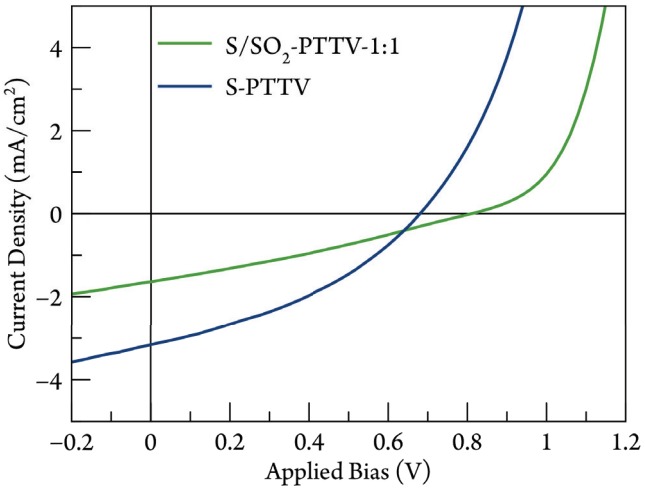

Fig. 2.10.: Current-voltage characteristics of bulk-heterojunction cells of **S/SO$_2$-PTTV-1:1** and **S-PTTV** in 1:1 PC$_{70}$BM.

2.4 Conclusion

We have reported new thienothiophene vinylene polymers whose electronic properties can be tuned by changing the oxidation state of the sulfur-containing side-chains. The sulfanyl and sulfonyl substituents show moderate and strong electron-withdrawing effects and their combination in random copolymers is a means to fine-tune the energy levels and achieve

a low band gap (1.5 eV) without affecting the uniformity of the conjugated backbone. Bulk-heterojunction photovoltaics based on the **S/SO_2-PTTV-1:1** random copolymer (with $PC_{70}BM$) displayed high V_{OC} of 0.8 V, but suffered from low I_{SC} due to poor charge mobility. The latter was attributed to poor of $\pi - \pi$ overlap between TT units caused by out-of-plane substituents, as corroborated by X-ray analysis. The oxidation state of the side chains controls the emissive properties of these materials; sulfonyl groups demonstrated dramatically increased fluorescence in dimers (PLQY of 45% vs 15% for sulfanyl) and polymers (PLQY of 17% vs ≈0% for sulfanyl).

Introducing a sulfur atom in various oxidation states (sulfanyl/sulfonyl) between the alkyl chain and the conjugated backbone represents a simple and predictable method for tuning the electronic and optical properties of organic semiconductors. This method can be a welcome alternative to designing more complex donor-acceptor motifs for new polymeric semiconductors.

2.5 Experimental Section

2.5.1 Polymer Characterization and Device Fabrication

Molecular weight measurements of the polymers were performed on a GPC PL 50 in THF at 30°C. UV/vis absorption and photoluminescence spectra were measured in $CHCl_3$ with a JACSO V670 UV–vis–NIR spectrometer and a Varian Eclipse Fluorometer, respectively. The fluorescence quantum yields of the polymers were determined versus cresyl violet in MeOH (PLQY = 0.54), while the quantum yields of the dimers were determined versus fluorescein in 0.1 M NaOH (PLQY = 0.79). Cyclic voltammetry was performed on a CH670 potentiostat from CH-Instruments in a three-electrode cell using a propylene carbonate solution of 0.1 M $(TBA)PF_6$ as an electrolyte, at scan rates of 100 mV s^{-1}. Pt disk and Pt wire were used as the working and counter electrodes, respectively, and a Ag/AgCl or $Ag/AgNO_3$ electrode was used as the reference. All potentials were adjusted vs ferrocene (internal standard).

OPV devices were prepared on ITO-coated glass substrates that had been cleaned with detergent and rinsed by sonicating in deionized water, acetone, and finally isopropanol for 20 min each. PEDOT:PSS (Clevios P Al 4083) was spin-cast onto the ITO-coated glass at 4,000 rpm for 30 seconds and then baked at 140°C for 10 minutes. Solutions of $PC_{71}BM$ and polymer in 1:1 ratios and 1 mg/mL concentrations in chlorobenzene were prepared by stirring overnight at 70°C under inert atmosphere. The photoactive layer was spin-cast at various rates for 60 seconds each. Next, thermal evaporation of 5 nm of Ca and/or 100 nm

of Al was performed to form the top contacts. Standard solar cell characterizations were carried out in a nitrogen environment under simulated 100 mW/cm^2 AM1.5G irradiation from a 300 W Xe arc lamp with an AM 1.5 global filter. All measurements were repeated on at least 4 devices.

2.5.2 Computational Methods

DFT calculations were performed using the Gaussian 09W program at the B3LYP level with a 6-31G(d) basis set.[35] All geometry optimization calculations were started with the substituents in the anti-orientation, at 90° angles to the TT plane. The dihedral angles reported were averaged from internal TT–vinylene dihedrals in geometry-optimized oligomers. The PBC calculation for polymer were performed at the same level, with various unit cell size to enable different dihedral angles (one monomer per unit cell necessarily affords a planar polymer; two monomers allow the optimization of the dihedral angle, with alternating clock-wise/anticlockwise rotation; six monomers per units cell allows helical twisting with 60° pitch, close to the optimized 55° for **S-PTT**). The energy of rotation of a TT unit vs the vinylene spacer was performed on optimized dimers while freezing the dihedral angle to the second TT unit. The energy diagrams of full, 360° rotations of substituents were calculated from optimized dimers with both TT–vinylene dihedral angles frozen.

2.5.3 Synthesis

All lithiation and polymerization reactions were performed under inert atmosphere, with flame-dried glassware and anhydrous solvents. 3,6-dibromothieno[3,2-*b*]thiophene was synthesized in four steps following literature procedures.[25][36]

3,6-Bis(hexylsulfanyl)thieno[3,2-*b*]thiophene (2.1a)
n-BuLi (0.60 mL, 1.5 mmol) was added at −75°C to a stirring solution of 3,6-dibromothieno[3,2-*b*]thiophene (0.379 g, 0.127 mmol) in diethyl ether (20 mL) and the reaction mixture stirred for 1 h. Dihexyldisulfide (0.42 g, 1.4 mmol) was added and the reaction was allowed to warm to room temperature overnight. The next day the reaction mixture was cooled back to −75°C and a second dose of n-BuLi added. After an hour, dihexyldisulfide was added and the reaction was allowed to warm to room temperature and stirred overnight a second time. The reaction was then quenched with H_2O (20 mL), the organics were washed with NH_4Cl solution (20 mL), H_2O (2 × 20 mL), then dried over Na_2SO_4, and concentrated in vacuo. The crude oil was then distilled in a Kugelrohr apparatus (170°C, 0.16 bar) to yield pure **2.1a** as a colorless oil (0.319 g, 67%). ^{1}HNMR (acetone-d_6, 400 MHz): δ 7.54 (s, 2H), 2.99 (t, J = 7.2 Hz, 4H), 1.63 (m, 4H), 1.44 (m, 4H), 1.27 (m, 8H), 0.87 (t, J = 6.8 Hz, 6H). ^{13}CNMR ($CDCl_3$, 125 MHz): δ 141.2, 127.0, 125.0, 34.6, 31.3, 29.6, 28.2, 22.5, 14.0. HR-MS (ESI): m/z = 373.1150 [M+1] (calcd for $C_{18}H_{29}S_4$, m/z = 373.1147).

3,6-Bis(dodecylsulfanyl)thieno[3,2-*b*]thiophene (2.1b)
The compound was synthesized in the same manner as described for **2.1a**. Kugelrohr distillation was not effective for separation, so the product was recrystallized from pentane in a −18°C in freezer to give tan crystals in a 30% yield. ^{1}HNMR (acetone-d_6, 400 MHz): δ

7.54 (s, 2H), 3.00 (t, J = 7.2 Hz, 4H), 1.63 (m, 4H), 1.44 (m, 4H), 1.27 (m, 16H), 0.88 (t, J = 6.8 Hz, 6H). ^{1}HNMR ($CDCl_3$, 400 MHz): δ 7.24 (s, 2H, overlaps with $CHCl_3$), 2.90 (t, J = 7.6 Hz, 4H), 1.61 (m, 4H), 1.40 (m, 4H), 1.24 (m, 16H), 0.88 (t, J = 7.2 Hz, 6H). ^{13}CNMR ($CDCl_3$, 125 MHz): δ 141.1, 126.9, 125.0, 34.6, 31.9, 29.6, 29.6, 29.5, 29.3, 29.1, 28.5, 22.7, 14.1.

3,6-Bis(2-ethylhexylsulfanyl)thieno[3,2-*b*]thiophene (2.1c)
The compound was synthesized and purified as described for **2.1a** to give a clear oil in 78% yield. ^{1}HNMR ($CDCl_3$, 400 MHz): δ 7.24 (s, 2H), 2.92 (d, J = 6.0 Hz, 4H), 1.40 (m, 9H), 1.25 (m, 9H), 0.87 (m, 12H). HR-MS (ESI): m/z = 429.1782 [M+1] (calcd for $C_{22}H_{37}S_4$, m/z = 429.1773).

3,6-Bis(butylsulfanyl)thieno[3,2-*b*]thiophene (2.1d)
The compound was synthesized and purified as described for **2.1a** to give a clear oil in 43% yield. ^{1}HNMR (acetone-d_6, 400 MHz): δ 7.53 (s, 2H), 2.99 (t, J = 8.0 Hz, 4H), 1.61 (m, 4H), 1.46 (m, 4H), 0.89 (t, J = 7.2 Hz, 6H). HR-MS (ESI): m/z = 317.0524 [M+1] (calcd for $C_{14}H_{21}S_4$, m/z = 317.0521).

2,5-Dibromo-3,6-bis(dodecylsulfanyl)thieno[3,2-*b*]thiophene (2.2b)
Thienothiophene **2.1b** (82.4 mg, 0.152 mmol) was dissolved in $CHCl_3$ (2 mL) and acetic acid (2 mL) and cooled to −40°C. NBS (82.6 mg, 0.464 mmol) was added and the reaction warmed slowly to room temperature protected from light with foil. After being stirred for 24 h, the reaction was treated with saturated $Na_2S_2O_3$ solution (5 mL). The reaction mixture was then diluted with H_2O and extracted with $CHCl_3$ (2 × 20 mL). The solvent was removed in vacuo and the resulting product was passed through a silica plug with hexane to yield pure bromide **2.2b** as a white solid (77.5 mg, 73%). ^{1}HNMR (CD_2Cl_2, 400 MHz): δ 2.89 (t, J = 7.2 Hz, 4H), 1.54 (m, 4H), 1.40 (m, 4H), 1.25 (m, 16H), 0.89 (t, J = 6.8 Hz, 6H).

2,5-Dibromo-3,6-bis(hexylsulfanyl)thieno[3,2-*b*]thiophene (2.2a)
The compound was synthesized as described for **2.2b** to give an orange oil in 33% yield. ^{1}HNMR (acetone-d_6, 400 MHz): δ 2.97 (t, J = 7.2 Hz, 4H), 1.55 (p, J = 7.6 Hz, 4H), 1.44 (p, J = 7.6 Hz, 4H), 1.26 (m, 8H), 0.86 (t, J = 7.2 Hz, 6H). ^{13}CNMR ($CDCl_3$, 75 MHz): δ 139.3, 125.5, 119.1, 34.6, 31.3, 30.0, 28.2, 22.5, 14.1. HR-MS (ESI): m/z = 528.9348 [M+1] (calcd for $C_{18}H_{27}Br_2S_4$, m/z = 528.9357).

2,5-Dibromo-3,6-bis((2-ethylhexyl)sulfanyl)thieno[3,2-*b*]thiophene (2.2c)
Compound was synthesized as described above to give an orange oil in 42% yield. ^{1}HNMR ($CDCl_3$, 300 MHz): δ 2.87 (d, J = 3.0 Hz), 1.42 (m, 9H), 1.25 (m, 9H), 0.87 (t, J = 7.2 Hz, 12H). HR-MS (APCI): m/z = 584.9954 [M+1] (calcd for $C_{22}H_{34}Br_2S_4$, m/z = 584.9983).

2,5-Dibromo-3,6-bis(dodecylsulfonyl)thieno[3,2-*b*]thiophene (2.3b)
Sulfide **2.2b** (0.1195 g, 0.1710 mmol) was dissolved in $CHCl_3$ (5 mL) and cooled to 0°C under nitrogen gas. MPCBA, purified from commercial reagent by washing with pH 7.5 phosphate buffer, (0.1520 g, 0.8808 mmol) was added, and the reaction mixture was allowed to warm to room temperature and stirred for 20 h. The reaction was then quenched with 0.1 M NaOH solution (25 mL), extracted with $CHCl_3$ (2 × 20 mL), and dried over Na_2SO_4. The solvent was removed in vacuo and the product was passed through a silica plug to afford pure sulfone **2.3b** as a white solid (0.122 g, 93%). ^{1}HNMR ($CDCl_3$, 300 MHz): δ 3.34 (t, J = 7.5 Hz, 4H), 1.75 (p, J = 7.8 Hz, 4H), 1.40 (m, 4H), 1.24 (m, 16H), 0.87 (t, J = 6.6 Hz, 6H).

^{13}CNMR ($CDCl_3$, 75 MHz): δ 135.9, 131.0, 122.1, 55.4, 31.9 29.5, 29.5, 29.4, 29.3, 29.2, 28.9, 28.1, 22.7, 22.2, 14.1. HR-MS (ESI) *m/z* = 761.1021 [M+1] (calcd for $C_{30}H_{51}Br_2O_4S_4$, *m/z* = 761.1031).

2,5-Dibromo-3,6-bis(2-ethylhexylsulfonyl)thieno[3,2-*b*]thiophene (2.3c)
The compound was synthesized in the same manner as described above to give a yellow solid in 82% yield. ^{1}HNMR (acetone-d_6, 300 MHz): δ 3.45 (d, *J* = 6.0 Hz, 4H), 1.44 (m, 10H), 1.24 (m, 8H), 0.86 (t, *J* = 7.2 Hz, 12H). ^{13}CNMR ($CDCl_3$, 125 MHz): δ 135.8, 131.8, 122.0, 58.8, 34.6, 32.5, 28.2, 25.9, 22.6, 14.0, 10.3. HR-MS (ESI): *m/z* = 648.9771 [M+1] (calcd for $C_{22}H_{35}Br_2O_4S_4$, *m/z* = 648.9779).

2-Bromo-3,6-bis(butylsulfanyl)thieno[3,2-*b*]thiophene (2.4)
3,6-Bis(butylsulfanyl)thieno[3,2-*b*]thiophene **2.1d** (0.1667 g, 0.5266 mmol) was cooled to −75°C in dry Et_2O. nBuLi was added dropwise and the reaction was stirred for 40 min at −75°C before being warmed to −10°C for 1 h. The reaction mixture was then cooled back to −75°C, and carbon tetrabromide (0.1665 g, 0.5021 mmol), dissolved in 1 mL of dry Et_2O, was added dropwise. After 2 h, the reaction mixture was quenched with H_2O (10 mL), diluted in Et_2O (25 mL), washed with H_2O and $NaHCO_3$ solution, and then dried over Na_2SO_4. The product was purified by silica-gel column chromatography with hexane and $CHCl_3$ as eluent (1:0 to 9:1 gradient) to afford a yellow oil (0.126 g, 61% yield). ^{1}HNMR (acetone-d_6, 400 MHz): δ 7.65 (s, 1H), 2.985 (t, *J* = 7.2 Hz, 2H), 2.978 (t, *J* = 7.2 Hz, 2H) 1.61 (m, 4H), 1.46 (m, 4H), 0.895 (t, *J* = 7.2 Hz, 3H), 0.870 (t, *J* = 7.2 Hz, 3H).

2-Bromo-3,6-bis(butylsulfonyl)thieno[3,2-*b*]thiophene (2.5)
Compound was synthesized in the same manner as described for compound **2.3** to give a yellow solid in 86% yield. ^{1}HNMR (acetone-d_6, 300 MHz): δ 8.59 (s, 1H), 3.50 (t, *J* = 7.5 Hz, 2H), 3.39 (t, *J* = 7.8 Hz, 2H), 1.72 (m, 4H), 1.45 (m, 4H), 0.89 (t, *J* = 6.9 Hz, 6H).

General Procedure for Stille Polycondensation Polymerization
The TT and (E)-1,2-bis(tributylstannyl)ethene monomers were weighed out and transferred to a pear-shaped flask and placed under a stream of nitrogen gas. Pd(PPh3)4 (10 mol%) was weighed out into a dry 25 mL Schlenk tube in a glovebox. The monomer mixture was transferred to the reaction flask, rinsing with dry toluene (2 mL). The mixture was degassed by freeze–pump–thaw (2 × 15 min at −75°C). The reaction was then heated to reflux (110°C) and sealed under nitrogen gas. The polymerization was monitored by UV over 48 h, but no further shift in the UV absorption onset was observed after 15 h. The reaction product was then precipitated by dropwise addition into MeOH (100 mL) and collected by filtration on PTFE membrane. The polymers are purified by Soxhlet extraction by sequential washing with ethanol, acetone, and hexane and finally collected in chloroform or chlorobenzene.

(E)-1,2-Bis(3,6-bis(butylsulfanyl)thieno[3,2-*b*]thiophen-2-yl)ethene (S-2TTV)
2.4 (49.9 mg, 0.126 mmol) and (E)-1,2-bis(tributylstannyl)-ethene (33.3 μL, 0.0632 mmol) were loaded into a 25 mL Schlenk tube. Dry toluene (2 mL) was added and the tube was flushed with N_2 before the addition of $Pd(PPh_3)_4$ (15.5 mg, 0.0134 mmol). The reaction was heated to 100°C, sealed under N_2, and stirred overnight. After cooling, the reaction mixture was diluted in EtOAc and washed with NH_4Cl solution (50 mL). The organics

were then washed with 1 M KF solution (2 × 20 mL) with vigorous shaking. The combined KF fractions were extracted with EtOAc and the organic phases dried with Na_2SO_4. The organics were then filtered through cotton and the solvent removed in vacuo. The product was flashed through silica with hexane and $CHCl_3$ as eluent (9:1) and further purified by recrystallization from hexane to afford 18.8 mg (46% yield) of **S-2TTV** as an orange powder. ^{1}HNMR ($CDCl_3$, 300 MHz): δ 7.49 (s, 2H), 7.22 (s, 2H), 2.887 (t, *J* = 7.2 Hz, 4H), 2.822 (t, *J* = 7.2 Hz, 4H), 1.50 (m, 16H), 0.863 (t, *J* = 7.2 Hz, 6H), 0.830 (t, *J* = 6.9 Hz, 6H). ^{13}CNMR (dimethyl sulfoxide-d_6, 500 MHz, 83°C): δ 144.9, 143.7, 137.8, 128.2, 125.2, 124.0, 122.0, 35.1, 34.1, 32.0, 31.7, 21.42, 21.27, 13.67, 13.64. HR-MS (ESI): *m/z* = 657.0978 [M+1] (calcd for $C_{30}H_{41}S_8$, *m/z* = 657.0968). Single crystals were grown by dissolving **S-2TTV** in a hot toluene/hexane/ethanol mixture and cooling overnight.

(E)-1,2-Bis(3,6-bis(butylsulfonyl)thieno[3,2-*b*]thiophen-2-yl)ethene (SO2-2TTV)

The same procedure as above was used with **2.5** as starting material. The product was flashed through silica with DCM, concentrated, then recrystallized from propanol and centrifuged to remove the propanol supernatant to afford 30.2 mg (45% yield) of pure **SO_2-2TTV** as an orange powder. ^{1}HNMR ($CDCl_3$, 300 MHz): δ 8.20 (s, 2H), 8.01 (s, 2H), 3.24 (t, *J* = 8.1 Hz, 8H), 1.79 (m, 8H), 1.46 (m, 8H), 0.937 (t, *J* = 7.2 Hz, 6H), 0.913 (t, *J* = 7.2 Hz, 6H). ^{13}CNMR (dimethyl sulfoxide-d_6, 500 MHz, 83°C): δ 148.5, 139.9, 139.2, 134.0, 132.6, 129.7, 123.9, 56.8, 55.9, 24.7, 24.7, 21.08, 21.05, 13.56, 13.55. HR-MS (ESI): *m/z* = 785.0569 [M+1] (calcd for $C_{30}H_{41}O_8S_8$, *m/z* = 785.0562). Mp >300°C (dec.)

References

(1) a) Perepichka, I. F.; Perepichka, D. F., *Handbook of Thiophene-Based Materials*; John Wiley & Sons, Ed., New York, 2009; b) Mishra, A.; Ma, C.-Q.; Segura, J. L.; Bäuerle, P. In *Handb. Thiophene-Based Mater.* Perepichka, I. F., Perepichka, D. F., Eds.; John Wiley & Sons, Ltd: Chichester, UK, 2009; Vol. 1, pp 1–155.

(2) Zhao, G.; He, Y.; Li, Y. No Title. *Adv. Mater.* **2010**, *22*, 4355.

(3) Son, H. J.; He, F.; Carsten, B.; Yu, L. Are we there yet? Design of better conjugated polymers for polymer solar cells. *J. Mater. Chem.* **2011**, *21*, 18934.

(4) Shi, C.; Yao, Y.; Yang, Y.; Pei, Q. Regioregular copolymers of 3-alkoxythiophene and their photovoltaic application. *J. Am. Chem. Soc.* **2006**, *128*, 8980.

(5) Chochos, C.; Economopoulos, S.; Deimede, V.; Gregoriou, V.; Lloyd, M.; Malliaras, G.; Kallitsis, J. Synthesis of a Soluble n-Type Cyano Substituted Polythiophene Derivative: A Potential Electron Acceptor in Polymeric Solar Cells. *J. Phys. Chem. C* **2007**, *111*, 10732.

(6) Babudri, F.; Farinola, G. M.; Naso, F.; Ragni, R. Fluorinated organic materials for electronic and optoelectronic applications: the role of the fluorine atom. *Chem. Commun. (Camb).* **2007**, 1003.

(7) Li, L.; Collard, D. M. Tuning the Electronic Structure of Conjugated Polymers with Fluoroalkyl Substitution: Alternating Alkyl/Perfluoroalkyl-Substituted Polythiophene. *Macromolecules* **2005**, *38*, 372.

(8) Huo, L.; Zhang, S.; Guo, X.; Xu, F.; Li, Y.; Hou, J. Replacing alkoxy groups with alkylthienyl groups: a feasible approach to improve the properties of photovoltaic polymers. *Angew. Chem. Int. Ed. Engl.* **2011**, *50*, 9697.

(9) Casalbore-Miceli, G.; Gallazzi, M.; Zecchin, S.; Camaioni, N.; Geri, a.; Bertarelli, C. A Donor–Acceptor Polymer with a Peculiar Negative-Charge-"Trapping" Characteristic. *Adv. Funct. Mater.* **2003**, *13*, 307.

(10) Dey, T.; Invernale, M. A.; Ding, Y.; Buyukmumcu, Z.; Sotzing, G. A. Poly(3,4-propylenedioxythiophene)s as a Single Platform for Full Color Realization. *Macromolecules* **2011**, *44*, 2415.

(11) Zhang, Q. T.; Tour, J. M. Alternating Donor/Acceptor Repeat Units in Polythiophenes. Intramolecular Charge Transfer for Reducing Band Gaps in Fully Substituted Conjugated Polymers. *J. Am. Chem. Soc.* **1998**, *120*, 5355.

(12) Liang, Y.; Feng, D.; Wu, Y.; Tsai, S.-T.; Li, G.; Ray, C.; Yu, L. Highly efficient solar cell polymers developed via fine-tuning of structural and electronic properties. *J. Am. Chem. Soc.* **2009**, *131*, 7792.

(13) Cremer, L.; De Verbiest, T.; Koeckelberghs, G. Influence of the Substituent on the Chiroptical Properties of Poly(thieno[3,2- b]thiophene)s. *Macromolecules* **2008**, *41*, 568.

(14) Huo, L.; Zhou, Y.; Li, Y. Alkylthio-Substituted Polythiophene: Absorption and Photovoltaic Properties. *Macromol. Rapid Commun.* **2009**, *30*, 925.

(15) Pozo-Gonzalo, C.; Khan, T.; McDouall, J. J. W.; Skabara, P. J.; Roberts, D. M.; Light, M. E.; Coles, S. J.; Hursthouse, M. B.; Neugebauer, H.; Cravino, A.; Sariciftci, N. S. Synthesis and electropolymerisation of 3′,4′-bis(alkylsulfanyl)terthiophenes and the significance of the fused dithiin ring in 2,5-dithienyl-3,4-ethylenedithiothiophene (DT-EDTT). *J. Mater. Chem.* **2002**, *12*, 500.

(16) a) Dane, E. L.; King, S. B.; Swager, T. M. Conjugated polymers that respond to oxidation with increased emission. *J. Am. Chem. Soc.* **2010**, *132*, 7758; b) King, S. M.; Perepichka, I. I.; Perepichka, I. F.; Dias, F. B.; Bryce, M. R.; Monkman, A. P. Exploiting a Dual-Fluorescence Process in Fluorene-Dibenzothiophene-S , S -dioxideCo-Polymers to Give Efficient Single Polymer LEDs with Broadened Emission. *Adv. Funct. Mater.* **2009**, *19*, 586.

(17) a) Sasabe, H.; Seino, Y.; Kimura, M.; Kido, J. A m -Terphenyl-Modifed Sulfone Derivative as a Host Material for High-Efficiency Blue and Green Phosphorescent OLEDs. *Chem. Mater.* **2012**, *24*, 1404; b) Malashikhin, S.; Finney, N. S. Fluorescent signaling based on sulfoxide profluorophores: application to the visual detection of the explosive TATP. *J. Am. Chem. Soc.* **2008**, *130*, 12846; c) Lee, W.; Jenks, W. S. Photophysics and Photostereomutation of Aryl Methyl Sulfoxides 1. *J. Org. Chem.* **2001**, *66*, 474; d) Christensen, P. R.; Nagle, J. K.; Bhatti, A.; Wolf, M. O. Enhanced Photoluminescence of Sulfur-Bridged Organic Chromophores. *J. Am. Chem. Soc.* **2013**, *135*, 8109.

(18) One example of a low band gap copolymer incorporating an alkylsulfonyl substituent was recently reported, but did not include electronic effects of fluorescence: Huang, Y.; Huo, L.; Zhang, S.; Guo, X.; Han, C. C.; Li, Y.; Hou, J. *Chem. Commun* **2011**, 8904.

(19) Medina, B. M.; Van Vooren, A.; Brocorens, P.; Gierschner, J.; Shkunov, M.; Heeney, M.; McCulloch, I.; Lazzaroni, R.; Cornil, J. Electronic Structure and Charge-Transport Properties of Polythiophene Chains Containing Thienothiophene Units: A Joint Experimental and Theoretical Study. *Chem. Mater.* **2007**, *19*, 4949.

(20) McCulloch, I.; Heeney, M.; Bailey, C.; Genevicius, K.; Macdonald, I.; Shkunov, M.; Sparrowe, D.; Tierney, S.; Wagner, R.; Zhang, W.; Chabinyc, M. L.; Kline, R. J.; McGehee, M. D.; Toney, M. F. Liquid-crystalline semiconducting polymers with high charge-carrier mobility. *Nat. Mater.* **2006**, *5*, 328.

(21) Lee, J. S.; Son, S. K.; Song, S.; Kim, H.; Lee, D. R.; Kim, K.; Ko, M. J.; Choi, D. H.; Kim, B.; Cho, J. H. Importance of Solubilizing Group and Backbone Planarity in Low Band Gap Polymers for High Performance Ambipolar field-effect Transistors. *Chem. Mater.* **2012**, *24*, 1316.

(22) Spencer, H. J.; Skabara, P. J.; Giles, M.; McCulloch, I.; Coles, S. J.; Hursthouse, M. B. The first direct experimental comparison between the hugely contrasting properties of PEDOT and the all-sulfur analogue PEDTT by analogy with well-defined EDTT–EDOT copolymers. *J. Mater. Chem.* **2005**, *15*, 4783.

(23) Scharber, M. C.; Mühlbacher, D.; Koppe, M.; Denk, P.; Waldauf, C.; Heeger, A. J.; Brabec, C. J. Design Rules for Donors in Bulk-Heterojunction Solar Cells—Towards 10 % Energy-Conversion Efficiency. *Adv. Mater.* **2006**, *18*, 789.

(24) Zade, S. S.; Bendikov, M. Twisting of conjugated oligomers and polymers: case study of oligo- and polythiophene. *Chemistry (Easton).* **2007**, *13*, 3688.

(25) McCulloch, I.; Heeney, M.; Chabinyc, M. L.; DeLongchamp, D.; Kline, R. J.; Cölle, M.; Duffy, W.; Fischer, D.; Gundlach, D.; Hamadani, B.; Hamilton, R.; Richter, L.; Salleo, A.; Shkunov, M.; Sparrowe, D.; Tierney, S.; Zhang, W. Semiconducting Thienothiophene Copolymers: Design, Synthesis, Morphology, and Performance in Thin-Film Organic Transistors. *Adv. Mater.* **2009**, *21*, 1091.

(26) Reddinger, J. L.; Reynolds, J. R. *J. Org. Chem.* **1996**, *61*, 4833 (Contrary to this report, our yields were improved by warming to room temperature after each addition of disulfide.)

(27) a) Ko, S.; Mondal, R.; Risko, C.; Lee, J. K.; Hong, S.; McGehee, M. D.; Brédas, J.-L.; Bao, Z. Tuning the Optoelectronic Properties of Vinylene-Linked Donor-Acceptor Copolymers for Organic Photovoltaics. *Macromolecules* **2010**, *43*, 6685; b) Wu, P.-t.; Ren, G.; Jenekhe, S. A. Crystalline Random Conjugated Copolymers with Multiple Side Chains: Tunable Intermolecular Interactions and Enhanced Charge Transport and Photovoltaic Properties. *Macromolecules* **2010**, *43*, 3306; c) Nielsen, C. B.; Ashraf, R. S.; Schroeder, B. C.; D'Angelo, P.; Watkins, S. E.; Song, K.; Anthopoulos, T. D.; McCulloch, I. Random benzotrithiophene-based donor-acceptor copolymers for efficient organic photovoltaic devices. *Chem. Commun. (Camb).* **2012**, *48*, 5832.

(28) Chapman, C. J.; Frost, C. G.; Mahon, M. F. Structure and reactivity of new phosphine ligands containing the hemi-labile sulfone moiety. *Dalton Trans.* **2006**, 2251.

(29) He, Y.; Wu, W.; Zhao, G.; Liu, Y.; Li, Y. Poly (3, 6-dihexyl-thieno [3, 2-b] thiophene vinylene): Synthesis, Field-Effect Transistors, and Photovoltaic Properties. *Macromolecules* **2008**, *41*, 9760.

(30) The MW of **SO_2-PTTV** corresponds to an average chain length of 14 repeat units. Extrapolating the DFT data (Figure 2.2) for an oligomer of 14 repaeat units predicts a band gap of 1.75 eV.

(31) Perepichka, I. F.; Perepichka, D. F.; Meng, H.; Wudl, F. Light-Emitting Polythiophenes. *Adv. Mater.* **2005**, *17*, 2281.

(32) Jeeva, S.; Lukoyanova, O.; Karas, A.; Dadvand, A.; Rosei, F.; Perepichka, D. F. Highly Emissive and Electrochemically Stable Thienylene Vinylene Oligomers and Copolymers: An Unusual Effect of Alkylsulfanyl Substituents. *Adv. Funct. Mater.* **2010**, *20*, 1661.

(33) D'Andrade, B. W.; Datta, S.; Forrest, S. R.; Djurovich, P.; Polikarpov, E.; Thomson, M. E. No Title. *Org. Electron.* **2005**, 11.

(34) a) Zhang, Y.; Dang, X.-D.; Kim, C.; Nguyen, T.-Q. Effect of Charge Recombination on the Fill Factor of Small Molecule Bulk Heterojunction Solar Cells. *Adv. Energy Mater.* **2011**, *1*, 610; b) Kroon, R.; Lenes, M.; Hummelen, J. C.; Blom, P. W. M.; de Boer, B. Small Bandgap Polymers for Organic Solar Cells (Polymer Material Development in the Last 5 Years). *Polym. Rev.* **2008**, *48*, 531.

(35) Frisch, M. J.; Trucks, G. W.; Schlegel, H. B.; Scuseria, G. E.; Robb, M. A.; Cheeseman, J. R.; Scalmani, G.; Barone, V.; Mennucci, B.; Petersson, G. A.; Nakatsuji, H.; Caricato, M.; Li, X.; Hratchian, H. P.; Izmaylov, A. F.; Bloino, J.; Zheng, G.; Sonnenberg, J. L.; Hada, M.; Ehara, M.; Toyota, K.; Fukuda, R.; Hasegawa, J.; Ishida, M.; Nakajima, T.; Honda, Y.; Kitao, O.; Nakai, H.; Vreven, T.; Montgomery, J. A.; Peralta, J. E.; Ogliaro, F.; Bearpark, M.; Heyd, J. J.; Brothers, E.; Kudin, K. N.; Staroverov, V. N.; Kobayashi, R.; Normand, J.; Raghavachari, K.; Rendell, A.; Burant, J. C.; Iyengar, S. S.; Tomasi, J.; Cossi, M.; Rega, N.; Millam, J. M.; Klene, M.; Knox, J. E.; Cross, J. B., et al. Gaussian09 Revision D.01., Gaussian Inc. Wallingford CT 2009.

(36) Henssler, J. T.; Matzger, A. J. Facile and scalable synthesis of the fused-ring heterocycles thieno[3,2-b]thiophene and thieno[3,2-b]furan. *Org. Lett.* **2009**, *11*, 3144.

2.6 Supporting Information for Chapter 2

2.6.1 Calculated band gaps and rotation energies.

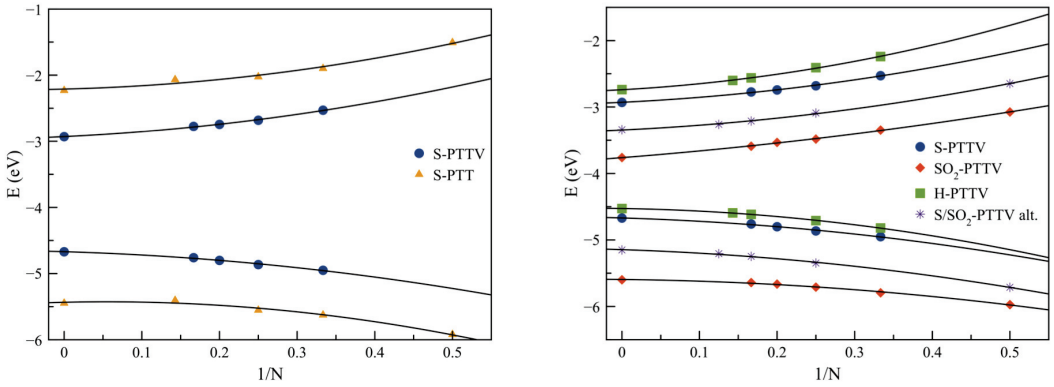

Figure S2.1. Calculated HOMO and LUMO energy levels of oligomers and infinite chains modeled with PBC. The vinyl spacer in S-PTTV shrinks the band gap by 1.48 eV vs. S-PTT (left) and the sulfanyl and sulfonyl substituents lower the energy levels (right).

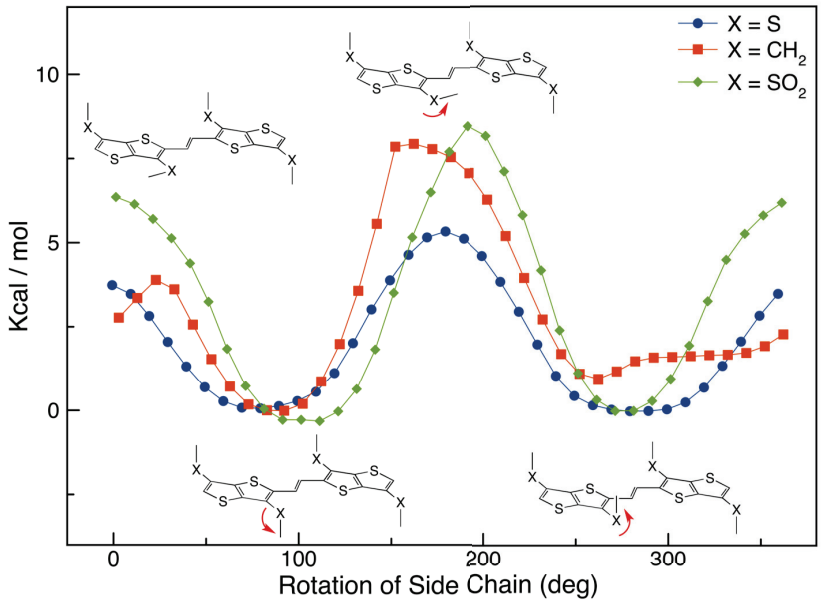

Figure S2.2. Plot of the energy of rotation of –SMe and –CH_2CH_3 in a substituted TTV dimer kept in a planar configuration.

2.6.2 Optical Spectroscopy and Electrochemistry

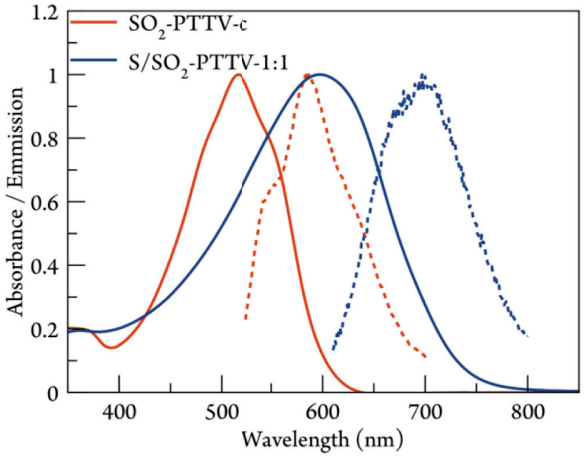

Figure S2.3. Absorption and emission spectra of **SO_2-PTTV** and **S/SO_2-PTTV-1:1**.

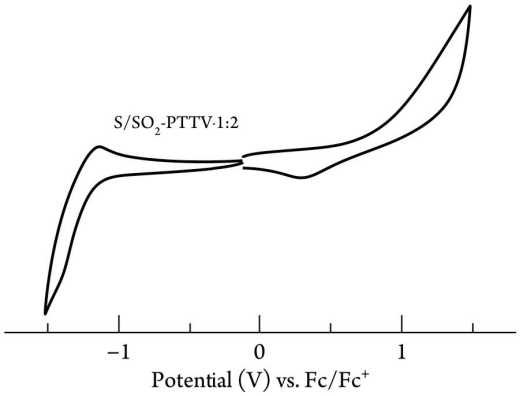

Figure S2.4. Cyclic voltammogram of **1:2 S/SO_2-PTTVc** (0.1 M Bu_4NPF_6 /propylene carbonate as electrolyte; scan rate 0.2 V/s).

2.6.3 AFM of Photovoltaic Device

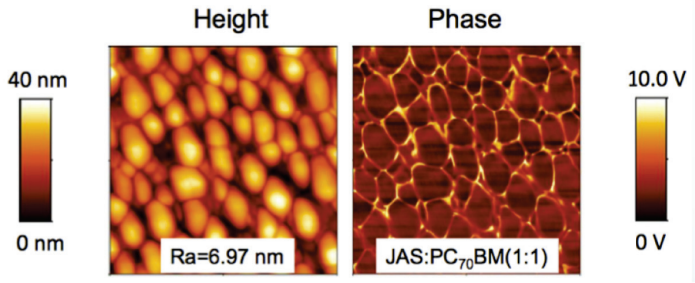

Figure S2.5. 2μm × 2μm AFM scan of a photovoltaic device: **S/SO$_2$-PTTV**:PC$_{70}$BM 1:1 blend, 1% in chlorobenzene spun-cast on PEDOT:PSS.

2.6.4 NMR Data

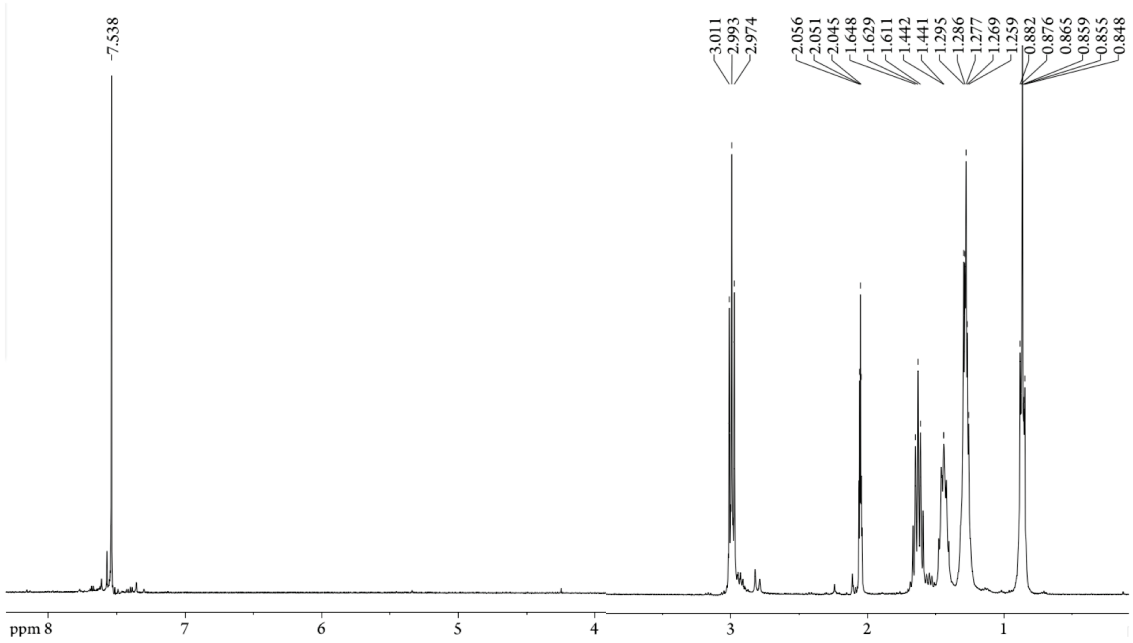

^{1}H NMR spectrum of compound **2.1a** in acetone-d_6.

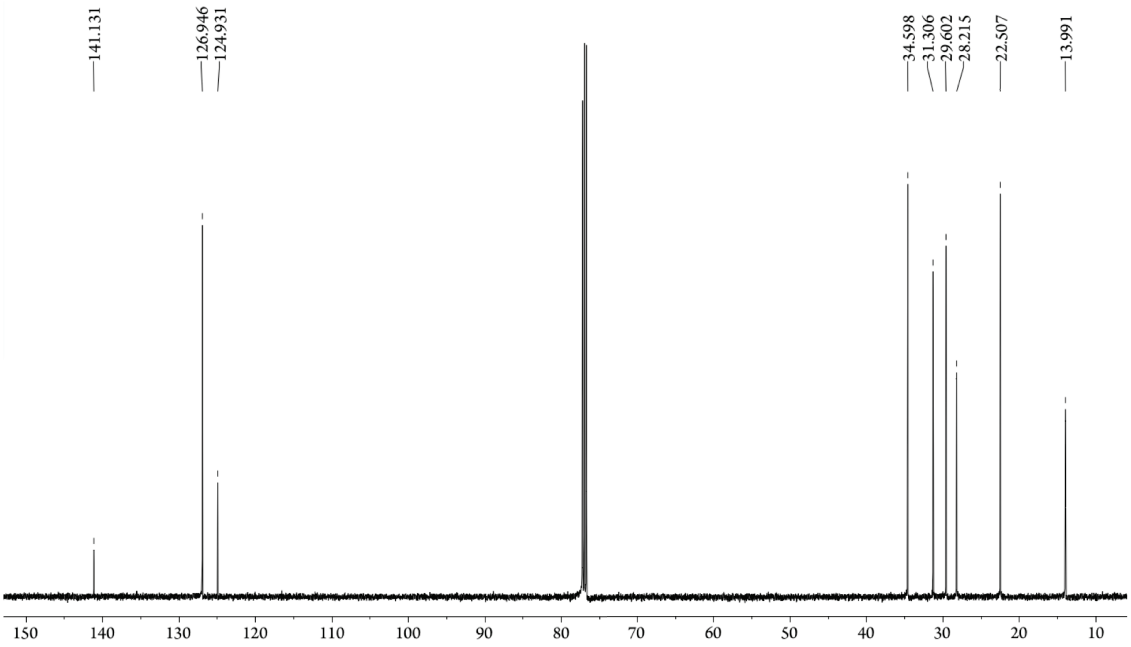

^{13}C NMR spectrum of compound **2.1a** in $CDCl_3$.

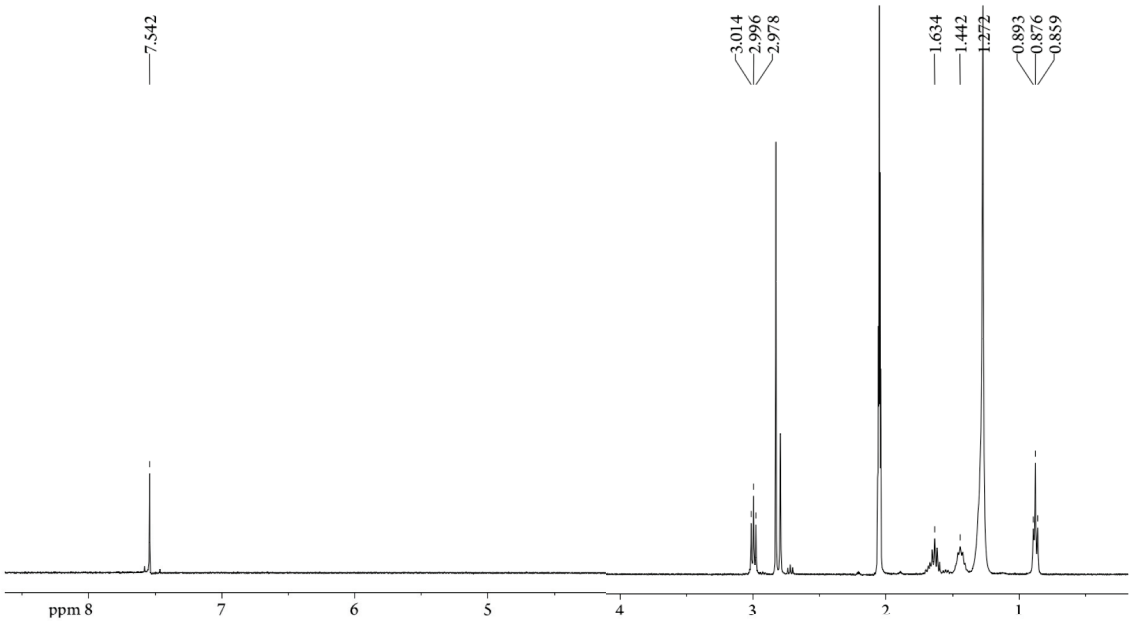

^{1}H NMR spectrum of compound **2.1b** in acetone-d_6.

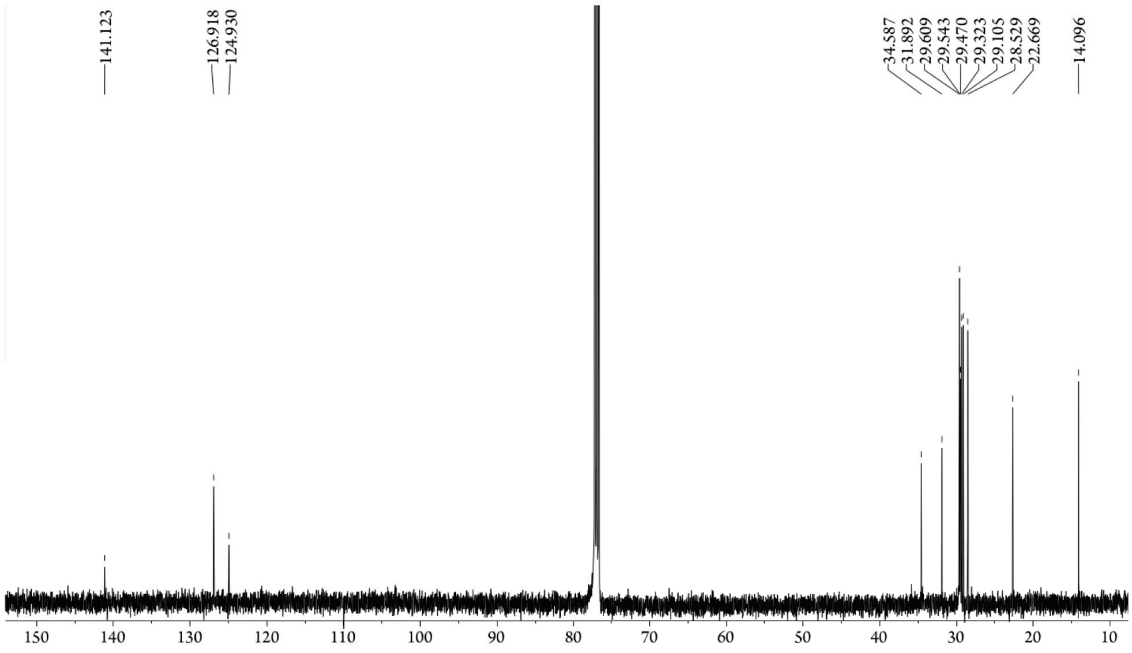

^{13}C NMR spectrum of compound **2.1b** in $CDCl_3$.

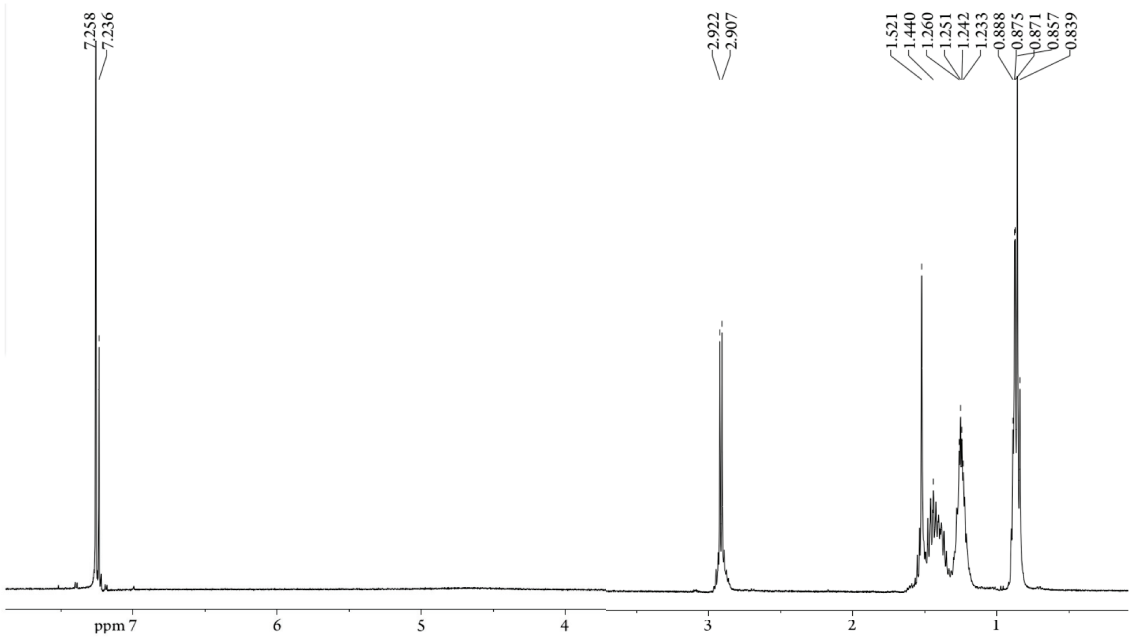

^{1}H NMR spectrum of compound **2.1c** in $CDCl_3$.

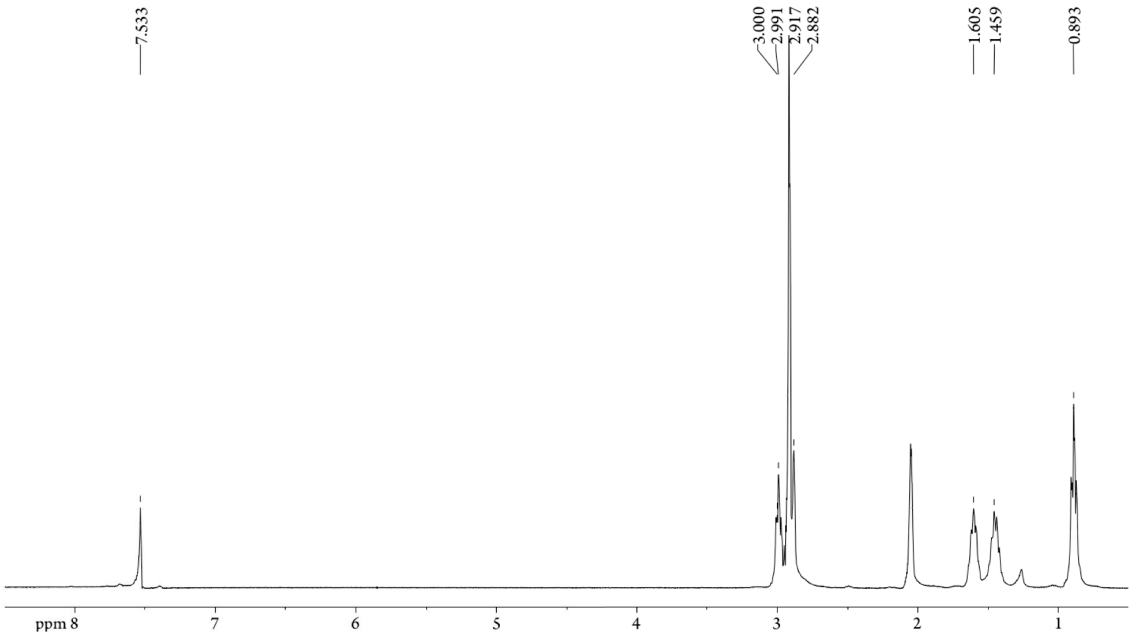

^{1}H NMR spectrum of compound **2.1d** in acetone-d_6.

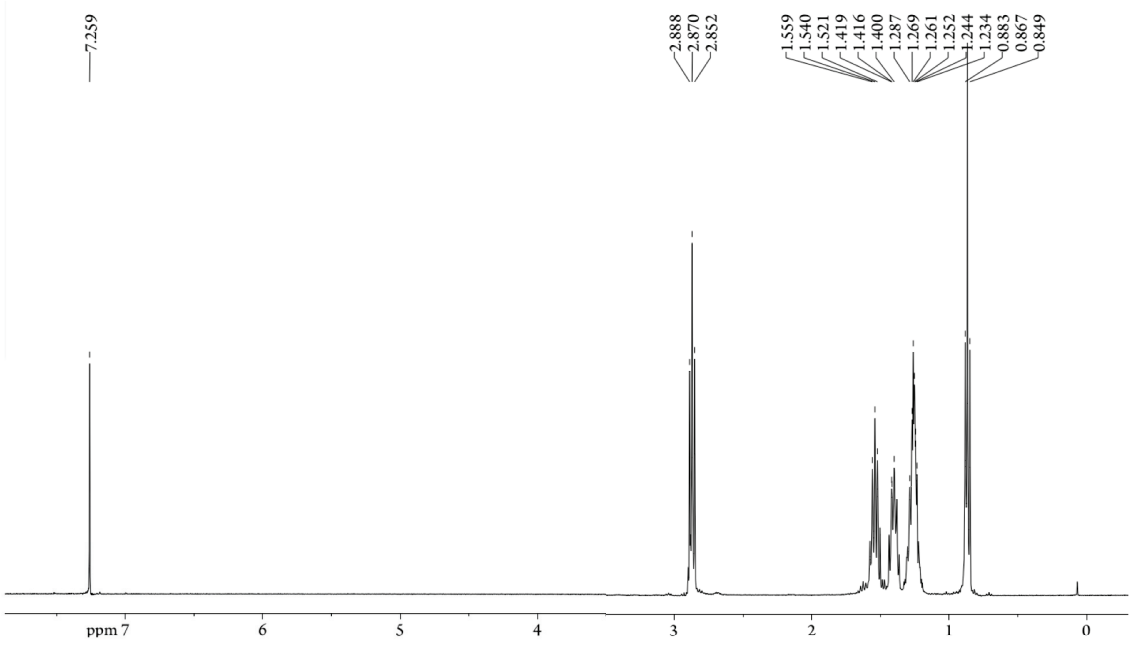

^{1}H NMR spectrum of compound **2.2a** in $CDCl_3$.

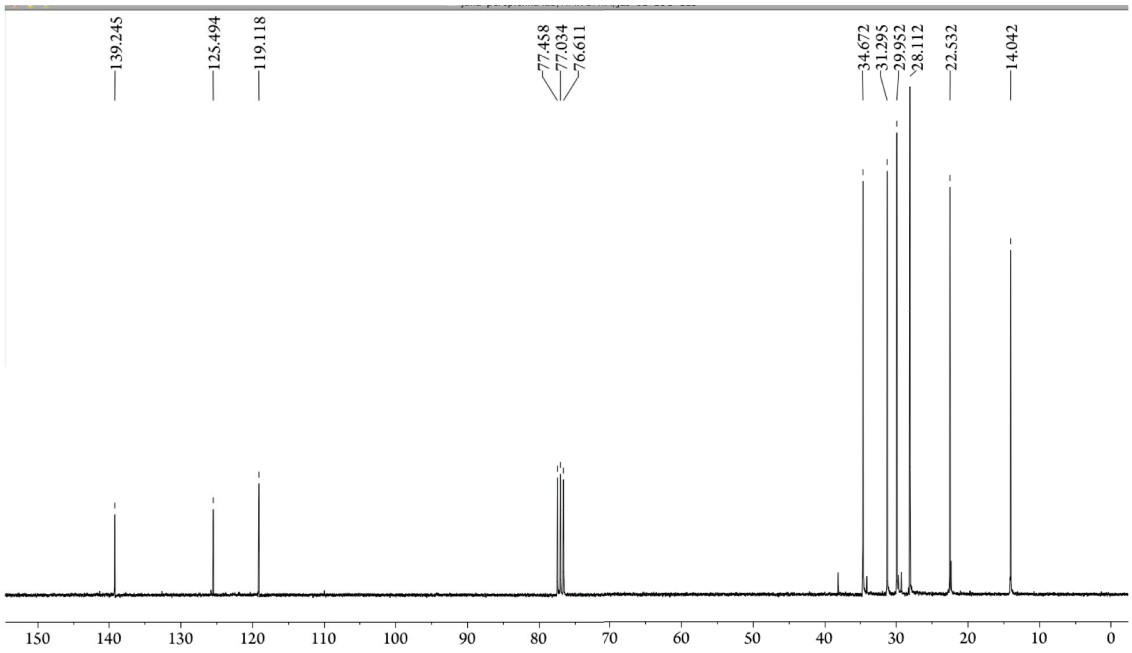

^{13}C NMR spectrum of compound **2.2a** in $CDCl_3$.

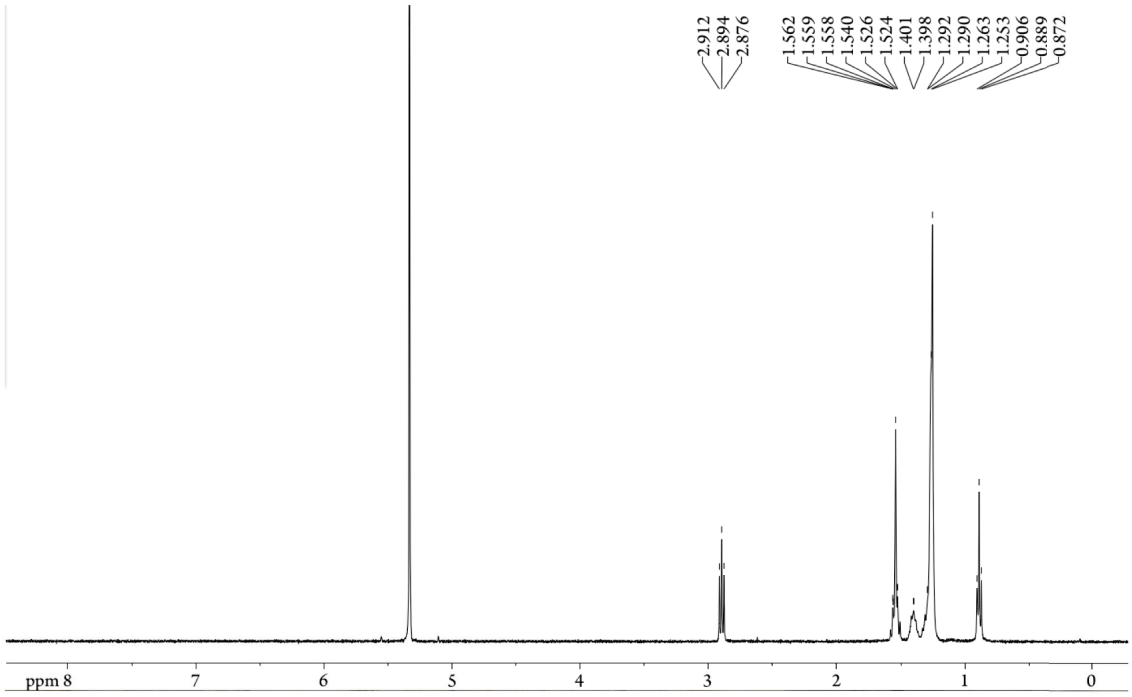

^{1}H NMR spectrum of compound **2.2b** in CD_2Cl_2.

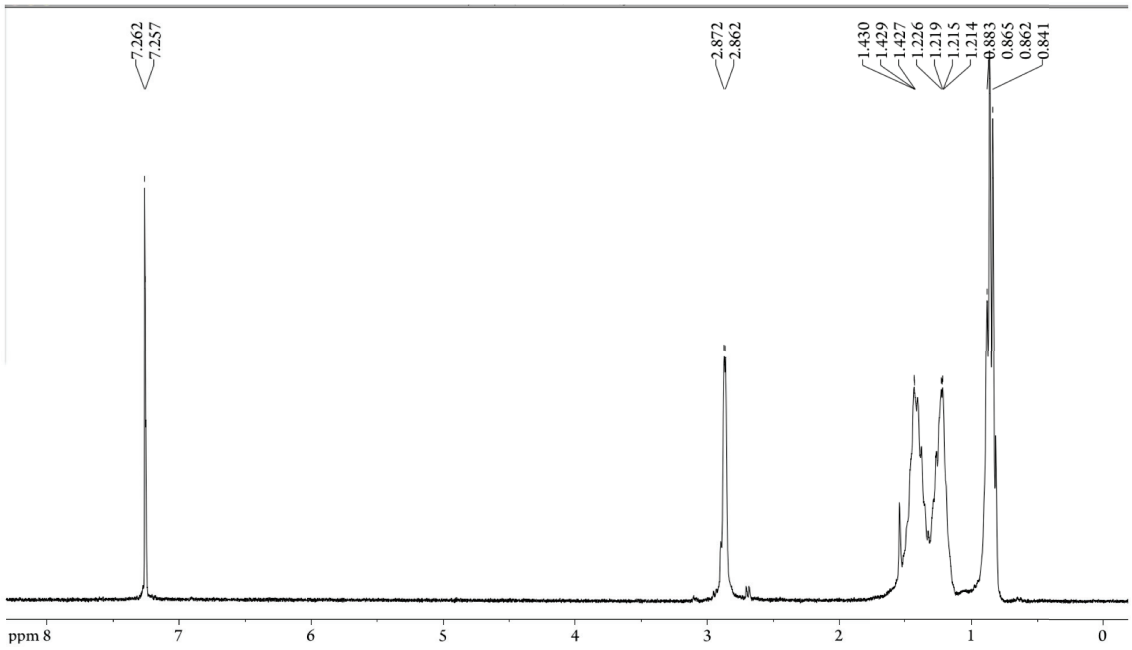

^{1}H NMR spectrum of compound **2.2c** in $CDCl_3$.

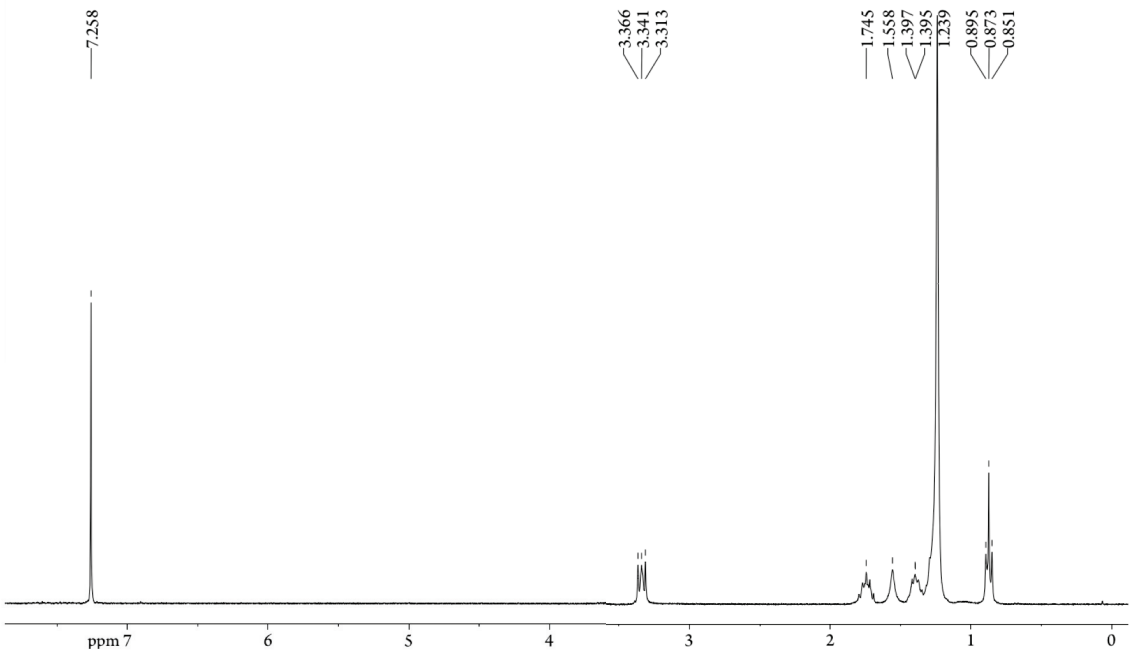

^{1}H NMR spectrum of compound **2.3b** in $CDCl_3$.

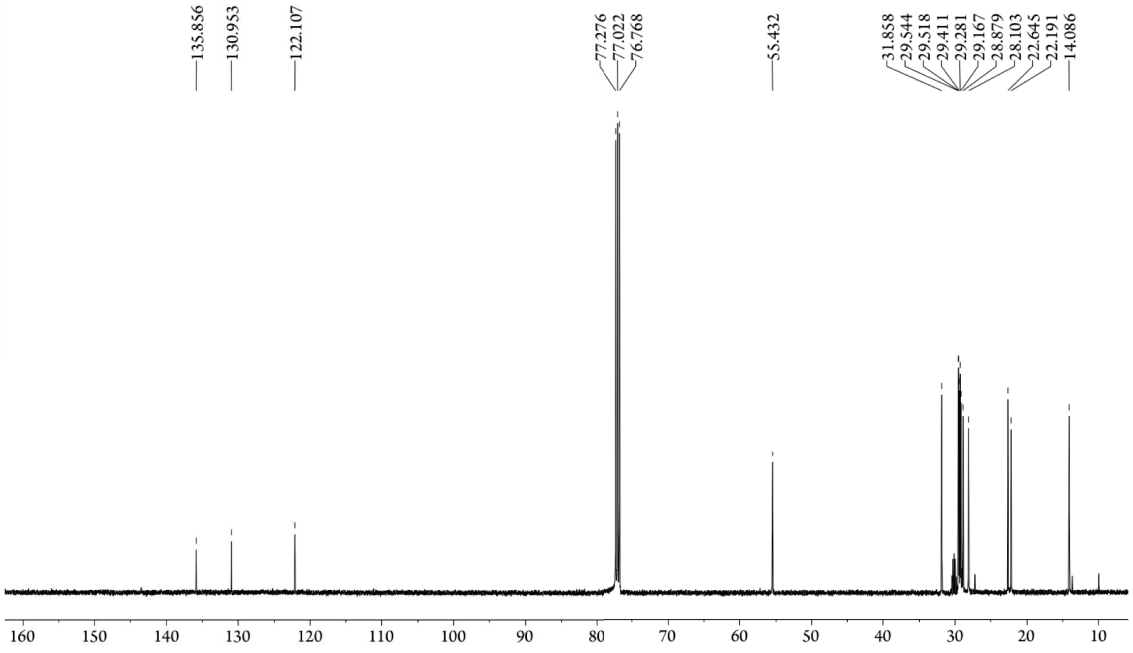

^{13}C NMR spectrum of compound **2.3b** in $CDCl_3$.

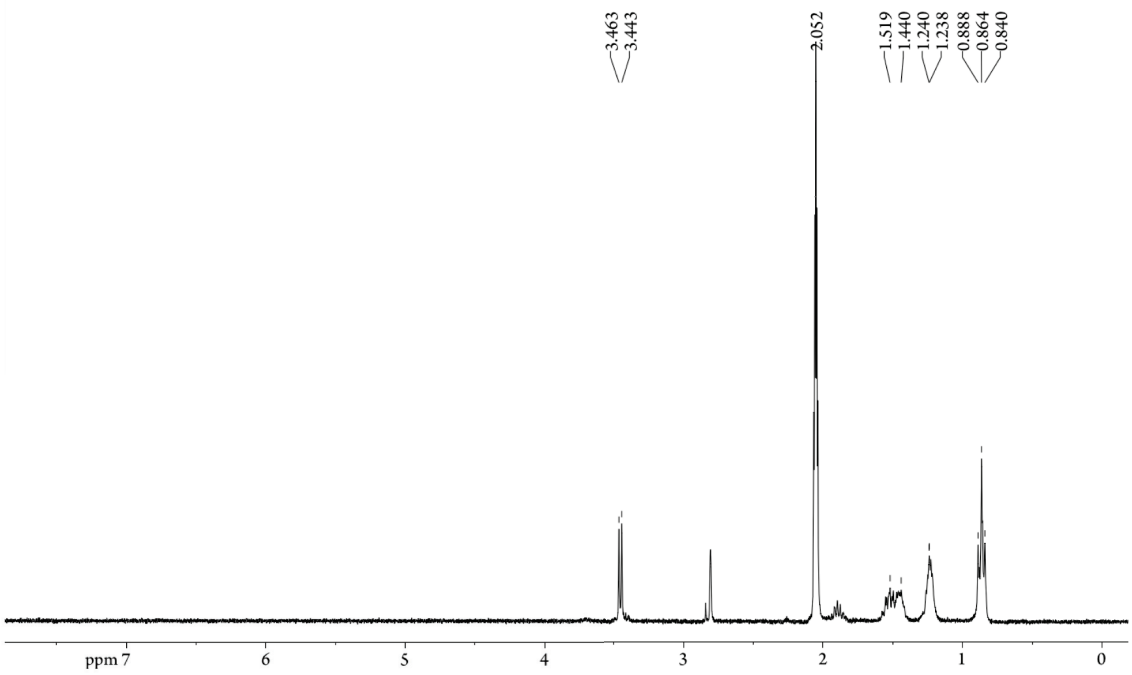

^{1}H NMR spectrum of compound **2.3c** in acetone-d_6.

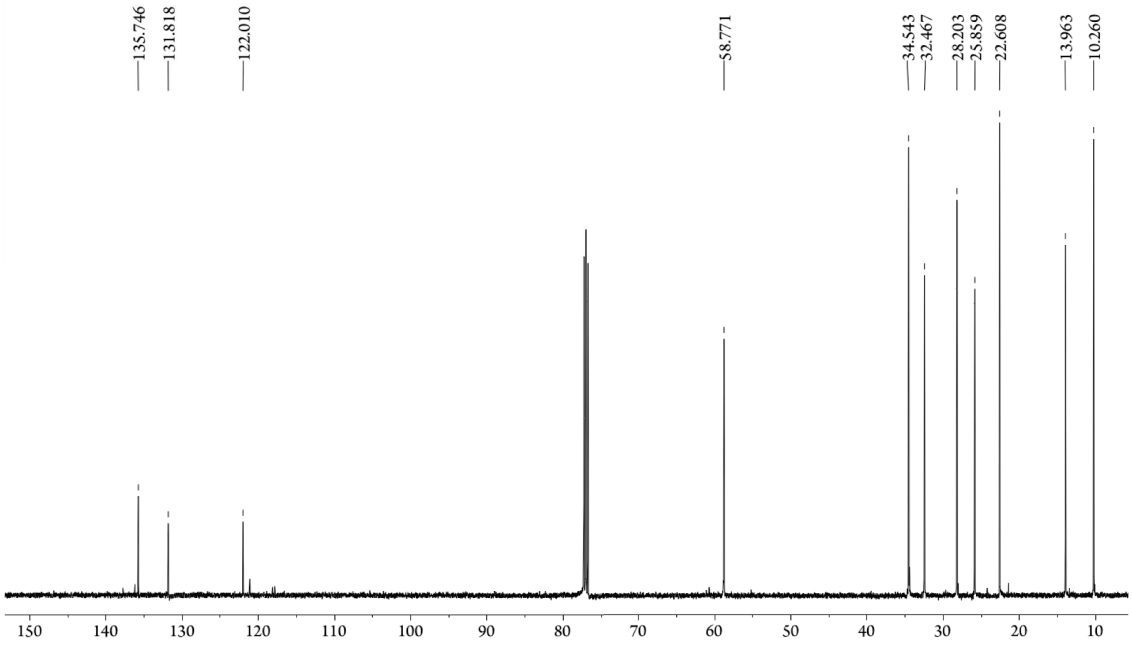

^{13}C NMR spectrum of compound **2.3c** in $CDCl_3$.

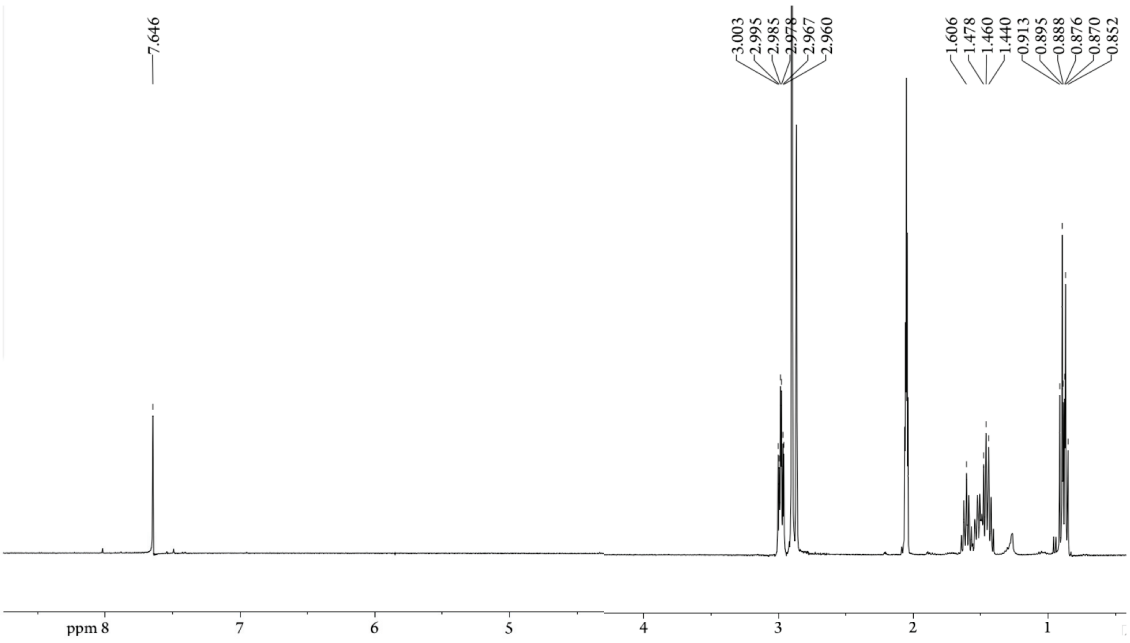

^{1}H NMR spectrum of compound **2.4** in $CDCl_3$.

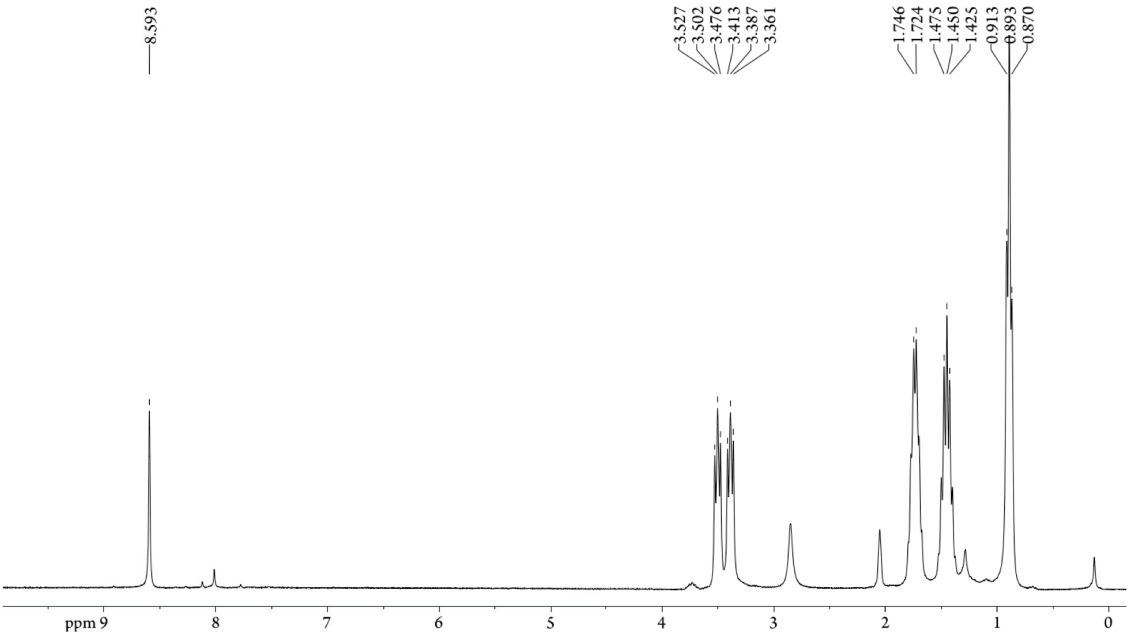

^{1}H NMR spectrum of compound **2.5** in acetone-d_6.

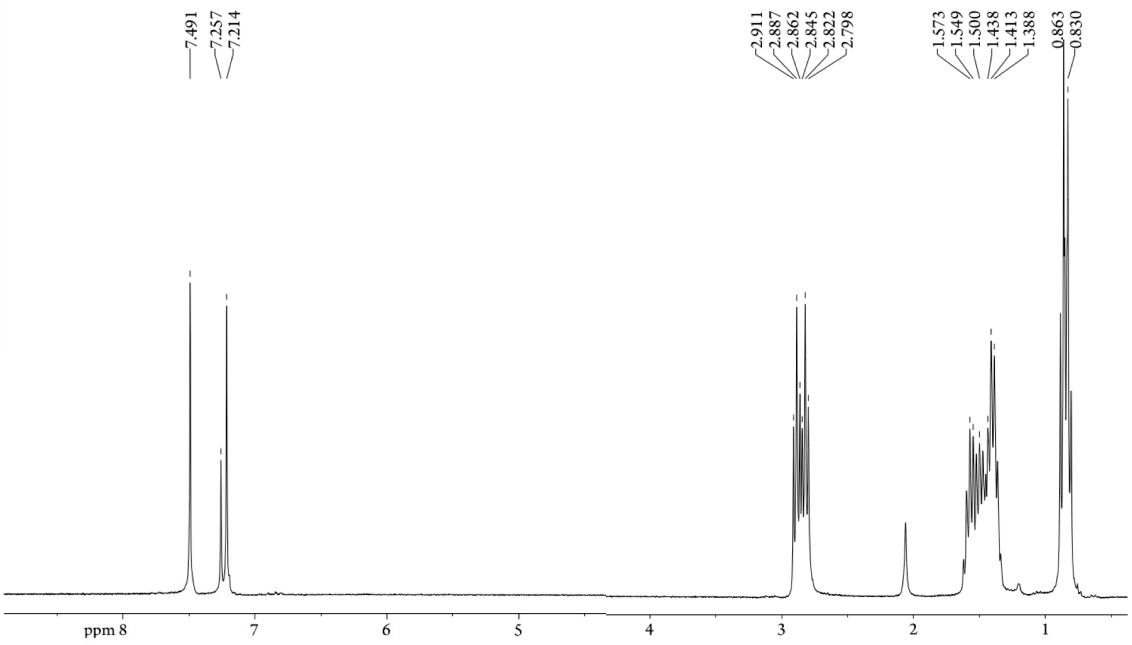

^{1}H NMR spectrum of compound **S-2TTV** in $CDCl_3$.

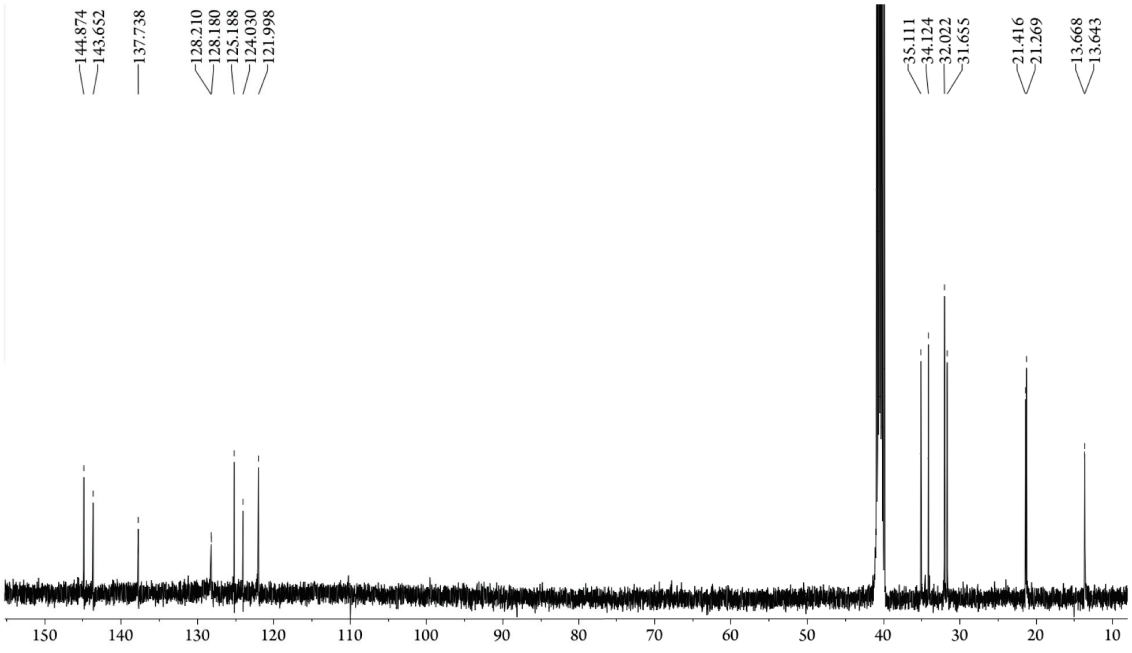

^{13}C NMR spectrum of compound **S-2TTV** in dimethyl sulfoxide-d_6 at 83 °C.

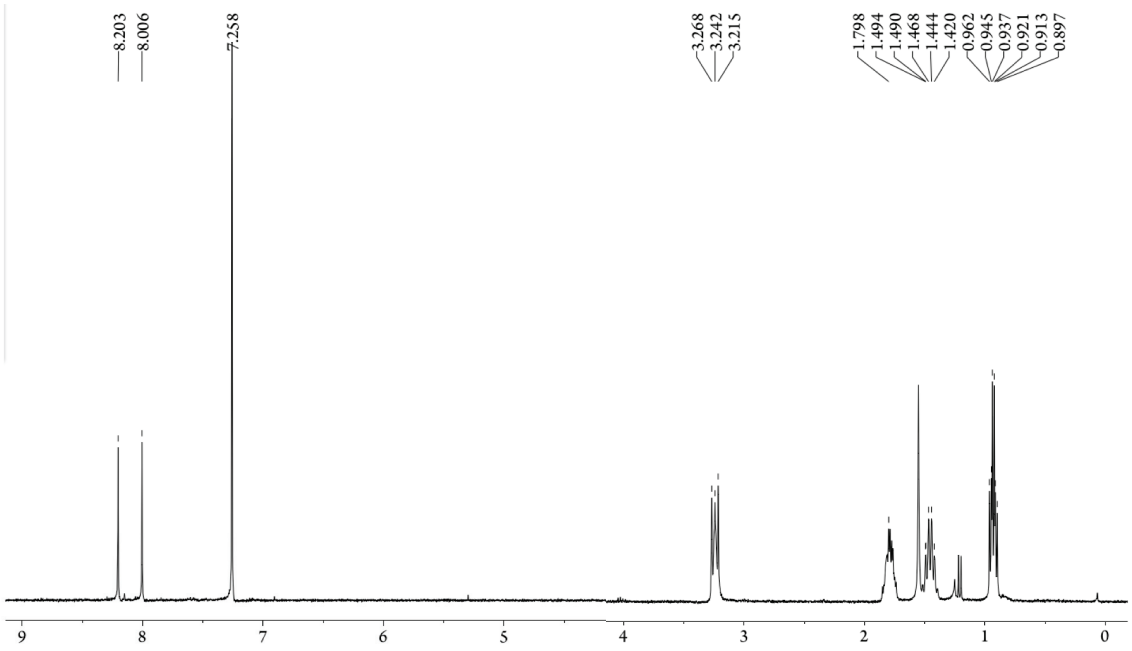

^{1}H NMR spectrum of compound **SO_2-2TTV** in $CDCl_3$.

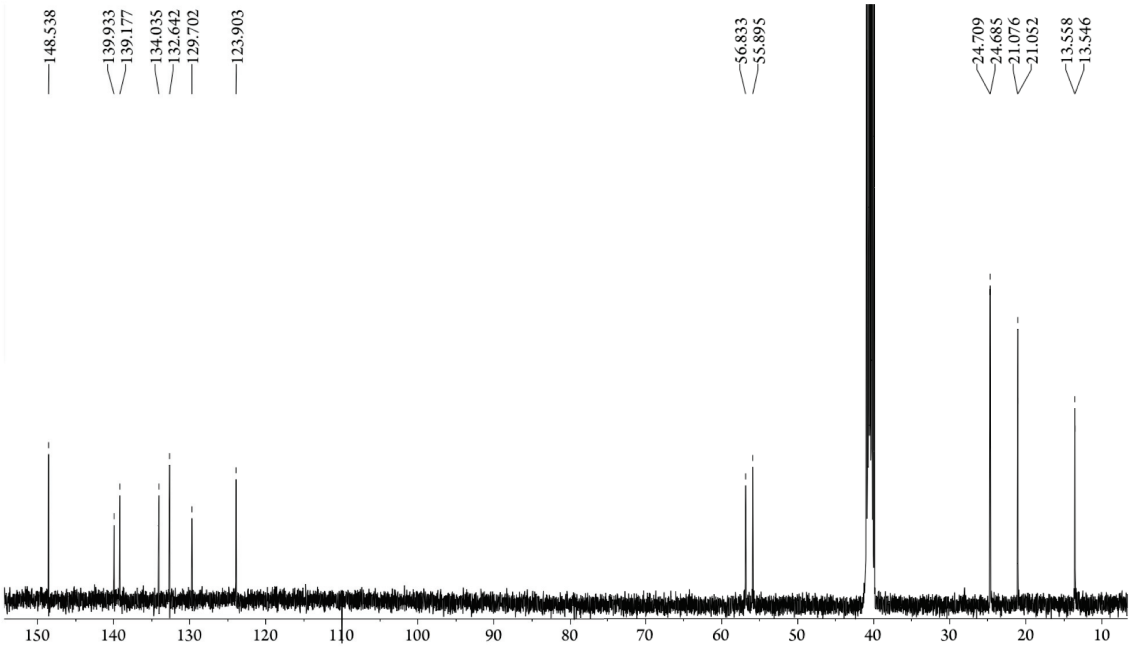

^{13}C NMR spectrum of compound **SO_2-2TTV** in dimethyl sulfoxide-d_6 at 90 °C.

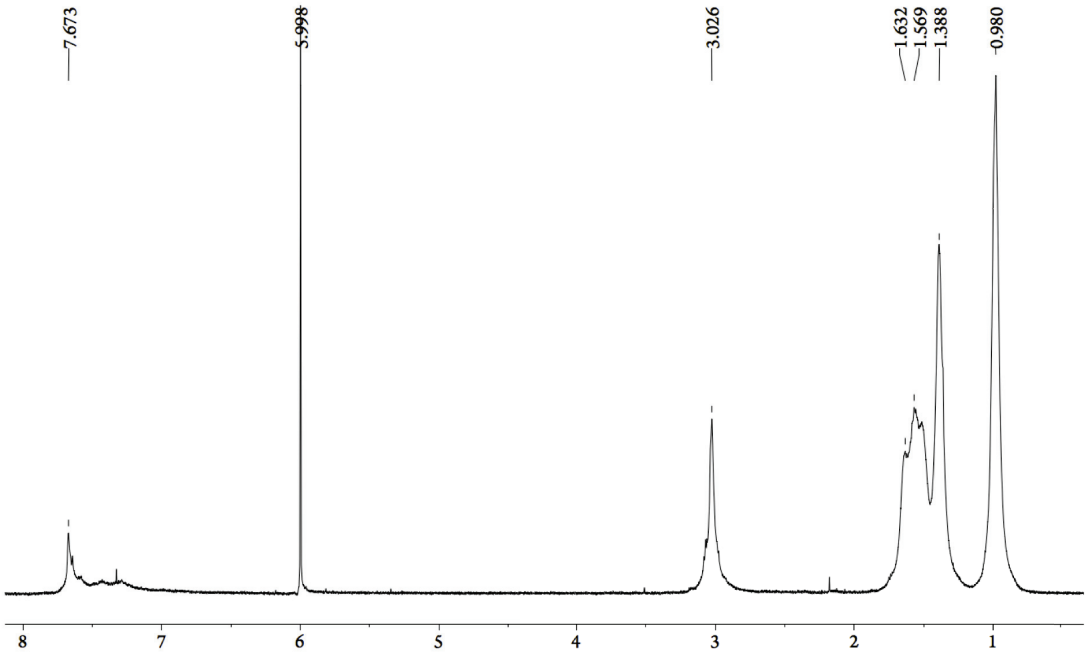

^{1}H NMR spectrum of compound **S-PTTVc** in TCE-d_2 at 120 °C.

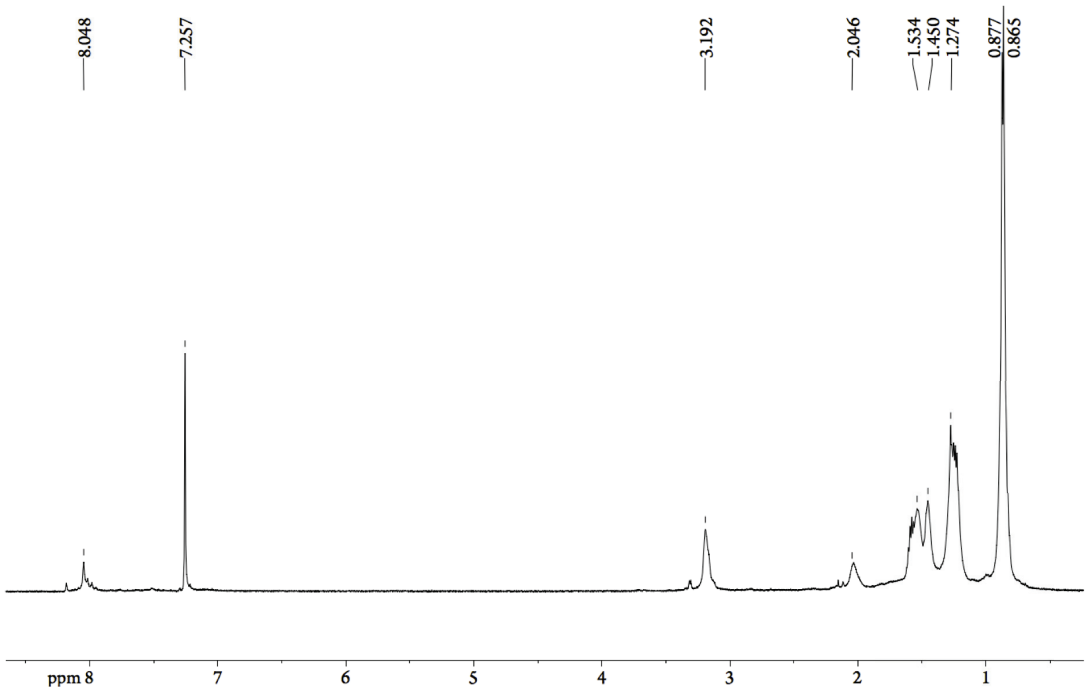

^{1}H NMR spectrum of compound **SO_2-PTTVc** in $CDCl_3$ at 55 °C.

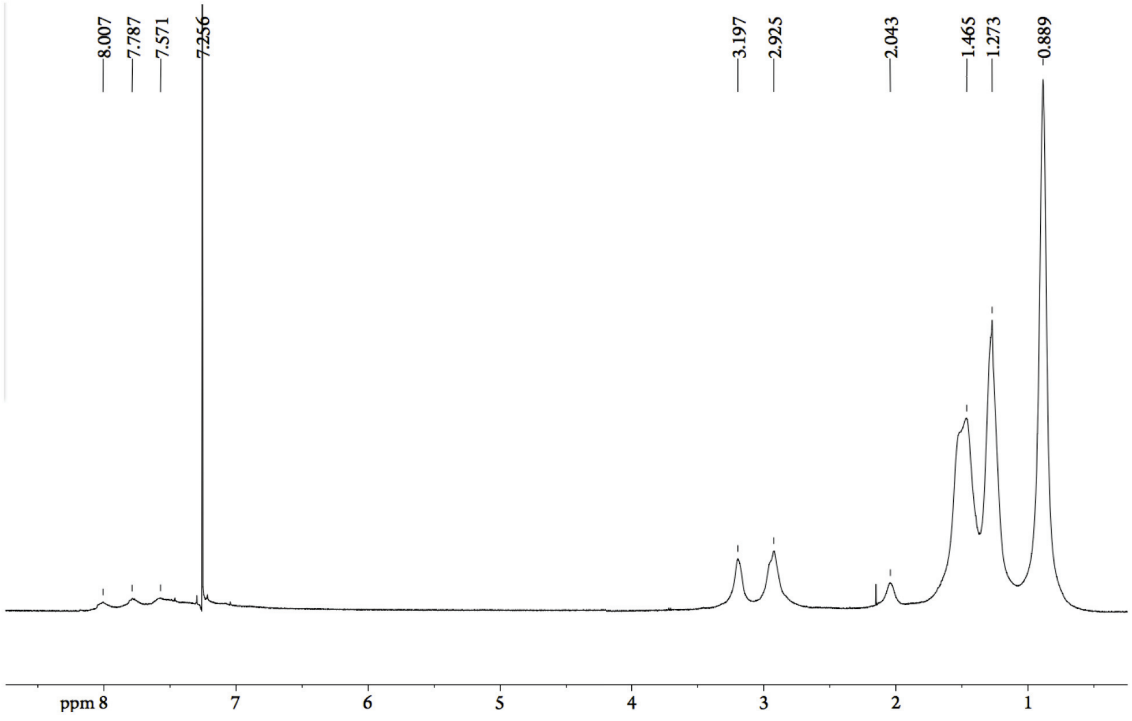

^{1}H NMR spectrum of compound **S/SO$_2$-PTTV-1:1** in CDCl$_3$ at 55 °C.

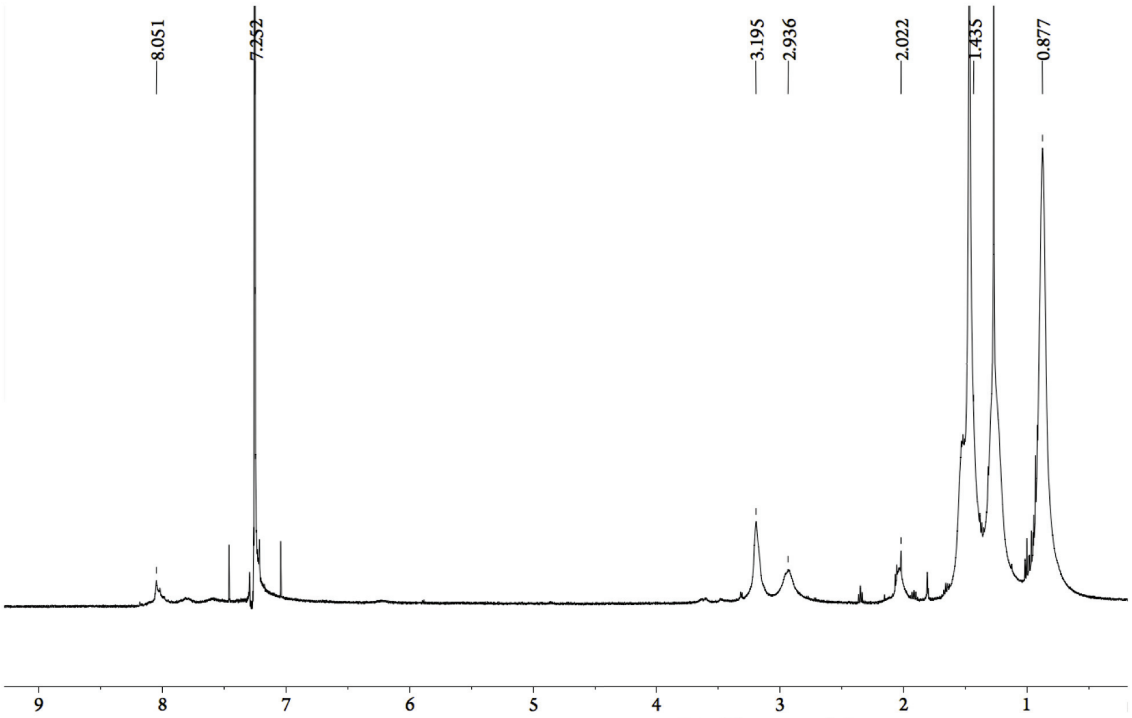

^{1}H NMR spectrum of compound **S/SO$_2$-PTTV-1:2** in CDCl$_3$ at 55 °C.

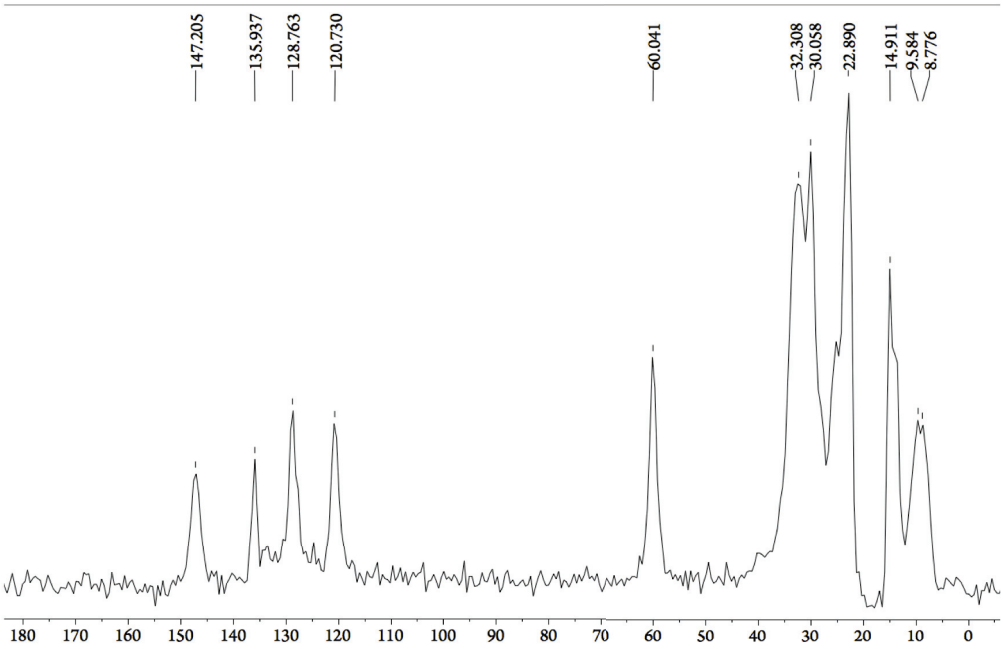

CP-MAS ^{13}C NMR spectrum of compound **SO_2-PTTVc** in the solid state. (TOSS: Total Suppression of Spinning Sidebands)

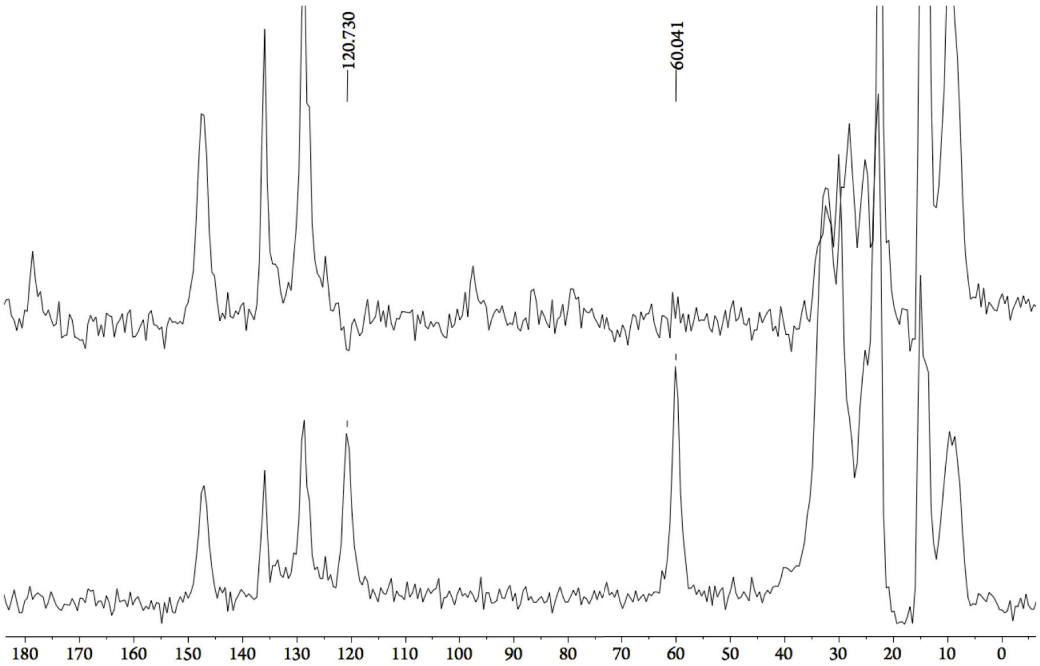

CP-MAS ^{13}CNMR spectra of compound **SO_2-PTTVc** (bottom) showing the suppression of the non-quaternary carbons on the vinyl group and part of side-chain under Dipolar Dephasing (top).

2.6.5 Photovoltaic Properties

Table S1. Photovoltaic properties of devices based on **S/SO$_2$-PTTVc-1:1**.

Conditions			Isc (mA/cm^2)	Voc (V)	FF	PCE
PCBM & ratio to polymer	top contact	spin rate				
PC$_{70}$BM 1:1 in CB	Ca+Al	1,000 rpm	2.37	0.78	0.31	0.57%
PC$_{70}$BM 2:1 in CB	Ca+Al	1,000 rpm	0.97	0.76	0.32	0.24%
PC$_{70}$BM 3:1 in CB	Ca+Al	1,000 rpm	1.04	0.77	0.32	0.25%
PC$_{70}$BM 1:1 in CB	Al	1,000 rpm	1.58	0.80	0.25	0.32%
PC$_{70}$BM 1:1 in CB	Al	1,500 rpm	1.78	0.80	0.29	0.41%
PC$_{70}$BM 1:1 in CB	Ca+Al	1,500 rpm	1.64	0.82	0.29	0.39%
PC$_{60}$BM 1:1 in CF	Al	1,000 rpm	0.81	0.76	0.25	0.16%
PC$_{60}$BM 1:1 in CF	Al	1,500 rpm	0.86	0.74	0.23	0.15%
PC$_{60}$BM 1:1 in CF	Al	1,000 rpm	0.66	0.76	0.24	0.12%
PC$_{60}$BM 1:1 in CF	Al	1,500 rpm	1.28	0.78	0.25	0.25%
PC$_{70}$BM 1:1 in CB no additive	Ca+Al	1,400 rpm	2.68	0.64	0.29	0.51%
PC$_{70}$BM 1:1 in CB 0.5% DIO	Ca+Al	1,400 rpm	4.07	0.66	0.29	0.78%
PC$_{70}$BM 1:1 in CB 1% DIO	Ca+Al	1,400 rpm	4.03	0.64	0.27	0.70%
PC$_{70}$BM 1:1 in CB 2% DIO	Ca+Al	1,400 rpm	3.97	0.64	0.29	0.73%
PC$_{70}$BM 1:1 in CB 3% DIO	Ca+Al	1,400 rpm	3.84	0.50	0.31	0.59%
PC$_{70}$BM 1:1 in CB no additive	Ca+Al	1,400 rpm	2.68	0.64	0.29	0.51%
PC$_{70}$BM 1:1 in CB 0.5% CN	Ca+Al	1,400 rpm	3.79	0.74	0.29	0.81%
PC$_{70}$BM 1:1 in CB 1% CN	Ca+Al	1,400 rpm	4.10	0.74	0.27	0.70%
PC$_{70}$BM 1:1 in CB 2% CN	Ca+Al	1,400 rpm	3.99	0.70	0.26	0.74%
PC$_{70}$BM 1:1 in CB 3% CN	Ca+Al	1,400 rpm	4.46	0.70	0.27	0.84%

Table S2. Photovoltaic properties of devices based on **S-PTTV**.

Conditions			Isc (mA/cm^2)	Voc (V)	FF	PCE
PCBM & ratio to polymer	top contact	spin rate				
PC$_{70}$BM 1:1 in CB	Ca+Al	1,000 rpm	2.92	0.67	0.27	0.52%
PC$_{70}$BM 1:1 in CB	Ca+Al	1,500 rpm	3.19	0.69	0.30	0.65%
PC$_{70}$BM 1:1 in CB	Ca+Al	2,000 rpm	3.14	0.68	0.34	0.72%
PC$_{70}$BM 1:1 in CB	Ca+Al	2,500 rpm	3.16	0.68	0.37	0.79%
PC$_{70}$BM 1:1 in CB	Ca+Al	3,000 rpm	3.04	0.68	0.36	0.74%

2.6.6 Computational Data

Computational data for P3MT (SCF total energy = –1182.263464 hartrees)

Periodic Boundary Conditions

Gaussian 09 Method: RB3LYP Basis set: 6-31G (d)

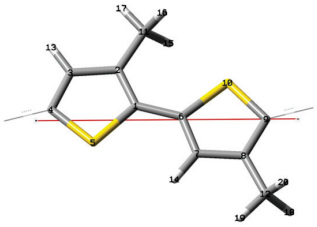

	Coordinates (Angstroms)		
Atom	X	Y	Z
1	3.017078	0.328786	0.453021
2	2.37889	1.56607	0.427785
3	0.967995	1.444802	0.410682
4	0.47962	0.150251	0.421956
5	1.83097	-0.973377	0.456727
6	4.41622	-0.020326	0.473197
7	4.971941	-1.287335	0.486516
8	6.387328	-1.333722	0.505499
9	6.959466	-0.064302	0.506776
10	5.706436	1.173444	0.485631
11	3.060844	2.909246	0.417093
12	7.138874	-2.639247	0.520742
13	0.318172	2.313864	0.388849
14	4.368387	-2.189416	0.481468
15	3.712164	3.031718	-0.456762
16	3.682304	3.060977	1.307978
17	2.317878	3.712096	0.391425
18	7.797347	-2.743906	-0.350056
19	6.438972	-3.480225	0.509519
20	7.765642	-2.741407	1.414972
21	7.858552	0.208103	0.097581

Computational data for H-PTTV (SCF total energy = –1103.6243489 hartrees)

Periodic Boundary Conditions

Gaussian 09 Method: RB3LYP Basis set: 6-31G (d)

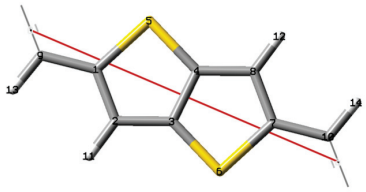

	Coordinates (Angstroms)		
Atom	X	Y	Z
1	1.904455	0.247009	-0.051134
2	2.881394	1.210363	-0.250786
3	4.185855	0.683396	-0.14176
4	4.232604	-0.683451	0.141444
5	2.62185	-1.344205	0.278448
6	5.796608	1.344148	-0.27877
7	6.514003	-0.247061	0.050828
8	5.537064	-1.210418	0.250469
9	0.486545	0.464964	-0.096145
10	7.931913	-0.465016	0.095844
11	2.64214	2.245915	-0.465192
12	5.776318	-2.245971	0.464873
13	0.200797	1.494654	-0.309622
14	8.217661	-1.494707	0.309317
15	8.418186	-0.000257	-0.000914

Computational data for S-PTT (SCF total energy = –11407.2568657 hartrees)

Periodic Boundary Conditions

Gaussian 09 Method: RB3LYP Basis set: 6-31G (d)

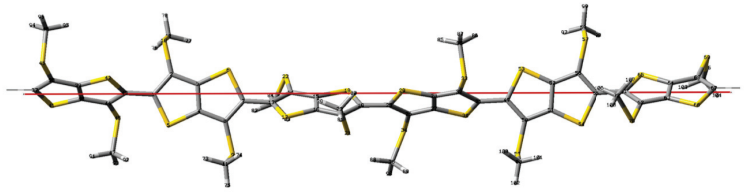

	Coordinates (Angstroms)		
Atom	X	Y	Z
1	6.634635	0.320019	-0.446091
2	7.559098	1.201359	0.088479
3	8.894278	0.783823	-0.197242
4	8.989609	-0.379691	-0.944787
5	7.412672	-1.018795	-1.304616
6	10.466435	1.452375	0.125815
7	11.246676	0.132296	-0.762431
8	10.322643	-0.77046	-1.271192
9	10.712704	-2.157512	-2.316988
10	7.16167	2.677604	1.003773
11	10.478508	-3.567932	-1.162622
12	7.250836	3.930428	-0.33932
13	12.703904	0.068451	-0.795172
14	13.614674	1.016376	-1.235089
15	14.956053	0.591814	-1.002351
16	15.073267	-0.655556	-0.407344
17	13.509458	-1.35483	-0.114705
18	16.517808	1.253624	-1.386723
19	17.323405	-0.175618	-0.716978
20	16.414486	-1.108158	-0.23361
21	16.831464	-2.721861	0.391479
22	13.231097	2.58184	-1.995744
23	16.521179	-2.510387	2.190292
24	12.518708	2.033412	-3.596927
25	18.780595	-0.202697	-0.654982
26	19.706866	-0.023756	-1.671049
27	21.039578	-0.046428	-1.165099
28	21.137261	-0.244989	0.204329
29	19.562824	-0.414028	0.920414
30	22.613216	0.034565	-1.899965
31	23.393614	-0.201092	-0.33037
32	22.472635	-0.33104	0.698896
33	22.876178	-0.702782	2.39208
34	19.350064	0.204982	-3.40237
35	22.59518	0.923005	3.201156
36	18.765568	-1.47404	-3.863854
37	0.570976	0.230569	0.046463
38	1.512164	0.122759	1.056457
39	2.838779	0.171733	0.531168
40	2.912655	0.326388	-0.844674
41	1.323615	0.396871	-1.547788
42	4.424716	0.137024	1.242737
43	5.177411	0.336283	-0.345197
44	4.239562	0.414002	-1.363087
45	4.617212	0.720103	-3.075443
46	1.147	-0.040229	2.792788
47	4.365582	-0.946163	-3.808313
48	1.285644	1.71476	3.324007
49	24.851034	-0.163723	-0.25221
50	25.783159	-0.975306	-0.878303
51	27.114632	-0.555813	-0.579534
52	27.201713	0.539553	0.265485
53	25.619792	1.111989	0.705887
54	28.693043	-1.159048	-0.989066
55	29.464425	0.093652	-0.001294
56	28.533127	0.928756	0.600683
57	28.916397	2.230187	1.753817
58	25.402313	-2.372137	-1.916704
59	28.657467	3.726992	0.71961
60	25.615031	-3.746826	-0.714059
61	30.92081	0.183271	0.010324
62	31.855628	-0.778473	0.359243

63	33.184789	-0.312749	0.135128
64	33.269867	0.977685	-0.366768
65	31.68875	1.668047	-0.575935
66	34.765133	-0.976199	0.428684
67	35.530685	0.5111	-0.145947
68	34.600897	1.462179	-0.537854
69	34.993308	3.118714	-1.056463
70	31.514966	-2.404713	1.003689
71	34.659616	3.023201	-2.860895
72	30.82331	-1.994594	2.654679
73	9.481415	-3.552612	-0.716646
74	11.242386	-3.563251	-0.381469
75	10.586373	-4.473349	-1.766132
76	6.494672	3.731423	-1.101735
77	8.245588	3.952947	-0.790087
78	7.047487	4.89632	0.131179
79	15.504331	-2.157613	2.377707
80	17.246468	-1.823593	2.633062
81	16.643923	-3.500855	2.636936
82	11.596517	1.46977	-3.441816
83	13.23986	1.433324	-4.155796
84	12.294907	2.945578	-4.156872
85	21.5867	1.293646	3.003344
86	23.337653	1.654533	2.873293

87	22.708813	0.751223	4.275029
88	17.847536	-1.727806	-3.329708
89	19.537765	-2.220464	-3.665968
90	18.561075	-1.439625	-4.937497
91	3.365704	-1.327483	-3.588551
92	5.124422	-1.646397	-3.451195
93	4.471088	-0.821103	-4.889445
94	0.523447	2.326133	2.83614
95	2.281048	2.111947	3.112551
96	1.118545	1.719407	4.404677
97	27.658525	3.73395	0.277515
98	29.417842	3.796491	-0.061884
99	28.755932	4.581593	1.394604
100	24.883995	-3.669319	0.093638
101	26.62858	-3.760601	-0.306882
102	25.440843	-4.66962	-1.274288
103	33.642863	2.674765	-3.056816
104	35.38391	2.372432	-3.356614
105	34.768501	4.04146	-3.244226
106	29.884095	-1.446063	2.559244
107	31.540952	-1.417741	3.241756
108	30.634812	-2.951042	3.149979
109	36.416591	0.340594	-0.276348

Computational data for S-PTT (planar, D = 0º)

(SCF total energy = –1901.2081061 hartrees)

Periodic Boundary Conditions

Gaussian 09 Method: RB3LYP Basis set: 6-31G (d)

	Coordinates (Angstroms)		
Atom	X	Y	Z
1	5.392124	-0.096771	-0.045839
2	4.486108	-0.738745	0.811241
3	3.139775	-0.432347	0.486716
4	2.979308	0.412512	-0.592082
5	4.515086	0.865116	-1.276373
6	1.604009	-0.884875	1.171071
7	0.726969	0.07703	-0.059454
8	1.632987	0.719029	-0.916512
9	1.270487	1.773967	-2.305643
10	4.848629	-1.793538	2.200474
11	1.199927	3.421013	-1.491156
12	4.919175	-3.440669	1.386182
13	2.127661	3.624321	-0.951857
14	0.344426	3.483808	-0.814683
15	1.080413	4.15349	-2.294334
16	5.774523	-3.503464	0.709512
17	3.991337	-3.64415	0.847121
18	5.038944	-4.173031	2.189425
19	6.114973	-0.204826	0.012928

Computational data for S-PTTV (SCF total energy = –1978.6261487 hartrees)

Periodic Boundary Conditions

Gaussian 09 Method: RB3LYP Basis set: 6-31G (d)

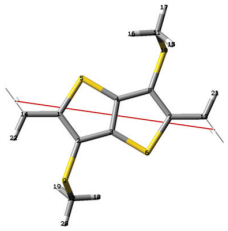

	Coordinates (Angstroms)		
Atom	X	Y	Z
1	1.87681	-0.191551	-0.201093
2	2.866198	-0.869918	-0.918595
3	4.166573	-0.482824	-0.504471
4	4.194985	0.479907	0.497309
5	2.581938	0.935842	0.975471
6	5.779621	-0.938761	-0.982628
7	6.484748	0.188639	0.193928
8	5.49536	0.867001	0.911433
9	2.546676	-2.100951	-2.163382
10	5.814877	2.098024	2.156231
11	5.574889	1.111525	3.690442
12	2.786718	-1.11448	-3.697603
13	7.90315	0.333975	0.345531
14	0.458409	-0.336885	-0.352698
15	6.316301	0.312243	3.758432
16	4.566678	0.693272	3.733271
17	5.711552	1.80551	4.524403
18	3.794945	-0.696264	-3.740426
19	2.045335	-0.315174	-3.765612
20	2.65004	-1.808473	-4.531554
21	8.191473	1.06374	1.100085
22	0.170084	-1.06665	-1.107251
23	8.400969	0	0

Computational data for SO_2-PTTV (SCF total energy = –4558.7752141 hartrees)

Periodic Boundary Conditions

Gaussian 09 Method: RB3LYP Basis set: 6-31G (d)

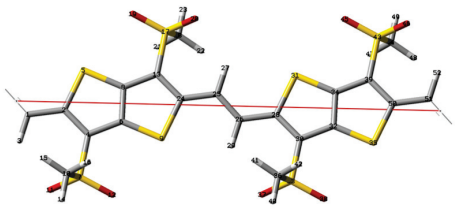

	Coordinates (Angstroms)		
Atom	X	Y	Z
1	0.461574	-0.508697	-0.09665
2	1.88531	-0.298209	-0.084086
3	0.159098	-1.552715	-0.131612
4	2.882906	-1.265367	0.040968
5	2.584531	1.319244	-0.25242
6	4.188881	-0.7163	-0.013914
7	2.620614	-3.014009	0.325731
8	4.198352	0.668462	-0.17672
9	5.802731	-1.36686	0.063451
10	2.267604	-3.115446	2.096897
11	1.416624	-3.450631	-0.395908
12	3.922257	-3.658069	0.088192
13	5.504293	1.217627	-0.231169
14	2.118754	-4.175554	2.318362
15	1.360389	-2.549093	2.316117
16	3.121775	-2.725217	2.653635
17	5.766324	2.96564	-0.519904
18	6.118497	3.062442	-2.291565
19	4.464733	3.610229	-0.283506
20	6.970589	3.404299	0.200036
21	5.264199	2.670417	-2.846854
22	7.02577	2.49575	-2.509671
23	6.266905	4.121982	-2.516022
24	6.501936	0.250779	-0.103816
25	7.925475	0.46195	-0.087324
26	8.863308	-0.523808	-0.07585
27	8.227303	1.506268	-0.056348
28	10.286881	-0.311669	-0.063625
29	8.562419	-1.568663	-0.099923
30	11.284724	-1.27357	0.094513
31	10.985341	1.299954	-0.282282
32	12.59047	-0.725663	0.025236
33	11.021368	-3.010518	0.441739
34	12.599418	0.65344	-0.180691
35	14.204535	-1.372411	0.12533
36	10.651911	-3.04485	2.212127
37	9.824671	-3.475625	-0.274275
38	12.325669	-3.661902	0.241263
39	13.90519	1.201271	-0.250254
40	10.501598	-4.095824	2.472647
41	9.74256	-2.471107	2.401082
42	11.500804	-2.632805	2.761166
43	14.168781	2.938992	-0.593479
44	14.539012	2.977991	-2.363549
45	12.864459	3.589932	-0.391769
46	15.365237	3.402056	0.124266
47	13.690196	2.567801	-2.914087
48	15.448237	2.404433	-2.553652
49	14.689856	4.029623	-2.621086
50	14.902988	0.239009	-0.094343
51	16.326757	0.450405	-0.086025
52	16.628278	1.494994	-0.058001
53	16.802493	-0.027201	0.013424

Computational data for S/SO_2-PTTV (alternating)

(SCF total energy = –4258.0159246 hartrees)

Periodic Boundary Conditions

Gaussian 09 Method: RB3LYP Basis set: 6-31G (d)

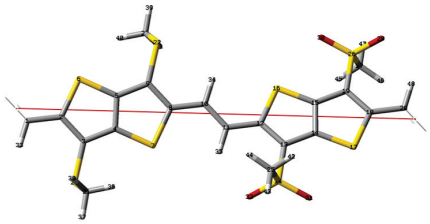

	Coordinates (Angstroms)		
Atom	X	Y	Z
1	16.324027	0.469067	0.058822
2	14.903438	0.274901	0.032326
3	13.927316	1.257521	0.221812
4	12.6211	0.711832	0.128257
5	12.580849	-0.657921	-0.111821
6	14.185206	-1.32438	-0.238458
7	11.016809	1.378347	0.254983
8	10.298515	-0.220865	-0.016045
9	11.274601	-1.203605	-0.205207
10	8.877903	-0.414778	-0.043003
11	7.935236	0.524371	0.242733
12	6.513282	0.319407	0.15772
13	5.501481	1.14347	0.649661
14	4.201646	0.642844	0.376582
15	4.209509	-0.561288	-0.322849
16	5.833765	-1.098447	-0.655624
17	2.57737	1.179977	0.70937
18	1.897883	-0.237984	-0.103777
19	2.909692	-1.061933	-0.595892
20	14.280222	2.984117	0.461553
21	13.834157	3.197575	2.233186
22	10.921452	-2.93023	-0.444266
23	11.369785	-3.145277	-2.215116
24	5.745539	2.617265	1.629686
25	6.138752	1.978876	3.275975
26	2.665678	-2.535532	-1.57622
27	2.272195	-1.896733	-3.222284
28	0.475953	-0.443257	-0.188406
29	1.48522	-3.265486	-1.088775
30	3.979902	-3.195553	-1.652502
31	4.43139	3.277474	1.705621
32	6.926151	3.346914	1.142158
33	16.625117	1.480474	0.326571
34	8.576665	-1.426121	-0.310804
35	8.232679	1.523061	0.553609
36	12.785736	2.948118	2.410627
37	13.992651	4.255881	2.456965
38	14.480202	2.591328	2.871829
39	11.211099	-4.203699	-2.438216
40	12.418556	-2.896472	-2.391406
41	10.72486	-2.539276	-2.855123
42	5.300738	1.376822	3.63243
43	6.283867	2.85122	3.918548
44	7.054854	1.387492	3.220897
45	3.110154	-1.294573	-3.578703
46	1.356104	-1.305357	-3.166934
47	2.126987	-2.768906	-3.865066
48	0.178637	-1.442	-0.499224
49	16.790859	-0.026577	-0.038888

Computational data for S/SO_2-PTTV (AADD-"block")

(SCF total energy = –8516.0303799 hartrees)

Periodic Boundary Conditions

Gaussian 09 Method: RB3LYP Basis set: 6-31G (d)

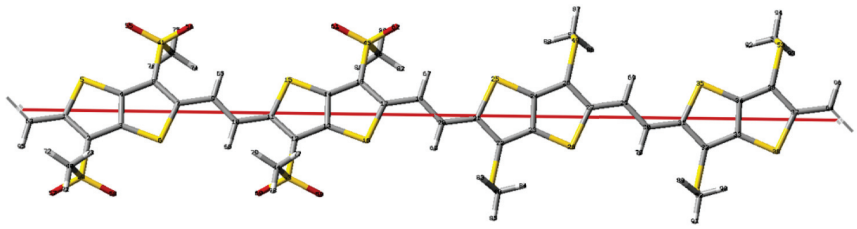

	Coordinates (Angstroms)		
Atom	X	Y	Z
1	31.700335	0.068774	0.247679
2	30.686838	0.244907	1.190247
3	29.387761	0.122335	0.631469
4	29.398021	-0.149484	-0.734977
5	31.02352	-0.260779	-1.35498
6	27.763881	0.241784	1.250212
7	27.086989	-0.096019	-0.350688
8	28.100507	-0.272763	-1.293021
9	25.66671	-0.17577	-0.567333
10	24.713911	0.146917	0.349335
11	23.293805	0.067782	0.13092
12	22.278524	0.247489	1.070789
13	20.981963	0.125535	0.51005
14	20.994892	-0.148634	-0.855902
15	22.619825	-0.271885	-1.470853
16	19.355086	0.241448	1.125791
17	18.681567	-0.08928	-0.478016
18	19.696993	-0.269469	-1.417662
19	17.261214	-0.158749	-0.694503
20	16.3147	0.223998	0.206259
21	14.895396	0.126036	0.035546
22	13.919154	0.573545	0.93168
23	12.613802	0.316361	0.443233
24	12.571876	-0.326669	-0.789547
25	14.174583	-0.629091	-1.399424
26	11.007885	0.621879	1.047902
27	10.288012	-0.133187	-0.388115
28	11.265756	-0.582858	-1.280253
29	8.867391	-0.233787	-0.556312
30	7.92295	0.212756	0.315456
31	6.502226	0.111567	0.149003
32	5.525974	0.557651	1.04459
33	4.219112	0.299998	0.556856
34	4.175043	-0.340207	-0.677342
35	5.780014	-0.64105	-1.287071
36	2.617677	0.59664	1.172676
37	1.894268	-0.157087	-0.261669
38	2.868796	-0.599631	-1.162212
39	30.928249	0.485549	2.944086
40	31.31621	-1.172151	3.55659
41	27.863524	-0.532844	-3.047356
42	27.493005	1.120052	-3.681975
43	22.512202	0.510663	2.825094
44	22.878425	-1.141552	3.463995
45	19.459333	-0.512578	-3.171691
46	19.075126	1.144715	-3.78764
47	14.266741	1.417419	2.45921
48	13.905385	0.091102	3.681681
49	10.927342	-1.420802	-2.813303
50	11.154591	-0.049453	-4.018475
51	5.866603	1.392267	2.578969
52	5.649182	0.016305	3.780693
53	2.518338	-1.440772	-2.690585
54	2.872831	-0.11093	-3.911232
55	29.176839	-0.934019	-3.578495
56	26.675305	-1.371536	-3.263476

57	32.111219	1.32986	3.169986
58	29.613825	0.868514	3.485595
59	21.198476	0.915263	3.35261
60	23.701491	1.347633	3.042018
61	20.774459	-0.898291	-3.709503
62	18.275703	-1.355588	-3.399007
63	33.121133	0.141682	0.459978
64	0.47471	-0.258915	-0.427597
65	25.37934	-0.550309	-1.547071
66	25.000813	0.521712	1.329103
67	16.96716	-0.567989	-1.657968
68	16.613382	0.661017	1.157703
69	8.567681	-0.724012	-1.480793
70	8.223038	0.702582	1.240032
71	31.458116	-1.076037	4.636185
72	32.23316	-1.524331	3.080058
73	30.47767	-1.836488	3.339081
74	26.575109	1.485402	-3.217506
75	27.357978	1.011052	-4.761242
76	28.335094	1.780571	-3.466442
77	22.035615	-1.801052	3.24816

78	23.011392	-1.030451	4.543308
79	23.796643	-1.509546	3.002258
80	18.935267	1.04713	-4.867368
81	19.914229	1.808119	-3.569454
82	18.157757	1.499034	-3.313509
83	14.590931	-0.749693	3.555701
84	12.871062	-0.25013	3.59921
85	14.058244	0.539192	4.667159
86	10.420334	0.741565	-3.850331
87	10.997859	-0.486285	-5.008503
88	12.166519	0.357963	-3.963247
89	6.386049	-0.771193	3.607532
90	4.638736	-0.395054	3.72767
91	5.807582	0.450701	4.771526
92	3.906711	0.232294	-3.831529
93	2.185971	0.728154	-3.781057
94	2.717549	-0.557129	-4.897192
95	33.41719	0.54878	1.423739
96	0.174011	-0.693768	-1.379401
97	33.591009	0.023707	-0.017731

3

Polymorphism in New Thienothiophene–Thiazolothiazole Organic Semiconductors

Whereas Chapter 2 focused entirely on sulfur heteroatoms, Chapter 3 discusses the incorporation of both sulfur and nitrogen heteroatoms. Again, a donor–acceptor strategy is adopted in the combination of electron rich thienothiophene moieties and electron deficient thiazolothiazole moieties to form small molecular trimers. Calculations are used to determine what effect the incorporation of thiazole-type nitrogens has on energy levels, reorganization energy and BLA, as compared to an all-sulfur thienothiophene trimer. This chapter also looks at the different heteroatom interactions in the solid-state packing of polymorphs of the trimers.

Reprinted with permission from: Schneider, J. A.; Black, H.; Lin, H.-P.; Perepichka, D. F. *ChemPhysChem* **2015**, *16*, 1173-1178.

3.1 Abstract

Charge transport in organic semiconductors is heavily influenced by their solid-state packing. To separate intermolecular packing effects from molecular electronic effects, we have synthesized two polymorphs of crystalline thienothiophene-thiazolothiazole trimers and studied them by DFT calculations, optical spectroscopy, single-crystal X-ray diffraction and charge-transport measurements in field-effect transistors. One polymorph was found to be a p-type semiconductor with a hole mobility of 3.3×10^{-3} cm^2/Vs, while the other was insulating. The different charge-transport behavior and optical properties of the two polymorphs are strongly related to the topology of their π–stacks. Subtle differences between the polymorphs, including S···S close contacts and bond-length alternation are also discussed for their possible effects on charge transport.

3.2 Introduction

Undeniably, organic semiconductors will play an important role in future electronic technologies. Charge mobilities in organic semiconductors are continuously being improved through the tuning of molecular structures and advances in fabrication techniques.[1] With these performance improvements comes greater scrutiny into how supramolecular ordering dictates charge transport. It is evident that the solid-state packing of a material will have a critical impact on its transport properties,[2] yet there is no consensus as to which packing motifs are most favorable.[3] Consequently, designing new semiconducting materials is still an empirical exercise, with morphological justifications for device performance mostly limited to after the fact discussions. Trends observed for one class of compounds do not always hold true for the next since charge transport is controlled by both the molecular structure and its supramolecular assembly.

The best way to isolate packing effects from molecular structure effects is to study polymorphs of the same material. Polymorphs of small molecules can indeed display vastly different charge mobilities, demonstrating the importance of variations in solid-state packing. For example, one polymorph of dihydrodiazapentalene, DHDAP, exhibits a charge

mobility 5,000 times greater than that of two other polymorphs.[4] Rubrene, one of the most studied semiconductors, has several polymorphs, where the monoclinic, triclinic and orthorhombic forms all display different hole mobilities.[5] Polymorphism has also been observed in thiophene-based materials, most notably the high- and low-temperature forms of sexithiophene.[6]

Thiophene-based materials are ubiquitous in organic electronics because of their synthetic accessibility, relatively low aromatic stabilization (beneficial for extended electron delocalization) and the electronegativity of sulfur being close to that of carbon. Thieno[3,2-*b*]thiophene (TT), a popular building block in organic semiconductors, has a fused bicyclic structure that enhances electron delocalization, promotes π–π stacking, and forms rod-like molecular structures owing to its 180° coupling geometry. TT units have been successfully incorporated into conjugated polymers[7] and oligomers[8] leading to an increase in charge mobility. Thiazolo[5,4-*d*]thiazole's (TzTz) structure is isoelectronic to TT's and is nearly identical except for the addition of electron deficient nitrogen. A recent review[9] on TzTz as a building block in organic electronics covers known structures very well so we will only mention a few significant advances. Takimiya et al. achieved high efficiencies in OPVs with thiophene–TzTz copolymers where the TzTz moiety imparted strong π–π stacking to the crystalline films.[10] Ando's group screened a series of TzTz-containing oligomers in FET devices and found that good n-type properties could be achieved by combining TzTz with electron withdrawing CF_3Ph– groups, but that derivatives with thiophene rings at the termini displayed only modest p-type mobilities.[11]

Combining both TT and TzTz building blocks creates a linear planar molecule with donor–acceptor behavior, structural rigidity and the possibility of S···S close contacts. In this work, we report on two polymorphs of novel thieno[3,2-*b*]thiophene-thiazolo[5,4-*d*]thiazole oligomers, TT–TzTz–TT (**3.1** and **3.2**, Scheme 3.1) and analyze the structure-property relationships, including the effects of heteroatoms and packing geometry.

Scheme 3.1: Synthesis of the TT-TzTz-TT oligomers.

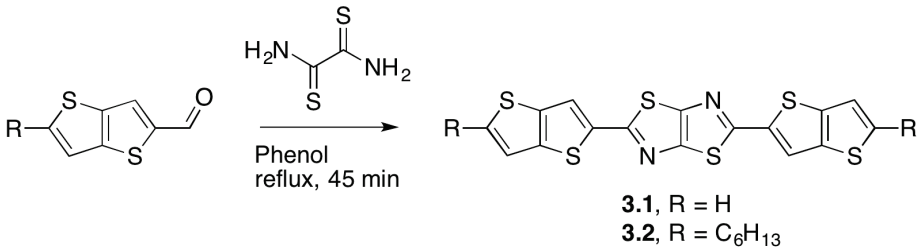

3.3 Results and Discussion

3.3.1 Synthesis and Molecular Properties

The thiazolothiazole core of the oligomers was synthesized by heating thieno[3,2-*b*]thiophene-2-carbaldehydes with dithiooxamide following the classic Ketcham synthesis (Scheme 3.1).[12] Hexyl groups were introduced in **3.2** to improve solubility and film-forming properties. The oligomers were purified by sublimation to yield bright orange solids. The

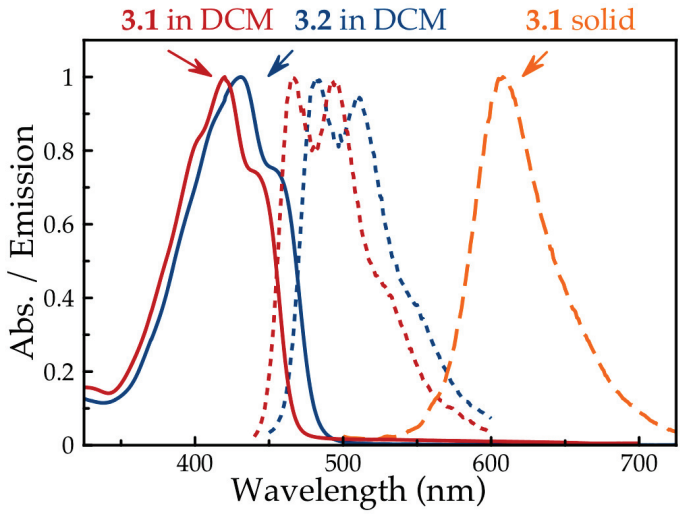

Fig. 3.1.: Absorption (—) and emission (- - -) spectra of **3.1** and **3.2** in CH_2Cl_2 solutions and the solid-state emission of **3.1**.

absorption and emission spectra of **3.1** and **3.2**, recorded in CH_2Cl_2 solutions, both reveal pronounced vibronic structures ($\Delta h\nu$ = 1200 cm^{-1}), as expected for rigid non-polar molecules of this type (Figure 3.1, Table 3.1). Introducing alkyl chains in **3.2** results in 10 nm

Tab. 3.1.: Calculated[a] energy levels, reorganization energies, and bond-length alternation and optical properties of **3.1**, **3.2** and the heteroanalogues 3–TT and 3–TzTz.

	HOMO (eV)	LUMO (eV)	E_g (eV)	λ_h (eV)	λ_e (eV)	Abs max (nm)	Em max (nm)	BLA[c] (Å)
3.1	–5.32	–2.35	2.97	0.317	0.231	420	465	0.0494
3.2	–5.12	–2.20	2.91	—	—	431	482	—
3–TT	–5.05	–1.97	3.08	0.330	0.302	401[b]	448[b]	0.0426
3–TzTz	–5.97	–2.97	3.00	0.306	0.283	—	—	0.0621

[a] Calculated on Gaussian 09 using B3LYP, 6-31G(d).
[b] Literature value (ref. [13]).
[c] Defined here as the average of the difference in length between adjacent single and double bonds.

and 17 nm shifts of the absorption and emission peaks, respectively. This is due to increased donor character from the hexyl–TT moieties which enhance the donor–acceptor interaction in this D–A–D system. The 0–0 transitions for **3.1** and **3.2** (455 and 469 nm, determined as a crossing of the absorption and emission curves) are 2.73 and 2.64 eV, respectively, slightly lower than the DFT-calculated HOMO–LUMO gap of 2.97 and 2.91 eV (Table 3.1). **3.1** and **3.2** are both fluorescent with identical quantum yields of 37% in CH_2Cl_2 solution (lifetimes τ=0.58 ns for **3.1**).

We compared the electronic properties of **3.1** to those of terthieno[3,2-*b*]thiophene (3–TT) and terthiazolo[5,4-*d*]thiazole (3–TzTz), which consist of only donor or acceptor units, respectively (Table 3.1). All three compounds are isoelectronic, differing by the number of nitrogen atoms in the TT framework (0, 2 or 6). As expected, the frontier orbitals of **3.1** lie between those of 3–TT and 3–TzTz, and its HOMO–LUMO gap is slightly lowered due to donor–acceptor interactions. This is confirmed by a ≈20 nm red-shift in the experimental absorption maxima of **3.1** versus 3–TT.[13] Bond length alternation (BLA) in the trimers was calculated given that BLA is a major contributor to band gap reduction in linear conjugated systems and correlates with the ratio of aromatic versus quinoidal character in polyaromatics.[14] The largest contributor to BLA is the bond-length difference between the interring C—C single bond and the N=C double bond in the ring. It follows therefore

that 3–TzTz has the largest BLA and 3–TT the smallest. The calculated BLA of TT–TzTz–TT is lower, however, than the average of the other two trimers, implying a stabilization of the quinoidal form through D–A effects. Reorganization energies were also calculated for both holes and electrons. Not surprisingly, the λ_h of **3.1** fell between that of the other two trimers, but the λ_e was significantly lower than both indicating good electron delocalization through the TzTz moiety (Table 3.1).

Electrochemical measurements of **3.2** were performed in dichlorobenzene and the cyclic voltammogram showed a reversible oxidation at 0.61 V (vs. Fc/Fc+) (Figure 3.2). This indicates a HOMO level of –5.4 eV (assuming Fc HOMO at –4.8 eV). At 0.85 V a second, quasi-reversible oxidation is visible. No reduction waves were observed in the accessible electrochemical window owing to the relatively high band gap.

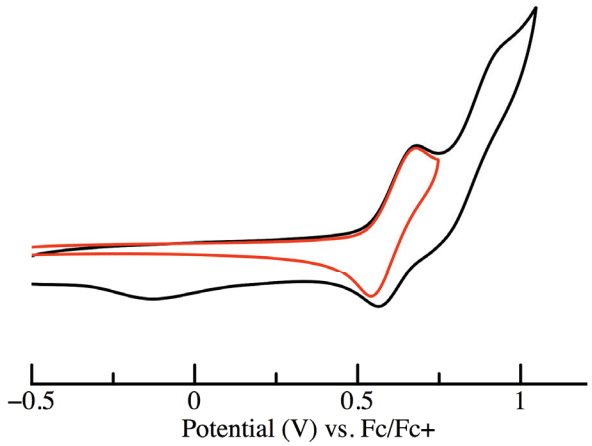

Fig. 3.2.: Cyclic voltammogram of **3.2** showing the first (red curve) and second (black curve) oxidations (0.1M Bu_4NPF_6 in DCB as electrolyte; scan rate 0.1 Vs^{-1}).

3.3.2 Solid–State Properties

Single crystals of **3.1** were grown by physical vapor transport in a horizontal temperature-gradient oven and yielded two polymorphs: red needle-like crystals (**3.1-Red**) in the warmer section and yellow crystals with a more plate-like appearance (**3.1-Yellow**) in the cooler section (Figure 3.3a and 3.4a). The crystal structures of both were determined by X-ray

analysis, revealing the same monoclinic $P2_1/c$ space group for both polymorphs (CCDC 1045343–<1045344, also see the Supporting Information).

The TT–TzTz–TT core in both **3.1-Red** and **3.1-Yellow** polymorphs is nearly planar; the average interring torsion angle is 1.5° and 3.0°, respectively. X-ray analysis shows that the BLA is very similar to the calculated gas-phase value (Table 3.1) and might be slightly smaller for the **3.1-Yellow** polymorph (0.049(3)Å) than for **3.1-Red** (0.054(7)Å), although the difference is not statistically significant. In **3.1-Red** the molecules arrange in a slipped-

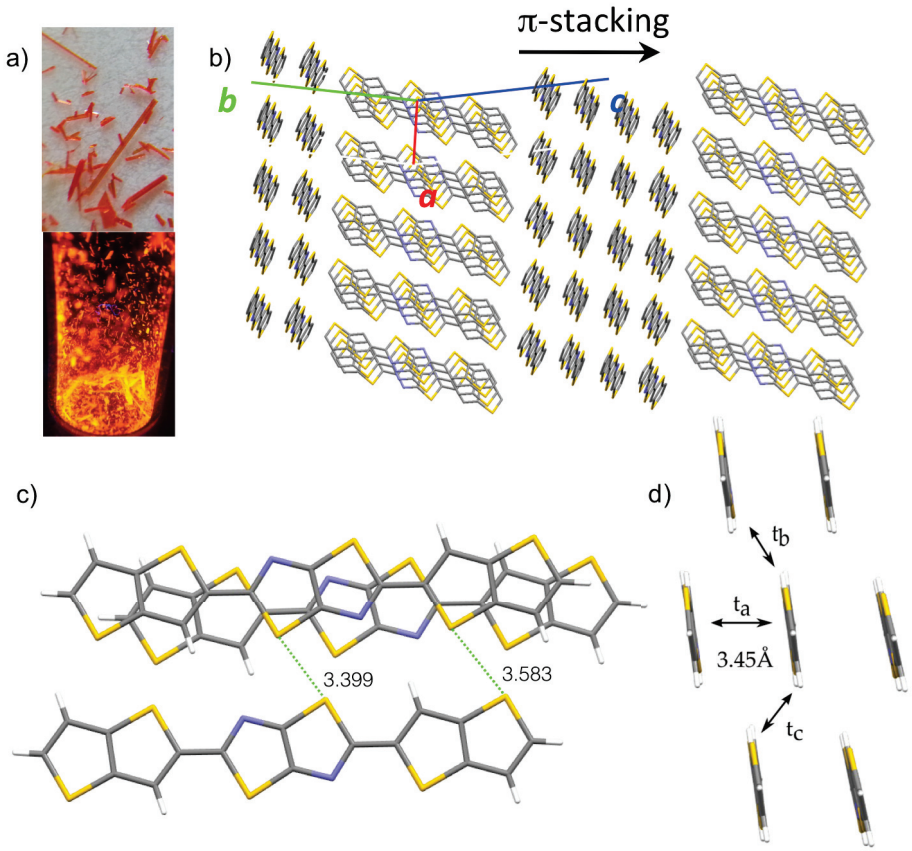

Fig. 3.3.: a) Images of the crystals under normal and UV light. Crystal structure of **3.1-Red** showing the b) lattice, c) unit cell and d) slipped-stacked packing. S···S close contacts and π–π distances are labeled.

stacked packing architecture with an interplanar distance of ≈3.45Å(Figure 3.3d). However, the resulting isolated π–stacks consist of only four molecules and these tetramers meet at 69.3° angles. Therefore, no continuous π–π stacking network capable of long-range trans-

port exists (Figure 3.3b). This is not the case for **3.1-Yellow**, which contains uninterrupted π–stacks with a slightly smaller interplanar distance of ≈3.41Å(Figure 3.4d). Adjacent molecules of the π–stacks in both polymorphs are laterally shifted along both the short and the long axes, but they do so to a much greater extent in **3.1-Yellow** than in **3.1-Red**. The adjacent π–stacks in **3.1-Red** are co-parallel forming a continuous one-dimensional channel (oriented vertically in Figure 3.3b). In **3.1-Yellow**, the molecules of adjacent π–stacks meet at an angle, forming a herringbone sheet-like arrangement, in both *bc* (Figure 3.4b) and *ab* (Figure 3.4d) planes. The packing of **3.1-Yellow** has four S···S close contacts, whereas

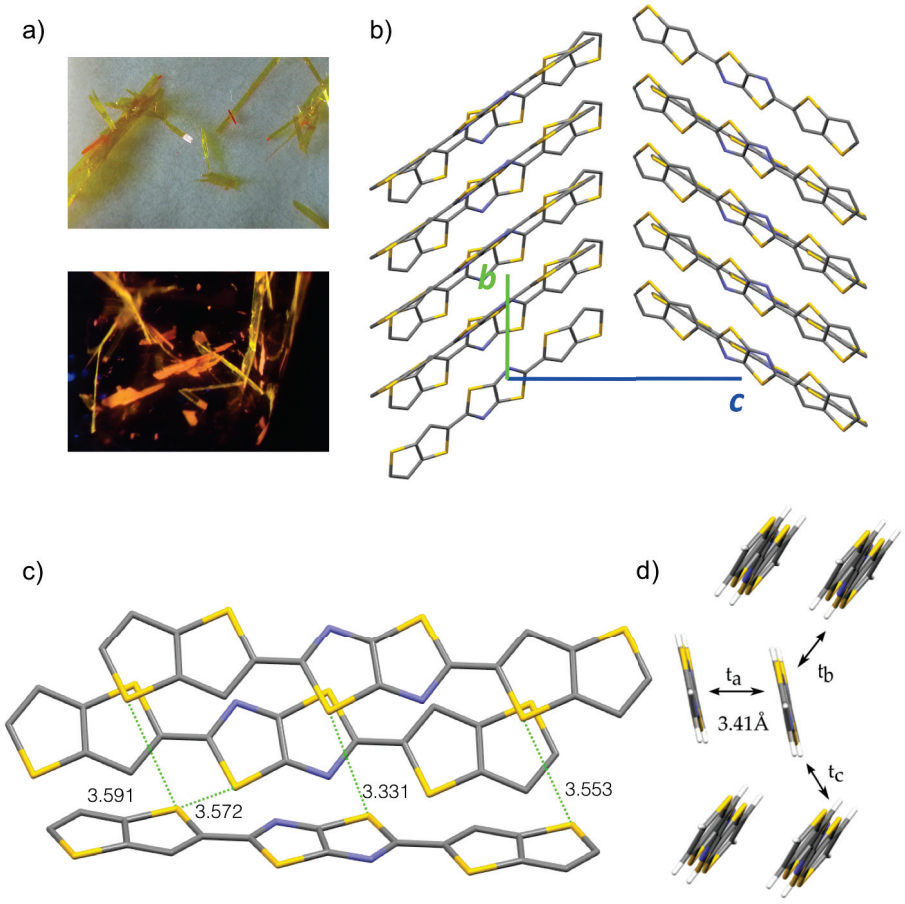

Fig. 3.4.: a) Images of the crystals under normal and UV light. Crystal structure of **3.1-Yellow** showing the b) lattice, c) unit cell and d) herring-bone packing. S···S and S···H close contacts and π–π distances are labeled.

3.1-Red has only two (Figure 3.3c and 3.4c). In both polymorphs, the S···S contacts between TzTz sulfur atoms were shorter than the contacts between TT sulfur atoms by ≈0.2–0.4Å.

Tab. 3.2.: Calculated electronic couplings in three directions.[a]

	3.1-Red		3.1-Yellow	
	hole (meV)	electron (meV)	hole (meV)	electron (meV)
t_a	–194.9	–11.6	–88.5	54.0
t_b	2.2	11.8	–0.4	–8.7
t_b	0.3	–6.9	2.3	27.4

[a] Electronic coupling, $V = \frac{J - 1/2(\epsilon_1 + \epsilon_2)S}{1 - S^2}$, where J is the transfer integral, S the overlap, and ϵ the site energy. Calculated using GGA:PW91, TZP with ADF software.

Using the experimental crystal structures, the electronic coupling between molecular dimers was calculated (Table 3.2). Both polymorphs display a pronounced anisotropy of the valence band: there is a strong electronic coupling of HOMOs between face-to-face pairs (along t_a, Figures 3.3d and 3.4d), but very little between edge-to-edge molecules (along t_b, t_c). The highest electronic coupling (t_a) for **3.1-Red** is much larger than that of **3.1-Yellow**, attributed to the smaller lateral shift between adjacent molecules in the π–stack. Unfortunately, this strong coupling in **3.1-Red** is limited to the previously described π–tetramers and does not result in a continuous p-channel. The strong coupling (t_a) in **3.1-Yellow** takes place along the continuous π–stacks defining the direction of high-conductance. The absolute value of coupling along t_a is similar to that of high mobility semiconductors of comparable size, but the coupling in the other direction is much lower (e.g. dianthra-TT: $t_{a,b,c} = 70, 88, 35$ meV; $\mu_h \approx 3.0 \times 10^{-5}$ cm^2/Vs.[8]

Interestingly, we see much less anisotropy in the electronic coupling of the LUMOs, with higher absolute values for the t_b and t_c pairs. The LUMO has a high coefficient at the sulfur atoms, explaining why t_b and t_c, the pairs with S···S contacts, should experience stronger electronic coupling.[15] The HOMO has a zero coefficient at sulfur, thus S···S contacts do not contribute to HOMO coupling between those pairs (see the SI for MO surfaces).

The emission of the solid (powder) sample of **3.1** is deeply red-shifted compared to that in solution (by 0.62 eV), signifying a substantial exciton delocalization (Figure 3.1). Fluores-

cence microscopy of the individual **3.1-Yellow** and **3.1-Red** polymorphs reveals emission maxima of 591 and 622 nm, respectively (Figure 3.5). **3.1-Red** is clearly more fluorescent than **3.1-Yellow**. However, both crystals show the same emission lifetimes ($\tau = 4.7$ ns), indicating a lower radiative rate in **3.1-Yellow** ($K_r = \Phi/\tau$) (Figure S4). The red shift and faster radiative transition of **3.1-Red** are likely explained by the strong coupling of molecular chromophores in this polymorph, and can be linked to the different packing modes described above.

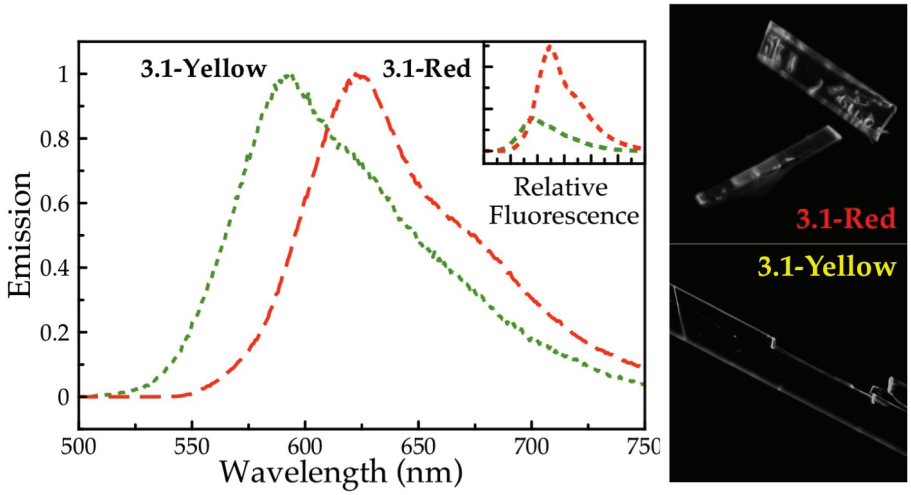

Fig. 3.5.: Fluorescence spectra of the crystal polymorphs of **3.1**. The inset shows their relative emissive intensities. On the right are microscope images of the polymorphs.

3.3.3 Device Studies

Single-crystal field-effect transistors (SCFETs) were fabricated from both polymorphs. We used a top-contact, bottom-gate geometry and tested the crystals on bare SiO_2/Si, poly(methyl methacrylate) (PMMA) and hexamethyldisilazane (HMDS) treated substrates, with the HMDS-treated substrates giving the best results. **3.1-Yellow** showed good transfer characteristics and a hole mobility (μ_h) of $3.3\text{x}10^{-3}\text{cm}^2/\text{Vs}$ (Figure 3.6a). The linear shape of the output curve at low V_{DS} bias indicates that contact resistance is not a major limiting factor in this device. We thus attributed the modest measured mobility primarily to the distinct one-dimensional nature of the electronic coupling (Table 3.2). **3.1-Red**, on the other hand, showed no gate-modulated current ($\mu_h < 10^{-7}\text{cm}^2/\text{Vs}$), as was expected

from its crystal structure. For the alkylated oligomer **3.2**, thin film transistors (TFTs) were made on bare SiO_2/Si substrates by high-vacuum deposition. The films exhibited p-type semiconducting behavior with hole mobilities of 1.0×10^{-3} cm^2/Vs, similar to that of SCFET of **3.1** (Figure 3.6b). No substantial electron mobility was measured for any of the materials/device configurations. This can be attributed to the rather high LUMO of both materials, which leads to a large electron injection barrier from the high-work function gold electrode (≈5.3 eV) and to facile charge trapping by O_2 and H_2O atmospheric impurities.

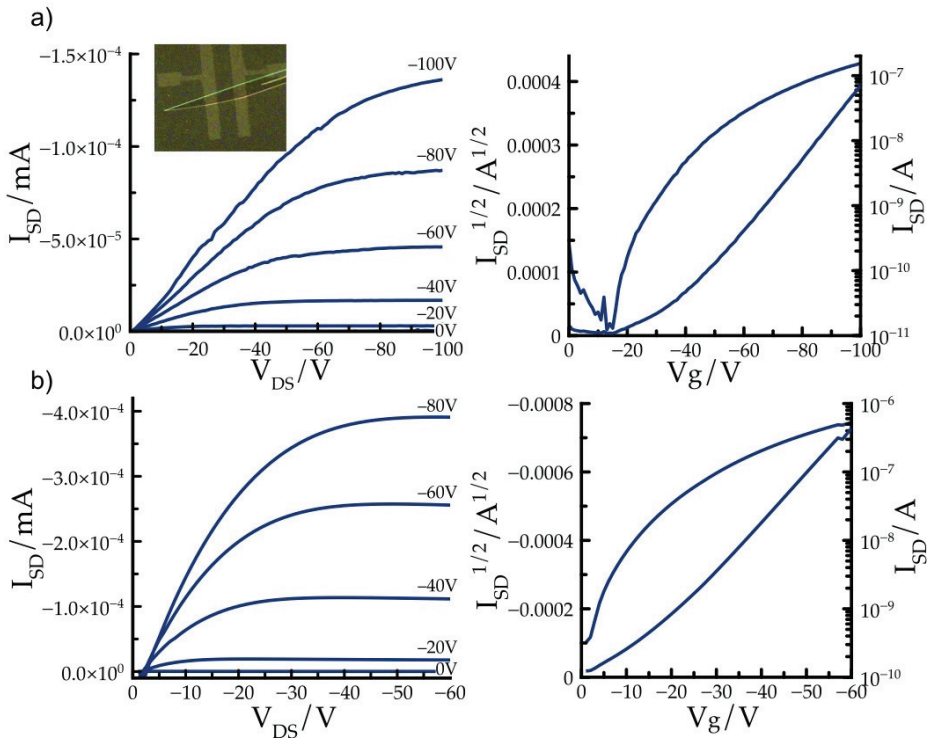

Fig. 3.6.: a) Output (top left) and transfer (top right) characteristics of single-crystal transistors made from **3.1-Yellow** ($\mu_h = 3.3 \times 10^{-3}$ cm^2/Vs). b) Output (bottom left) and transfer (bottom right) characteristics of thin-film transistors made from **3.2** ($\mu_h = 1.0 \times 10^{-3}$ cm^2/Vs).

3.4 Conclusions

In summary, we have synthesized new organic semiconductors combining isoelectronic donor (thienothiophene) and acceptor (thiazolothiazole) building blocks and grew two

crystal polymorphs of the material, namely, **3.1-Red** and **3.1-Yellow**. **3.1-Red** was found to have a slipped-stacked packing architecture and a large calculated electronic coupling between face-to-face molecules, which gives rise to a pronounced bathochromic shift of the absorbance and a characteristic red color. However, these π–stacking molecules exist in isolated groups of tetramers, leaving no possibility for long-range transport. **3.1-Yellow** possesses a smaller electronic coupling (thus exhibiting a smaller bathochromic shift), but also more S···S close contacts and a herringbone packing motif with continuous π–π stacking. Both polymorphs were fluorescent and exhibited large red-shifts in their solid-state emission. SCFETs were fabricated from both polymorphs, but only **3.1-Yellow** displayed semiconductive properties. TFTs were also fabricated from the alkylated oligomer **3.2**. Though calculations suggest the possibility of n-type character, both **3.1-Yellow** and **3.2** displayed only p-type behavior proceeding from poor charge injection due to gold's high work function, and possible electron trapping. Our study has made tangible the connection between the crystal packing and device performance of thienothiophene–thiazolothiazole semiconductors. An understanding of polymorphism and this type of structure-property relationship will be paramount for further rational design of organic semiconductors.

3.5 Experimental Section

3.5.1 Optical Spectroscopy

UV/Vis absorption and photoluminescence spectra were measured in CH_2Cl_2 with a JACSO V670 UV-Vis-NIR spectrometer and a Varian Eclipse Fluorimeter, respectively. The fluorescence quantum yields were determined relative to fluorescein in 0.1 M NaOH (PLQY=0.79). Solid-state fluorescence data was acquired for powders using an integrating sphere.

3.5.2 Electrochemistry

Cyclic voltammetry studies were performed on a CH670 potentiostat from CH-Instruments in a three-electrode cell using a 0.1 M $TBAPF_6$/*o*-dichlorobenzene electrolyte solution, at scan rates of 100 mV s^{-1}. A Pt disk and a Pt wire were used as the working and counter electrodes, respectively, and an Ag/AgCl electrode was used as the reference. All potentials were adjusted versus ferrocene (internal standard).

3.5.3 Synthesis

Thieno[3,2-*b*]thiophene-2-carbaldehyde was synthesized according to literature procedures.[13]

Scheme 3.2: Synthesis of 5-hexylthieno[3,2-*b*]thiophene-2-carbaldehyde.

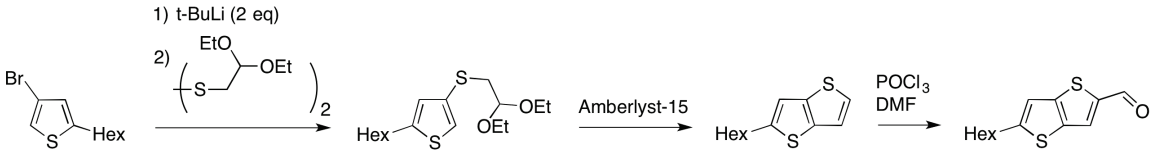

4-((2,2-diethoxyethyl)thio)-2-hexylthiophene
In a dry flask, 1.7 M tert-butyllithium in pentane (100 mL, 0.170 mol) was added dropwise to a solution of 3-bromo-5-hexylthiophene (18.2 g, 0.074 mol) in ether (500 mL) at −78°C under a N_2 atmosphere. The addition complete, the reaction stirred for 30 min at this temperature, then 1,2-bis(2,2-diethoxyethyl)disulfide (24.6 g, 0.083 mol) was added dropwise and the reaction mixture allowed to warm to room temperature. The reaction stirred for 2 days and was quenched with water. The organic layer was extracted with ether (100 mL), washed with 1 M aqueous NaOH (4 x 100 mL) and brine (100 mL). After drying the organic layer over anhydrous Na_2SO_4 the solvent was removed in vacuo to yield a brown oil which was used directly in the next step without purification.

2-hexylthieno[3,2-*b*]thiophene
Anhydrous amberlyst 15 ion exchange resin (50 g) was added to a stirring solution of crude 4-((2,2-diethoxyethyl)thio)-2-hexylthiophene in ether (500 mL) and the reaction mixture was heated to reflux for 12 hours. The solution was then decanted and poured through a Buchner funnel fitted with filter paper. Fresh ether (400 mL) was added to the amberlyst beads and brought to reflux for 2 hours in order to extract the residual product. This solution was combined with the reaction mixture upon decanting through the Buchner funnel. After removing the solvent in vacuo the residue was passed through a silica plug with hexane to afford a red oil. The product was purified by distillation at 70°C, under a pressure of 150 microns to afford a solid (2.53 g, 15% yield over two steps) with spectral characteristics as previously reported.[16] ^{1}HNMR ($CDCl_3$, 500 MHz, 25°C) δ 7.29 (d, J = 5.5 Hz, 1H), 7.20 (d, J = 5.5 Hz, 1H), 6.98 (s, 1H), 2.90 (t, J = 7.6, 2H), 1.74 (m, 2H), 1.41 (m, 2H), 1.33 (m, 4H), 0.91 (t, J = 7.1 Hz, 3H).

5-hexylthieno[3,2-*b*]thiophene-2-carbaldehyde
DMF (0.34 mL, 4.410 mmol) was cooled to 0°C under a flow of N_2 and $POCl_3$ (0.41 mL, 4.399 mmol) was added dropwise. The reaction mixture warmed to room temperature and was diluted in dry chloroform (15 mL). After stirring for 1 hour, 2-hexylthieno[3,2-*b*]thiophene (0.399 g, 1.776 mmol) is added under positive pressure. A condenser is attached and the reaction brought to reflux overnight. The next day, the reaction is cooled, a sodium acetate solution in water is added (0.761 g in 5 mL) and the reaction is refluxed for 30 more minutes. The reaction mixture is extracted with DCM (3 x 20 mL) and the organics are washed with a saturated solution of $NaHCO_3$ (2 x 50 mL) before being dried over Na_2SO_4. The solvent is removed in vacuo to afford a dark oily solid. The product was purified by column

chromatography using a 20% to 80% dichloromethane in hexane gradient eluent system to afford peach-colored crystals (0.357 g, 80% yield) with spectral characteristics as previously reported.[16] ^{1}HNMR ($CDCl_3$, 500 MHz, 25°C) δ 9.94 (s, 1H), 7.87 (s, 1H), 7.04 (s, 1H), 2.94 (t, J = 7.2, 2H), 1.76 (m, 2H), 1.42 (m, 2H), 1.34 (m, 4H), 0.92 (t, J = 7.1 Hz, 3H). ^{13}CNMR ($CDCl_3$, 125 MHz, 25°C) δ 183.3, 156.3, 146.1, 143.7, 137.5, 129.4, 117.1, 31.6, 31.5, 31.2, 28.7, 22.6, 14.1.

2,5-bis(thieno[3,2-*b*]thiophen-2-yl)thiazolo[5,4-*d*]thiazole (3.1)
Thieno[3,2-*b*]thiophene-2-carbaldehyde (0.202 g, 1.20 mmol, 2.0 eq), dithiooxamide (0.073 g, 0.61 mmol, 1 eq), and phenol (0.248 g, 2.63 mmol, 4.3 eq) were loaded into a 25 mL round-bottom flask equipped with a condenser. The reaction was refluxed at 180°C for 45 min. Once cooled, the solid reaction mixture was dispersed in Et_2O, filtered and washed with Et_2O. The dark solids were purified by sublimation at 230°C, at pressures of $\approx 3\times10^{-5}$ torr to yield a bright orange powder (0.031 g, 13% yield). Crystals were grown by physical vapor transport (PVT) in a tube furnace at 300°C under a flow of nitrogen. HR-MS (APCI) m/z=418.8945 [M+1] (calcd. for $C_{16}H_7N_2S_6$: m/z=418.8928).

2,5-bis(5-hexylthieno[3,2-*b*]thiophen-2-yl)thiazolo[5,4-*d*]thiazole (3.2)
was synthesized as described above to yield an orange powder in a 14% yield. HR-MS (APCI) m/z=587.0821 [M+1] (calcd. for $C_{28}H_{31}N_2S_6$: m/z=587.0806).

3.5.4 Computational Methods

Geometries were calculated at the B3LYP/6-31G(d) level of theory using the Gaussian 09W program.[17] The reorganization energies, shown in Table 3.1, are calculated based on the four-point scheme neglecting the outer-sphere contributions.[18] The bond-length alternation values in Table 3.1 were calculated as the average of the difference between single- and double-bond lengths along the conjugation pathway. Charge-transfer integrals were calculated according to the site-energy corrected method[19] with the PW91 functional and Slater-type triple-ζ plus polarization (TZP) basis sets using the ADF (Amsterdam Density Functional) package.[20]

3.5.5 Device Fabrication

For all FET devices, heavily n-doped Si wafers (Sb, ρ=0.005–0.025 ohm cm) with 200 nm SiOx (Ci=17.2 nF cm^{-2}) were used as gate electrode and dielectric, respectively. Wafers were cleaned by submerging in "piranha" solution at 80°C for 15 min, sonicated in isopropyl alcohol for 30 min, then rinsed with distilled H_2O and dried under N_2. For HMDS-treated substrates, the wafers were heated in a HMDS/toluene solution at 60°C for one hour. Crystals suitable for devices were then located under a magnifying lens and transferred to the surface with the tip of a needle. A shadow mask was carefully placed over the crystals and 80 nm Au source/drain electrodes were deposited via thermal evaporation at pressures $< 5\text{x}10^{-6}$torr. For thin-film devices, vacuum deposition of **3.2** for a nominal thickness of 50 nm was performed at pressures $\approx 1\text{x}10^{-6}$ torr with an evaporation rate of 0.1–0.2 Ås^{-1}. Gold (50 nm) was then evaporated through a shadow mask to define the source/drain

electrodes. The active channel length was defined by the mask at 50 μm, while the channel width was determined by the crystal size, as measured using an optical microscope.

References

(1) a) Gundlach, D. J.; Royer, J. E.; Park, S. K.; Subramanian, S.; Jurchescu, O. D.; Hamadani, B. H.; Moad, a. J.; Kline, R. J.; Teague, L. C.; Kirillov, O.; Richter, C. A.; Kushmerick, J. G.; Richter, L. J.; Parkin, S. R.; Jackson, T. N.; Anthony, J. E. Contact-induced crystallinity for high-performance soluble acene-based transistors and circuits. *Nat. Mater.* **2008**, *7*, 216; b) Yuan, Y.; Giri, G.; Ayzner, A. L.; Zoombelt, A. P.; Mannsfeld, S. C. B.; Chen, J.; Nordlund, D.; Toney, M. F.; Huang, J.; Bao, Z. Ultra-high mobility transparent organic thin film transistors grown by an off-centre spin-coating method. *Nat. Commun.* **2014**, *5*, 3005; c) Wang, C.; Dong, H.; Hu, W.; Liu, Y.; Zhu, D. Semiconducting π-conjugated systems in field-effect transistors: a material odyssey of organic electronics. *Chem. Rev.* **2012**, *112*, 2208; d) Jiang, L.; Dong, H.; Hu, W. Organic single crystal field-effect transistors: advances and perspectives. *J. Mater. Chem.* **2010**, *20*, 4994.

(2) Coropceanu, V.; Cornil, J.; da Silva Filho, D. a.; Olivier, Y.; Silbey, R.; Brédas, J.-L. Charge transport in organic semiconductors. *Chem. Rev.* **2007**, *107*, 926.

(3) Anthony, J. E. Functionalized acenes and heteroacenes for organic electronics. *Chem. Rev.* **2006**, *106*, 5028.

(4) Tang, Q.; Zhang, D.; Wang, S.; Ke, N.; Xu, J.; Yu, J. C.; Miao, Q. A Meaningful Analogue of Pentacene: Charge Transport, Polymorphs, and Electronic Structures of Dihydrodiazapentacene. *Chem. Mater.* **2009**, *21*, 1400.

(5) a) Yassar, A. Recent trends in crystal engineering of high-mobility materials for organic electronics. *Polym. Sci. Ser. C* **2014**, *56*, 4; b) Matsukawa, T.; Yoshimura, M.; Sasai, K.; Uchiyama, M.; Yamagishi, M.; Tominari, Y.; Takahashi, Y.; Takeya, J.; Kitaoka, Y.; Mori, Y.; Sasaki, T. Growth of thin rubrene single crystals from 1-propanol solvent. *J. Cryst. Growth* **2010**, *312*, 310.

(6) Fichou, D. Structural order in conjugated oligothiophenes and its implications on opto-electronic devices. *J. Mater. Chem.* **2000**, *10*, 571.

(7) a) McCulloch, I.; Heeney, M.; Chabinyc, M. L.; DeLongchamp, D.; Kline, R. J.; Cölle, M.; Duffy, W.; Fischer, D.; Gundlach, D.; Hamadani, B.; Hamilton, R.; Richter, L.; Salleo, A.; Shkunov, M.; Sparrowe, D.; Tierney, S.; Zhang, W. Semiconducting Thienothiophene Copolymers: Design, Synthesis, Morphology, and Performance in Thin-Film Organic Transistors. *Adv. Mater.* **2009**, *21*, 1091; b) Schneider, J. A.; Dadvand, A.; Wen, W.; Perepichka, D. F. Tuning the Electronic Properties of Poly(thienothiophene vinylene)s via Alkylsulfanyl and Alkylsulfonyl Substituents. *Macromolecules* **2013**, *46*, 9231.

(8) Niimi, K.; Shinamura, S.; Osaka, I.; Miyazaki, E.; Takimiya, K. Dianthra[2,3-b:2′, 3′-f]thiophene (DATT): Synthesis, Characterization , and FET Characteristics of New π-Extended Heteroarene with Eight Fused Aromatic Rings. *J. Am. Chem. Soc.* **2011**, *133*, 8732.

(9) Bevk, D.; Marin, L.; Lutsen, L.; Vanderzande, D.; Maes, W. Thiazolo[5,4-d]thiazoles – promising building blocks in the synthesis of semiconductors for plastic electronics. *RSC Adv.* **2013**, *3*, 11418.

(10) Osaka, I.; Saito, M.; Koganezawa, T.; Takimiya, K. Thiophene-thiazolothiazole copolymers: significant impact of side chain composition on backbone orientation and solar cell performances. *Adv. Mater.* **2014**, *26*, 331.

(11) Ando, S.; Nishida, J.-i.; Tada, H.; Inoue, Y.; Tokito, S.; Yamashita, Y. High performance n-type organic field-effect transistors based on pi-electronic systems with trifluoromethylphenyl groups. *J. Am. Chem. Soc.* **2005**, *127*, 5336.

(12) Johnson, J. R.; Ketcham, R. Thiazolothiazoles. I. The Reaction of Aromatic Aldehydes with Dithioöxamide 1. *J. Am. Chem. Soc.* **1960**, *82*, 2719.

(13) Henssler, J. T.; Matzger, A. J. Facile and scalable synthesis of the fused-ring heterocycles thieno[3,2-b]thiophene and thieno[3,2-b]furan. *Org. Lett.* **2009**, *11*, 3144.

(14) Brédas, J. L. Relationship between band gap and bond length alternation in organic conjugated polymers. *J. Chem. Phys.* **1985**, *82*, 3808.

(15) a) Shinamura, S.; Osaka, I.; Miyazaki, E.; Takimiya, K. Air-stable and high-mobility organic semiconductors based on heteroarenes for field-effect transistors. *Heterocycles* **2011**, *83*, 1187; b) Osaka, I.; Kakara, T.; Takemura, N.; Koganezawa, T.; Takimiya, K. Naphthodithiophene-naphthobisthiadiazole copolymers for solar cells: Alkylation drives the polymer backbone flat and promotes efficiency. *J. Am. Chem. Soc.* **2013**, *135*, 8834.

(16) Kim, K. H.; Chi, Z.; Cho, M. J.; Jin, J. I.; Cho, M. Y.; Kim, S. J.; Joo, J. S.; Choi, D. H. Soluble star-shaped molecules based on thiophene derivatives as organic semiconductors for field-effect transistor applications. *Chem. Mater.* **2007**, *19*, 4925.

(17) Frisch, M. J.; Trucks, G. W.; Schlegel, H. B.; Scuseria, G. E.; Robb, M. A.; Cheeseman, J. R.; Scalmani, G.; Barone, V.; Mennucci, B.; Petersson, G. A.; Nakatsuji, H.; Caricato, M.; Li, X.; Hratchian, H. P.; Izmaylov, A. F.; Bloino, J.; Zheng, G.; Sonnenberg, J. L.; Hada, M.; Ehara, M.; Toyota, K.; Fukuda, R.; Hasegawa, J.; Ishida, M.; Nakajima, T.; Honda, Y.; Kitao, O.; Nakai, H.; Vreven, T.; Montgomery, J. A.; Peralta, J. E.; Ogliaro, F.; Bearpark, M.; Heyd,

J. J.; Brothers, E.; Kudin, K. N.; Staroverov, V. N.; Kobayashi, R.; Normand, J.; Raghavachari, K.; Rendell, A.; Burant, J. C.; Iyengar, S. S.; Tomasi, J.; Cossi, M.; Rega, N.; Millam, J. M.; Klene, M.; Knox, J. E.; Cross, J. B., et al. Gaussian09 Revision D.01., Gaussian Inc. Wallingford CT 2009.

(18) Brédas, J.-L.; Beljonne, D.; Coropceanu, V.; Cornil, J. Charge-transfer and energy-transfer processes in pi-conjugated oligomers and polymers: a molecular picture. *Chem. Rev.* **2004**, *104*, 4971.

(19) Senthilkumar, K.; Grozema, F. C.; Bickelhaupt, F. M.; Siebbeles, L. D. A. Charge transport in columnar stacked triphenylenes: Effects of conformational fluctuations on charge transfer integrals and site energies. *J. Chem. Phys.* **2003**, *119*, 9809.

(20) ADF2008.01 SCM, Theoretical Chemistry, Vrije Universiteit: Amsterdam, The Netherlands, http://www.scm.com.

3.6 Supporting Information for Chapter 3

3.6.1 Bond Lengths and Unit Cell Parameters of the Polymorphs

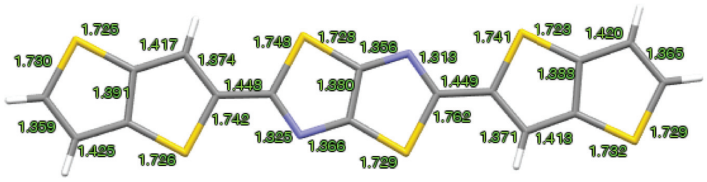

Figure S1. Crystal structure of **3.1-Red** showing bond lengths.

Table S1. Crystal data and structure refinement for **3.1-Red**.

Identification code	PERE52
Empirical formula	$C_{16}H_6N_2S_6$
Formula weight	418.59
Temperature/K	150
Crystal system	monoclinic
Space group	$P2_1/c$
a/Å	5.8770(2)
b/Å	19.1682(7)
c/Å	27.9627(10)
α/°	90
β/°	92.9500(18)
γ/°	90
Volume/Å^3	3145.87(19)
Z	8
ρ_{calc}g/cm^3	1.768
μ/mm^{-1}	5.238
F(000)	1696.0
Crystal size/mm^3	0.15 × 0.05 × 0.02
Radiation	GaKα (λ = 1.34139)
2Θ range for data collection/°	4.864 to 121.238
Index ranges	-7 ≤ h ≤ 6, -24 ≤ k ≤ 24, -36 ≤ l ≤ 36
Reflections collected	45871
Independent reflections	7215 [R_{int} = 0.0701, R_{sigma} = 0.0451]
Data/restraints/parameters	7215/0/433
Goodness-of-fit on F^2	1.013
Final R indexes [I>=2σ (I)]	R_1 = 0.0410, wR_2 = 0.0973
Final R indexes [all data]	R_1 = 0.0685, wR_2 = 0.1116
Largest diff. peak/hole / e Å^{-3}	0.45/-0.38

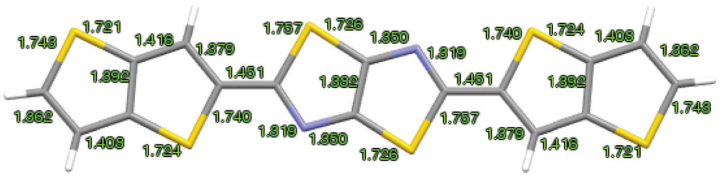

Figure S2. Crystal structure of **3.1-Yellow** showing bond lengths.

Table S2. Crystal data and structure refinement for **3.1-Yellow**.

Identification code	pere53
Empirical formula	$C_{16}H_6N_2S_6$
Formula weight	418.59
Temperature/K	150
Crystal system	monoclinic
Space group	$P2_1/c$
a/Å	10.7767(5)
b/Å	4.6154(2)
c/Å	31.9504(15)
α/°	90
β/°	99.453(2)
γ/°	90
Volume/Å^3	1567.59(12)
Z	4
ρ_{calc}g/cm^3	1.774
μ/mm^{-1}	5.256
F(000)	848.0
Crystal size/mm^3	0.2 × 0.1 × 0.05
Radiation	GaKα (λ = 1.34139)
2Θ range for data collection/°	4.878 to 121.468
Index ranges	-14 ≤ h ≤ 13, -5 ≤ k ≤ 5, -41 ≤ l ≤ 41
Reflections collected	51814
Independent reflections	3798 [R_{int} = 0.1005, R_{sigma} = 0.0416]
Data/restraints/parameters	3798/0/218
Goodness-of-fit on F^2	1.070
Final R indexes [I>=2σ (I)]	R_1 = 0.1043, wR_2 = 0.2862
Final R indexes [all data]	R_1 = 0.1190, wR_2 = 0.2958
Largest diff. peak/hole / e Å^{-3}	1.82/-0.83

3.6.2 Computational Data

Computational data for TT-TzTz-TT (SCF total energy = –3111.92527400 hartrees)

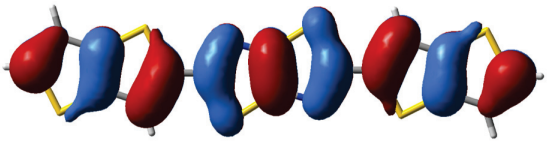

HOMO

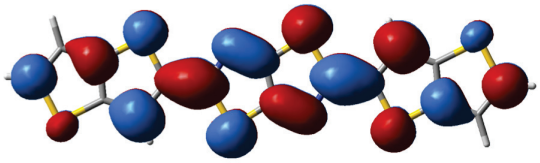

LUMO

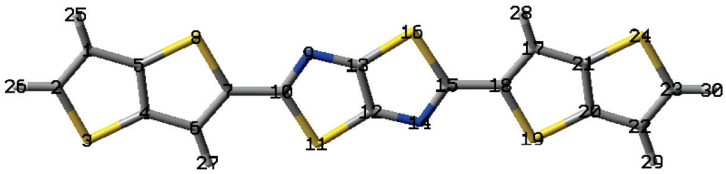

Coordinates (Å)			
Atom Label	X	Y	Z
1	-0.3607	2.151271	0.175206
2	-1.22177	1.174998	-0.24509
3	-0.41272	-0.26865	-0.81461
4	1.143554	0.450532	-0.48229
5	0.994319	1.735726	0.039046
6	2.488996	0.033401	-0.61971
7	3.369337	1.010419	-0.19884
8	2.541074	2.464432	0.374731
9	5.546033	1.986309	0.253989
10	4.809423	0.982292	-0.17548
11	5.724245	-0.44914	-0.74215
12	7.190417	0.415113	-0.35241
13	6.854376	1.664647	0.152777
14	8.498765	0.09343	-0.45356
15	9.235363	1.097505	-0.02419
16	8.320545	2.528872	0.54258
17	11.55577	2.046548	0.419769

Coordinates (Å)			
Atom Label	X	Y	Z
18	10.67546	1.069511	-0.00111
19	11.50381	-0.38411	-0.57561
20	13.05052	0.344384	-0.23924
21	12.90122	1.629416	0.28248
22	14.40556	-0.07108	-0.37546
23	15.26658	0.905226	0.04484
24	14.45745	2.348441	0.615342
25	-0.68282	3.111951	0.559439
26	-2.30299	1.212204	-0.25691
27	2.802701	-0.93017	-1.00539
28	11.24203	3.009906	0.805947
29	14.72773	-1.0316	-0.76005
30	16.34781	0.868163	0.056408

Computational data for 3-TT (SCF total energy = –-3079.83242836 hartrees**)**

Coordinates (Å)			
Atom Label	X	Y	Z
1	-1.12986	9.38077	-0.01957
2	-1.08995	8.014519	-0.07196
3	0.252368	7.539833	-0.06667
4	1.21408	8.544599	-0.00967
5	0.457555	10.11707	0.038701
6	1.004864	5.966897	-0.1182
7	2.619982	6.698395	-0.03588
8	2.55272	8.075479	0.010778
9	3.793805	5.855751	-0.02967
10	3.87944	4.506531	0.251933
11	5.208852	4.027888	0.162675
12	6.149461	4.995927	-0.18184
13	5.380873	6.543203	-0.42629
14	5.977436	2.480607	0.407107
15	7.564531	3.168088	0.010617
16	7.478881	4.517297	-0.27104
17	8.738366	2.325468	0.016924
18	8.805655	0.948368	-0.02926
19	10.14431	0.479281	-0.00883
20	11.10601	1.484084	0.047676
21	10.35349	3.057027	0.098728
22	10.90085	-1.0932	-0.05671
23	12.48827	-0.35684	0.001063
24	12.44833	1.009426	0.052969
25	-2.00635	10.01481	-0.01275
26	-1.97338	7.388197	-0.11299
27	3.429373	8.709466	0.079732
28	3.022308	3.904771	0.531694
29	8.336014	5.119072	-0.55077
30	7.929009	0.314331	-0.09783
31	13.36477	-0.99087	-0.00566
32	13.33175	1.63578	0.093654

Computational data for 3-TzTz (SCF total energy = –3111.92527400 hartrees**)**

	Coordinates (Å)		
Atom Label	X	Y	Z
1	-0.84832	9.185508	0.089858
2	-0.86426	7.88484	-0.01582
3	0.418243	7.432538	0.006008
4	1.438183	8.371037	0.127905
5	0.731906	9.963306	0.224106
6	1.11064	5.836809	-0.09051
7	2.705122	6.610363	0.044357
8	2.713501	7.921602	0.150001
9	3.904318	5.806677	0.035334
10	3.897911	4.494543	-0.06996
11	5.170688	4.0441	-0.04736
12	6.192064	4.986887	0.075078
13	5.498107	6.583522	0.170791
14	5.864646	2.447466	-0.14308
15	7.458435	3.224313	-0.00763
16	7.464842	4.536444	0.097679
17	8.657632	2.420625	-0.01665
18	8.649255	1.109388	-0.1223
19	9.924572	0.659951	-0.10017
20	10.94451	1.598448	0.021775
21	10.25211	3.19418	0.118249
22	10.63085	-0.93232	-0.19636
23	12.21107	-0.15452	-0.06204
24	12.22701	1.146143	0.043662
25	-1.7452	9.793837	0.098141
26	13.10795	-0.76286	-0.07028

3.6.3 NMR Data

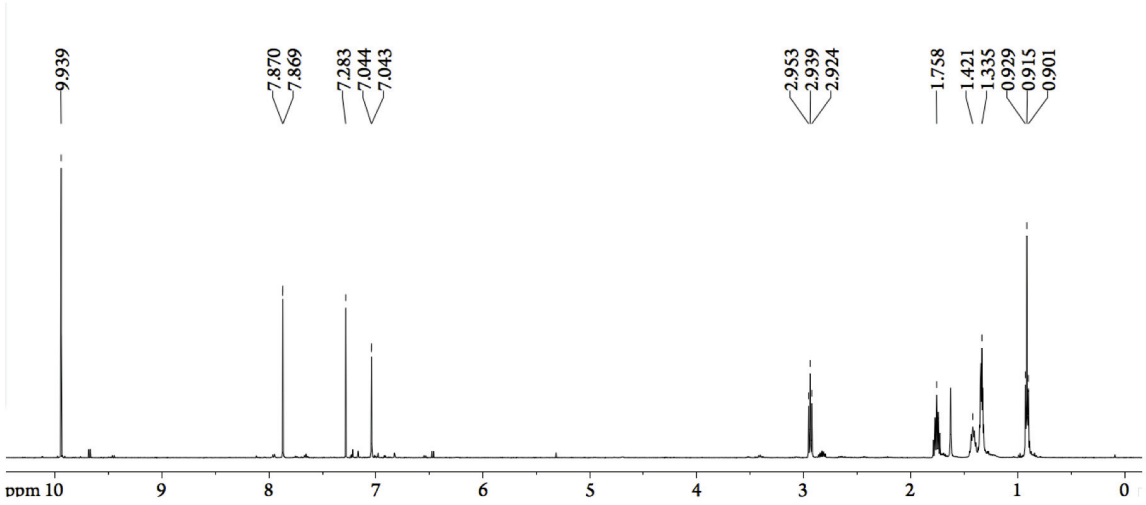

^{1}H NMR spectrum of **5-hexylthieno[3,2-*b*]thiophene-2-carbaldehyde** in $CDCl_3$.

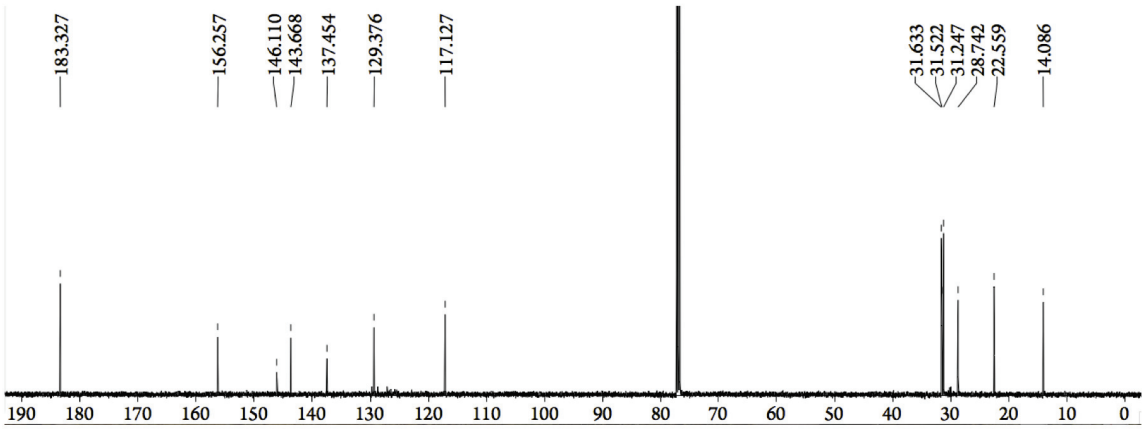

^{13}C NMR spectrum of **5-hexylthieno[3,2-*b*]thiophene-2-carbaldehyde** in $CDCl_3$.

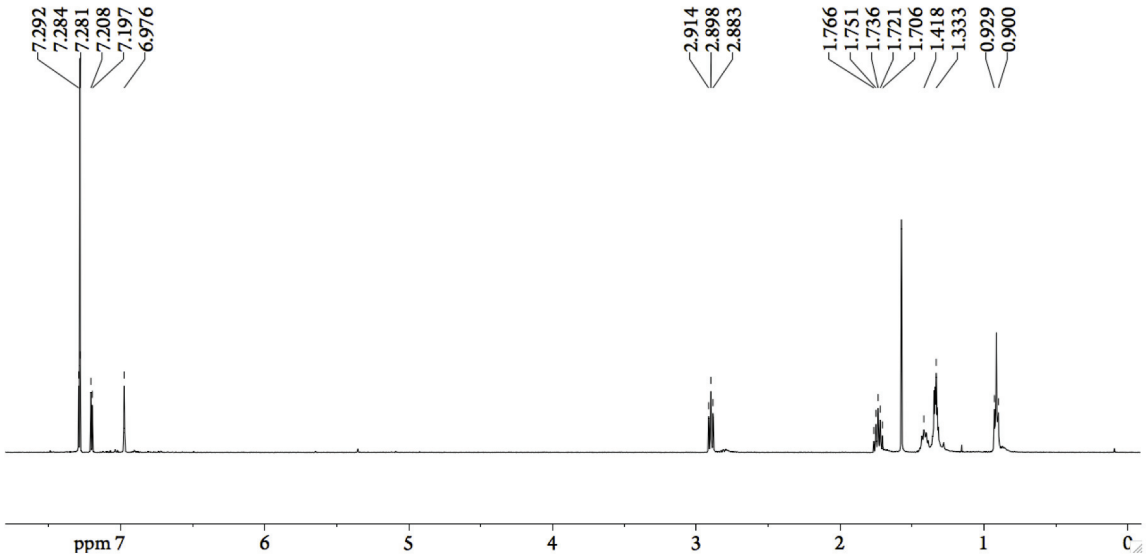

^{1}H NMR spectrum of **2-hexylthieno[3,2-*b*]thiophene** in $CDCl_3$.

3.6.4 Lifetime Plots

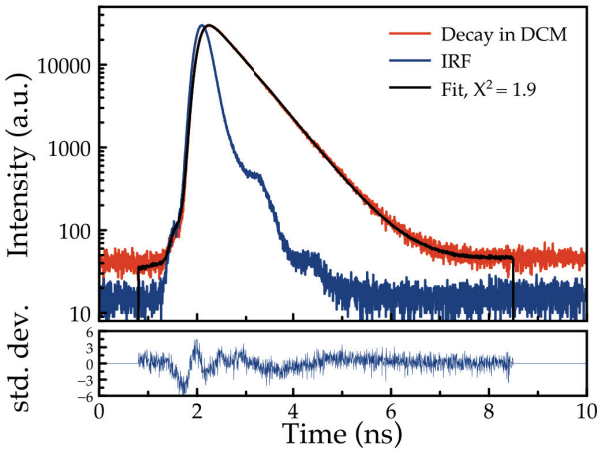

Figure S3.3. Fluorescence intensity decay of **3.1** in CH_2Cl_2 with a single exponential fit ($\tau = 0.58$ ns). The high χ^2 value is not improved by adding more exponential components and is attributed to the limited number of data points due to the short lifetime.

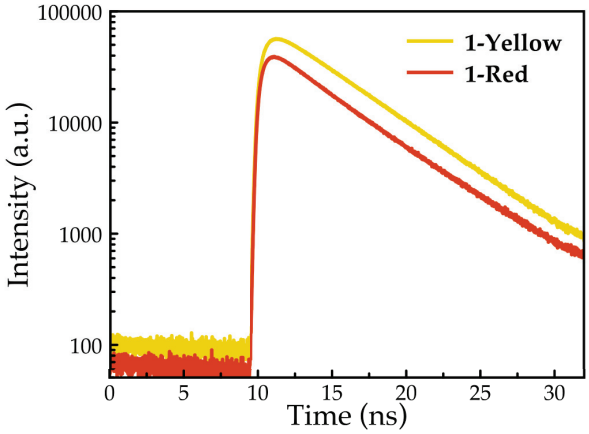

Figure S3.4. Identical fluorescence intensity decays of **3.1-Red** and **3.1-Yellow** crystals ($\tau = 4.7$ ns) (χ^2 typically under 1.1).

4 A New Approach to Polycyclic Azaarenes: Synthesis of Diazabenzopyrene and Diazaperylene.

While Chapter 3 demonstrated the efficacy of using nitrogen heteroatoms to lower the frontier energy levels of a material, it also suggests that sulfur heteroatoms, if present, will dominate self-assembly, as well as counteract the electronegativity of the nitrogen. Chapter 4, therefore, focuses on the synthesis of novel nitrogen-containing π–conjugated materials without sulfur. As was discussed in Chapter 1, extended non-linear fused arenes are more stable than their linear counterparts, so the focus is on the synthesis of non-linear polycyclic N-heteroaromatic compounds (N-PAHs), which are less well known than azaacenes. Diazabenzopyrene and diazaperylene, which are structural isomers, are synthesized and the location of the nitrogen heteroatoms in the π–conjugated core is shown to impact the optical properties of the molecules in polar media and in the presence of acid.

4.1 Introduction

Polycyclic aromatic hydrocarbons (PAHs) are an interesting class of π–functional materials, comprised of linear acenes (for example, pentacene), non-linear PAHs (perylene), and substituted PAHs (rubrene), all of which have been extensively studied as organic semiconductors in transistor devices[1], emitters in organic light emitting diodes (OLEDs)[2] or as fluorescent probes.[3]

Perylene and its derivatives are widely used as blue, green, and red dopant materials in OLEDs.[2] Indeed, the first multilayer electroluminescent device (the basis of today's OLED technology), employed perylene as an (orange) emitting layer.[4] Perhaps the most studied PAHs in terms of photophysical properties, however, is pyrene.[5] Pyrene forms excimers in concentrated solutions, which have a distinct fluorescence band from that of the monomer.[6] This concentration dependent emission profile makes pyrene a useful molecular probe to investigate surfactant micelle formation, phospholipid vesicles, and polymer aggregates.[7] Pyrene also shows an affinity for the surface of graphene and carbon-nanotubes, making it a popular moiety for the non-covalent functionalization of these structures.[8]

Most PAHs show p-type charge transport, but they can be structurally modified to exhibit n-type or ambipolar transport properties. Complementary circuits, desired for their low power consumption, rely on a combination of p- and n-type transistors and their development has been slow due in part to the relative scarcity of n-type semiconductors.[9] Current approaches to access n-type transport in PAHs include employing anti-aromatic cores[10] or electron withdrawing substituents[11], as well as the inclusion of nitrogen heteroatoms (see Figure 4.1 for examples).[12] The high electronegativity of nitrogen can lower the LUMO energy of polycyclic N-heteroaromatic compounds (N-PAHs) facilitating the injection of electrons and increasing the stability of the resulting radical anion charge carriers. Importantly for charge transport, the introduction of nitrogen into the cyclic framework does not increase the reorganization energy of the molecule as much as peripheral electron withdrawing substituents. Accordingly, azaacene **4.i** is one of the best n-type organic semiconductors displaying impressive electron transport properties in thin film FETs ($\mu_e = 3.3\ cm^2/Vs$).[13] Nitrogen heteroatoms may also play an important role in the supramolecular ordering of a material. Thus hydrogen bonding in N-PAHs has been used to direct and stabilize certain assemblies.[14] For example, in quinacridone **4.ii**, a widely used magenta pigment, self-complementary hydrogen bonding causes a slipped stacked arrangement with closer π–π distances than seen in the herringbone structure of pentacene.[15] Reasonably efficient ambipolar charge transport ($\mu_h = 0.2\ cm^2/Vs$, $\mu_e = 0.01\ cm^2/Vs$) has been observed for **4.ii** in thin film FETs.

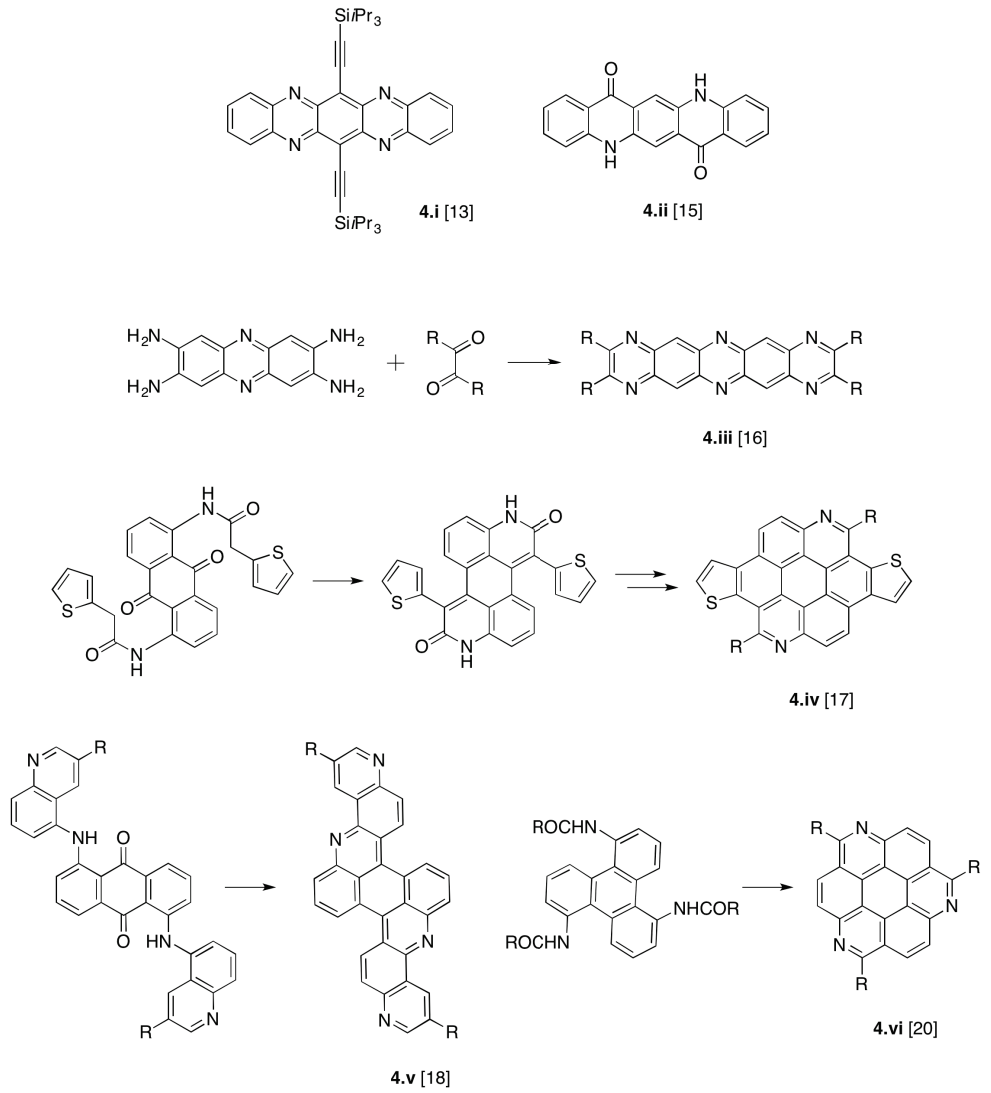

Fig. 4.1.: Polycyclic N-heteroaromatic compounds reported in the literature and some of their synthetic pathways.

It is useful to note that in pyrrole, a 5-membered N-heterocycle, the nitrogen is electron donating as its lone pair is in conjugation with the aromatic ring. Accordingly, 6-membered N-heterocycles with unsaturated nitrogens (C–N=C) are sought after for molecules with lowered HOMO/LUMO energy levels. While there are multiple ways to synthesize 6-membered N-heterocycles, only a few of these (i-iii) are easily applicable for larger N-PAHs. (i) Nucleophilic condensation of ortho-diamines with ortho-quinones (or dihydroxybenzoquinones), as used in the synthesis of extended azaacenes such as **4.iii**.[16] This method is limited to the formation of pyrazine units, however, and reduced (hydrogenated) structures are common side-products. A similar nucleophilic cyclization reaction was used to synthesize **4.iv** via the condensation of an amide and a quinone.[17] (ii) Electrophilic cyclization via a Friedel-Crafts-like attack of the (amino-containing) carbonyl precursor on the neighboring aromatic ring, as used in the preparation of azaperylene **4.v**[18] (yet corresponding azapyrenes could only be formed in very low yields[19] or not at all[18]). A related approach was very recently reported for the preparation of triazacoronene **4.vi** via the cyclization of the triphenylenetriamide in molten $AlCl_3$–NaCl.[20] (iii) The cyclization of amines and internal alkynes to yield azapyrenes , though this technique leaves the final structure adorned with difficult to remove substituents, such as phenyl or alkyl groups.[21]

Therefore, it seems clear that additional synthetic avenues for the incorporation of nitrogen heteroatoms into π–conjugated systems would benefit the development of novel N-PAH materials with interesting optical and electronic properties.

Used in the synthesis of indoles and pyrroles, the Hemetsberger reaction begins with the transformation of a vinyl azide to an azirine intermediate (discernable through IR and NMR measurements and isolable depending on the substituents).[22] The thermolysis of vinyl-2H-azirine produces a vinyl-nitrene intermediate (trappable with triphenylphosphine) that through electrocyclization and a [1,5]-sigmatropic hydrogen shift forms the desired indole or pyrrole (Scheme 4.1).[23] While pyrrole formation is generally favored, vinyl azides have also been used to synthesize pyridine if an allylic or benzylic carbon is available to form a 6-membered ring.[24] We theorized that 6-membered rings could also be achieved on *peri*-substituted PAH where no *ortho*-position is free for pyrrole formation.

Scheme 4.1: The Hemetsberger reaction proceeding via azirine and nitrene intermediates.

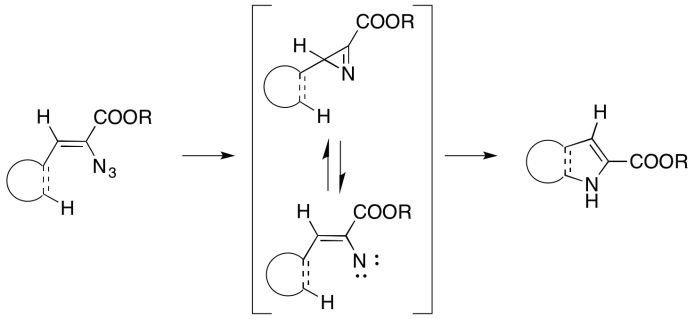

Here, we report the synthesis of two novel polycyclic N-heteroaromatic compounds, 1,8-diazabenzo[e]pyrene and 3,9-diazaperylene from 9,10-disubstituted anthracene. We utilize a Hemetsberger-type reaction in an unprecedented way to access fused pyridines and explore the reaction's regioselectivity under different conditions. The photophysical properties of the compounds are compared to those of their homocyclic analogues. The incorporation of nitrogen leads to the stabilization of the frontier orbitals of the compounds and new stimuli-responsive behavior (dual-channel fluorescence sensing of acids) while maintaining the optical band-gap and fluorescent efficiency of the parent compounds.

4.2 Results and Discussion

When Hemetsberger and Knittel first reported their reaction is 1972, they had also explored 6-membered ring formation, but concluded that "an insertion in the *peri*-position could not be achieved if the 2-position was substituted, as in [1-(2-methoxy-naphthyl)] and [9-anthryl precursors]. In these cases, only undefined resins occur."[23] As the mechanistic reasons for this failure were not clear, we decided to revisit Hemetsberger's original reaction with 9-anthryl derivatives. The reaction generates several unstable side-products and the expected product **4.2** was not isolated, but we found that insertion at the *peri*-position does occur, as evidenced by the formation of the oxidized polycyclic compound **4.3** (Scheme 4.2).

Deducing that fused pyridine **4.3** was the product of the spontaneous oxidation of **4.2** (calculated HOMO = –4.5 eV), we hypothesized that the cyclization of a bis(azidoacrylate) would lead directly to the aromatized diazaarene (Scheme 4.3).

Scheme 4.2: Synthesis of **4.3** demonstrating 6-membered ring formation.

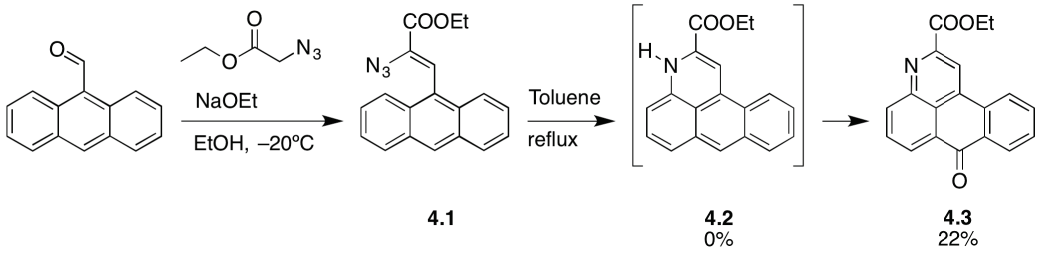

Scheme 4.3: The synthesis of **4.10** and **4.11** via thermolysis or photolysis.

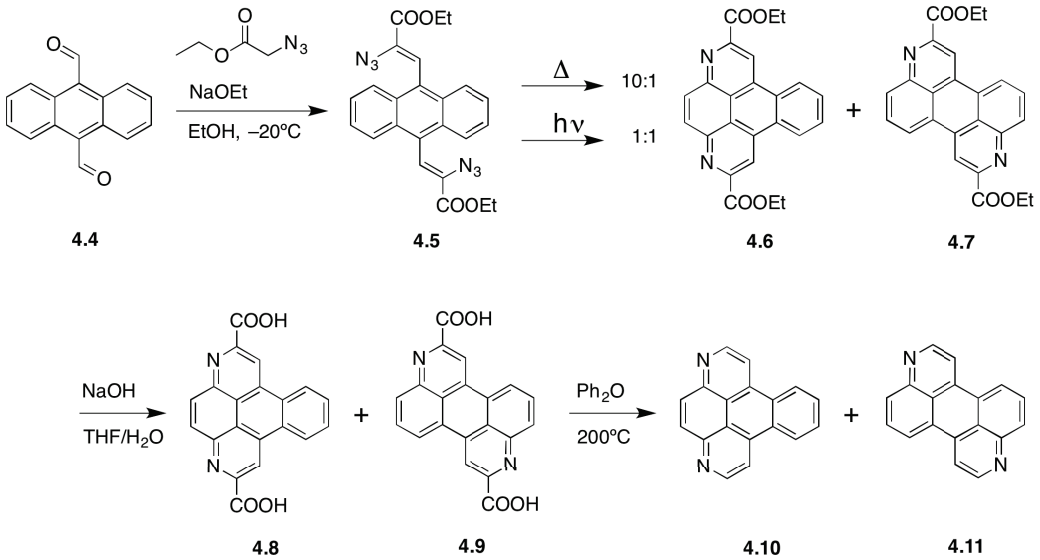

4.2.1 Synthesis

Bis(azidoacrylate) precursor **4.5** was prepared by the base-promoted Knoevenagel condensation of ethyl azidoacetate and 9,10-anthracenedicarbaldehyde **4.4** (Scheme 4.3).[25] Two cyclization routes could be anticipated for **4.5**: "cis" nitrogen insertion at the 1,4-positions to form diazabenzopyrene **4.6** and "trans" nitrogen insertion at the 1,5-positions to form diazaperylene **4.7**. Thermolysis of **4.5** under the classic Hemetsberger conditions (refluxing in toluene) leads predominantly to the formation of **4.6** (80% isolated yield) with typically less than 10% of **4.7**. Such selectivity can be rationalized by the electronic effect of the monocyclic intermediate (consider the structure of **4.2**) that activates the substituted benzene ring towards electrophilic attack, favoring the formation of **4.6**. It should be noted that the

dihydro analogues of **4.6** and **4.7** were never observed. Their high HOMO energies (–3.6 eV and –4.1 eV, respectively) suggest that dehydrogenation is spontaneous.

While repeating the cyclization reaction, however, we occasionally noticed higher amounts of **4.7**. At the same time, we found that solutions of **4.5**, a yellow solid, were quickly turning green, which we initially assumed was an indication of decomposition. An in situ NMR experiment revealed, however, that under visible light at room temperature, **4.5** undergoes a tandem photocyclization to form both **4.6** and **4.7** in a ~1:1 ratio (Scheme 4.3). The observed green color could be due to charge transfer complexes between dihydro precursors and the oxidized product. The photocyclization proceeds cleanly with no visible side products, though at lower temperatures (−10°C and below) we were able to identify an azirine intermediate through its characteristic proton shift at 4.17 ppm (Figure 4.2).[26]

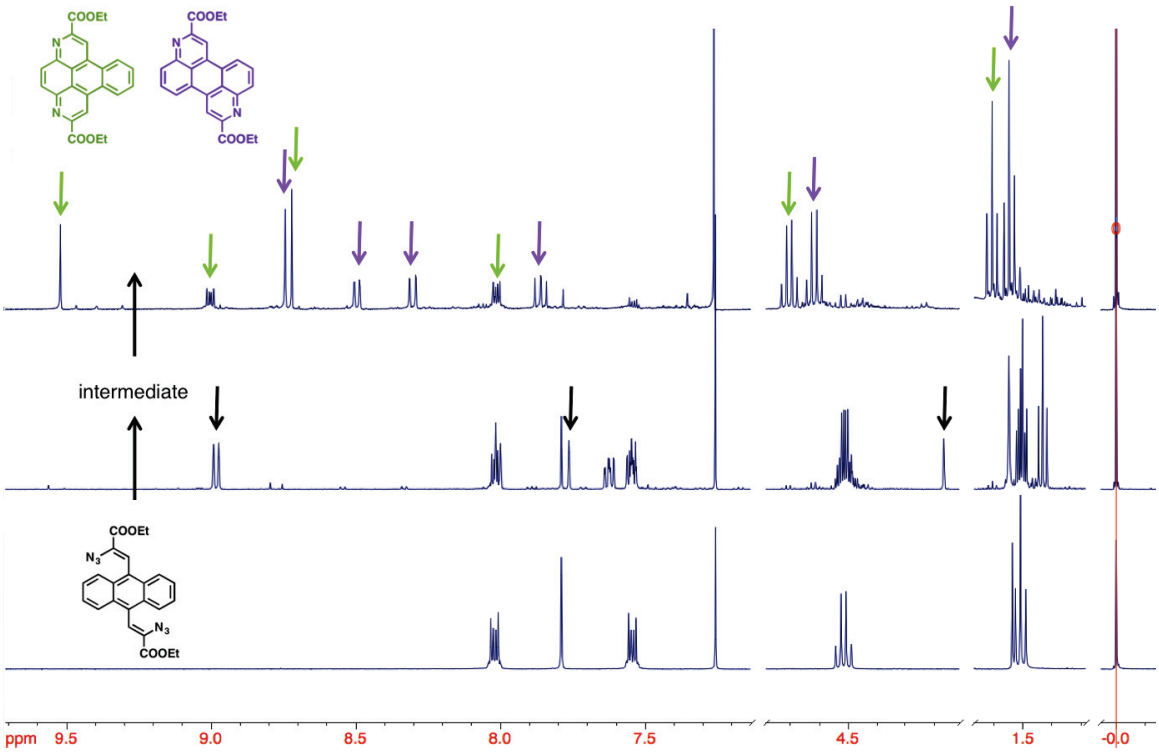

Fig. 4.2.: ^{1}HNMR spectra showing the progress of the photocyclization at −50°C in $CDCl_3$. The bottom spectrum is of the starting vinyl azide **4.5**. A mixture of **4.5** and the mono-azirine intermediate (characteristic peaks shown with black arrows) is visible in the middle spectrum. The top spectrum shows that the cyclization has completed and a ~1:1 ratio of **4.6** (green) and **4.7** (purple) is present.

It is known that the extrusion of nitrogen from vinyl azides to form azirines can proceed thermally or photochemically and that azirines themselves are highly photochemically active.[27] Only recently, however, Farney and Yoon demonstrated that visible light along with a ruthenium photocatalyst could be used to synthesize pyrroles from dienyl azides via an azirine intermediate.[28] In our case, the anthracene core of **4.5** likely acts as an antenna chromophore, allowing it to react under visible-light without the aid of a photocatalyst. The reaction, which proceeds quickly at room temperature, was also monitored by UV-vis spectroscopy where the appearance of sharp vibronic bands indicated formation of cyclized products (Figure S4.1). Both the thermolysis reaction and the photocyclization proceed cleanly and in near quantitative yields. A proposed mechanism for the reactions, proceeding via nitrene formation and subsequent insertion into the *peri*-position C-H bond, is shown in Scheme 4.4.

Scheme 4.4: Proposed mechanism via nitrene C-H insertion.

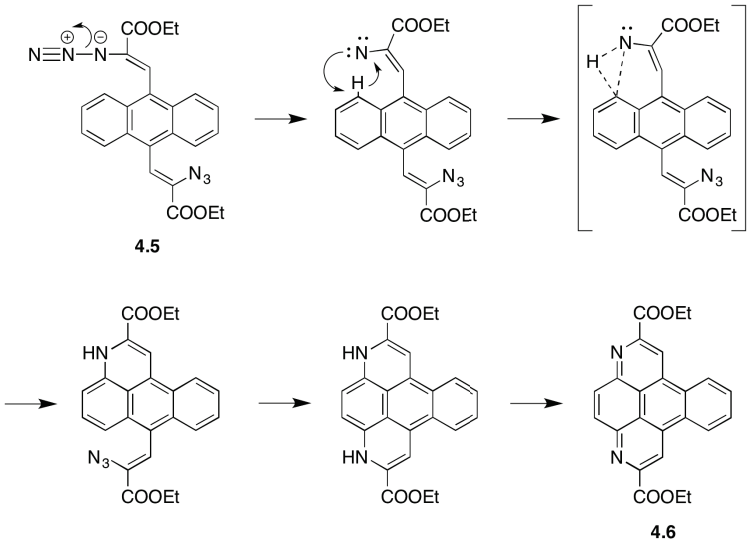

The ester groups of the above cyclization products were removed by hydrolysis and decarboxylation, affording 95% pure 1,8-diazabenzo[e]pyrene **4.10** in 30% yields from the thermolysis method or a mixture of **4.10** and 3,9-diazaperylene **4.11** (23% combined yield) from photolysis (Scheme 4.3). Analytically pure **4.11** was separated from **4.10** in this mixture by preparative reverse phase HPLC, as yellow and white solids, respectively.

Tab. 4.1.: Calculated frontier orbitals,[a] HOMO–LUMO gaps, and optical properties[b] of synthesized N-PAHs and their PAH analogues.

	HOMO (eV)	LUMO (eV)	E_g (eV)	Abs max (nm)	Em max (nm)	Em max solid (nm)	PLQY[c]
4.6	–6.57	–2.49	4.08	336	407		0.03
4.10	–6.16	–2.06	4.11	368.5	370	480	0.12
4.10-2H$^+$			3.23	358[d]	459[d]		0.10[d]
Benzo[e]pyrene	–5.41	–1.39	4.02	340[29]	391[29]	475[30]	0.04[29]
4.7	–6.06	–2.92	3.14				
4.11	–5.67	–2.49	3.18	423	431	619	0.82
4.11-2H$^+$			2.99	451[d]	460[d]		0.78[d]
Perylene	–4.95	–1.89	3.06	435[e][31]	436[e][31]	570[32]	0.94[e][31]

[a] DFT calculations at the B3LYP, 6-31G(d) level.
[b] Measured in CH_2Cl_2 solutions unless noted.
[c] Anthracene in ethanol was used as the standard (PLQY = 0.27).
[d] Measured in 1% TFA in CH_2Cl_2.
[e] Measured in cyclohexane.

4.2.2 Optoelectronic Properties

In order to investigate the effect of nitrogen insertion on the optoelectronic properties of N-PAHs, we performed DFT calculations and photophysical experiments on **4.10** and **4.11**. Calculations confirmed that the HOMO and LUMO energy levels of **4.10** and **4.11** were stabilized by 0.6–0.7 eV compared to their hydrocarbon analogues benzo[e]pyrene and perylene (Table 4.1), with a slightly stronger stabilizing effect in **4.10**. The frontier orbitals of **4.6** and **4.7** were both further lowered by two ester substituents by 0.4 eV.

The much smaller HOMO-LUMO gap of **4.11** vs **4.10** (3.18 eV vs. 4.11 eV) mirrors the differences between their homocyclic analogues, perylene and benzo[e]pyrene (Table 4.1), and could be rationalized by fewer aromatic Clar's sextets and thus better electron delocalization in **4.11**. Accordingly, a large red-shift was observed for **4.11** vs **4.10** in the UV-vis absorption spectra (Figure 4.3). Both the absorption and emission bands of **4.10** and **4.11** show a very pronounced vibronic splitting ($\Delta h\nu \sim 1300$ cm^{-1}), indicative of the molecules' rigid π–conjugated structures. **4.11** emits strongly in solution (PLQY = 0.82 in CH_2Cl_2),

while **4.10** is a much weaker emitter (PLQY = 0.12). These values are similar to the quantum yields of their parent PAHs (Table 4.1) and are in agreement with TD-DFT calculations that predict a lower transition oscillator strength for **4.10** (0.13) than for **4.11** (0.34). Curious to see if **4.10** or **4.11** shared pyrene's characteristic excimer formation at high concentration, we studied their emission at increasing concentrations and in water fractions to induce aggregation. Neither compound exhibited excimer formation, as evidenced by the lack of red-shifted emission bands in concentrated solutions (Figure S4.3). In water/MeCN solutions, however, **4.10** exhibits a continuous enhancement in fluorescence, likely due to increase of the solvent polarity (Figure 4.4). The fluorescence of **4.11** is unaffected, probably due to its lower polarity, which also causes it to precipitate in water fractions above 60%.

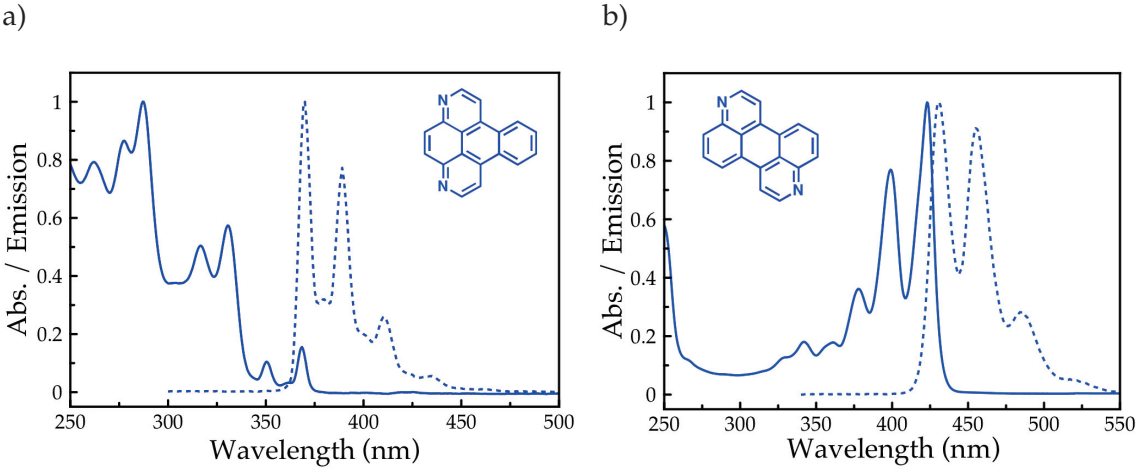

Fig. 4.3.: Absorption (—) and emission (- -) spectra of **4.10** (a) and **4.11** (b) in CH_2Cl_2 solutions.

In the solid state, **4.10** is more emissive than **4.11** (Figure 4.5) and both materials show large red shifts (110 nm for **4.10** and 188 nm for **4.11**) indicating that fluorescence originates from delocalized excitons. We also observe spectral broadening and the disappearance of vibrational structures, details previously reported for the solid emission of perylene and pyrene.[32] Excitation scans of the compounds reveal considerable overlap between the absorption and emission regions of **4.10** and to a lesser extent of **4.11**, which may be partly responsible for the low observed quantum yields (Φ = 0.03 for **4.10** and 0.01 for **4.11**) due to self-absorption. These values are much lower than those recorded in powder

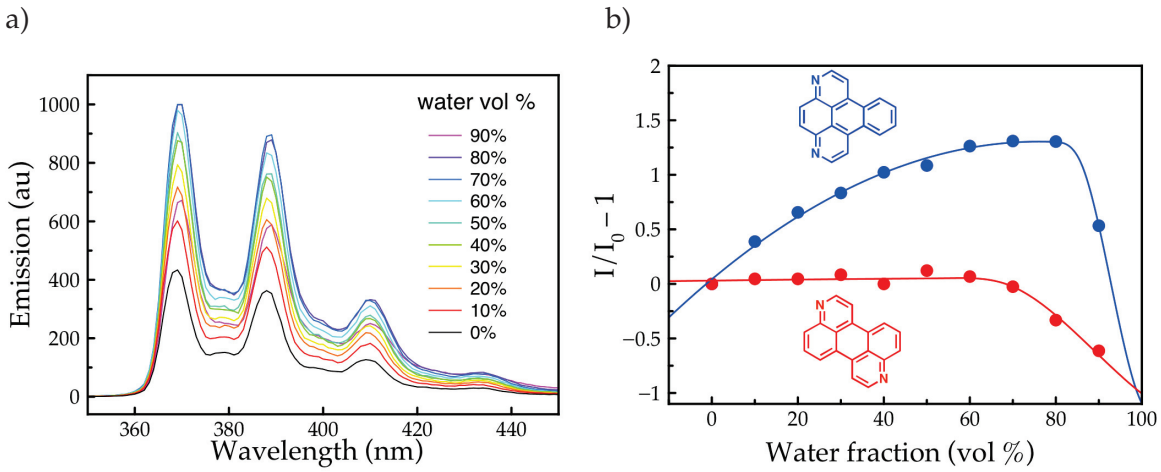

Fig. 4.4.: a) Emission spectra of **4.10** in MeCN-water solutions show polarity-induced enhanced emission. b) Plot of variations in PL peak intensities of **4.10** and **4.11** versus water fraction.

samples of perylene (Φ = 0.18) and pyrene (Φ = 0.67).[32] While the solid-state emission of **4.10** resembles that of benzo[e]pyrene, the solid-state emission of **4.11** is approximately 50 nm red-shifted compared to solid perylene (Table 4.1). This and its decreased solid-state fluorescence could be due to stronger intermolecular coupling.

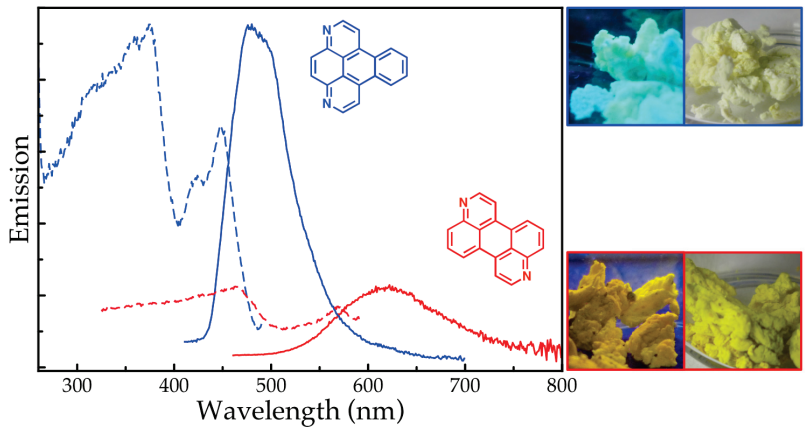

Fig. 4.5.: Solid-state emission spectra (—) and excitation (- -) spectra normalized to the respective emissions of **4.10** and **4.11** with images of the material under UV and natural light.

Due to the presence of basic nitrogen centers, **4.10** and **4.11** undergo pronounced spectroscopic changes when exposed to acids as a result of the nitrogen heteroatoms (Figure

4.6). Titration experiments with trifluoroacetic acid (TFA) reveal a very quick broadening and red-shift in the absorption spectra of **4.10** and **4.11** in MeCN with 0.01–0.05% TFA. This is accompanied by quenching of fluorescence, attributed to the low emissivity of the mono-protonated species, **4.10-H**$^+$ and **4.11-H**$^+$. Continued acidification of the solutions is expected to produce the diprotonated species, **4.10-2H**$^+$ and **4.11-2H**$^+$, concomitant with marked increases in fluorescence from 0.1% to 1% TFA. The emission bands of **4.10-2H**$^+$ and **4.11-2H**$^+$ are distinctly red-shifted from those of **4.10** and **4.11** (90 nm and 35 nm respectively), suggesting that these compounds could be useful as dual-band fluorescence pH sensors.[33] Of particular significance for applications in fluorescence imaging are the comparable quantum yields between **4.10**/**4.11** and **4.10-2H**$^+$/**4.11-2H**$^+$, suggesting these compounds could be used as ratiometric probes (Table 4.1).

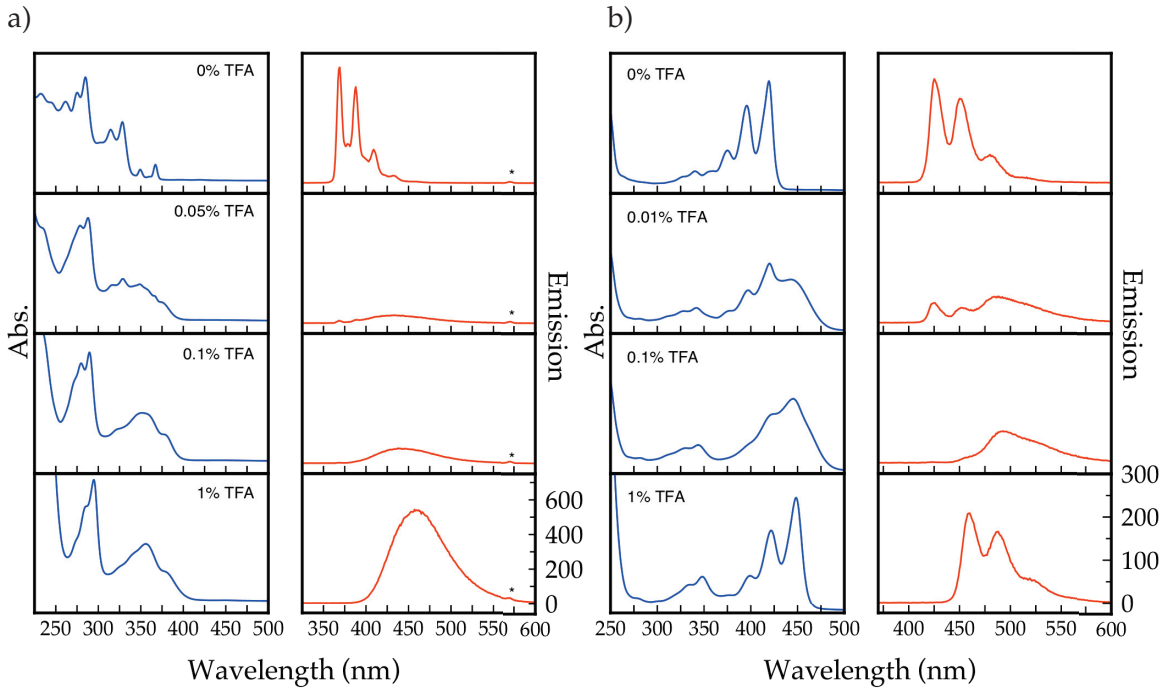

Fig. 4.6.: The change in absorption (blue) and emission (red) spectra of a) **4.10** and b) **4.11** in MeCN solutions with increasing concentrations of trifluoroacetic acid. Asterisks denote the 2nd order excitation peak.

4.3 Conclusions

We have demonstrated that vinyl azide derivatives of PAHs with available *peri*-positions can cyclize to form fused pyridine-like structures in near-quantitative yield, representing a new avenue for the synthesis of novel polycyclic N-heteroaromatic compounds. The regioselectivity of tandem cyclizations can be altered through the reaction conditions, as the cyclization can be induced either thermally or photochemically without a metal catalyst or high-energy light source. The two novel N-PAHs reported herein, 1,8-diazabenzo[e]pyrene and 3,9-diazaperylene, are calculated to have significantly lower HOMO/LUMO levels compared to their parent PAHs. Diazaperylene's exhibits better electron delocalization and high quantum yields in solution (82%) compared to diazapyrene (10%). The heteroatoms greatly alter the optoelectronic properties, as exemplified, e.g., by the "turn-off" and "turn-on" pH fluorescence sensing behavior of these compounds. We have demonstrated that nitrogen heteroatoms can be used to tune the energy levels of known PAH emitters without significantly changing the HOMO-LUMO gap or emission efficiency. The documented properties of these molecules have positive implications for their potential use as n-type semiconductors, fluorescent sensors, and light-emitting materials.

4.4 Experimental Section

4.4.1 Optical Spectroscopy

UV/Vis absorption and photoluminescence spectra were measured in CH_2Cl_2 with a JACSO V670 UV-Vis-NIR spectrometer and a Varian Eclipse Fluorimeter, respectively. The fluorescence quantum yields were determined relative to anthracene in EtOH (Φ = 0.27). Solid-state fluorescence was acquired for powders using an integrating sphere on a FluoroLog-3 spectrofluorometer (Horiba Jobin Yvon Inc.).

4.4.2 Computational Methods

Geometries, molecular orbital energies, and electronic transitions were calculated at the B3LYP/6–31G(d) level of theory using the Gaussian 09W program.[34]

4.4.3 Synthesis

Ethyl 2-azidoacetate (Warning: Highly flammable liquid and vapour. Reaction performed behind blast shield.)
Ethyl chloroacetate (10 mL, 0.093 mol) in EtOH (40 mL) was cooled to 0°C in an ice bath. Sodium azide (7.0 g, 0.11 mol) was weighed out, dissolved in H_2O (20 mL) and added to the cold reaction mixture. The solution was stirred at 0°C for 20 minutes before being brought to reflux for 4.5 hrs. After cooling, the reaction mixture was washed with H_2O (60 mL) and extracted with Et_2O (3 × 50 mL). The combined organics were washed with H_2O (3 × 50 mL), dried over Na_2SO_4, and the solvent was removed in vacuo to afford a clear oil (11 g, 95% yield). NMR data was in agreement with literature. ^{1}HNMR ($CDCl_3$, 500 MHz, 25°C) δ 4.29 (q, *J* = 7.2 Hz, 2H), 3.88 (s, 2H), 1.34 (t, *J* = 7.2 Hz, 3H). ^{13}CNMR ($CDCl_3$, 125 MHz, 25°C) δ 168.3, 61.8, 50.3, 14.04.

Ethyl (Z)-3-(anthracen-9-yl)-2-azidoacrylate (4.1)
In a dry 2-neck flask, sodium (0.20 g, 8.7 mmol) was added to dry EtOH (15 mL) under a N_2 atmosphere and the solution was stirred till no sodium remained. In a second dry flask, anthracene-9-carbaldehyde (0.39 g, 1.9 mmol) and ethyl 2-azidoacetate (1.20 g, 9.3 mmol) were combined with dry EtOH (15 mL) and cooled to −20°C under a N_2 atmosphere. The fresh NaOEt solution was slowly transferred via cannula and the reaction mixture was stirred overnight at −20°C. The reaction mixture was then poured into saturated $NaHCO_3$ (10 mL) chilled with ice and extracted with ethyl acetate (3 × 25 mL). The solvent was removed in vacuo and the product purified by column chromatography in 60:40 hexane:chloroform to afford a yellow solid (0.24 g, 40% yield). ^{1}HNMR ($CDCl_3$, 500 MHz, 25°C) δ 8.51 (s, 1H), 8.07 (d, *J* = 7.5 Hz, 2H), 8.01 (d, *J* = 8.5 Hz, 2H), 7.86 (s, 1H), 7.54 (m, 4H), 4.54 (q, *J* = 7.0 Hz, 2H), 1.53 (t, *J* = 7.5 Hz, 3H). ^{13}CNMR ($CDCl_3$, 125 MHz, 25°C) δ 162.7, 131.14, 131.12, 128.97, 128.95, 128.2, 126.9, 125.6, 125.4, 123.8, 62.6, 14.3.

Ethyl 7-oxo-7H-naphtho[1,2,3-de]quinoline-2-carboxylate (4.3)
Compound **4.1** (0.20 g, 0.62 mol) is dissolved in dry toluene (20 mL) and brought to reflux under a N_2 atmosphere. The reaction is monitored by TLC and when complete, cooled and the solvent removed in vacuo. The crude product was purified by column chromatography using a gradient of 100% hexane to 40% tetrahydrofuran to afford **4.3** as a dark solid (0.04 g, 22% yield). ^{1}HNMR ($CDCl_3$, 500 MHz, 25°C) δ 9.03 (s, 12H), 8.83 (dd, *J* = 7.3, 1.3 Hz, 1H), 8.80 (d, *J* = 8.1 Hz, 1H), 8.57 (dd, *J* = 7.8, 1.1 Hz, 1H), 8.52 (d, *J* = 7.9 Hz, 1H), 8.08 (t, *J* = 8.0 Hz, 1H), 7.84 (td, *J* = 7.6, 1.5 Hz, 1H), 7.76 (td, *J* = 7.6, 1.0 Hz, 1H), 4.68 (q, *J* = 7.1 Hz, 1H), 1.60 (t, *J* = 7.1 Hz, 1H). ^{13}CNMR ($CDCl_3$, 125 MHz, 25°C) δ 182.1, 165.0, 149.1, 146.8, 137.2, 136.8, 134.0, 133.4, 132.2, 131.5, 131.2, 130.8, 128.64, 128.58, 124.4, 124.3, 116.7, 62.8, 14.4. HR-MS (APCI) *m/z* = 304.0962 [M+1] (calcd. for $C_{19}H_{14}NO_3$: *m/z* = 304.0968).

Diethyl 3,3′-(anthracene-9,10-diyl)(2Z,2′Z)-bis(2-azidoacrylate) (4.5)
In a dry 2-neck flask, sodium (2.2 g, 0.095 mol) was added to dry EtOH (100 mL) under a N_2 atmosphere and the solution was stirred till no sodium remained. In a second dry flask, **4.4** (2.6 g, 0.011 mol) and ethyl azidoacetate (11.4 g, 0.088 mol) were combined with dry EtOH (150 mL) and cooled to −20°C under a N_2 atmosphere. The fresh NaOEt solution was slowly transferred via cannula and the reaction mixture was stirred overnight at −10°C. The reaction mixture was then poured into saturated $NaHCO_3$ (20 mL) and ice and let

stand in at 6°C for 3 hours. The resulting yellow precipitate was collected by filtration and washed with water to afford a bright yellow solid (3.0 g, 59%) The product can be used without further purification or purified by column chromatography using a gradient of 100% hexane to 100% dichloromethane, however solutions of 4.5 will react if exposed to light. ^{1}HNMR ($CDCl_3$, 500 MHz, 25°C) δ 8.02 (dd, *J* = 6.7, 3.3 Hz, 4H), 7.79 (s, 2H), 7.55 (dd, *J* = 6.8, 3.2 Hz, 4H), 4.52 (q, *J* = 7.2 Hz, 4H), 1.51 (t, *J* = 7.2 Hz, 6H). ^{13}CNMR ($CDCl_3$, 125 MHz, 25°C) δ 162.6, 131.5, 128.7, 128.4, 126.2, 126.1, 123.5, 62.7, 14.3. HR-MS (ESI) *m/z* = 495.1187 [M+K]+ (calcd. for $C_{24}H_{20}KN_6O_4$: *m/z* = 495.1178).

Diethyl dibenzo[f,lmn][2,9]phenanthroline-2,7-dicarboxylate (4.6)
Thermolysis Method Compound **4.5** (0.74 g, 1.6 mmol) is suspended in dry toluene (50 mL) and brought to reflux under a N_2 atmosphere. After refluxing overnight the reaction is cooled and the solvent removed in vacuo. The crude product was purified recrystallization from hot tetrahydrofuran to afford a tan powder of **4.6** (0.52 g, 80% yield) containing 6% of **4.7** as an impurity). ^{1}HNMR ($CDCl_3$, 500 MHz, 25°C) δ 9.56 (s, 2H), 9.03 (dd, *J* = 6.1, 3.4 Hz, 2H), 8.75 (s, 2H), 8.03 (dd, *J* = 6.2, 3.3 Hz, 2H), 4.71 (q, *J* = 7.2 Hz, 4H), 1.61 (t, *J* = 7.1 Hz, 6H). ^{13}CNMR (CD_2Cl_2, 125 MHz, 25°C) δ 165.4, 148.3, 147.4, 136.92, 133.7, 130.7, 129.5, 124.9, 119.0, 115.6, 62.4, 14.3. HR-MS (ESI) *m/z* = 421.1156 [M+Na]+ (calcd. for $C_{24}H_{18}N_2NaO_4$: *m/z* = 421.1159).

Dibenzo[f,lmn][2,9]phenanthroline-2,7-dicarboxylic acid (4.8)
NaOH (0.079 g, 2.0 mmol) was added to a suspension of **4.6** (0.30 g, 0.75 mmol) in a THF/H_2O (40 mL/10 mL) solution. The reaction is stirred for 2 hrs and then acidified with HCl. The THF is removed in vacuo and the product dissolved in a minimum amount of H_2O. HCl is added to the aqueous solution until no more precipitate is observed. The product is then filtered, washed with H_2O and MeOH, and fully dried to afford a dark brown acid **4.8** (0.25 g, 98% yield) which was used in the next step without purification. ^{1}HNMR ($(CD_3)_2SO$), 500 MHz, 25°C) δ 13.64 (s, br, 2H), 9.37 (s, 2H), 9.06 (d, br, 2H), 8.52 (s, 2H), 7.99 (d, br, 2H). ^{13}CNMR (($(CD_3)_2SO$), 125 MHz, 25°C) δ 167.0, 148.4, 147.8, 136.6, 133.7, 131.4, 129.2, 125.6, 118.5, 115.7. HR-MS (ESI) *m/z* = 343.0717 [M+] (calcd. for $C_{20}H_{11}N_2O_4$: *m/z* = 343.0713).

Dibenzo[f,lmn][2,9]phenanthroline (1,8-diazabenzo[e]pyrene 4.10)
A dry flask was charged with **4.8** (0.25 g, 0.73 mmol) and diphenyl ether (20 mL). The flask was evacuated and refilled with N_2 and then brought to reflux for 3.5 hrs. The diphenyl ether is distilled off under vacuum and the resulting solids are sonicated into Et_2O and filtered to afford yellow powder of **4.8** (0.06 g, 31% yield) containing 6% of **4.11** as an impurity. The product was further purified by sublimation at 140°C. ^{1}HNMR ($CDCl_3$, 500 MHz, 25°C) δ 9.39 (d, *J* = 5.2 Hz, 2H), 8.87 (dd, *J* = 6.1, 3.3 Hz, 2H), 8.66 (d, *J* = 5.3 Hz, 2H), 8.56 (s, 2H), 7.93 (dd, *J* = 6.2, 3.3 Hz, 2H). ^{13}CNMR ($CDCl_3$, 125 MHz, 25°C) δ 148.7, 148.2, 135.5, 132.8, 130.0, 129.7, 124.6, 118.2, 114.3. HR-MS (APCI) *m/z* = 255.0928 [M+] (calcd. for $C_{18}H_{11}N_2$: *m/z* = 255.0917).

Diethyl dibenzo[f,lmn][2,9]phenanthroline-2,7-dicarboxylate (4.6) and
diethyl benzo[1,2,3-de:4,5,6-d'e']diquinoline-2,8-dicarboxylate (4.7)
Photocyclization Method Compound **4.5** (52 mg, 0.11 mmol) is loaded into a dry reaction vessel under a N_2 atmosphere and dry CH_2Cl_2 (10 mL) is syringed in. The reaction is

stirred at −80°C under illumination from a 100W compact fluorescent bulb with a 5,000K color temperature. The reaction is monitored by UV-vis and when complete the solvent is removed in vacuo to afford a dark green solid (48 mg, >100% yield). The mixture of products was used in the next reaction without purification. ^{1}HNMR ($CDCl_3$, 500 MHz, 25°C) δ 9.43 (s, 2H), 8.91 (dd, *J* = 6.1, 3.4 Hz, 2H), 8.642 (s, 2H) 8.635 (s, 2H), 8.39 (d, *J* = 6.9 Hz, 2H), 8.22 (d, *J* = 8.4 Hz, 2H), 7.93 (dd, *J* = 6.1, 3.3 Hz, 2H), 7.77 (t, *J* = 8.0 Hz, 2H), 4.63 (q, *J* = 7.1 Hz, 4H), 4.54 (q, *J* = 7.1 Hz, 4H), 1.62 (t, *J* = 7.1 Hz, 6H), 1.57 (t, *J* = 7.1 Hz, 6H).

Dibenzo[f,lmn][2,9]phenanthroline-2,7-dicarboxylic acid (4.8) and **benzo[1,2,3-de:4,5,6-d′e′]diquinoline-2,8-dicarboxylic acid (4.9)** were prepared in the same manner as described above for compound **4.8** in a 70% yield. The mixture of products was used in the next reaction without purification.

Dibenzo[f,lmn][2,9]phenanthroline (1,8-diazabenzo[e]pyrene 4.10) and **benzo[1,2,3-de:4,5,6-d′e′]diquinoline (3,9-diazaperylene 4.11)** were prepared in the same manner as described above for compound **4.10** in a 23% yield after sublimation. The two isomers are then separated on a C18 prep HPLC column running a gradient from 100% H_2O to 100% MeCN.

(4.10) Spectroscopic data is identical to the product prepared (above) by thermolysis method.

(4.11) ^{1}HNMR ($(CD_3)_2SO$), 500 MHz, 50°C) δ 8.88 (d, *J* = 4.8 Hz, 2H), 8.55 (d, *J* = 7.5 Hz, 2H), 8.25 (d, *J* = 4.8 Hz, 2H), 7.99 (d, *J* = 8.3 Hz, 2H), 7.81 (t, *J* = 7.9 Hz, 2H). ^{13}CNMR ($((CD_3)_2SO$), 125 MHz, 70°C) δ 152.1, 149.5, 137.6, 131.6, 130.4, 128.8, 123.6, 123.3, 115.2. HR-MS (ESI) *m/z* = 255.0909 [M+] (calcd. for $C_{18}H_{11}N_2$: *m/z* = 255.0917).

References

(1) a) Pisula, W.; Feng, X.; Müllen, K. Charge-Carrier Transporting Graphene-Type Molecules. *Chem. Mater.* **2011**, *23*, 554; b) Zhang, L.; Cao, Y.; Colella, N. S.; Liang, Y.; Bredas, J. L.; Houk, K. N.; Briseno, A. L. Unconventional, chemically stable, and soluble two-dimensional angular polycyclic aromatic hydrocarbons: from molecular design to device applications. *Acc Chem Res* **2015**, *48*, 500; c), *Polycyclic Arenes and Heteroarenes*; Miao, Q., Ed.; Wiley-VCH Verlag GmbH & Co. KGaA: Weinheim, Germany, 2015.

(2) a) Türker, L.; Tapan, A.; Gümüş, S. Electroluminescent properties of certain polyaromatic compounds: Part 2–Organic emitters. *Polycycl. Aromat. Compd.* **2009**, *29*, 139; b) Su, S.; Herron, N.; Meng, H. In *Org. Light. Mater. Devices (2nd Ed.)* Li, Z. R., Ed.; CRC Press: Boca Raton, FL, 2015; Chapter 3, pp 310–452.

(3) a) Ren, R. X.-F.; Chaudhuri, N. C.; Paris, P. L.; Rumney; Kool, E. T. Naphthalene, Phenanthrene, and Pyrene as DNA Base Analogues: Synthesis, Structure, and Fluorescence in DNA. *J. Am. Chem. Soc.* **1996**, *118*, 7671; b) Yuan, L.; Lin, W.; Zheng, K.; Zhu, S. FRET-based small-molecule fluorescent probes: Rational design and bioimaging applications. *Acc. Chem. Res.* **2013**, *46*, 1462; c) Pak, Y.; Swamy, K.; Yoon, J. Recent Progress in Fluorescent Imaging Probes. *Sensors* **2015**, *15*, 24374.

(4) Adachi, C.; Tokito, S.; Tsutsui, T.; Saito, S. Electroluminescence in Organic Films with Three-Layer Structure. *Jpn. J. Appl. Phys.* **1988**, *27*, L269.

(5) Figueira-Duarte, T. M.; Müllen, K. Pyrene-based materials for organic electronics. *Chem. Rev.* **2011**, *111*, 7260.

(6) Birks, J.; Christophorou, L. Excimer fluorescence spectra of pyrene derivatives. *Spectrochim. Acta* **1963**, *19*, 401.

(7) a) Kalyanasundaram, K.; Thomas, J. K. Environmental effects on vibronic band intensities in pyrene monomer fluorescence and their application in studies of micellar systems. *J. Am. Chem. Soc.* **1977**, *99*, 2039; b) Jiang, J.; Tong, X.; Zhao, Y. A New Design for Light-Breakable Polymer Micelles. *J. Am. Chem. Soc.* **2005**, *127*, 8290; c) Bains, G.; Patel, A. B.; Narayanaswami, V. Pyrene: A Probe to Study Protein Conformation and Conformational Changes. *Molecules* **2011**, *16*, 7909.

(8) a) Britz, D. A.; Khlobystov, A. N. Noncovalent interactions of molecules with single walled carbon nanotubes. *Chem. Soc. Rev.* **2006**, *35*, 637; b) Georgakilas, V.; Otyepka, M.; Bourlinos, A. B.; Chandra, V.; Kim, N.; Kemp, K. C.; Hobza, P.; Zboril, R.; Kim, K. S. Functionalization of graphene: Covalent and non-

covalent approaches, derivatives and applications. *Chem. Rev.* **2012**, *112*, 6156; c) Kuila, T.; Bose, S.; Mishra, A. K.; Khanra, P.; Kim, N. H.; Lee, J. H. Chemical functionalization of graphene and its applications. *Prog. Mater. Sci.* **2012**, *57*, 1061.

(9) Usta, H.; Facchetti, A.; Marks, T. J. N-channel semiconductor materials design for organic complementary circuits. *Acc. Chem. Res.* **2011**, *44*, 501.

(10) a) Chase, D. T.; Fix, A. G.; Kang, S. J.; Rose, B. D.; Weber, C. D.; Zhong, Y.; Zakharov, L. N.; Lonergan, M. C.; Nuckolls, C.; Haley, M. M. 6,12-Diarylindeno[1,2-b]fluorenes: Syntheses, photophysics, and ambipolar OFETs. *J. Am. Chem. Soc.* **2012**, *134*, 10349; b) Fix, A. G.; Deal, P. E.; Vonnegut, C. L.; Rose, B. D.; Zakharov, L. N.; Haley, M. M. Indeno[2,1- c]fluorene: A New Electron-Accepting Scaffold for Organic Electronics. *Org. Lett.* **2013**, *15*, 1362.

(11) a) Swartz, C. R.; Parkin, S. R.; Bullock, J. E.; Anthony, J. E.; Mayer, A. C.; Malliaras, G. G. Synthesis and characterization of electron-deficient pentacenes. *Org. Lett.* **2005**, *7*, 3163; b) Sakamoto, Y.; Suzuki, T.; Kobayashi, M.; Gao, Y.; Fukai, Y.; Inoue, Y.; Sato, F.; Tokito, S. Perfluoropentacene: High-performance p-n junctions and complementary circuits with pentacene. *J. Am. Chem. Soc.* **2004**, *126*, 8138; c) Tang, M. L.; Reichardt, A. D.; Wei, P.; Bao, Z. Correlating carrier type with frontier molecular orbital energy levels in organic thin film transistors of functionalized acene derivatives. *J. Am. Chem. Soc.* **2009**, *131*, 5264; d) Tang, M. L.; Oh, J. H.; Reichardt, A. D.; Bao, Z. Chlorination: a general route toward electron transport in organic semiconductors. *J. Am. Chem. Soc.* **2009**, *131*, 3733.

(12) Bunz, U. H. F.; Engelhart, J. U.; Lindner, B. D.; Schaffroth, M. Large N-heteroacenes: new tricks for very old dogs? *Angew. Chem. Int. Ed. Engl.* **2013**, *52*, 3810.

(13) a) Miao, S.; Appleton, A. L.; Berger, N.; Barlow, S.; Marder, S. R.; Hardcastle, K. I.; Bunz, U. H. F. 6,13-Diethynyl-5,7,12,14-tetraazapentacene. *Chem. - A Eur. J.* **2009**, *15*, 4990; b) Liang, Z.; Tang, Q.; Mao, R.; Liu, D.; Xu, J.; Miao, Q. The position of nitrogen in N-heteropentacenes matters. *Adv. Mater.* **2011**, *23*, 5514; c) Miao, Q. Ten years of N-heteropentacenes as semiconductors for organic thin-film transistors. *Adv. Mater.* **2014**, *26*, 5541.

(14) a) Tang, Q.; Liang, Z.; Liu, J.; Xu, J.; Miao, Q. N-heteroquinones: quadruple weak hydrogen bonds and n-channel transistors. *Chem. Commun. (Camb).* **2010**, *46*, 2977; b) He, Z.; Liu, D.; Mao, R.; Tang, Q.; Miao, Q. Hydrogen-Bonded Dihydrotetraazapentacenes. *Org. Lett.* **2012**, *14*, 1050.

(15) Głowacki, E. D.; Romanazzi, G.; Yumusak, C.; Coskun, H.; Monkowius, U.; Voss, G.; Burian, M.; Lechner, R. T.; Demitri, N.; Redhammer, G. J.; Sünger, N.; Suranna, G. P.; Sariciftci, S. Epindolidiones-Versatile and Stable Hydrogen-Bonded Pigments for Organic Field-Effect Transistors and Light-Emitting Diodes. *Adv. Funct. Mater.* **2015**, *25*, 776.

(16) Li, G.; Wu, Y.; Gao, J.; Wang, C.; Li, J.; Zhang, H.; Zhao, Y.; Zhao, Y.; Zhang, Q. Synthesis and physical properties of four hexazapentacene derivatives. *J. Am. Chem. Soc.* **2012**, *134*, 20298.

(17) a) He, B.; Pun, A. B.; Klivansky, L. M.; McGough, A. M.; Ye, Y.; Zhu, J.; Guo, J.; Teat, S. J.; Liu, Y. Thiophene fused azacoronenes: Regioselective synthesis, self-organization, charge transport and its incorporation in conjugated polymers. *Chem. Mater.* **2014**, *26*, 3920; b) He, B.; Dai, J.; Zherebetskyy, D.; Chen, T. L.; Zhang, B. A.; Teat, S. J.; Zhang, Q.; Wang, L.; Liu, Y. A divergent route to core- and peripherally functionalized diazacoronenes that act as colorimetric and fluorescence proton sensors. *Chem. Sci.* **2015**, *6*, 3180.

(18) Sarkar, P.; Jeon, I.-R.; Durola, F.; Bock, H. Tetraazaarenes by the ceramidonine approach. *New J. Chem.* **2012**, *36*, 570.

(19) Tokita, S.; Watanabe, T.; Fujita, Y.; Iijima, H.; Terazono, S. Molecular Design and Synthesis of Novel Analogues of Benzodixanthene and Anthradichromene. *Mol. Cryst. Liq. Cryst. Sci. Technol. Sect. A.* **1997**, *297*, 269.

(20) Tan, Q.; Chen, H.; Xia, H.; Liu, B.; Xu, B. Parent and trisubstituted triazacoronenes: synthesis, crystal structure and physicochemical properties. *Chem. Commun.* **2016**, *52*, 537.

(21) a) He, T.; Too, P. C.; Chen, R.; Chiba, S.; Sun, H. Concise Synthesis and Two-Photon-Excited Deep-Blue Emission of 1,8-Diazapyrenes. *Chem. - An Asian J.* **2012**, *7*, 2090; b) Baranov, D. S.; Popov, A. G.; Uvarov, M. N.; Kazantsev, M. S.; Mostovich, E. A.; Glebov, E. M.; Kulik, L. V. Naphtho[4,3,2,1-lmn][2,9]phenanthrolines: Synthesis, characterization, optical properties and light-induced electron transfer in composites with the semiconducting polymer MEH-PPV. *Synth. Met.* **2015**, *201*, 43.

(22) Isomura, K.; Okada, M.; Taniguchi, H. Azirine formation by decomposition of terminal vinyl azides. *Tetrahedron Lett.* **1969**, *10*, 4073.

(23) a) Hemetsberger, H.; Knittel, D. Synthese und Thermolyse von a-Azidoacrylestern. *Monatshefte fur Chemie* **1972**, *103*, 194; b) Pearson, W. H.; Lian, B. W.; Bergmeier, S. C. In *Compr. Heterocycl. Chem. II*, 1996, pp 1–60.

(24) a) Padwa, A.; Smolanoff, J.; Tremper, A. Intramolecular Reorganization of Some Unsaturated 2H-Azirines. *J. Org. Chem.* **1976**, *41*, 543; b) Gilchrist, T. L.; Rees, C. W.; Rodrigues, J. A. R. Synthesis of fused pyridines under neutral conditions. *J. Chem. Soc. Chem. Commun.* **1979**, 627.

(25) Heaner IV, W. L.; Gelbaum, C. S.; Gelbaum, L.; Pollet, P.; Richman, K. W.; DuBay, W.; Butler, J. D.; Wells, G.; Liotta, C. L. Indoles via Knoevenagel–Hemetsberger reaction sequence. *RSC Adv.* **2013**, *3*, 13232.

(26) Henn, L.; Hickey, D. M. B.; Moody, C. J.; Rees, C. W. Formation of indoles, isoquinolines, and other fused pyridines from azidoacrylates. *J. Chem. Soc. Perkin Trans. 1* **1984**, *104*, 2189.

(27) a) Swenton, J. S.; Ikeler, T. J.; Williams, B. H. Photochemistry of singlet and triplet azide excited states. *J. Am. Chem. Soc.* **1970**, *92*, 3103; b) Palacios, F.; de Retana, A. M. O.; de Marigorta, E. M.; de los Santos, J. M. 2H-Azirines as Synthetic Tools in Organic Chemistry. *European J. Org. Chem.* **2001**, *2001*, 2401; c) Gritsan, N.; Platz, M. In *Organic Azides: Syntheses and Applications*, 2010, pp 311–372.

(28) Farney, E. P.; Yoon, T. P. Visible-light sensitization of vinyl azides by transition-metal photocatalysis. *Angew. Chem. Int. Ed. Engl.* **2014**, *53*, 793.

(29) Ilhan, F.; Tyson, D. S.; Meador, M. A. Phenacenes from Diels-Alder trapping of photogenerated o-xylylenols: phenanthrenes and benzo[e]pyrene bisimide. *Org. Lett.* **2006**, *8*, 577.

(30) Lewitzka, F.; Niessner, R. Application of time-resolved fluorescence spectroscopy on the analysis of PAH-coated aerosols. *Aerosol Sci. Technol. Amsterdam, Netherlands* **1995**, *23*, 454.

(31) Berlman, I. B. In *Handb. Fluoresc. Spectra Aromat. Mol.* Berlman, I. B., Ed., Second; Elsevier: 1971, pp 107–415.

(32) Katoh, R.; Suzuki, K.; Furube, A.; Kotani, M.; Tokumaru, K. Fluorescence Quantum Yield of Aromatic Hydrocarbon Crystals. *J. Phys. Chem. C* **2009**, *113*, 2961.

(33) a) Grover, A.; Schmidt, B. F.; Salter, R. D.; Watkins, S. C.; Waggoner, A. S.; Bruchez, M. P. Genetically Encoded pH Sensor for Tracking Surface Proteins through Endocytosis. *Angew. Chemie Int. Ed.* **2012**, *51*, 4838; b) Han, J. M.; Xu, M.; Wang, B.; Wu, N.; Yang, X.; Yang, H.; Salter, B. J.; Zang, L. Low dose detection of γ radiation via solvent assisted fluorescence quenching. *J. Am. Chem. Soc.* **2014**, *136*, 5090.

(34) Frisch, M. J.; Trucks, G. W.; Schlegel, H. B.; Scuseria, G. E.; Robb, M. A.; Cheeseman, J. R.; Scalmani, G.; Barone, V.; Mennucci, B.; Petersson, G. A.; Nakatsuji, H.; Caricato, M.; Li, X.; Hratchian, H. P.; Izmaylov, A. F.; Bloino, J.; Zheng, G.; Sonnenberg, J. L.; Hada, M.; Ehara, M.; Toyota, K.; Fukuda, R.; Hasegawa, J.; Ishida, M.; Nakajima, T.; Honda, Y.; Kitao, O.; Nakai, H.; Vreven, T.; Montgomery, J. A.; Peralta, J. E.; Ogliaro, F.; Bearpark, M.; Heyd, J. J.; Brothers, E.; Kudin, K. N.; Staroverov, V. N.; Kobayashi, R.; Normand, J.; Raghavachari, K.; Rendell, A.; Burant, J. C.; Iyengar, S. S.; Tomasi, J.; Cossi, M.; Rega, N.; Millam, J. M.; Klene, M.; Knox, J. E.; Cross, J. B., et al. Gaussian09 Revision D.01., Gaussian Inc. Wallingford CT 2009.

4.5 Supporting Information for Chapter 4

4.5.1 Optical Spectroscopy

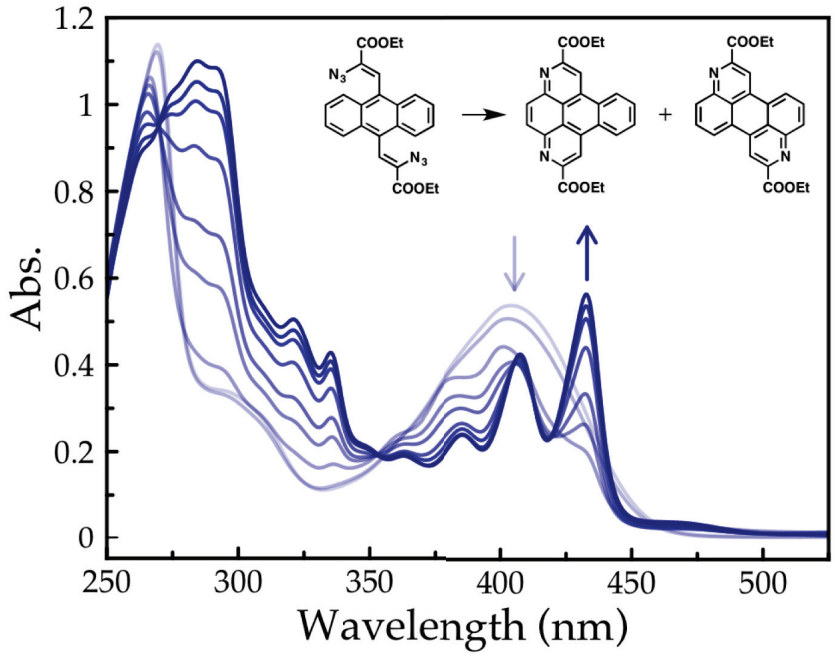

Figure S4.1. The absorption spectra showing the photocyclization of **4.5** at room temperature under ambient lighting. The broad peak of **4.5** is replaced by the sharper vibronic bands of cyclized **4.6** and **4.7**.

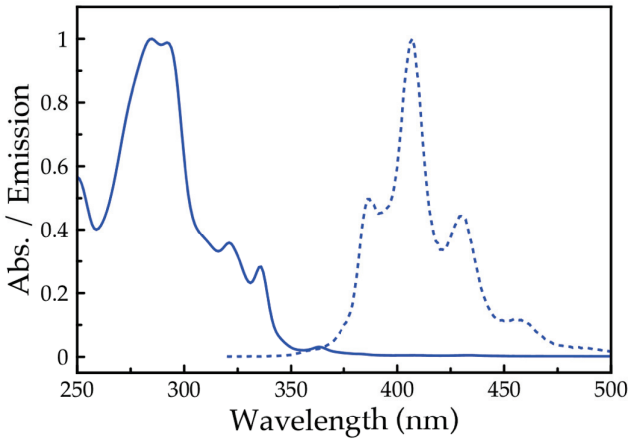

Figure S4.2. Absorption (—) and emission (- -) spectra of **4.6** in CH_2Cl_2 solution.

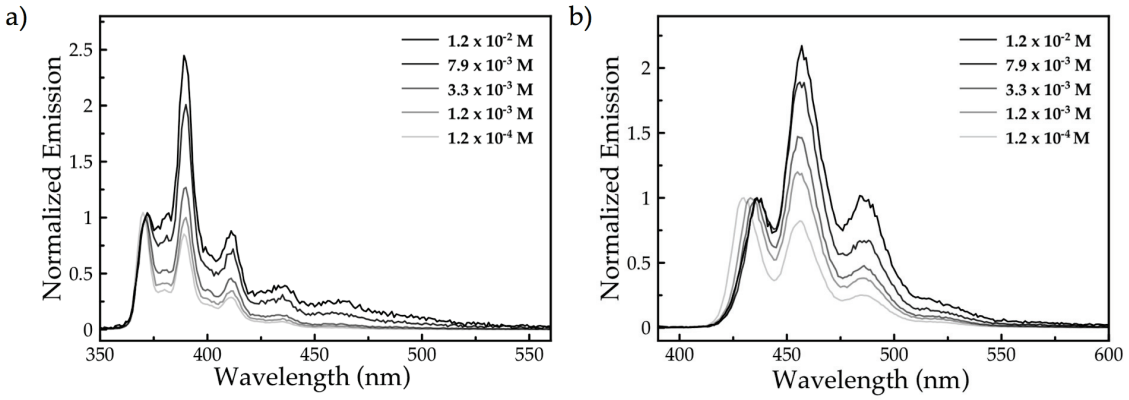

Figure S4.3. Emission spectra of **4.10** (a) and **4.11** (b) in increasing concentrations and normalized to the first emission band. The observed changes in the relative intensities of the vibronic bands can be explained by self-absorption.

4.5.2 NMR Data

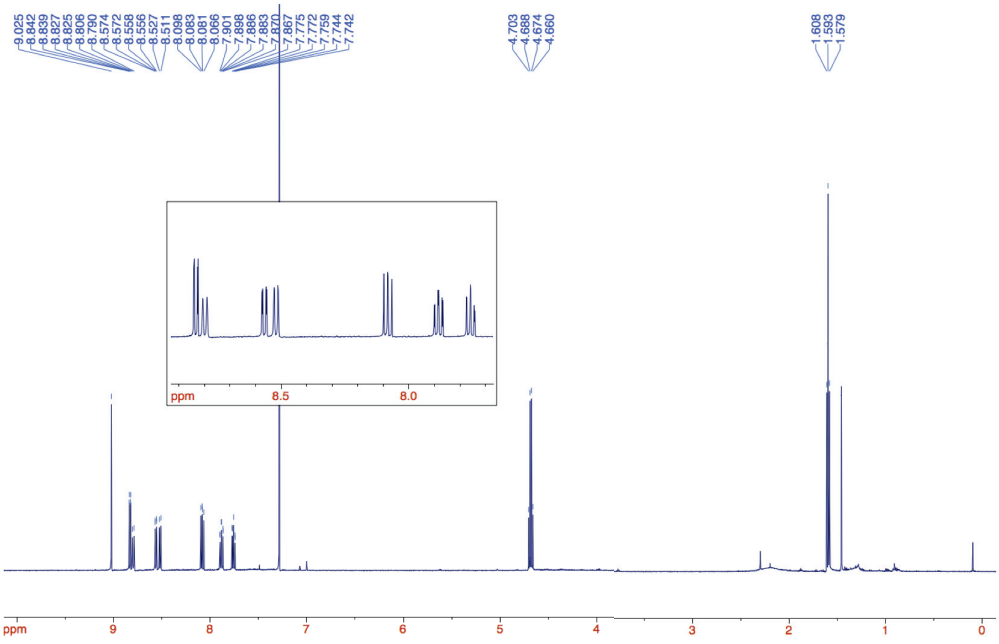

^{1}H NMR spectrum of compound **4.3** in $CDCl_3$.

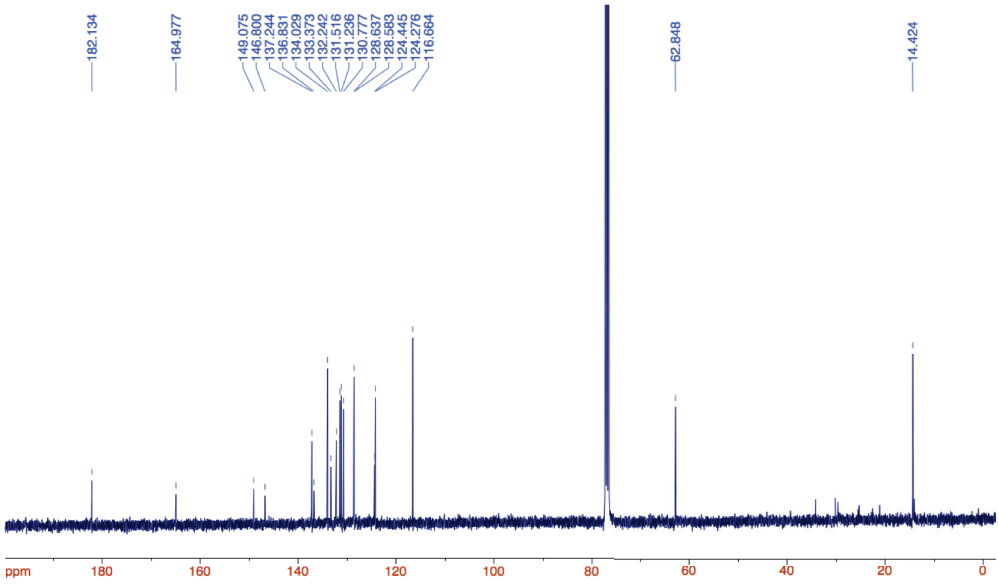

^{13}C NMR spectrum of compound **4.3** in $CDCl_3$.

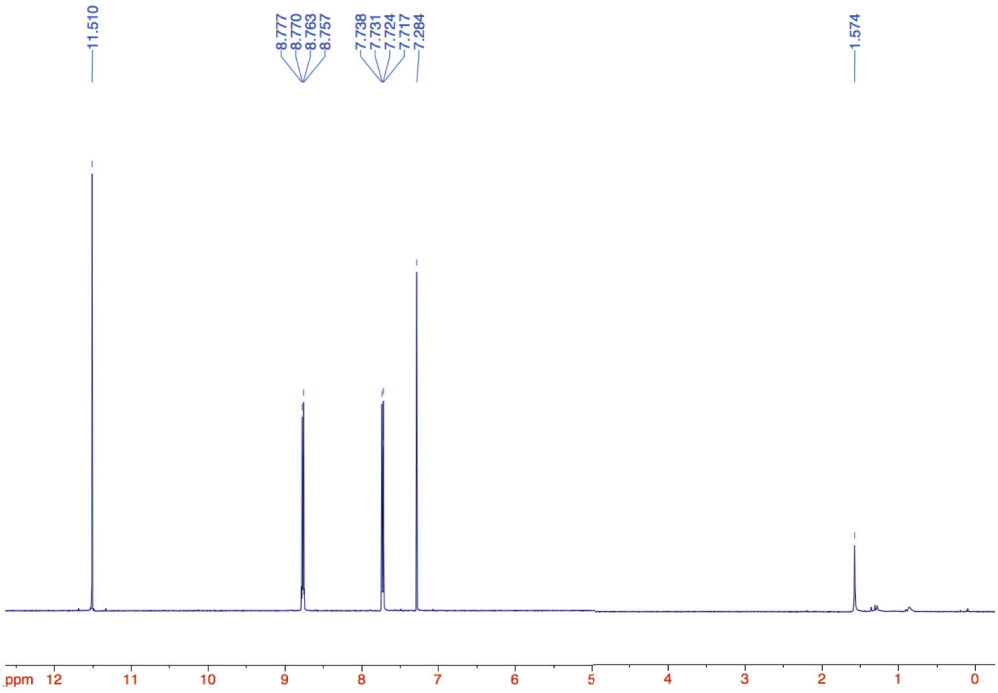

^{1}H NMR spectrum of compound **4.4** in $CDCl_3$.

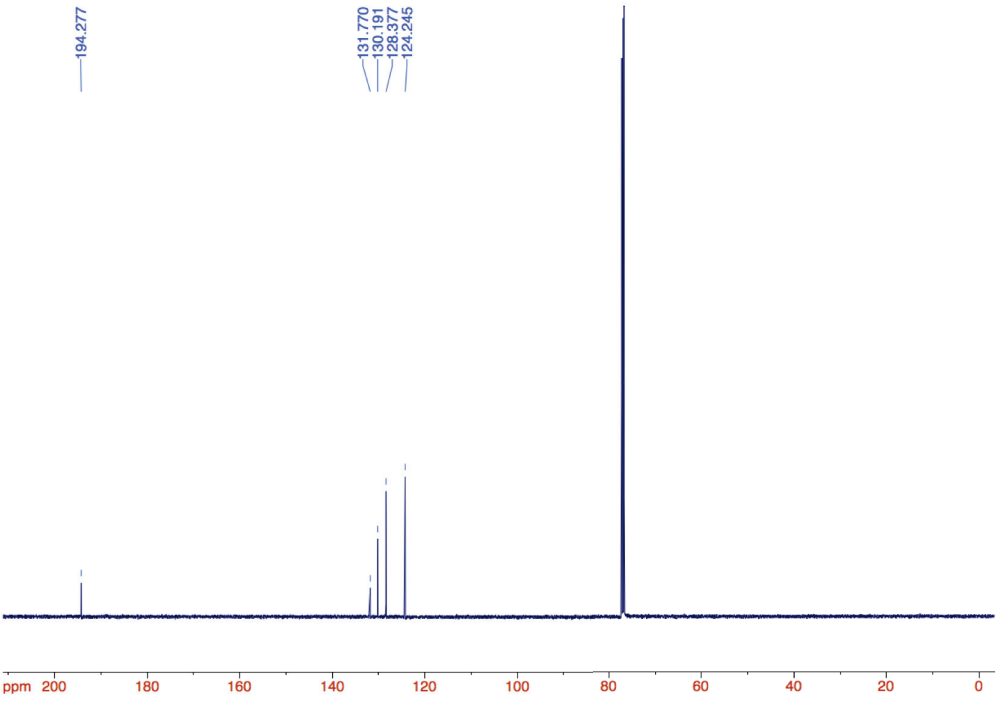

^{13}C NMR spectrum of compound **4.4** in $CDCl_3$.

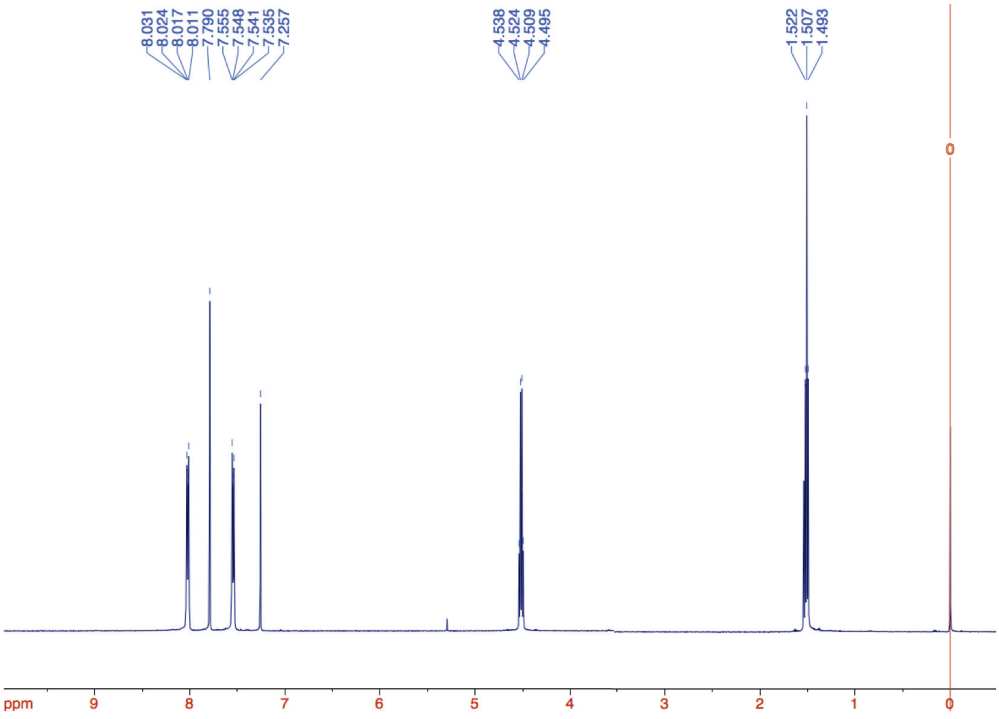

^{1}H NMR spectrum of compound **4.5** in $CDCl_3$.

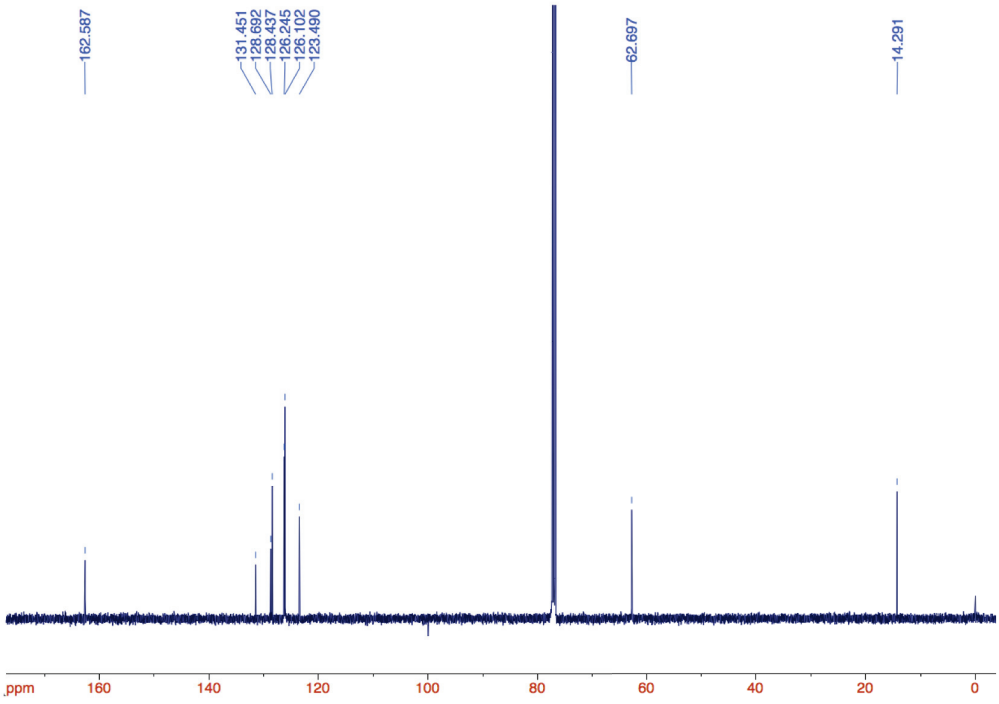

^{13}C NMR spectrum of compound **4.5** in $CDCl_3$.

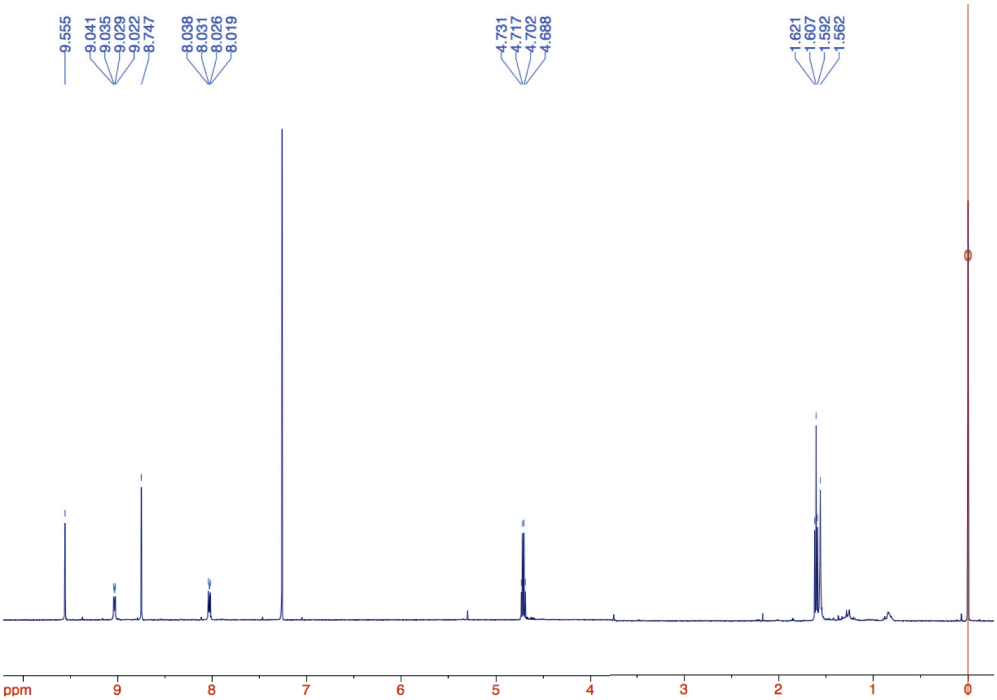

^{1}H NMR spectrum of compound **4.6** in $CDCl_3$.

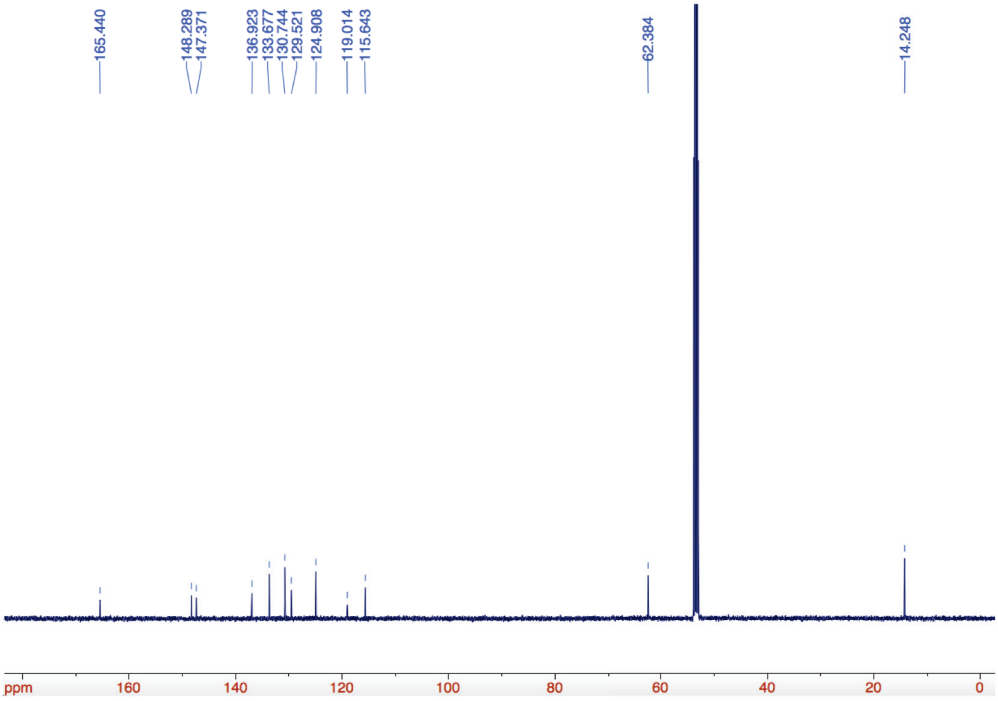

^{13}C NMR spectrum of compound **4.6** in $CDCl_3$.

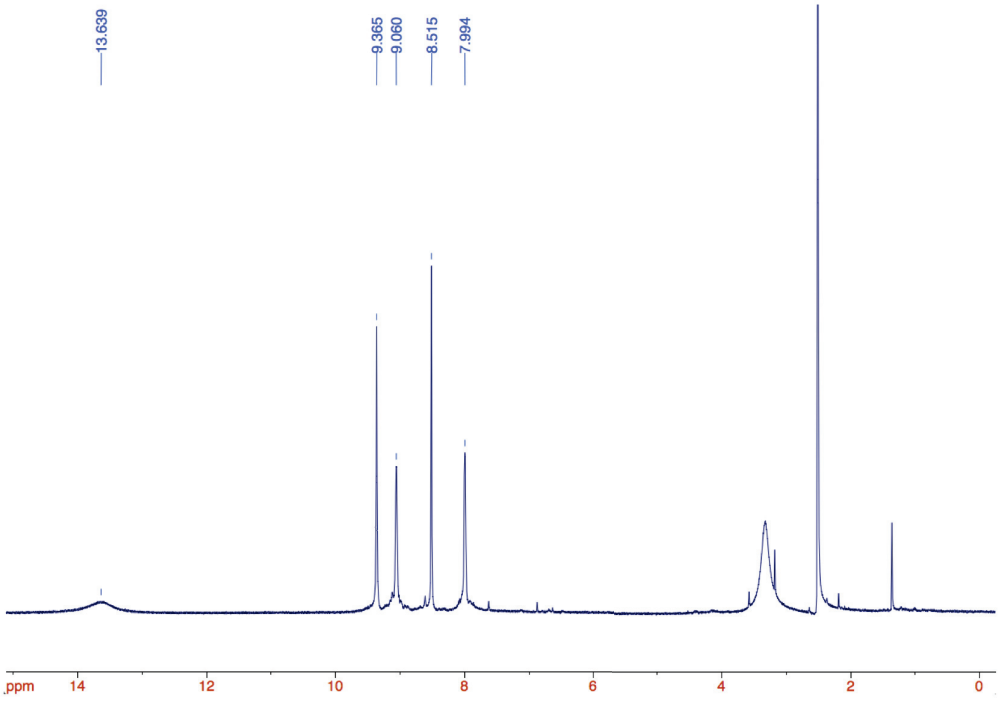

^{1}H NMR spectrum of compound **4.8** in $(CD_3)_2SO$.

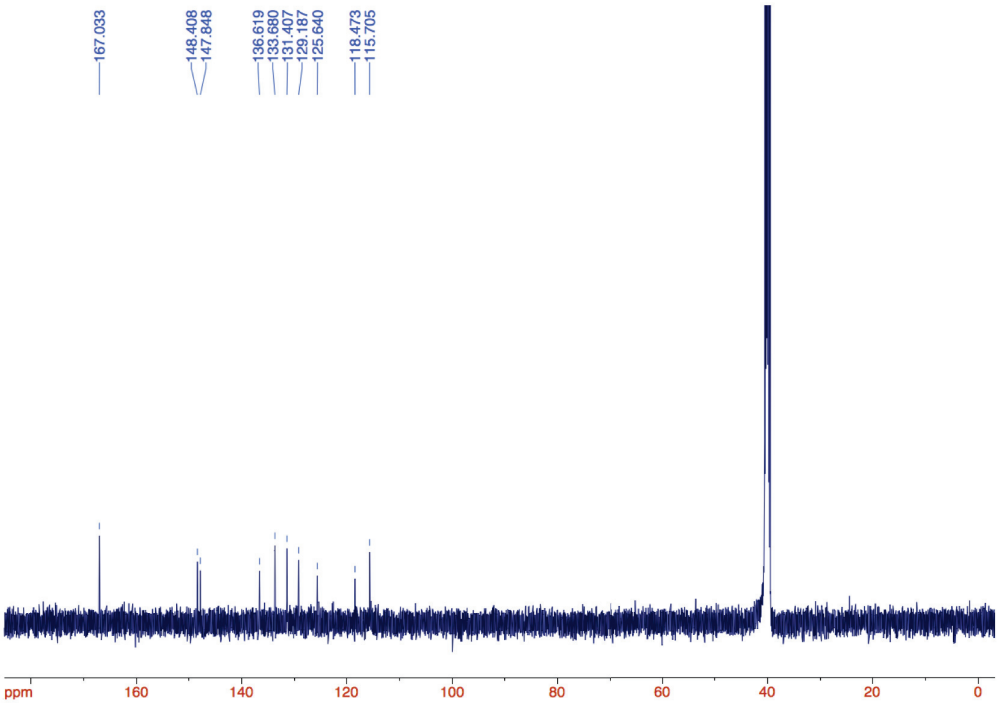

^{13}C NMR spectrum of compound **4.8** in $(CD_3)_2SO$.

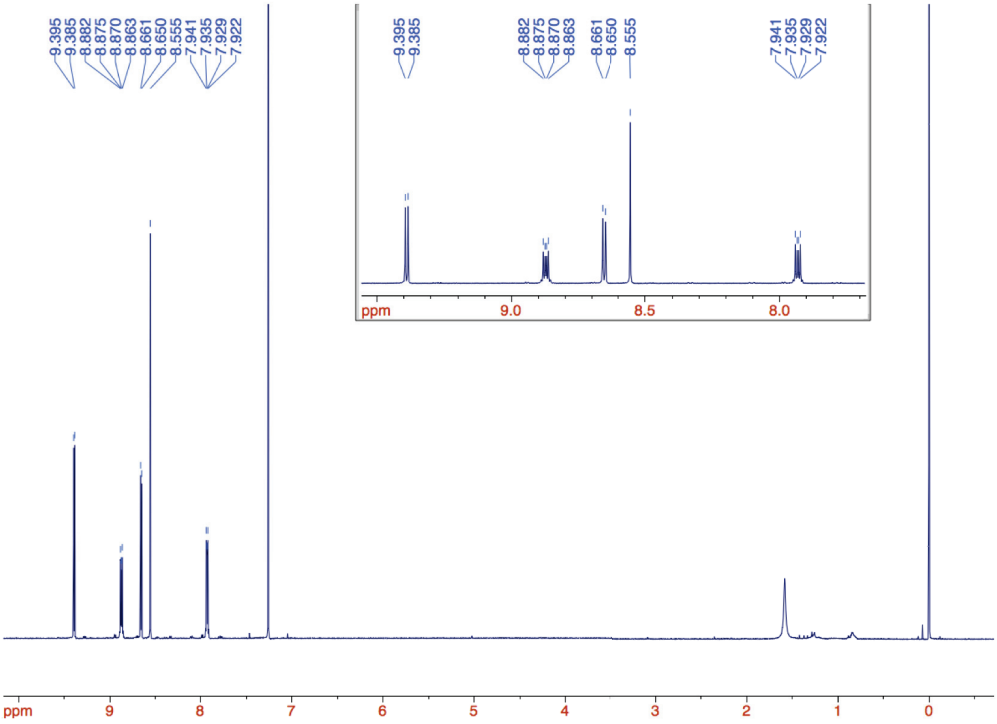

^{1}H NMR spectrum of compound **4.10** in $CDCl_3$.

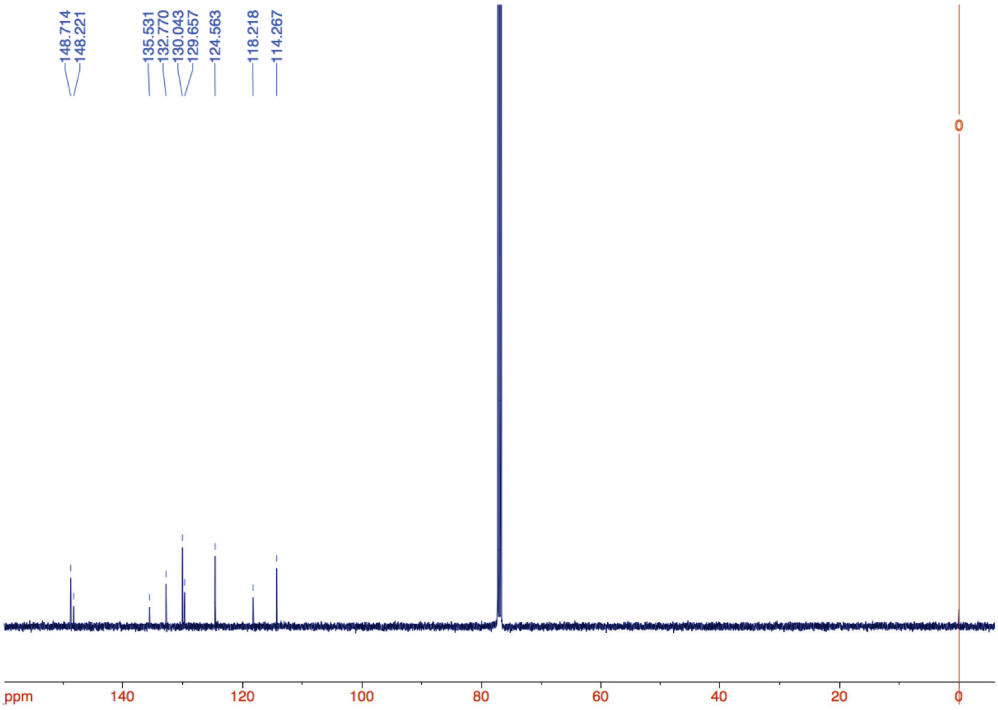

^{13}C NMR spectrum of compound **4.10** in $CDCl_3$.

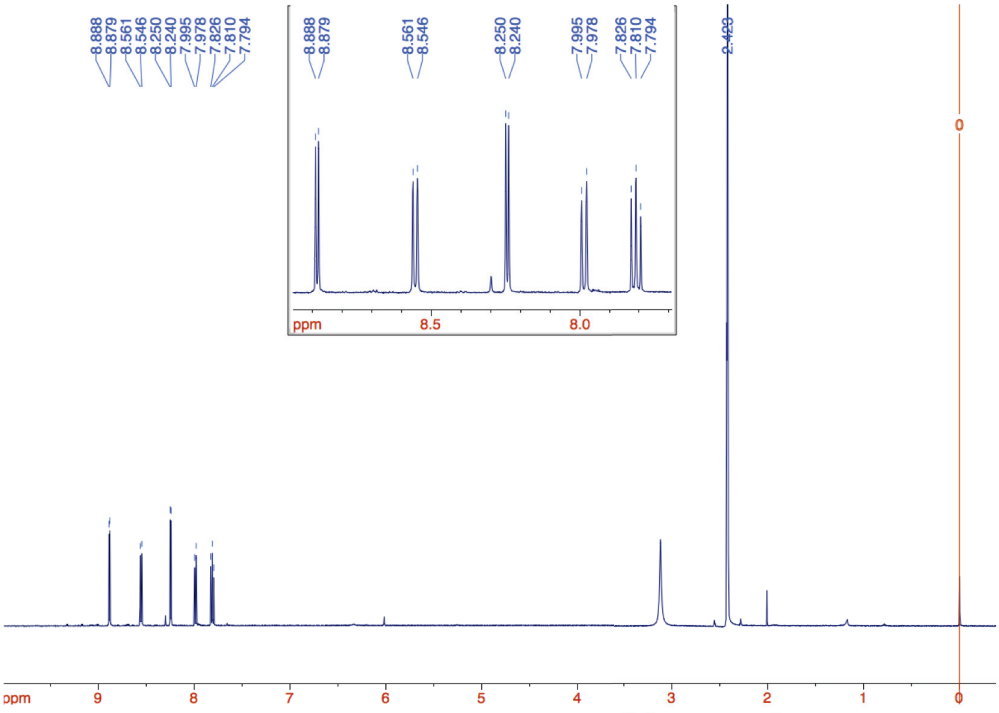

^{1}H NMR spectrum of compound **4.11** in $(CD_3)_2SO_3$ at 50 °C.

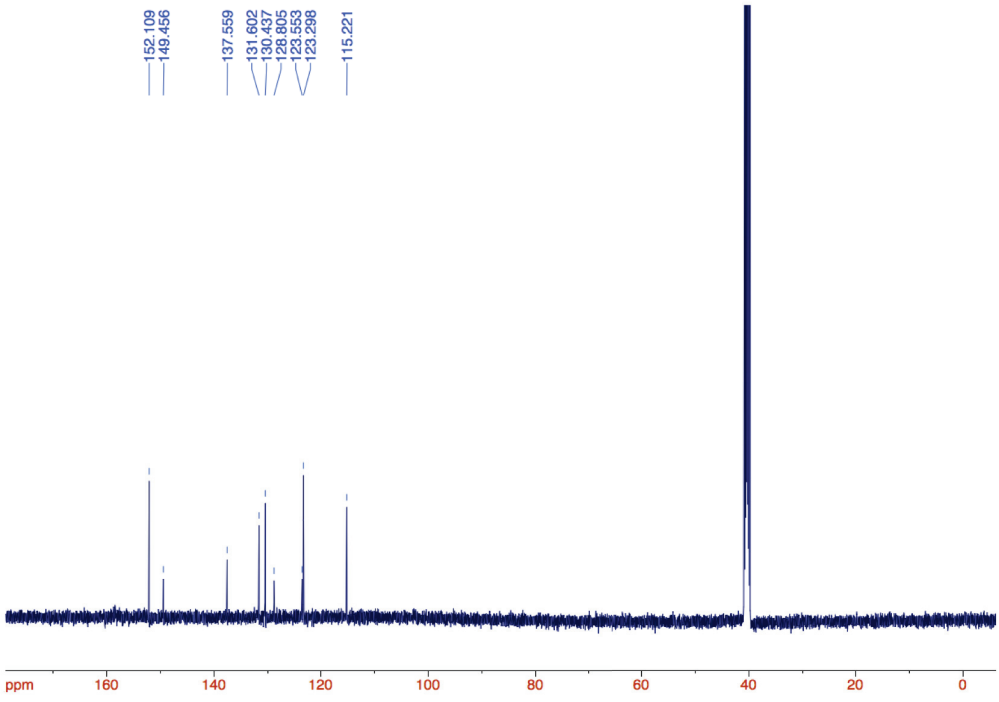

^{13}C NMR spectrum of compound **4.11** in $(CD_3)_2SO_3$ at 70 °C.

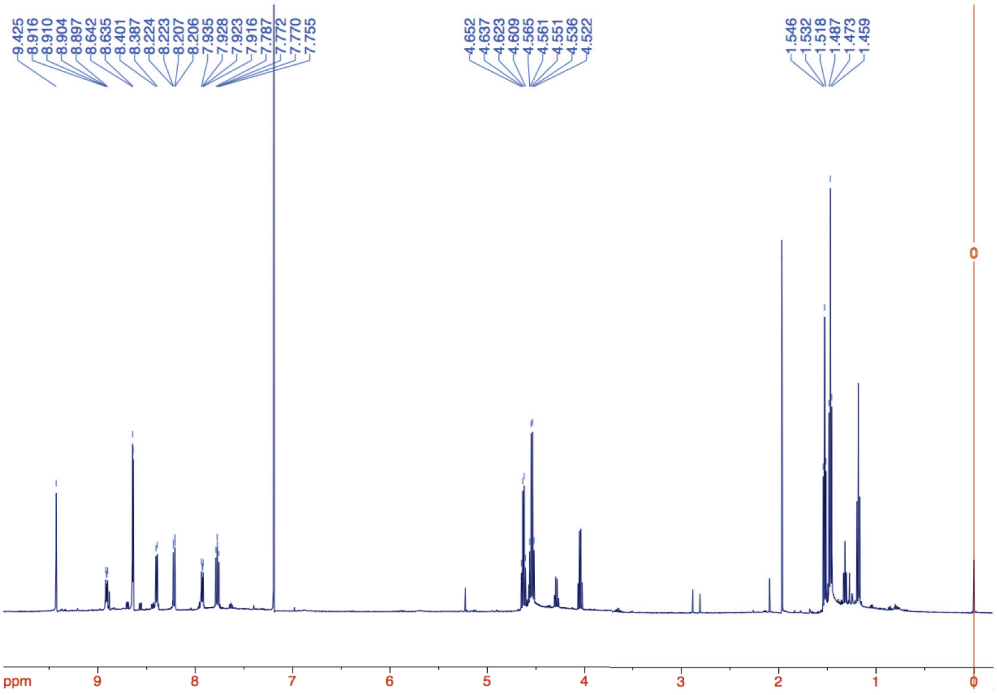

^{1}H NMR spectrum of crude compounds **4.6** and **4.7** in $CDCl_3$.

Anthracene-9,10-dicarbaldehyde (4.4)

In a dry flask, 2.5 M n-butyllithium in hexane (19 mL, 0.13 mol) was added dropwise to a solution of 9,10-dibromoanthracene (6.4 g, 19 mmol) in ether (250 mL) at –55 °C under a N_2 atmosphere. The addition complete the reaction stirred for 20 min at this temperature and was then warmed to 35 °C and stirred for 1 hr more. The reaction mixture was then cooled to –75 °C and DMF (6.0 mL, 78 mmol) was added. The reaction mixture was allowed to warm to room temperature, stirred overnight and was then quenched with water. A majority of the solvent was removed in vacuo and the product was precipitated with water. The product was filtered, rinsed with water and then purified by column chromatography using a gradient of 100% hexane to 100% chloroform to afford bright orange crystals (2.4 g, 54% yield). NMR data was in agreement with literature (*Tetrahedron Letters*, **2010**, *51*, 1161). ^{1}H NMR ($CDCl_3$, 500 MHz, 25°C) δ 11.51 (s, 2H), 8.77 (dd, J = 6.9, 3.3 Hz, 4H), 7.73 (dd, J = 6.9, 3.3 Hz, 4H). ^{13}CNMR ($CDCl_3$, 125 MHz, 25°C) δ 194.3, 131.8, 130.2, 128.4, 124.2.

4.5.3 Computational Data

Computational data for 4.6 (SCF total energy = – 1335.86041416 hartrees)

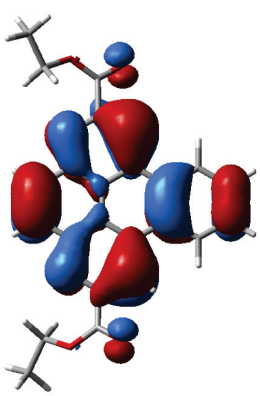

HOMO

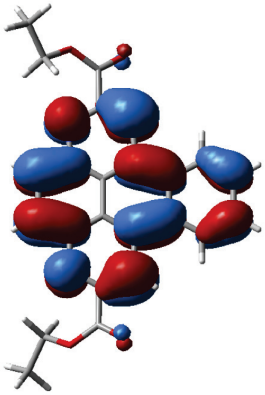

LUMO

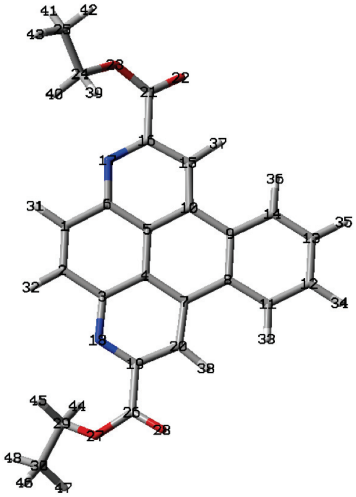

	Coordinates (Angstroms)		
Atom	X	Y	Z
1	0.355116	4.340952	-0.12501
2	0.355071	3.003521	0.125481
3	1.587289	2.274221	0.260092
4	2.822883	2.971544	0.132033
5	2.822931	4.372699	-0.13191
6	1.587383	5.070137	-0.2598
7	4.041362	2.255358	0.271962
8	5.312964	2.973243	0.134742
9	5.313012	4.37077	-0.13494

10	4.041459	5.088772	-0.272
11	6.547967	2.306575	0.263234
12	7.749045	2.98392	0.132543
13	7.749092	4.359866	-0.13304
14	6.54806	5.037323	-0.26359
15	3.937998	6.453721	-0.54235
16	2.673515	7.054846	-0.6342
17	1.522845	6.395281	-0.49779
18	1.522663	0.949082	0.498092
19	2.673288	0.289395	0.634311
20	3.937809	0.890418	0.542326
21	2.649412	8.525387	-0.99507
22	3.582597	9.013025	-1.5988
23	1.596208	9.300299	-0.68235
24	0.573762	8.966967	0.287952
25	-0.03262	10.2816	0.747372
26	2.649136	-1.18113	0.995279
27	1.596	-1.95614	0.682527
28	3.582227	-1.66868	1.599226
29	0.573759	-1.62321	-0.28813
30	-0.03237	-2.93804	-0.7473
31	-0.5672	4.90299	-0.23142
32	-0.56729	2.441571	0.232023
33	6.566333	1.242299	0.468618
34	8.687027	2.44637	0.236595
35	8.687111	4.897329	-0.23721
36	6.5665	6.101597	-0.46897
37	4.802166	7.08402	-0.70472
38	4.80194	0.260044	0.704595
39	1.01896	8.419612	1.124042
40	-0.16553	8.317818	-0.1845
41	-0.45633	10.82926	-0.10024
42	0.721624	10.91553	1.223954
43	-0.83359	10.08814	1.469883
44	1.019089	-1.07606	-1.12428
45	-0.16573	-0.974	0.18394
46	-0.45622	-3.4855	0.10037
47	0.722055	-3.57204	-1.22352
48	-0.83319	-2.74489	-1.47006

Computational data for 4.7 (SCF total energy = – -1335.85071464 hartrees)

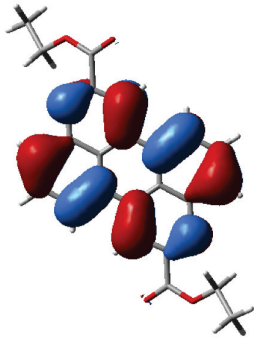

HOMO

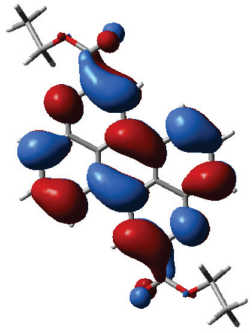

LUMO

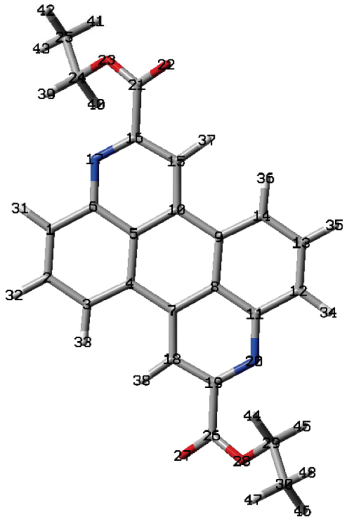

	Coordinates (Angstroms)		
Atom	X	Y	Z
1	-0.54369	5.89812	-1.88808
2	-1.18043	4.680904	-1.79265
3	-0.46009	3.521464	-1.44651
4	0.905833	3.56405	-1.19111
5	1.582661	4.818744	-1.28408
6	0.849075	5.993931	-1.63914
7	1.683983	2.369097	-0.82357
8	3.084294	2.498386	-0.56607
9	3.761106	3.753096	-0.65895
10	2.982988	4.948021	-1.02664
11	3.817881	1.323197	-0.21101
12	5.210616	1.41904	0.038097
13	5.847318	2.636289	-0.05715

14	5.126989	3.795722	-0.40333
15	3.534181	6.21449	-1.13305
16	2.725563	7.310447	-1.51028
17	1.431248	7.220034	-1.75694
18	1.132834	1.102586	-0.71741
19	1.941461	0.006623	-0.34022
20	3.235737	0.097068	-0.09337
21	3.400796	8.666644	-1.53625
22	4.394011	8.854531	-0.86422
23	2.905568	9.67895	-2.26817
24	1.924876	9.547037	-3.32651
25	2.071151	10.77579	-4.20711
26	1.266307	-1.34962	-0.31447
27	0.273507	-1.53766	-0.98706
28	1.760968	-2.36172	0.418133
29	2.741719	-2.22965	1.47641
30	2.595677	-3.45842	2.35701
31	-1.07481	6.806994	-2.15112
32	-2.24686	4.604697	-1.98357
33	-0.99739	2.581799	-1.38001
34	5.741742	0.510167	0.30114
35	6.913715	2.712528	0.133946
36	5.664256	4.735413	-0.46968
37	4.576179	6.415348	-0.9218
38	0.09087	0.901719	-0.92882
39	0.930582	9.477119	-2.88229
40	2.108414	8.627682	-3.89023
41	3.071867	10.8256	-4.64757
42	1.904456	11.68927	-3.62778
43	1.334316	10.74034	-5.01754
44	2.558047	-1.31032	2.040141
45	3.735967	-2.15957	1.032126
46	2.762549	-4.37188	1.77769
47	1.59497	-3.50842	2.797468
48	3.332507	-3.42282	3.167438

Computational data for 4.10 (SCF total energy = – -801.49470624 hartrees)

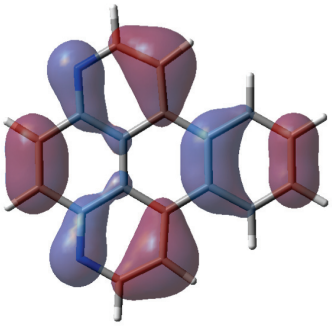

HOMO

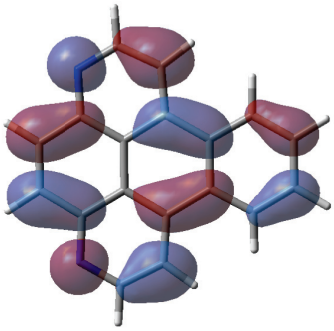

LUMO

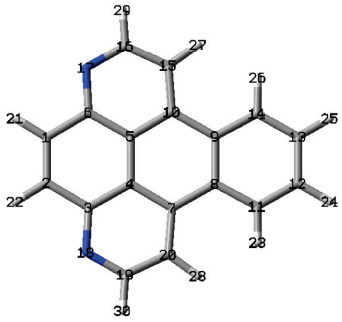

	Coordinates (Angstroms)		
Atom	X	Y	Z
1	0.360105	4.340085	-0.12981
2	0.360061	3.004383	0.130268
3	1.591057	2.274855	0.272459
4	2.827471	2.971258	0.136638
5	2.827518	4.372984	-0.1365
6	1.591149	5.0695	-0.27216
7	4.044994	2.254719	0.276678
8	5.316018	2.973495	0.136271
9	5.316065	4.370518	-0.13646
10	4.045088	5.08941	-0.2767
11	6.552973	2.309317	0.266157
12	7.754935	2.984262	0.134163
13	7.75498	4.359527	-0.13467
14	6.553063	5.034582	-0.26651
15	3.937815	6.45785	-0.54396
16	2.674087	7.045562	-0.65828
17	1.521173	6.392667	-0.53027
18	1.520992	0.951694	0.530578
19	2.673864	0.298693	0.65843
20	3.937631	0.886289	0.543951
21	-0.56076	4.904024	-0.23964
22	-0.56084	2.440528	0.240221
23	6.572254	1.24544	0.474655
24	8.692873	2.446443	0.239355
25	8.692954	4.89726	-0.23999
26	6.572414	6.098458	-0.47501
27	4.81356	7.084802	-0.66668
28	4.813334	0.259256	0.666554
29	2.597262	8.111749	-0.86658
30	2.596968	-0.76749	0.866742

Computational data for 4.11 (SCF total energy = – 801.4849891 hartrees)

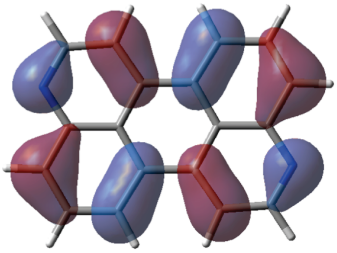

HOMO

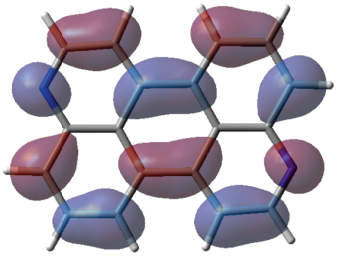

LUMO

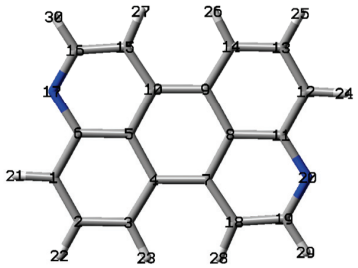

	Coordinates (Angstroms)		
Atom	X	Y	Z
1	-0.54084	5.903049	-1.88672
2	-1.17752	4.685184	-1.7998
3	-0.4582	3.524972	-1.45458
4	0.906223	3.566647	-1.19183
5	1.583091	4.823414	-1.27746
6	0.850078	6.001253	-1.62853
7	1.682894	2.369373	-0.82882
8	3.083865	2.49372	-0.57268
9	3.76073	3.75049	-0.65829
10	2.984066	4.947758	-1.02134
11	3.816879	1.315881	-0.22161
12	5.20779	1.414091	0.036616
13	5.844466	2.631962	-0.05027
14	5.125141	3.792173	-0.3955
15	3.533746	6.217544	-1.13391
16	2.719447	7.311662	-1.48666
17	1.425565	7.234165	-1.72986
18	1.133223	1.099579	-0.71629
19	1.947524	0.00546	-0.36355
20	3.241398	0.082962	-0.12031
21	-1.06854	6.813796	-2.15031
22	-2.2431	4.609249	-1.99728
23	-0.99635	2.584944	-1.39656
24	5.735493	0.503344	0.300214
25	6.910032	2.707903	0.147251
26	5.663286	4.732206	-0.45349
27	4.588213	6.396071	-0.95558
28	0.078763	0.921046	-0.89465
29	1.499438	-0.98424	-0.27939
30	3.16754	8.30135	-1.57086

Conclusions

5

The effect sulfur and nitrogen heteroatoms have on the properties of organic semiconductors has been examined through the synthesis and analysis of novel small molecules and polymers. Different structure-property relationships related to these heteroatoms were explored, from effects on energy levels, to supramolecular ordering, to pH sensitive optical properties.

While alkyl and alkoxy side chains are frequently used as substituents on conjugated polymers, examples of alkylsulfanyl side chain are scarce in the literature. We synthesized alkylsulfanyl-substituted thienothiophene vinylene polymers and fined-tuned the energy levels and band gaps of those polymers by oxidizing monomer side chains to electron withdrawing sulfoxyl and sulfonyl groups (Appendix, Chapter 2). The sulfonyl groups had a strong electron withdrawing effect compared to the modest effect of the sulfanyl groups. The sulfonyl groups also imparted greater disorder due to a lower rotation barrier, while sulfanyl substituted materials appeared more rigid. Copolymerization of alkylsulfanyl and alkylsulfonyl-substituted monomers yielded low band gap Donor-Acceptor polymers whose π–conjugated backbones are structurally homogeneous. While the polymers gave excellent open circuit voltages in PCBM bulk heterojunction solar cells, low short circuit currents limited efficiencies. AFM studies of the devices revealed large domains and very high surface roughness, suggesting charge transport was limited by the film's morphology. Single-crystal analysis of model dimers confirmed that alkylsulfanyl chains lie orthogonal to the conjugated backbone and inhibit π–π overlap between thienothiophene units. While this was likely detrimental for charge carrier mobility, fewer π–π interactions led to enhanced fluorescence compared to thiophene vinylene polymers with simple alkyl chains. Elucidating the electronic and structural effects of alkylsulfanyl and alkylsulfonyl substituents, has led to their subsequent use in new polymeric OSCs.

As we learned in Chapter 2, supramolecular ordering in the solid-state is critical to charge transport, yet discussions of structure-property relationships are usually limited to the

specific molecule being studied. To compare packing motifs in the absence of molecular structure effects, we studied two polymorphs of thienothiophene-thiazolothiazole trimers by measuring their charge transport properties in single-crystal field effect transistors. The polymorph with the stronger electronic coupling between cofacial molecules showed no charge transport, however, due to its slipped π–stacks being isolated into groups of tetramers. The second polymorph had weaker electronic couplings between molecules, but formed infinite π–stacks in a herringbone motif with S···S contacts in multiple directions, and therefore did display transistor properties. In both polymorphs only short S···S distances were observed, while the thiazolo nitrogen heteroatom appeared to have little influence on the solid-state packing of the molecule.

With the discovery of new nitrogen-containing polycyclic aromatic materials as our objective, we repurposed the Hemetsberger indolization reaction to synthesize fused pyridines. We found that an extended π–conjugated core allowed for the rare visible-light activation of vinyl azides without the use of a metal photocatalyst or a photoredox catalyst. Through high yielding photochemistry we synthesized diazabenzo[e]pyrene and diazaperylene. The insertion of nitrogen-heteroatoms proved an effective way to lower the energy levels of the PAH parent compounds. Both diazabenzo[e]pyrene and diazaperylene, as well as their protonated forms, retain the fluorescent properties of their respective PAH analogues, while introducing pH sensitive shifts in emission wavelengths.

Overall, this dissertation presents several novel organic semiconductors. The observed structure-property relationships of these materials is explained through the lens of heteroatom effects, thereby bettering our understanding of design strategies based on heteroatom incorporation. This has led to further progress in the synthesis of OSCs for high performance devices.

5.1 Future Work

Since our publication of Chapter 2, several polymers demonstrating high efficiencies in solar cells have been synthesized with alkylsulfanyl side chains.[1,2,3,4] In these examples the alkylsulfanyl substituent is placed away from the backbone of the polymer through the use of a thienyl or thioester group. This removed placement of the sulfanyl group may aid the materials' supramolecular assembly since, as we discovered, alkylsulfanyl chains have a propensity to lie orthogonal to the conjugated core, disrupting π-π stacking. This may not be the case, however, with longer linear chains that form lamellar structures through van der Waals interactions. Alkylsulfanyl substituents are readily introduced from thiols or disulfides onto halogenated aromatics and large variety of thiols are commercially available. This offers us the possibility of examining a series of substituents and comparing their dihedral angles (as –SR and $–SO_2R$). By studying crystalline small molecules, like substituted anthracenes for example, the effect of these substituents on supramolecular ordering, especially π-π distances, will be better understood. These findings will allow us to select appropriate side chains to alter the crystallinity or emissivity of conjugated polymers.

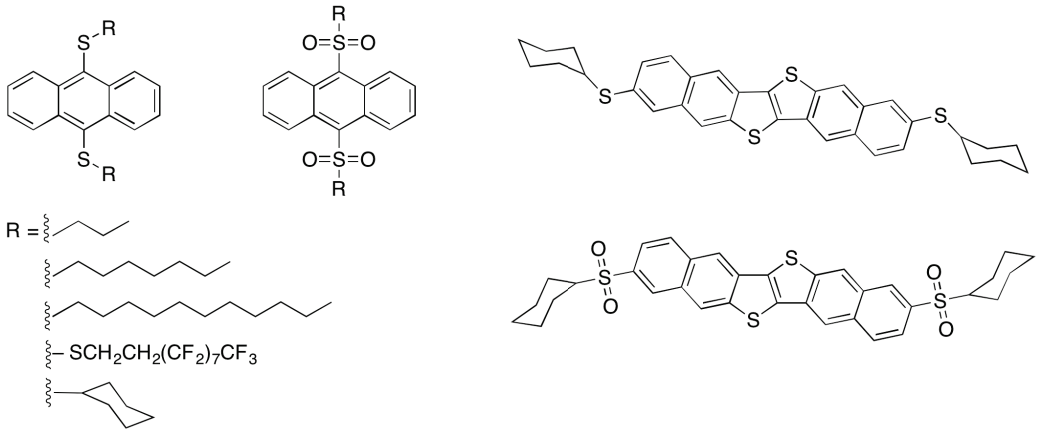

[1]Cui, C.; Wong, W.-Y.; Li, Y. *Energy Environ Sci.*, **2014**, *7*, 2276
[2]Ouyang, D.; Xiao, M.; Zhu, D.; Zhu, W.; Du, Z.; Wang, N.; Zhou, Y.; Bao, X.; Yang, R. *Polym. Chem.*, **2015**, *6*, 55
[3]Zhu, D.; Sun, L.; Bao, X.; Wen, S.; Han, L.; Gu, C.; Guo, J.; Yang, *R. RSC Adv.*, **2015**, *5*, 62336
[4]Zhu, D.; Sun, L.; Liu, Q.; Wen, S.; Han, L.; Bao, X.; Yang, R. *Macromol. Rapid. Commun.*, **2015**, *36*, 2065

Two thiols are especially interesting as possible substituents: semifluoroalkyl thiol and cyclohexyl thiol. Though fluoroalkyl substitutents have limited solubility they are often used as electron withdrawing groups to lower the energy levels of materials for n-channel transport. Fluroalkyl sulfanyl groups have not yet been studied in OSC and the possibility of further lowering HOMO/LUMO levels via oxidation to fluroalkyl sulfonyl is particularly interesting.

A second substituent of interest that has gone underutilized in organic electronics is the cyclohexyl group. Often seen in glassy polymers, cyclohexyl groups have a transition from their "chair" to "boat" conformation that grants the material molecular motion. Bao demonstrated that small molecule OSCs with cyclohexyl side chains exhibited vastly different film morphologies dependent on substrate temperature, while also being more soluble than hexyl-substituted versions of the same molecule.[5] By functionalizing small molecule OSCs with cyclohexylsulfanyl and cyclohexylsulfonyl groups, the electronic properties of the molecules could be tuned while exploring possible liquid crystalline behavior and changes in film morphologies. This could lead to high performance devices by means of controlling the crystallinity of thin films of OSCs with high mobilities, such as dinaphtothienothiophene.

The use of –SR and $–SO_2R$ substituents in the formation of donor-acceptor polymers was successfully demonstrated in Chapter 2, but in a random copolymer. The difference in the reactivity of the monomers causes uncertainty in the backbone structure of the polymer. By copolymerizing bromo- and stanyl-monomer units the alternating nature of the polymer would be guaranteed, which is expected to increase D—A interactions. This requires removing the vinylene spacer that reduced steric repulsions between the monomers. An attractive alternative is a benzodithiophene homopolymer where substituents do not contribute to the sterics between monomer units. Recently bulk heterojuction solar cells made with homopolymers of benzodithiophene were reported with efficiencies up to 6%.[6] By utilizing sulfanyl and sulfonyl substituents, new copolymers could be synthesized that would benefit

[5]Locklin, J.; Li, D.; Mannsfeld, S. C. B.; Borkent, E.-J.; Meng, H.; Advincula, R.; Bao, Z. *Chem. Mater.* **2005**, *17*, 3366
[6]Kang, T. E.; Kim, T.; Wang, C.; Yoo, S.; Kim, B. J. *Chem. Mater.* **2015**, *27*, 2653

from both the low band gap of a donor-acceptor polymer and the crystalline behavior of a homopolymer.

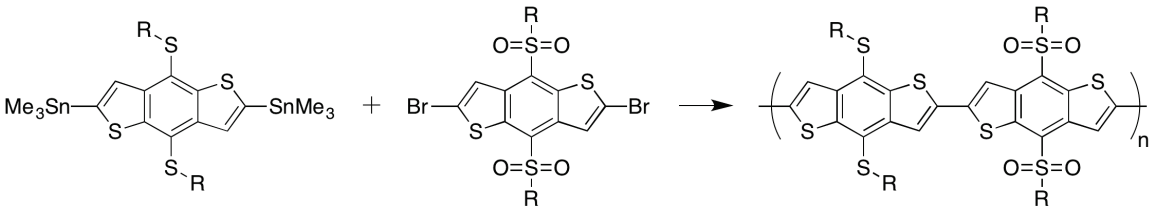

In Chapter 4 we demonstrated the visible-light activation of vinyl azides bound to an extended π-conjugated system. The scope of this reaction and its tolerance to functional group on the π-conjugated core should be explored. Electron donating and electron withdrawing substituents could potentially alter the regioselectivity of the reaction. Visible-light activation should also be applicable to the synthesis of indoles. Preliminary experiments showed that cyclization does occur in **A.17** (Figure A.7) under illumination, though a mixture of products was observed. Successful cyclization would yield benzodipyrrole, a nitrogen-analogue of benzodithiophene, a very popular building block in OSCs.

The regioselectivity of the cyclization can also be controlled by blocking certain positions with a heteroatom. For example a 1,5-diazaanthracene precursor would yield a perylene-like structure, with no possibility of forming benzopyrene. The same approach could also be used to access smaller structures such as 1,4,6,9-tetraazapyrene from a 2,6-naphthyridine precursor, though there is the risk of N–N bond formation, as observed in the synthesis of azaindoles via the thermolyis of vinyl azides.[7] Derivatives of 1,3,6,8-tetraazapyrenes have been previously reported to be strongly fluorescent and promising building blocks for n-type OSCs, while fused pyrazoles have yet to be studied for organic electronics.

[7] Roy, P. J.; Dufresne, C.; Lachance, N.; Leclerc, J. P.; Boisvert, M.; Wang, Z.; Leblanc, Y. *Synthesis*, **2005**, *16*, 2751

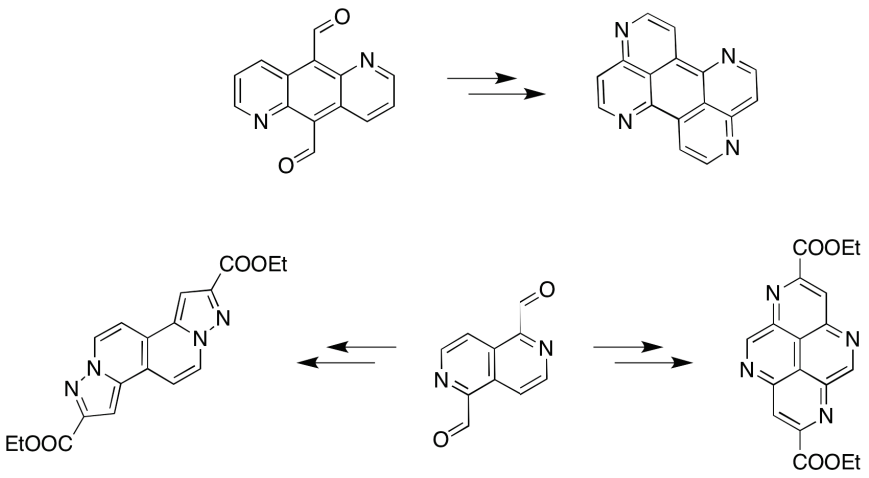

Finally, while the Hemetsberger reaction has been shown to form 5- and 6-membered rings, the formation of 7-membered rings by this method has yet to be studied. Recently Miao reported the first PAH OSCs containing 7-membered rings.[8] Their excellent charge transport properties demonstrated that heptagon- embedded PAHs are promising candidates for organic electronic materials. Starting from benzene trimers, shown below, the synthetic strategies from Chapter 4 could be used to achieve novel azepine-containing structures. The final structure is formally antiaromatic and benefits from a small band gap (2.0 eV), all the while being stabilized by its extended conjugation (HOMO = –4.7 eV, R = CH_3). These planar structures would be likely candidates for organic electronic materials and would represent the first azepine-containing small molecule OSCs.

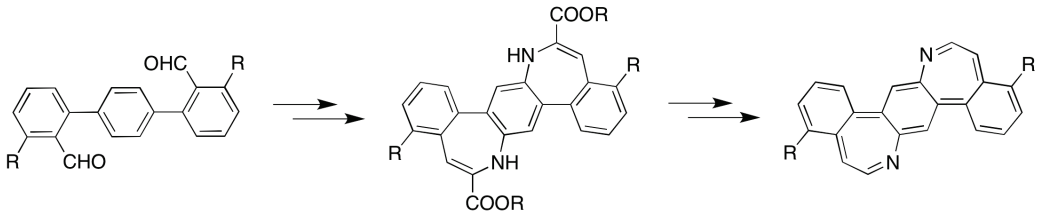

[8]Yang, X.; Liu, D.; Miao, Q. *Angew. Chem. Int. Ed.* **2014**, *53*, 6786

Appendix

A

A.1 Nonathio[9]circulene

Octathio[8]circulene, nicknamed Sulflower, is a circulene comprised of fused thiophene rings containing no hydrogen atoms.[1] The packing motif of the structure features several close S...S contacts. Octathio[8]circulene and nonathio[9]circulene were calculated to exist at a strain energy minimum and therefore be planar–the only two planar structures of the thiocirulene series. This project was an attempt to synthesize unreported nonathio[9]circulene (Scheme A.1). Thieno[2,3-*b*]thiophene was synthesized with the help of Violetta Toader, halogenated and coupled into dimers via an Ullmann-type nickel catalyzed reaction. We were unable to form cyclic tri-thieno[2,3-b]thiophene, however, owing to a high degree of cyclic strain which we calculated to be 39 Kcal/mol. By comparison, cyclic tetra-thiophene, the intermediate to Sulflower, has a calculated ring strain of only 4 Kcal/mol.

Scheme A.1: Synthetic Route to Nonacirculene.

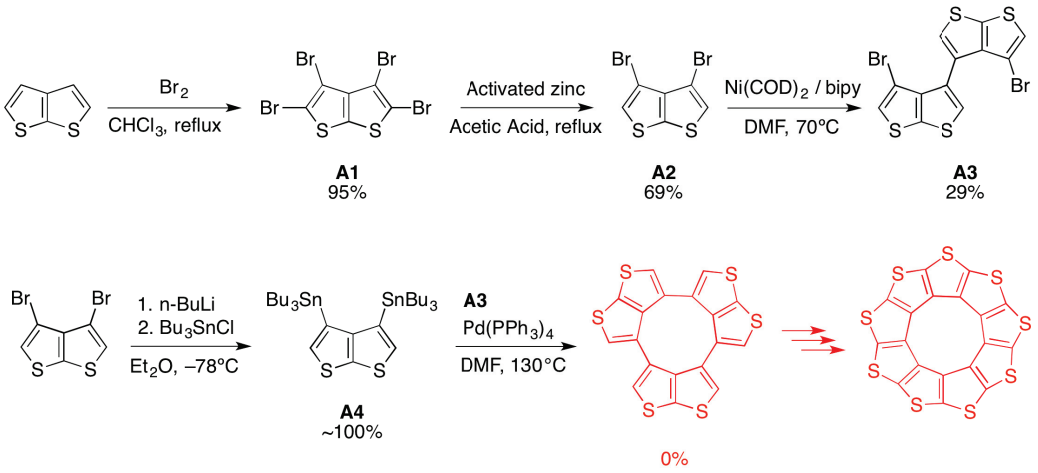

Tetrabromothieno[2,3-*b*]thiophene A1

Bromine (5.5 mL, 107 mmol) was added to a 0°C solution of thieno[2,3-*b*]thiophene (1.86 g, 13.3 mmol) in $CHCl_3$ (200 mL). The reaction was refluxed for 5 days and then quenched with 10% Na_2SO_3 solution (125 mL). The organics were extracted into $CHCl_3$ (50 mL) and washed with $NaHCO_3$ (150 mL). The solvent was removed in vacuo to yield **A1** in quantitative yields as a fluffy yellow powder. FTIR confirmed the disappearance of aromatic hydrogens.

3,4-Dibromothieno[2,3-*b*]thiophene A2

Freshly activated zinc (2 minutes in 10% HCl)(0.454 g, 6.94 mmol) was added to a stirring solution of tetrabromothieno[2,3-*b*]thiophene **A1** (0.871 g, 1.91 mmol) in acetic acid (10

mL). The reaction mixture was refluxed for 4 hours, then cooled and diluted with H_2O (70 mL). The aqueous mixture was kept in the cold room overnight and the resultant yellow precipitate was filtered an washed with H_2O to afford **A2** in quantitative yields. The solids can be further purified by recrystallization from hot hexane (0.393 g, 69% yield). ^{1}HNMR ($CDCl_3$, 400 MHz): δ 7.32 (s, 2H).

4,4′-Dibromo-3,3′-bithieno[2,3-*b*]thiophene A3
Bis(cyclooctadiene)nickel(0) (0.299 g, 1.09 mmol), 1,5-cyclooctadiene (0.14 mL, 1.1 mmol) and dimethylformamide (1 mL) were loaded into a 50 mL schlenk tube and degassed by freeze-pump-thaw. 2,2′-bipyridine (0.184 g, 1.18 mmol) was added and the reaction stirred at room temperature until a deep violet color was achieved (10 min). **A2** (0.294 g, 0.985 mmol) was added and the mixture was heated to 77°C and stirred for a week. The reaction mixture was cooled to room temperature, 5% HCl (5 mL) was added, and the mixture stirred for 5 minutes. The mixture was then diluted with H_2O (15 mL), extracted into $CHCl_3$ (3 × 10 mL), dried over Na_2SO_4, concentrated in vacuo, and passed through a silica plug washing with $CHCl_3$. The solvent was removed in vacuo and the resultant brown oil was dissolved in a minimum of DCM (1 mL). The product was crashed out with hexanes to afford **A3** (0.063 g, 29% yield) as a fine tan powder. ^{1}HNMR ($CDCl_3$, 400 MHz): δ 7.38 (s, 2H), 7.31 (s, 2H).

3,4-Bis(tributylstannyl)thieno[2,3-*b*]thiophene A4
n-Butyllithium (0.60 mL, 1.5 mmol) was added to a stirring solution of **A2** (0.199 g, 0.668 mmol) in dry diethyl ether (5 mL) at −75°C and the reaction mixture was stirred for 1 hour. Tributyltin (0.40 mL, 1.5 mmol) was added and the reaction was allowed to warm to room temperature. After stirring overnight the reaction was quenched with H_2O (25 mL), extracted into $CHCl_3$ (2 × 15 mL), dried over Na_2SO_4, and concentrated in vacuo to yield crude **A4** as a yellow oil in quantitative yields. ^{1}HNMR ($CDCl_3$, 400 MHz): δ 7.31 (s, 2H), and several aliphatic signals due to excess tributyltin.

A.2 Poly(thiophenevinylene)s with Alkylsulfanyl, Alkylsulfoxide, and Alkylsulfonyl Substituents

Concurrently to the work presented in Chapter 2, we also explored the effect of oxidation of the alkylsulfanyl substituents on poly(thiophenevinylene)s. Poly(thiophenevinylene) with alkylsulfanyl substituents had previously been reported, but the controlled oxidation of the substituent had not.[2] To this end we synthesized the polymers **S-PTV**, **SO-PTV**, and **SO_2-PTV** via Stille polycondensations with (E)-1,2-bis(tributylstannyl)ethene (Scheme A.2). The trends in the optical properties were consistent with those reported in Chapter 2 for poly(thienothiophenevinylenes) (Figure A.1). Only **SO_2-PTV** was emissive with a PLQY of 16%.

Scheme A.2: Synthesis of monomers and polymerization reactions of poly(thiophenevinylene)s.

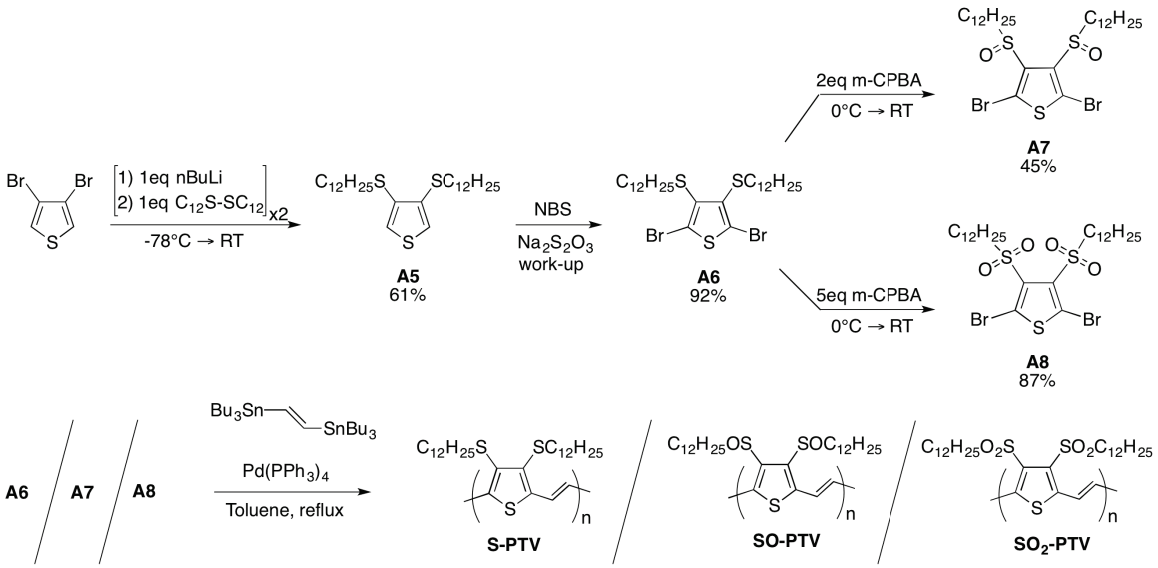

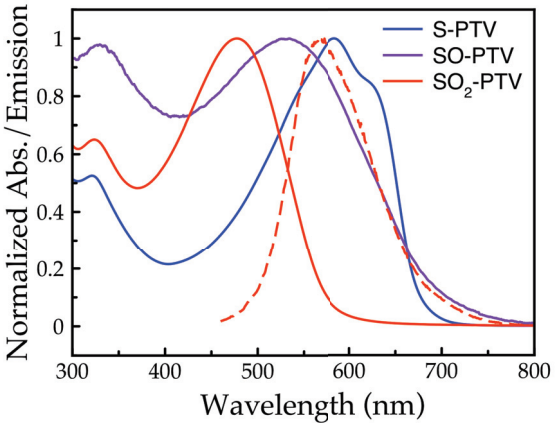

Fig. A.1.: Absorption (—) and emission (- -) spectra of **S-PTV**, **SO-PTV** and **SO_2-PTV** in chloroform solutions.

3,4-bis(dodecylthio)thiophene A5

n-BuLi (1.4 mL, 3.5 mmol) was added at −75°C to a stirring solution of 3,4-dibromothiophene (0.842 g, 3.48 mmol) in diethyl ether (60 mL) and the reaction mixture stirred for 1 h. Didodecyldisulfide (1.40 g, 3.48 mmol) was added and the reaction was allowed to warm to room temperature overnight. The next day the reaction mixture was cooled back to −75°C and a second dose of n-BuLi added. After an hour, didodecyldisulfide was added and the reaction was allowed to warm to room temperature and stirred overnight a second time. The reaction was then quenched with H_2O (20 mL), the organics were washed with NH_4Cl solution (50 mL), H_2O (2 × 50 mL), then dried over Na_2SO_4, and concentrated in vacuo. The crude oil was distilled in a Kugelrohr apparatus (160°C, 0.16 bar) to yield **A5** (1.03 g,

61% yield) as a yellow oil. ^{1}HNMR ($CDCl_3$, 400 MHz): δ 7.08 (s, 2H), 2.86 (t, *J* = 7.6 Hz, 4H), 1.64 (p, *J* = 7.6 Hz, 4H), 1.41 (m, 4H), 1.25 (m, 32H), 0.88 (t, *J* = 6.8 Hz, 6H). ^{13}CNMR ($CDCl_3$, 75 MHz): δ 133.9, 122.9, 34.4, 31.9, 29.7, 29.64, 29.60, 29.5, 29.4, 29.2, 29.0, 28.8, 22.7, 14.1.

2,5-Dibromo-3,4-bis(dodecylthio)thiophene A6

3,4-bis(dodecylthio)thiophene **A5** (0.243 g, 0.502 mmol) was dissolved in $CHCl_3$ (2.5 mL) and acetic acid (2.5 mL) and cooled to −20°C. NBS (0.200 g, 1.12 mmol) was added and the reaction warmed slowly to room temperature protected from light with foil. After being stirred for 24 h, the reaction was treated with saturated $Na_2S_2O_3$ solution (5 mL). The reaction mixture was then diluted with H_2O and extracted with $CHCl_3$ (2 × 30 mL). The solvent was removed in vacuo and the resulting product was passed through a silica plug with hexane. The product was further purified by column chromatography (100% hexane) to yield **A6** (0.173 g, 54% yield) as a white solid. ^{1}HNMR ($CDCl_3$, 400 MHz): δ 2.85 (t, *J* = 7.2 Hz, 4H), 1.52 (p, *J* = 7.2 Hz, 4H), 1.25 (s, 36H), 0.88 (t, *J* = 6.6 Hz, 6H). ^{13}CNMR ($CDCl_3$, 75 MHz): δ 136.3, 117.9, 36.0, 31.9, 29.7, 29.64, 29.60, 29.5, 29.4, 29.2, 29.1, 28.6, 22.7, 14.1.

2,5-Dibromo-3,4-bis(dodecylsulfinyl)thiophene A7

m-CPBA (37.0 mg, 0.214 mmol) was added to a stirring solution of **A6** (68.3 mg, 0.106 mmol) in $CHCl_3$ (2 mL) at 0°C under inert atmosphere. The reaction was allowed to warm to room temperature and stirred overnight. The reaction was quenched with 0.1 M NaOH (20 ml) and extracted with $CHCl_3$, dried over Na_2SO_4, and concentrated in vacuo to afford a yellow oil. The product was purified by column chromatography (4:1 hexane/ethyl acetate eluent mixture) to afford **A7** (32.2 mg, 45% yield) as a white crystalline solid. ^{1}HNMR ($CDCl_3$, 300 MHz): δ 3.67 (ddd, *J* = 12.7, 9.2, 5.4 Hz, 1H), 3.39 (ddd, *J* = 12.7, 9.4, 5.5 Hz, 1H), 3.33 (ddd, *J* = 12.7, 9.4, 6.6 Hz, 1H), 3.18 (ddd, *J* = 12.7, 9.6, 6.7 Hz, 1H), 1.77 (m, 4H), 1.45 (m, 4H), 1.24 (m, 32H), 0.87 (t, *J* = 6.5 Hz, 6H). ^{13}CNMR ($CDCl_3$, 75 MHz): δ 141.4, 139.8, 116.8, 115.1, 54.6, 54.4, 31.9 29.6, 29.5, 29.3, 29.2, 29.2, 28.6, 28.6, 23.4, 22.7, 14.1. HR-MS (ESI) *m/z* = 673.1396 [M+1] (calcd. for $C_{28}H_{51}Br_2O_2S_3$: *m/z* = 673.1412).

2,5-Dibromo-3,4-bis(dodecylsulfonyl)thiophene A8

Same procedure as **A7**, but with 5 equivalents of m-CPBA. (87% yield) ^{1}HNMR ($CDCl_3$, 400 MHz): δ 3.57 (t, *J* = 8.4 Hz, 4H), 1.85 (m, 4H), 1.43 (m, 4H), 1.25 (m, 32H), 0.88 (t, *J* = 7.2 Hz, 6H).

All polymerization were carried out as described in Chapter 2.

A.3 Ladder Polymers

In 2007, Takimiya's group reported the synthesis of dinaphthohtienothiophene (DNTT) via the iodine mediated cyclization of two methylsulfanyl substituents and vinylene.[3] Our **S-PTV** and **S-PTTV** polymers contain these same features, so we suspected a similar cyclization reaction could be possible, generating ladder polythiophene (**LPT**) (Scheme A.3). **LPT** was prepared on glass slides from spin-coated samples of polymers by exposing the slides to iodine vapors at 120°C (Figure A.2). Samples of LPT were also prepared with iodine in acetic acid solutions under pressure at 130°C. Samples were treated with hydrazine to reduce the iodine doped **LPT**.

Scheme A.3: The reported synthesis of DNTT. Below is the proposed synthesis of LPT from **S-PTV** and **S-PTTV** polymers.

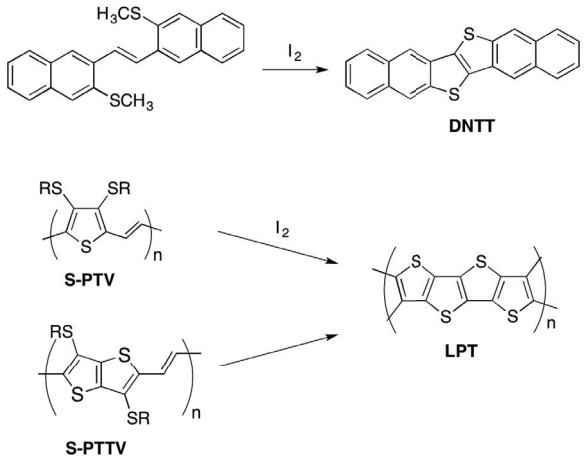

From the absorption spectra of the iodine treated films (Figure A.2) we see a significant blue-shift vs the untreated polymer films (Day 0) consistent with theoretical calculations predicting a band gap of 2.20 eV for **LPT**. Treatment with hydrazine causes a red-shift and the disappearance of a charge transfer band at 950 nm. Experiments on films of **S-PTTV** gave identical results. Unfortunately XPS measurements did not show the desired 2:1 carbon atom to sulfur atom ratio for the fully cyclized ladder polymer. Instead the ratio increased from 7:1 to 16:1. An increase in oxygen was also observed. From these results, we concluded that while some cyclization may be occurring, yielding an insoluble product, a majority of alkyl chains must still be present.

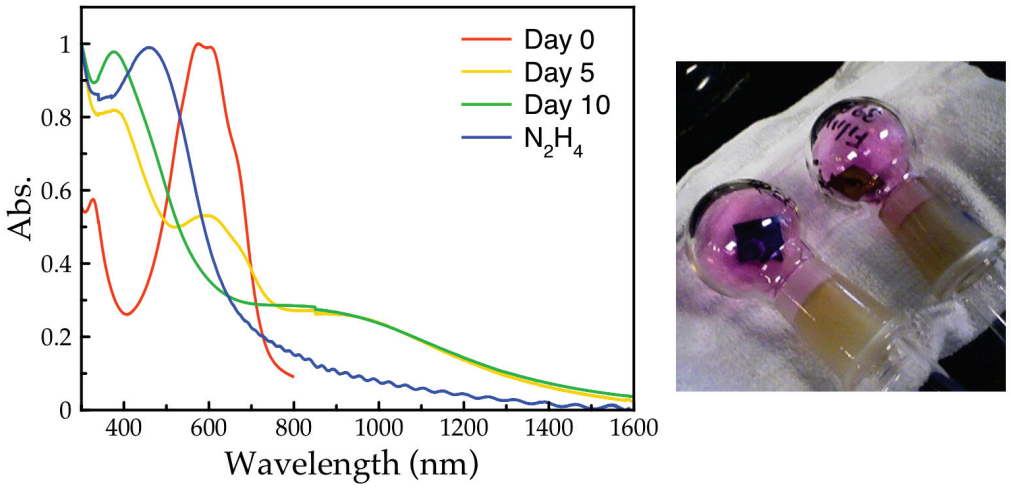

Fig. A.2.: Absorption spectra of a **S-PTV** film exposed to iodine vapors for several days and the film after after treatment with hydrazine. On the right is a picture of films in iodine chambers.

A.4 Pyrrolopyrrole

As a means to compare sulfur and nitrogen heteroatoms in conjugated polymers, we synthesized the nitrogen analogue of thienothiophene: pyrrolopyrrole (Scheme A.4). The pyrrole nitrogen on **A9** must be protected for the cyclization to proceed.[4] We found that the protecting group and pyrolle hydrogen could subsequently be replaced with alkyl groups in one step, though **A12** appeared less stable than **A11**. The goal of the project was to form a pyrrole-based semiconductive polymer, but was abandoned before polymers were made. We hoped to form pyrrolopyrrole vinylene monomers via McMurray coupling, but tests with pyrrole-2-carboxaldehydes gave impure polymerized material. Therefore we did not attempt to remove the ester substituent of **A12**. Another approach for this project in the future is the possible electropolymerization of 1,4-dihexylpyrrolo[3,2-*b*]pyrrole.

Methyl (Z)-2-azido-3-(1H-pyrrol-2-yl)acrylate A9
Into anhydrous methanol (6 mL) cooled to −20°C, was added solid sodium (0.345 g, 19.6 mmol). The reaction was stirred till all the sodium dissolved. 2-Pyrrolecarboxaldehyde (0.584 g, 6.14 mmol) was combined with methyl 2-azidoacetate (1.92 g, 16.7 mmol), then slowly added to the cold reaction via a syringe pump (0.05 mL/min). The reaction was kept at −20°C and stirred overnight. The reaction mixture was then poured into ice-cold water and extracted with diethyl ether. The solvent was removed in vacuo without warming and the resultant oil was purified by column chromatography using a gradient of 100% hexane to 20% ethyl acetate to afford **A9** (0.481 g, 41% yield) as a dark oil. ^{1}HNMR (acetone-d_6, 400 MHz) δ 7.06 (br, 1H), 6.90 (s, 1H), 6.63 (br, 1H), 6.23 (m, 1H), 3.84 (s, 3H).

Scheme A.4: Synthesis of pyrrolopyrrole and functionalization with alkyl groups.

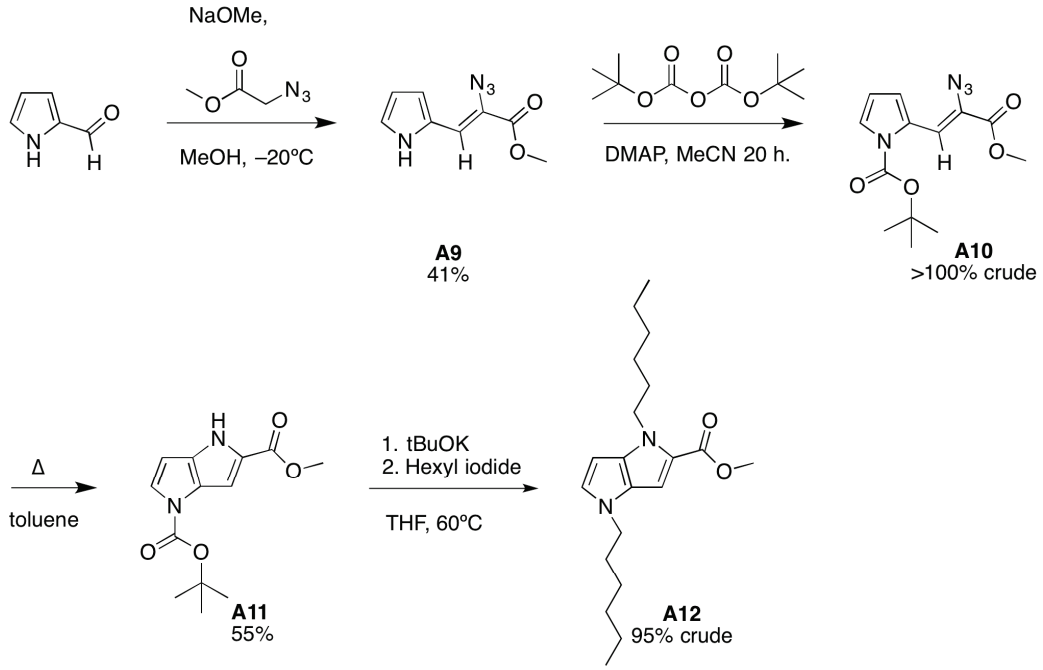

***tert*-Butyl (Z)-2-(2-azido-3-methoxy-3-oxoprop-1-en-1-yl)-1H-pyrrole-1-carboxylate A10**
Di-*tert*-butyl dicarbonate (0.86 mL, 3.74 mmol) was syringed into a solution of **A9** (0.481 g, 2.50 mmol) in dry acetonitrile (4 mL). 4-Dimethylaminopyridine (0.032 g, 0.26 mmol) was added and the reaction was covered in foil and allowed to stir overnight. The next day the reaction was diluted with DCM, poured into $NaHCO_3$, and extracted with more DCM. The organics were washed with NH_4Cl and brine before being dried over Na_2SO_4. The solvent was removed in vacuo to afford crude **A10** as a yellow oil. (Product can be used in the next cyclization step without further purification, but excess di-*tert*-butyl dicarbonate adds to the new pyrrole ring.) ^{1}HNMR ($CDCl_3$, 500 MHz): δ 7.90 (s, 1H), 7.41 (dd, J = 3.3, 1.6 Hz, 1H), 7.31 (dd, J = 3.7, 1.6 Hz, 1H), 6.31 (t, J = 3.5 Hz, 1H), 3.91 (s, 3H), 1.64 (s, 9H). ^{13}CNMR ($CDCl_3$, 125 MHz): δ 164.2, 146.7, 128.6, 124.6, 122.3, 120.0, 115.4, 111.8, 84.7, 52.8, 28.0.

1-(*tert*-Butyl) 5-methyl pyrrolo[3,2-*b*]pyrrole-1,5(4H)-dicarboxylate A11
Crude **A10** was dissolved in dry toluene (3 mL) and slowly added to 10 mL of refluxing toluene via a syringe pump (0.12 mL/min). Two hour after the completion of the addition, the reaction was cooled and the solvent was removed in vacuo. Purification by column chromatography in 100% hexane afforded **A11** (0.360 g, 55% yield) as a white solid. (Also collected 22% of di-Boc product.) ^{1}HNMR ($CDCl_3$, 500 MHz): δ 8.82 (br, 1H), 7.43 (br, 1H), 6.92 (br, 1H), 6.22 (s, 1H), 3.91 (s, 3H), 1.68 (s, 9H). (t, J = 3.5 Hz, 1H), 3.91 (s, 3H), 1.64 (s, 9H).

Methyl 1,4-dihexyl-1,4-dihydropyrrolo[3,2-*b*]pyrrole-2-carboxylate A12
Under inert atmosphere, tBuOK (0.160 g, 0.589 mmol) was transferred to a 25 mL Schlenk

tube. The tube was evacuated and refilled with nitrogen. Dry THF (2 mL) was added and the mixture cooled to 0°C. **A11** (0.033 g, 0.126 mmol) was added under positive pressure and the reaction was allowed to warm to room temperature over thirty minutes. 1-Iodohexane (0.20 mL, 1.35 mmol) was added and the reaction was warmed to 60°C and stirred for 2 hours. The reaction mixture was then poured into NH_4Cl and extracted with Et_2O (2 × 25 mL). The organic fractions were washed with H_2O and dried over Na_2SO_4 before removing the solvent in vacuo to afford **A12** (0.042 g, 95% crude yield) as a dark oil. ^{1}HNMR ($CDCl_3$, 500 MHz): δ 6.85 (br, 1H), 6.77 (s, 1H), 5.92 (br, 1H), 4.40 (t, J = 7.3 Hz, 2H), 3.92 (t, J = 7.1 Hz, 2H), 3.90 (s, 3H), 1.83 (m, 4H), 1.32 (m, 12H), 0.89 (m, 6H).

A.5 Dithienothiophene anthracene

While attempting to make thieno[3,2-*b*]thiophene-2,5-dicarbaldehyde we instead synthesized thieno[3,2-*b*]thiophene-2,3-dicarbaldehyde (**A13**). This ortho lithiation was surprising and was thought to occur due to the stabilization of the ortho-dianion by TMEDA. Thiophene-2,3-dicarbaldehyde had been used to synthesize acenedithiophenes with interesting crystal packing motifs and charge transport properties.[5][6] Following literature procedures we synthesized the novel dithienothiophene anthracene analogue (**A16**) (Scheme A.5. **A16** was emissive with a quantum yield of 40% (Figure A.3). The two regioisomers, which are formed in equal amounts, appeared to be separable by recrystallization, but the proper conditions were not found and pure isomers were not collected. The project was not submitted for publication because the formation of **A13** could not be predictably reproduced.

Scheme A.5: Synthesis of TIPS-anthradithienothiophene.

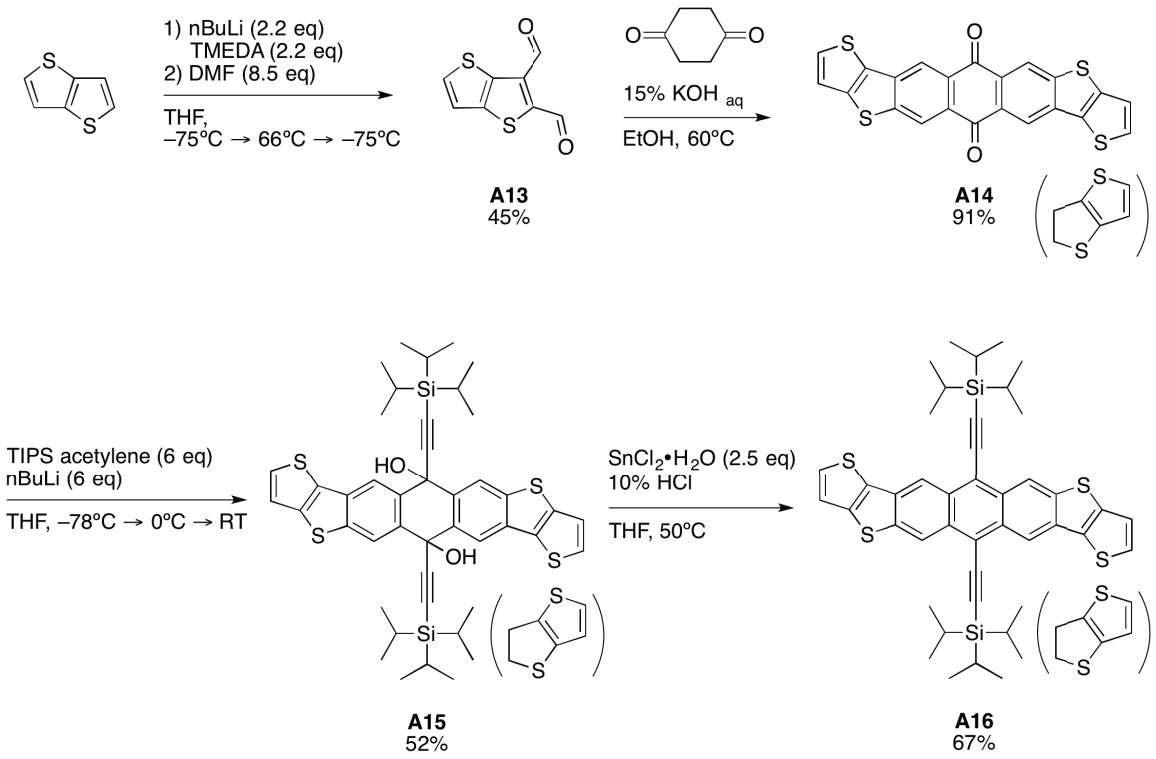

Thieno[3,2-*b*]thiophene-2,3-dicarbaldehyde A13

Thieno[3,2-*b*]thiophene (0.107 g, 0.762 mmol) in diethy ether was cooled to −75°C under N_2. TMEDA (0.25 mL, 1.65 mmol) and nBuli (0.67 mL, 1.68 mmol) were added successively via syringe and the reaction turned yellow. The reaction was heated to reflux for 30 minutes, then cooled back to −75°C. The reaction was quenched with DMF (0.50 mL, 6.5 mmol) and slowly allowed to warm to room temperature overnight. The next day the reaction

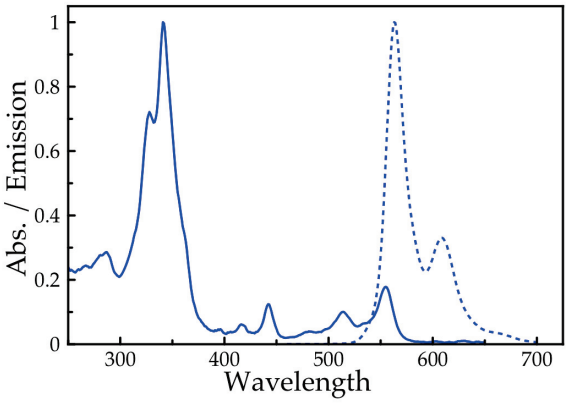

Fig. A.3.: Absorption (—) and emission (- - -) spectra of dithienothiophene anthracene **A16**.

was clear. Precipitates were observed after quenching with 2M HCl (30 mL) at −20°C. The reaction mixture was diluted in H_2O and extracted with DCM. The solvent was removed in vacuo to afford **A13** (0.1142g, 76% yield) as a yellow solid. ^{1}HNMR ($CDCl_3$, 300 MHz): δ 10.70 (s, 1H), 10.48 (s, 1H) 7.82 (d, J = 5.2 Hz, 1H), 7.38 (d, J = 5.1 Hz, 1H). ^{13}CNMR ($CDCl_3$, 75 MHz): δ 182.6, 181.7, 154.8, 148.7, 143.3, 138.7, 136.3, 119.1. HR-MS (APCI) m/z = 196.9718 [M+1] (calcd. for $C_8H_5O_2S_2$: m/z = 196.9725). Note: This reaction was successfully repeated twice, but failed with freshly distilled TMEDA. A ^{1}HNMR of the "old" TMEDA, however, showed no major impurities, but were shifted slightly up-field.

Anthra-dithieno[3,2-*b*]thiophene-dione A14

Thieno[3,2-b]thiophene-2,3-dicarbaldehyde **A13** (0.082 g, 0.42 mmol) was stirred in EtOH (8 mL) at 60°C till dissolved. 1,4-cyclohexane dione (0.024 g, 0.21 mmol) was added, followed by 15% aqueous KOH (0.34 mL, 0.91 mmol). The reaction mixture was stirred at 60°C for 1.5 hours. The dark reaction mixture for cooled and filtered. The bright yellow solids were washed with EtOH to afford **A14** (0.082 g, 91% yield), which was used without further purification. ^{1}HNMR ($CDCl_3$, 500 MHz): δ 8.90 (s, 1H), 8.88 (s, 1H), 8.85 (s, 1H), 8.84 (s, 1H), 7.74 (d, J = 5.0 Hz, 2H), 7.42 (d, J = 5.0 Hz, 2H). HR-MS (APCI) m/z = 432.9489 [M+1] (calcd. for $C_{22}H_9O_2S_4$: m/z = 432.9480).

Bis((triisopropylsilyl)ethynyl)-dihydroanthra-dithieno[3,2-*b*]thiophene-diol A15

Triisopropyl silyl acetylene (0.25 mL, 1.1 mmol) in dry THF (10 mL) was cooled to −75°C under inert atmosphere. nBuLi (0.44 mL, 1.1 mmol) was slowly added drop-wise. The reaction mixture was stirred at −75°C for 15 minutes and was then allowed to warm to 0°C for 15 minutes more. **A14** (0.082 g, 0.189 mmol) was added at 0°C under positive pressure, the reaction was warmed to room temperature and stirred overnight. The reaction was then quenched with saturated NH_4Cl (1 mL) and poured into H_2O (25 mL). The product was extracted into diethyl ether (2 x 20 mL) and dried over Na_2SO_4 before being concentrated in vacuo to afford a reddish brown oil. The product dissolved in a minimum of DCM and

crashed out in hexanes to afford **A15** (0.078 g, 52% yield) as red crystals. ^{1}HNMR ($CDCl_3$, 500 MHz): δ 8.80 (s, 1H), 8.70 (s, 1H), 8.69 (s, 1H), 8.60 (s, 1H), 7.58 (dd, *J* = 5.1, 1.2 Hz, 2H), 7.37 (d, *J* = 5.1 Hz, 2H), 1.11 (s, 36H).

Bis((triisopropylsilyl)ethynyl)anthra-dithieno[3,2-*b*]thiophene A16
A15 (0.069 g, 0.087 mmol) was dissolved in 2 mL of dry THF and the red solution was degassed with bubbling N_2. Tin(II) chloride dihydrate (0.051 g, 0.22 mmol) was added and the solution was degassed for 2 more minutes. The reaction was stirred for 4.5 hours and then filtered. The product was dissolved in refluxing hexane/DCM and quickly passed through a small silica plug while hot. The solvent was removed in vacuo to afford **A16** (0.044 g, 67% yield) as red solids. ^{1}HNMR ($CDCl_3$, 500 MHz): δ 9.20 (s, 1H), 9.17 (s, 1H), 9.14 (s, 1H), 9.12 (s, 1H), 7.66 (d, *J* = 5.0 Hz, 2H), 7.36 (d, *J* = 5.0 Hz, 2H), 0.91 (s, 36H). HR-MS (APCI) *m/z* = 763.2437 [M+1] (calcd. for $C_{44}H_{51}S_4Si_2$: *m/z* = 763.2407).

A.6 Bispyrrolobenzene

Using the chemistry learned from the synthesis of pyrollopyrroles, we theorized that we could synthesize benzodipyrrole, a nitrogen analogue to the well known benzodithiophene building block. The use of the Hemetesberger indolization reaction had previously been shown to work in very similar reactions.[7][8] In our hands, however, we were not able to obtain the desired cyclized product, though we tried several methods (Scheme A.6).

Scheme A.6: Synthesis of dimethoxy-phenylene-bis(2-azidoacrylate) and failed cyclization attempts.

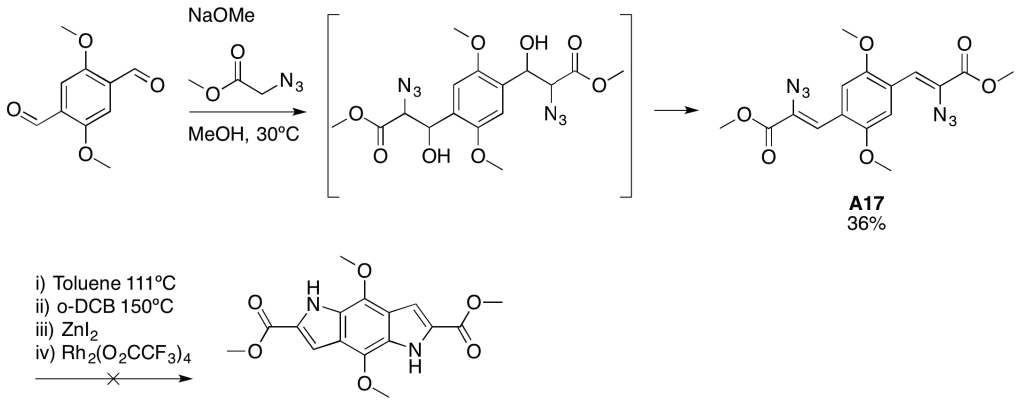

Fearing that the methoxy groups in **A17** were interfering with the cyclization, we also tried synthesizing the thiophene-substituted starting material **A22**, though this failed to cyclize as well (Scheme A.7).

Dimethyl 3,3′-(2,5-dimethoxy-1,4-phenylene)(2Z,2′Z)-bis(2-azidoacrylate) A17
Into anhydrous methanol (4 mL) cooled to −20°C, was added solid sodium (0.140 g, 6.06 mmol). The reaction was warmed to room temperature and stirred till all the sodium

Scheme A.7: Synthesis of dithiophenylphenylene-bis(2-azidoacrylate).

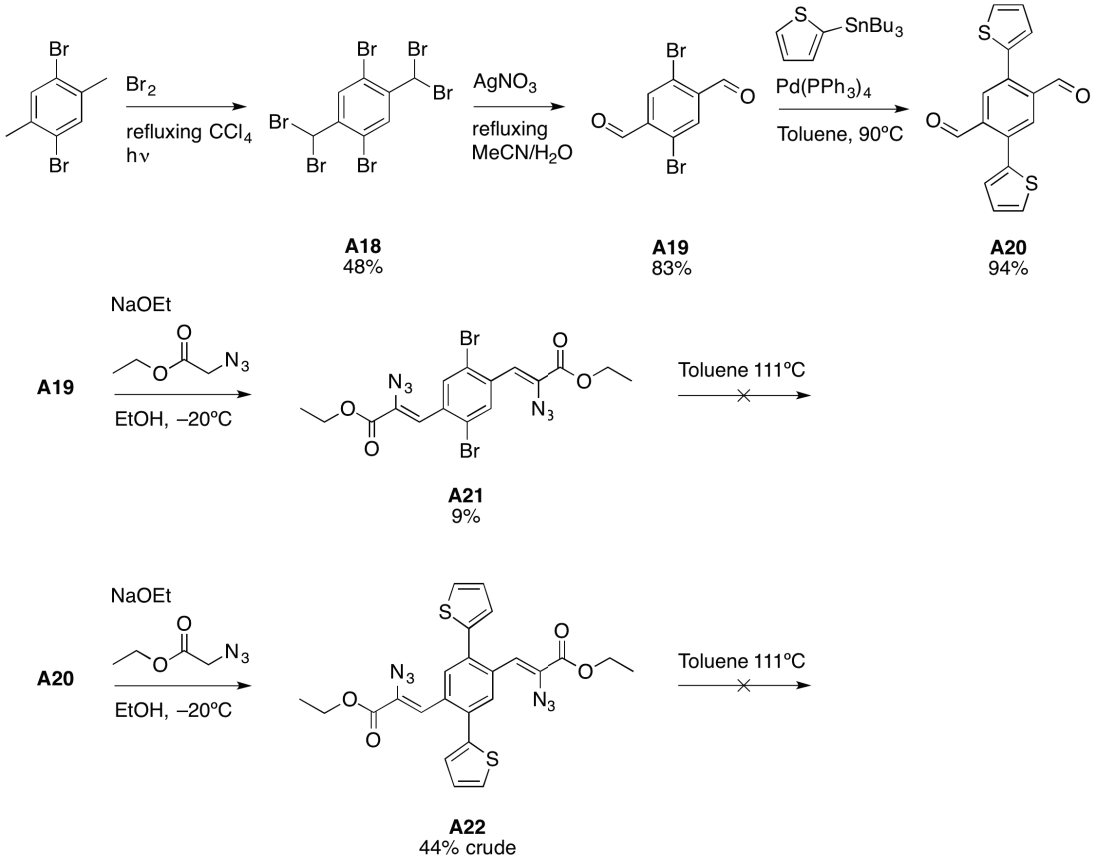

dissolved. At room temperature methyl 2-azidoacetate (0.890 g, 7.74 mmol), diluted in 4 mL of anhydrous methanol, and 2,5-dimethoxyterephthalaldehyde (0.249 g, 1.28 mmol) were added in alternating portions keeping the temperature constant. The reaction was then warmed to 30°C and stirred for 3 hours. The turbid reaction mixture was quenched with $NaHCO_3$ (15 mL), stirred for 5 minutes, then poured onto ice. The mixture was kept at 6°C for 1 hour before filtering and washing solids with H_2O. The solids were dried overnight under vacuum to yield an orange powder (0.179 g, 36% yield). ^{1}HNMR ($CDCl_3$, 500 MHz): δ 7.86 (s, 2H), 7.41 (s, 2H), 3.95 (s, 6H), 3.91 (s, 6H).

1,4-Dibromo-2,5-bis(dibromomethyl)benzene A18

Followed procedure from literature: *Angew. Chem. Int. Ed.*, **2014**, *53*, 6786. Collected **A18** (48% yield) as a white powder. ^{1}HNMR ($CDCl_3$, 500 MHz): δ 8.15 (s, 2H), 6.96 (s, 2H).

2,5-Dibromoterephthalaldehyde A19

Followed procedure from literature: *Angew. Chem. Int. Ed.*, **2014**, *53*, 6786. Collected **A19** (83% yield) as pale yellow needle-like crystals. ^{1}HNMR ($CDCl_3$, 500 MHz): δ 10.37 (s, 2H), 8.18 (s, 2H). ^{13}CNMR ($CDCl_3$, 125 MHz): δ 189.8, 137.3, 135.0, 125.5.

2,5-Di(thiophen-2-yl)terephthalaldehyde A20
2,5-Dibromoterephthalaldehyde **A19** (0.506 g, 1.73 mmol) and toluene (25 mL) were loaded into a schlenk tube and placed under inert atmosphere. Tetrakis(triphenylphosphine)palladium(0) (0.165 g, 0.143 mmol) was added under positive pressure, followed by tributyl(thiophen-2-yl)stannane (1.5 mL, 4.7 mmol) via syringe. The reaction mixture was heated to 88°C and stirred for 2 days while monitoring progress by TLC. Once the reaction complete, the mixture was cooled, diluted with ethyl acetate, and filtered through cotton to remove excess palladium. The solution was washed with 1M KF (25 mL), H_2O, and brine, dried over Na_2SO_4, and concentrated in vacuo. The product was purified by column chromatography using a gradient of 100% hexanes to 50% DCM to afford **A20** (0.488 g, 94% yield) as a yellow solid. ^{1}HNMR ($CDCl_3$, 500 MHz): δ 10.29 (s, 2H), 8.17 (s, 2H), 7.56 (dd, J = 5.1, 1.2 Hz, 2H), 7.22 (dd, J = 5.1, 3.5 Hz, 2H), 7.17 (dd, J = 3.5, 1.2 Hz, 2H). ^{13}CNMR ($CDCl_3$, 125 MHz): δ 191.2, 137.3, 137.0, 136.8, 130.9, 130.1, 128.3, 128.1.

Diethyl 3,3′-(2,5-dibromo-1,4-phenylene)(2Z,2′Z)-bis(2-azidoacrylate) A21
In a dry 2-neck flask under N_2, solid sodium (0.137 g, 5.96 mmol) was added into anhydrous ethanol (10 mL) cooled to −20°C, and stirred till all the sodium dissolved. 2,5-Dibromoterephthalaldehyde **A19** (0.206 g, 0.704 mmol) was combined with ethyl 2-azidoacetate (0.738 g, 5.72 mmol) and ethanol (10 mL) and cooled to −20°C in a separate flask. The freshly prepared NaOEt/EtOH solution was then slowly transfered to the reaction flask via cannula. The reaction was warmed to −10°C and stirred overnight under N_2. The reaction mixture was then poured into saturated $NaHCO_3$ (6 mL) and ice and kept at 6°C for one hour. The resultant precipitates were filtered and washed with H_2O. The product was purified by column chromatography (100% DCM) to afford **A21** (0.034 g, 9% yield) as a yellow powder. ^{1}HNMR (CD_2Cl_2, 500 MHz): δ 8.50 (s, 2H), 7.19 (s, 2H), 4.43 (q, J = 7.1 Hz, 4H), 1.44 (t, J = 7.1 Hz, 6H).

Diethyl 3,3′-(2,5-di(thiophen-2-yl)-1,4-phenylene)(2Z,2′Z)-bis(2-azidoacrylate) A22
Followed similar procedure as for **A21**, but did not cool the reaction. Instead warmed to 30°C after the addition of NaOEt and stirred for 5 hours. The reaction mixture was then poured into saturated $NaHCO_3$ (6 mL) and ice and kept at 6°C for one hour. The resultant precipitates were filtered and washed with H_2O to afford **A22** (44% crude yield) as light orange solids.

A.7 Thio-Coronene

The goal of this early project was to synthesize coronene with fused thiophene rings on its periphery. The hexakis(thiophenyl)benzene precursor was easily synthesized (Scheme A.8), but the complete bromination of **A26** was more difficult. Questions as to the selectivity of the following cyclization reaction led to the abandonment of this project.

Scheme A.8: Synthesis of thio-coronene precursors.

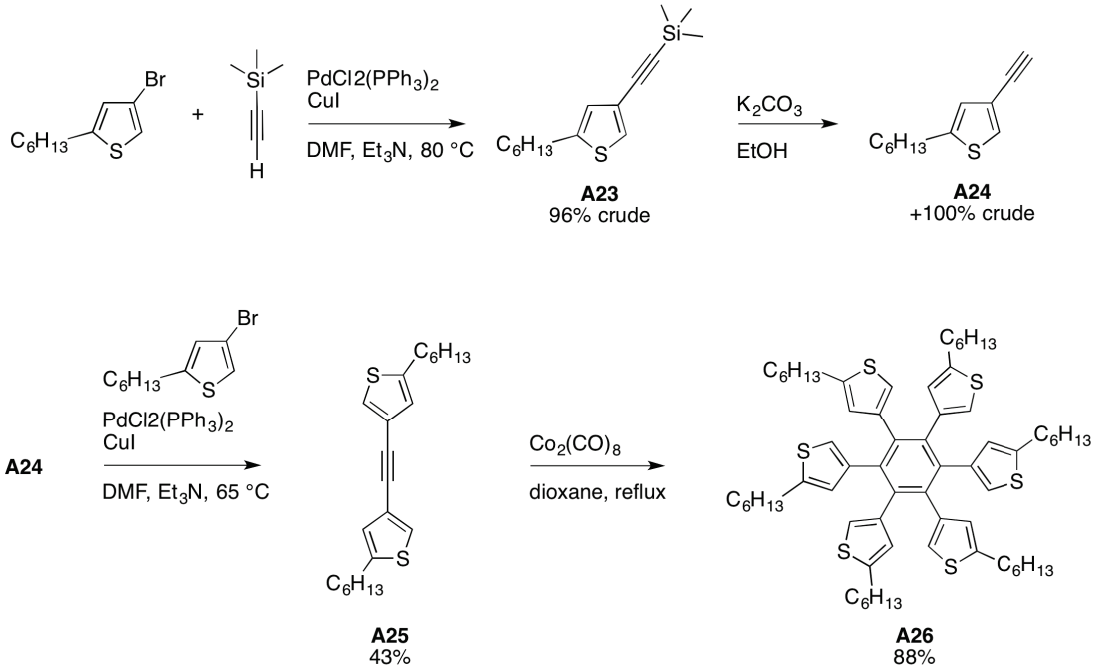

((5-Hexylthiophen-3-yl)ethynyl)trimethylsilane A23

To palladium(II)chloride (0.034 g, 0.19 mmol), copper(I)iodide (0.041 g, 0.21 mmol), and triphenylphosphine (0.10 g, 0.39 mmol) under inert atmosphere, was added 2-hexyl-4-bromothiophene (2.14 g, 8.65 mmol) via syringe. Dimethylformamide (12 mL) and triethylamine (5 mL) were subsequently added and the resulting solution was heated to 90°C and stirred for 30 minutes. Trimethylsilylacetylene (1.5 mL, 11 mmol) was then added to the reaction flask and the solution was stirred at 90°C overnight. The reaction mixture, containing crystals, was combined with DCM (80 mL) and the organic phase was washed with water (3 x 200 mL) and brine (2 x 200 mL). The organic fractions were then dried over $MgSO_4$ and passed through a silica plug. THe solvent was removed in vacuo to afford **A23** (2.20 g, 96% yield) as a bright orange oil. ^{1}HNMR ($CDCl_3$, 400 MHz): δ 7.26 (s, 1H), 6.79 (s, 2H), 2.74 (t, *J* = 7.2 Hz, 2H), 1.63 (m, 2H), 1.29 (m, 6H), 0.88 (t, *J* = 6.4 Hz, 3H), 0.23 (s, 9H).

4-Ethynyl-2-hexylthiophene A24

To a stirring solution of **A23** (2.19 g, 8.30 mmol) in ethanol (100mL) was added potassium carbonate (3.30 g, 23.9 mmol). After stirring at room temperature for 48 hours the reaction mixture was poured into water (100 mL), extracted with petroleum ether (3 x 50 mL), washed with brine (100 mL), and dried over $MgSO_4$. The solvent was removed in vacuo to afford crude **A24** (1.66 g, +100% yield) as an orange oil. ^{1}HNMR ($CDCl_3$, 400 MHz): δ 7.30 (s, 1H), 6.81 (s, 1H), 2.99 (s, 1H), 2.76 (t, *J* = 7.6 Hz, 2H), 1.65 (m, 2H), 1.31 (m, 6H), 0.88 (t, *J* = 6.8 Hz, 3H).

1,2-Bis(5-hexylthiophen-3-yl)ethyne A25

To palladium(II)chloride (0.023 g, 0.13 mmol), copper(I)iodide (0.027 g, 0.14 mmol), and triphenylphosphine (0.058 g, 0.22 mmol) under inert atmosphere was added 2-hexyl-4-bromothiophene (1.33 g, 5.39 mmol). Degassed dimethylformamide (4 mL) and triethylamine (2.8 mL) were then added and the resulting solution was heated to 60°C. After stirring for 30 minutes, 4-ethynyl-2-hexylthiophene **A24** (0.912 g, 4.744 mmol) was added and the reaction mixture was stirred overnight at 65°C. The reaction mixture was then diluted in DCM (50 ml), washed with water (3 x 100 mL), dried over $MgSO_4$, and concentrated in vacuo. The product was purified by column chromatography (100% hexanes) to afford **A25** (0.723 g, 47% yield) as a bright orange oil. ^{1}HNMR ($CDCl_3$, 400 MHz): δ 7.26 (s, 2H), 6.83 (s, 2H), 2.77 (t, J = 7.6 Hz, 4H), 1.66 (m, 4H), 1.30 (m, 12H), 0.89 (t, J = 6.8 Hz, 6H).

1,2,3,4,5,6-Hexakis(5-hexylthiophen-3-yl)benzene A26

A mixture of **A25** (0.257 g, 0.715 mmol) in 1-4 dioxane (10 mL) was degassed by "freeze-pump-thaw." To this was added octacarbonyl dicobalt (0.047 g, 0.14 mmol) and the reaction mixture was refluxed overnight under N_2. The reaction mixture was then cooled and poured into water (40 mL) and extracted with DCM (3 x 30 mL). The organic fractions were combined and washed with brine (50 mL), dried over $NaSO_4$ and concentrated in vacuo. The product was purified by column chromatography (100% hexanes to 10% EtOAc) to afford **A26** (0.226 g, 88% yield) as a sticky dark brown solid. ^{1}HNMR ($CDCl_3$, 400 MHz): δ 6.32 (s, 6H), 6.15 (s, 6H), 2.53 (t, J = 7.2 Hz, 12H); 1.42 (m, 12H), 1.22 (m, 36H), 0.88 (t, J = 7.2 Hz, 18H).

A.8 Additional known compounds

Scheme A.9: Synthesis of 2,5-di(pyridin-4-yl)thiazolo[5,4-d]thiazole. Knighton, R. C.; Hallett, A. J.; Kariuki, B. M.; Pope, S. J. A. *Tetrahedron Lett.* **2010**, *51*, 5419–5422.

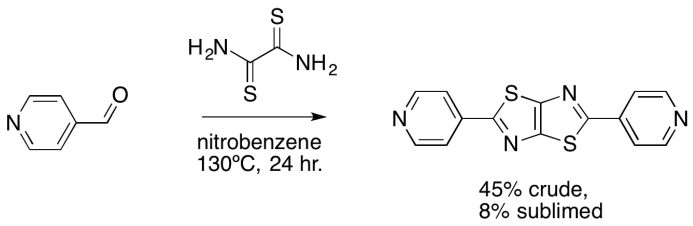

Scheme A.10: Synthesis of thieno[3,2-*b*]pyrroles.
Jiang, X.-D.; Zhang, H.; Zhang, Y.; Zhao, W. *Tetrahedron* **2012**, *68*, 9795–9801.

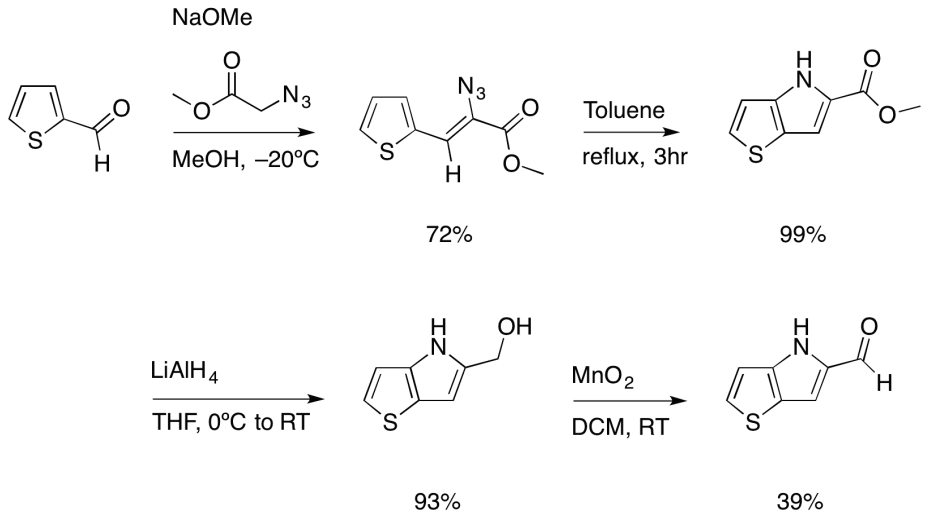

Scheme A.11: Synthesis of dihydrothieno[3,2-b:4,5-b′]dipyrrole.
Nguyen, H. Q.; Rainbolt, E. A.; Sista, P.; Stefan, M. C. *Macromol. Chem. Phys.* **2012**, *213*, 425–430.

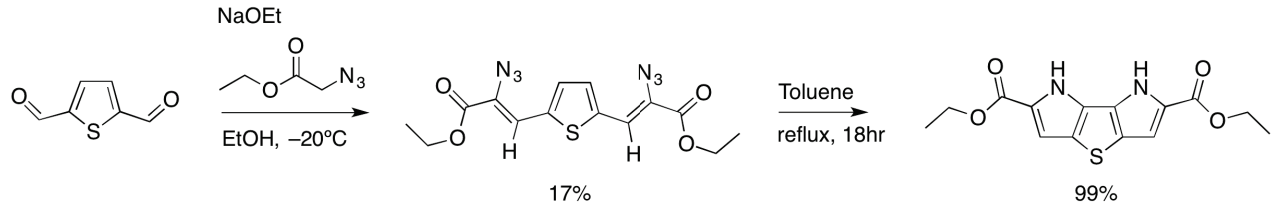

References

(1) Chernichenko, K. Y.; Sumerin, V. V.; Shpanchenko, R. V.; Balenkova, E. S.; Nenajdenko, V. G. "Sulflower": A new form of carbon sulfide. *Angew. Chemie - Int. Ed.* **2006**, *45*, 7367.

(2) Goldoni, F.; Janssen, R. a. J.; Meijer, E. Synthesis and characterization of new copolymers of thiophene and vinylene: Poly(thienylenevinylene)s and poly(terthienylenevinylene)s with thioether side chains. *J. Polym. Sci. Part A Polym. Chem.* **1999**, *37*, 4629.

(3) Yamamoto, T.; Takimiya, K. Facile Synthesis of Highly π-Extended Heteroarenes, Dinaphtho[2,3-b:2′,3′-f]chalcogenopheno[3,2-b]chalcogenophenes, and Their Application to Field-Effect Transistors. *J. Am. Chem. Soc.* **2007**, *129*, 2224.

(4) Stokes, B. J.; Dong, H.; Leslie, B. E.; Pumphrey, A. L.; Driver, T. G. Intramolecular C-H amination reactions: exploitation of the Rh(2)(II)-catalyzed decomposition of azidoacrylates. *J. Am. Chem. Soc.* **2007**, *129*, 7500.

(5) Payne, M. M.; Odom, S. a.; Parkin, S. R.; Anthony, J. E. Stable, crystalline acenedithiophenes with up to seven linearly fused rings. *Org. Lett.* **2004**, *6*, 3325.

(6) Wang, C.; Dong, H.; Hu, W.; Liu, Y.; Zhu, D. Semiconducting π-conjugated systems in field-effect transistors: a material odyssey of organic electronics. *Chem. Rev.* **2012**, *112*, 2208.

(7) Heaner IV, W. L.; Gelbaum, C. S.; Gelbaum, L.; Pollet, P.; Richman, K. W.; DuBay, W.; Butler, J. D.; Wells, G.; Liotta, C. L. Indoles via Knoevenagel–Hemetsberger reaction sequence. *RSC Adv.* **2013**, *3*, 13232.

(8) Curiel, D.; Espinosa, A.; Más-Montoya, M.; Sánchez, G.; Tárraga, A.; Molina, P. A new open benzodipyrrole-based chemosensor for hydrogenpyrophosphate anion in aqueous environment. *Chem. Commun. (Camb).* **2009**, 7539.